Late Quaternary Palaeoenvironmental Reconstruction in the Burydah Area, Central Saudi Arabia

Thesis submitted for the Degree of
Doctor of Philosophy at the University of Leicester

by

Ahmed Al dughairi

Supervisor: Dr Sue McLaren

Department of Geography
University of Leicester

JAN 2011

Abstract

Late Quaternary Palaeoenvironmental Reconstruction in the Burydah area, Central Saudi Arabia

Ahmed Al dughairi

Although investigations to find evidence for Quaternary environmental changes is conducted in Africa and the south Arabian Peninsula, in Saudi Arabia there are also vast areas covered with deposits that preserve detailed Quaternary histories of past climatic events. Unfortunately to date much of Saudi Arabia has not been explored in terms of past climatic changes, nor have in any sites been accurately dated using numerical dating techniques. As a result there is a scarcity of Quaternary palaeoclimatic archives set in a reliable temporal framework. This research aims to help remedy this situation through the examination and reconstruction of environmental changes in the area around Burydah, central Saudi Arabia.

The findings of this research have shown evidence for significant wet phases in Marine Isotope Stage (MIS) 7, as well as the MIS 5d, 5b and 5a, which coincide with wetter phases elsewhere in the Arabian Peninsula and Africa. A later wet phase is represented by palaeolake deposits formed in MIS4. Similar to most areas in the Arabian Peninsula and North Africa, there is no evidence of climatic conditions during the Last Glacial Maximum (LGM), perhaps suggesting that conditions were hyper-arid with an environment that was erosive rather than depositional. Moving into the Holocene, interdune lake tufa deposits formed at MIS 1 c. 12-7ka.

This research shows that dunes were forming during the early Holocene, as there were significant wet events in the Burydah, such as active wadis, and tufa deposits which formed at lake sites. Moving through to the mid-Holocene and towards present day, there is evidence for a drying out of the wadi systems and the establishment and growth of sand sheets covering the landscape. From c. 5ka onwards the Burydah area had become arid, with similar conditions to those that persist today.

Acknowledgements

All praise is due to Allah, most Gracious, most Merciful, for his help, blessing and guidance which gave me the patience and endurance to accomplish this work.

My great thanks to my supervisor, Dr. Sue McLaren for the effective guidance, valuable advice, useful comments and continuous encouragement and support throughout the process of conducting this research, and Dr Andrew Bradley for his generous investment of time, encouragement, suggestions and insightful counselling helped shape the directions taken in this study.

I would like also to thank all the people who agreed to participate in this research, including the fieldwork. I would like to express my deep and sincere appreciation to the many individuals and institutions who have given information and assistance in order to make this thesis a reality.

I am very grateful to personnel of many labs where measurements were conducted (e.g. Dr Mark Bateman, University of Sheffield; Dr Simon Kemp, Geological Survey, Gemma Black, University of Leicester.

I would like to express my sincere gratitude to Qassim University, for providing the scholarship and the assistance that enable me to carry on working this study.

My great appreciation goes to my father and mother for their moral support and prayers for my success. For the most, I am specifically grateful to my wife for her patience and to my children for their support and tolerance. Also, my great thanks go to my brothers: Ali; Mohamed; Omer; Abdulaziz; Abdullah and Abed Al Majied for their help and encouragement.

List of Abbreviations

^{14}C: Radiocarbon dating

De: Equivalent dose

ETM Landsat Enhanced Thematic Mapper

GIS: Geographic Information System

ITCZ: Intertropical Convergence Zone

KACST: King Abdulaziz City for Science and Technology

KSA: Kingdom of Saudi Arabia

LGM: Last Glacial Maximum

MMR: Milton Multiband Radiometer

MS: Magnetic Susceptibility

OSL: Optically Stimulated Luminescence

PCA: Principal Components Analysis

PMT: Photomultiplier tube filter

SAR: single aliquot regenerative dose

SCRS: Saudi Centre of Remote Sensing

TM: Landsat Thematic Mapper

XRD: X-Ray diffraction

Table of Contents

Chapter 3: Research Methodology and Techniques

Chapter 4*:* Results

List of Figures

List of Tables

CHAPTER ONE

1 The study area

1.1 Introduction

This chapter provides a general review of the physical characteristics of central Saudi Arabia, in particular the geology, geomorphology, climate, natural vegetation and soil characteristics, to provide a background for studying the area around Burydah, Qassim province. The chapter also provides an explanation as to why this study area was chosen, the research questions and the structure of this thesis.

1.2 The physical characteristics of central Saudi Arabia

Saudi Arabia is situated in southwest Asia and covers an area of 2.3 million km^2; it comprises about 5% of the world's arid zones. Ancient sedimentary and volcanic rocks (Precambrian) have been eroded and reduced to a nearly level plain (Brown et al., 1989). From Cambro-Ordovician to early Tertiary times, the shallow seas of the Tethys lapped onto Saudi Arabia's north-eastern plain, and marine sediments were deposited (Edgell, 2006).

1.2.1 The Arabian Shield and the Arabian Shelf

Saudi Arabia is divided into two main regions: the Arabian Shield in the west and the Arabian Shelf towards the east (Fig1.1). The Arabian Shield occupies one-third of Saudi Arabia, roughly 610,000 km^2 of the entire Arabian Peninsula (Alwelaie, 1985). It is mainly made up of metamorphosed sedimentary and volcanic rocks which relate to the Precambrian period (Powers et al., 1966), and others are covered by Quaternary sediments. The Arabian Shelf is located to the east of the Arabian Shield, where it occupies roughly two-thirds of the Arabian Peninsula. Its sequence is made up of continental and shallow marine sedimentary rocks (Chapman, 1978).

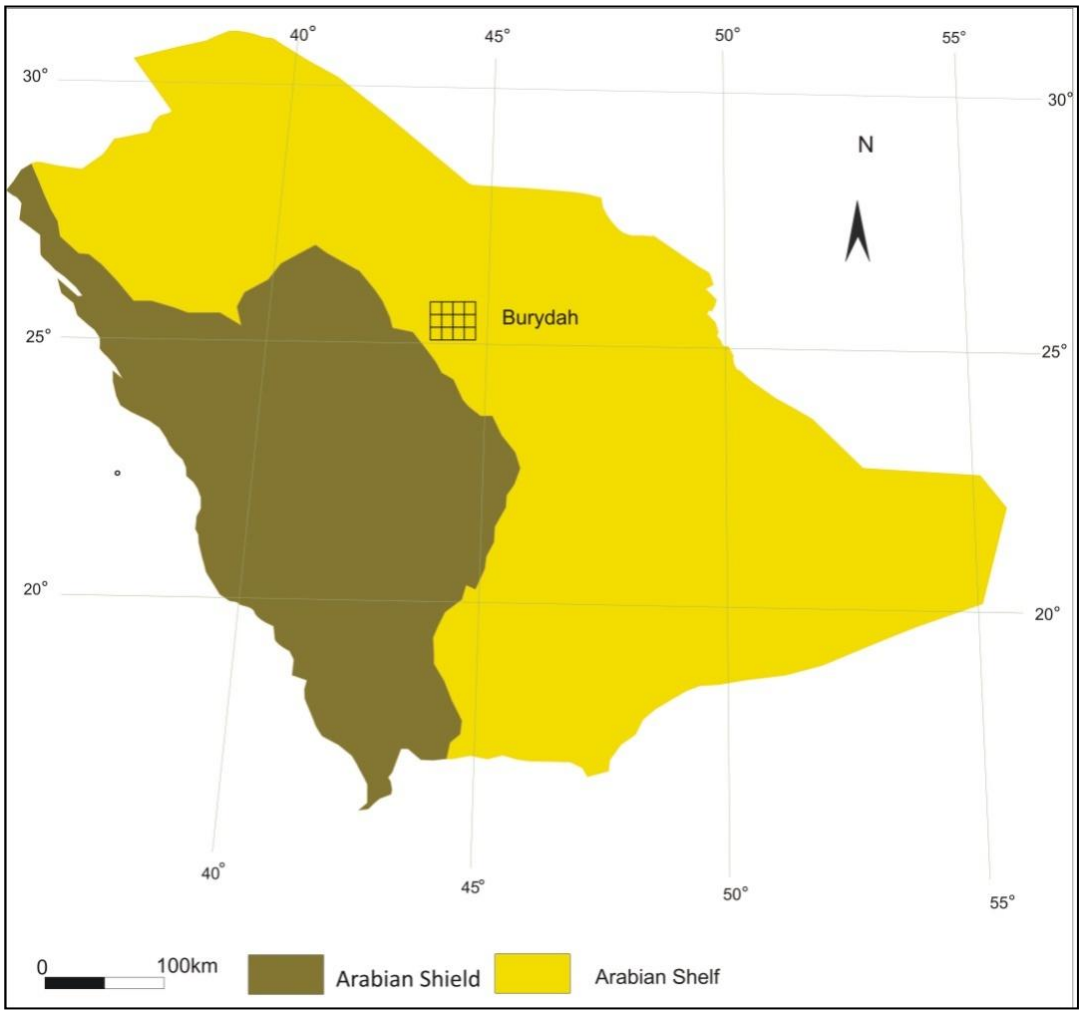

Figure 1.1: General Geological Map of the Arabian Shield and Arabian Shelf in Saudi Arabia, box represents the study area (*Source: Saudi Atlas, 1999).*

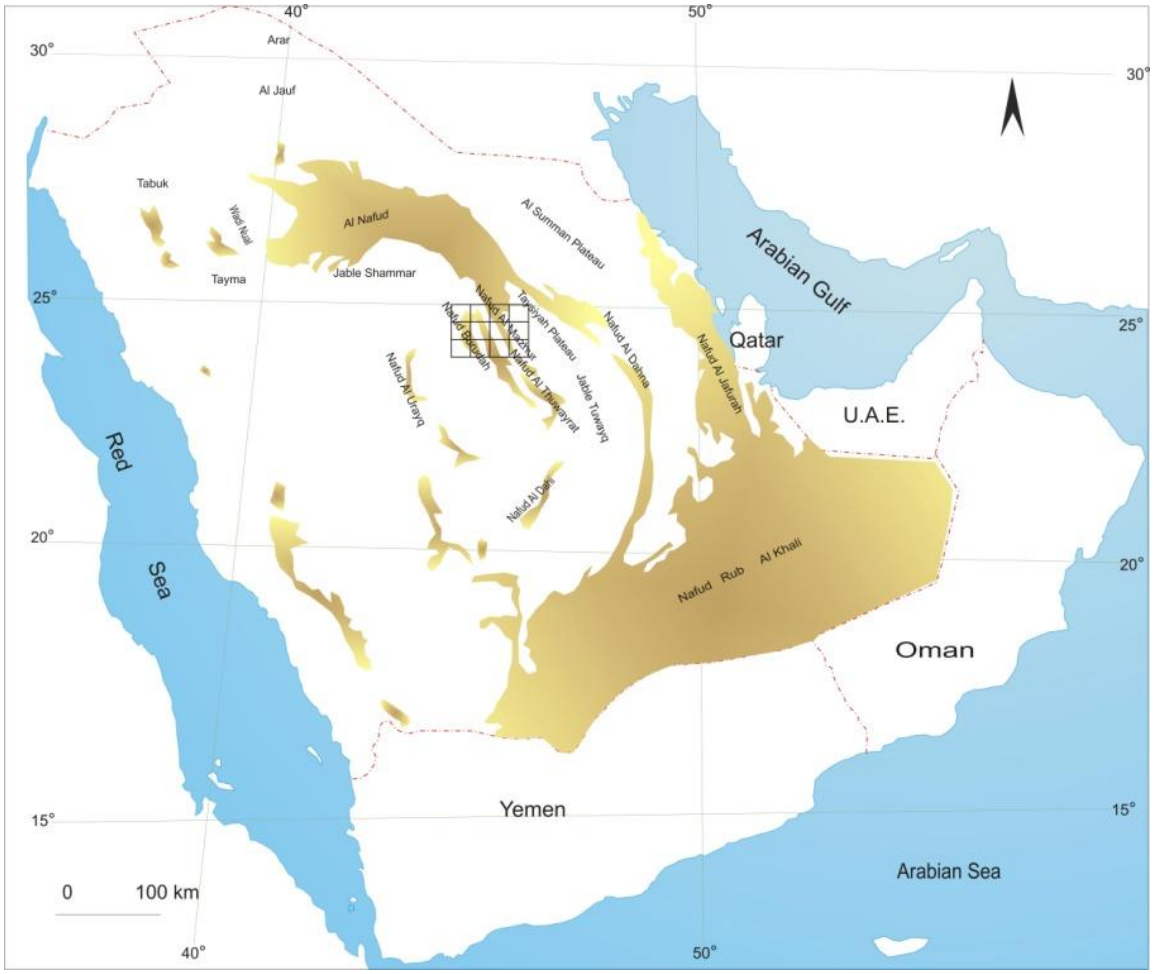

Figure 1.2: A general map showing the main dune fields in Saudi Arabia, box represents the study area

Source: Saudi Atlas 1999.

1.2.2 Distribution of Nafuds in Saudi Arabia

The Nafud is the common Arabic term for the sand dune fields; Rub Al Khali is the largest sand desert in Saudi Arabia, occupying an area of 600,000 km^2 (Al welaie, 1985) (Fig 1.2). The second largest dune field is Al Nafud, situated in the north of Saudi Arabia, occupying an area of 64,630 km^2 (Fig 1.3). Al Nafud is located to the north of the Burydah area (see Fig 1.2). The eastern parts of Al Nafud are gradually linked with Nafud Al Mazhur near Al Taysiyah Plateau, according to Hotzl (1984), Al welaie (1985) and Edgell (2006). Al Nafud has a rectangular shape trending NNW-SSE, joining the eastern part of the Great Nafud with Nafud Al Thuwayrat (Fig1.2).

Al Dahna dune field lies in the middle of Saudi Arabia (Fig1.2) and occupies an area of 40,789 km^2. It is a belt that extends for a distance of 1,300 km. The northern parts of the Burydah area are located on the east edge of Nafud Al Dahna, where Arq Al Dukhul and Arq Al Hamel are situated. The dunes extend across Al Taysiyah Plateau, flanked by Wadi Al Fuwayliq in the north and west and Al Dahna in the east (Fig 1.2).

1.2.3 Wadi Al Rimah in Saudi Arabia

Wadi systems extend in different parts of Saudi Arabia. For example, Wadi Al Rimah is one of the longest wadi systems in Saudi Arabia (Fig1.3) and extends for 970 km from Harrat Khaybar in the west (between latitudes 25° 43' and 40° 00') to the east of Saudi Arabia toward the Arabian Gulf (Al welaie, 1985). The uppermost wadi channel is a narrow gorge that cuts into Precambrian metamorphic and igneous rocks, namely schists, phyllites and granites (Hotzl et al., 1978), as well as large basalt flows from the Tertiary and Quaternary ages (Brown et al., 1963). The mid-drainage area is flat, with a low gradient and gentle slopes (Al Dughairi, 2003). Approximately 4 km to the west of Burydah City, the wadi runs into the surface of a cuesta, which consists mainly of Cambrian–Devonian sandstones. According to Hotzl et al. (1984), Wadi Al Rimah is a large, old river system crossing the Burydah area from west to east, with a channel of varying width at the eastern margin of the study area which cuts across a sabkhah until it becomes blocked by the sand dunes of Nafud Al Thuwayrat. Beyond Nafud Al Thuwayrat, Wadi Al Rimah takes on another name, 'Wadi Al Ajradi'; it then crosses the Al Taysiyah plateau, which is composed of limestone, dolomite and clays. When the wadi crosses the western edge of the Sulb Plateau it takes a turn towards Wadi Al Batin and continues on towards the eastern Saudi border with Iraq.

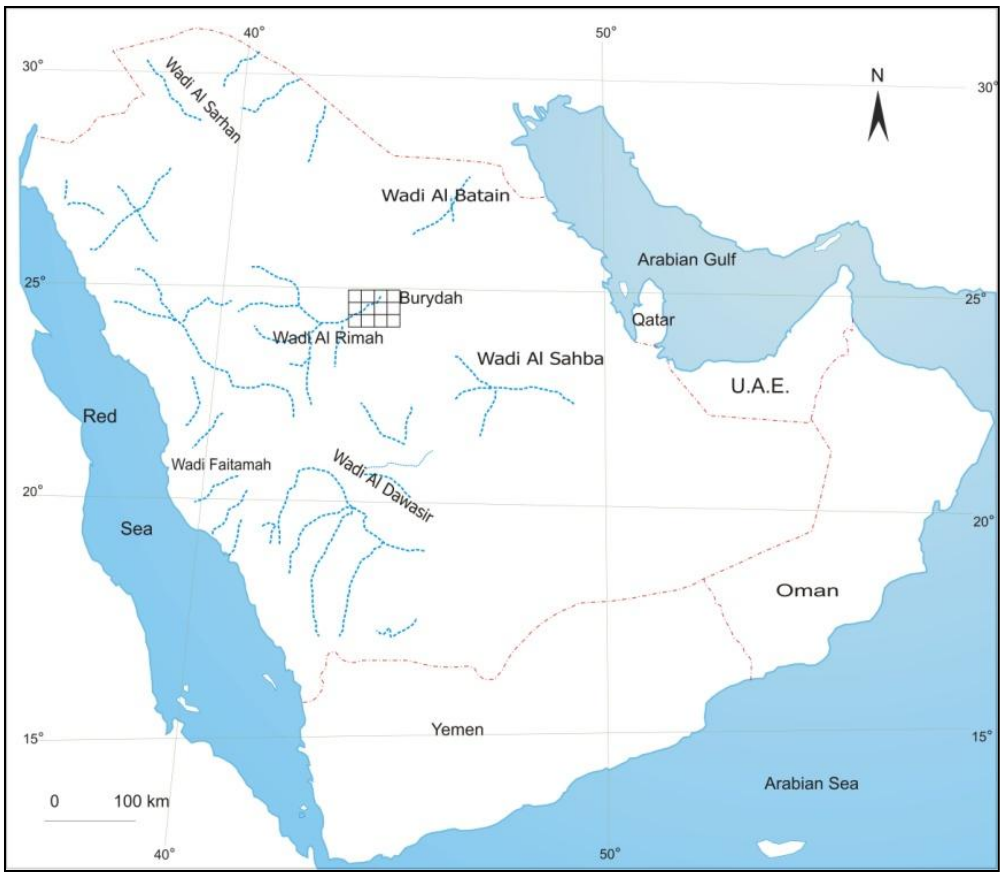

Figure 1.3: A general map showing the main wadis in Saudi Arabia, box represents the study area.

Source: Saudi Atlas 1999

1.3 The physical characteristics of the Burydah area

1.3.1 The Geological setting

The Burydah area is underlain by Phanerozoic sedimentary rocks on the western edge of the sedimentary basin that occupies the Arabian Shelf. These deposits crop out in a homocline and have been assigned to the following lithological formations of both the Paleozoic and Mesozoic Eras:

The Saq Sandstone (Cambrian to Early Ordovician in age), is composed of white, grey, or brown cross-bedded sandstones (Fig1.4).The Tabuk formation is Early Ordovician to Early Silurian and Devonian in age. This formation is composed of partly micaceous silty sandstone, varying from red to pink, light grey and brown buff (Al Welaie, 1996). It

crops out sporadically in the western part of the Burydah area. The formation is buried by Nafud Burydah around Wadi Al Rimah and also beneath Nafud Al Shuqayyiqah (Powers et al., 1966).

The Khuff formation is Permian in age. The full sequence crops out at Safra Al Shaquah, Safra Burydah in the north of the Burydah area, where it is around 50 m thick, and occurs in cuestas to the south of Wadi Al Rimah. It consists predominantly of grey limestone and greenish brownish shale, dark-grey dolomite, marl, clay and gypsum, with fossil wood at the base (Al Welaie, 1996; Powers et al., 1966).

The Sudair shale is Upper Permian to Lower Triassic in age. The outcrops at Safra Al Buatun and around Al Tarafiyah oasis are buried at the edge of Nafud Al Sirr and appear again at Jal Khartam. The Sudair formation comprises red, green, and brown shales, carbonates, clays, and gypsum (Al Welaie, 1996; Manivit et al., 1986; Powers et al.,1936).

The Jilh formation is Upper Permian to Lower Triassic in age. The uppermost parts consist predominantly of red to brown fine-grained bedded sandstone, pinkish gypsum, and yellow to golden brown dolomite and conglomerate (Al Welaie, 1996). The Jilh formation in the Burydah area forms the well-marked Safra Al Asyah cuesta, to the east of Nafud Al TarafIyah, and Safra Al Mistawi, to the east of Nafud as Sirr. It also forms the plateau further to the east near Nafud Al Thuwayrat which is covered with small parallel hills that appear to be dark red in colour as a result of the high amounts of iron oxide (Powers et al., 1936). The Minjur Sandstone is Triassic to Jurassic in age and forms a low-lying plain in eastern Burydah. The outcrops also lie between the Jilh Formation plateau and Nafud Al Thuwayrat and have been observed as small hills under Nafud Thuwayrat where much of the formation is buried. The rocks are composed of white, red or purplish pedogenised claystone with beds of white to pink, medium and fine grained sandstone, in locally cross-bedded sandstone (Manivit et al 1986, Powers et al., 1936). To the south of Wadi Al Rimah is a conglomeratic sandstone with a ferruginous cement and black to brown ironstone beds (Al welaie, 1996).

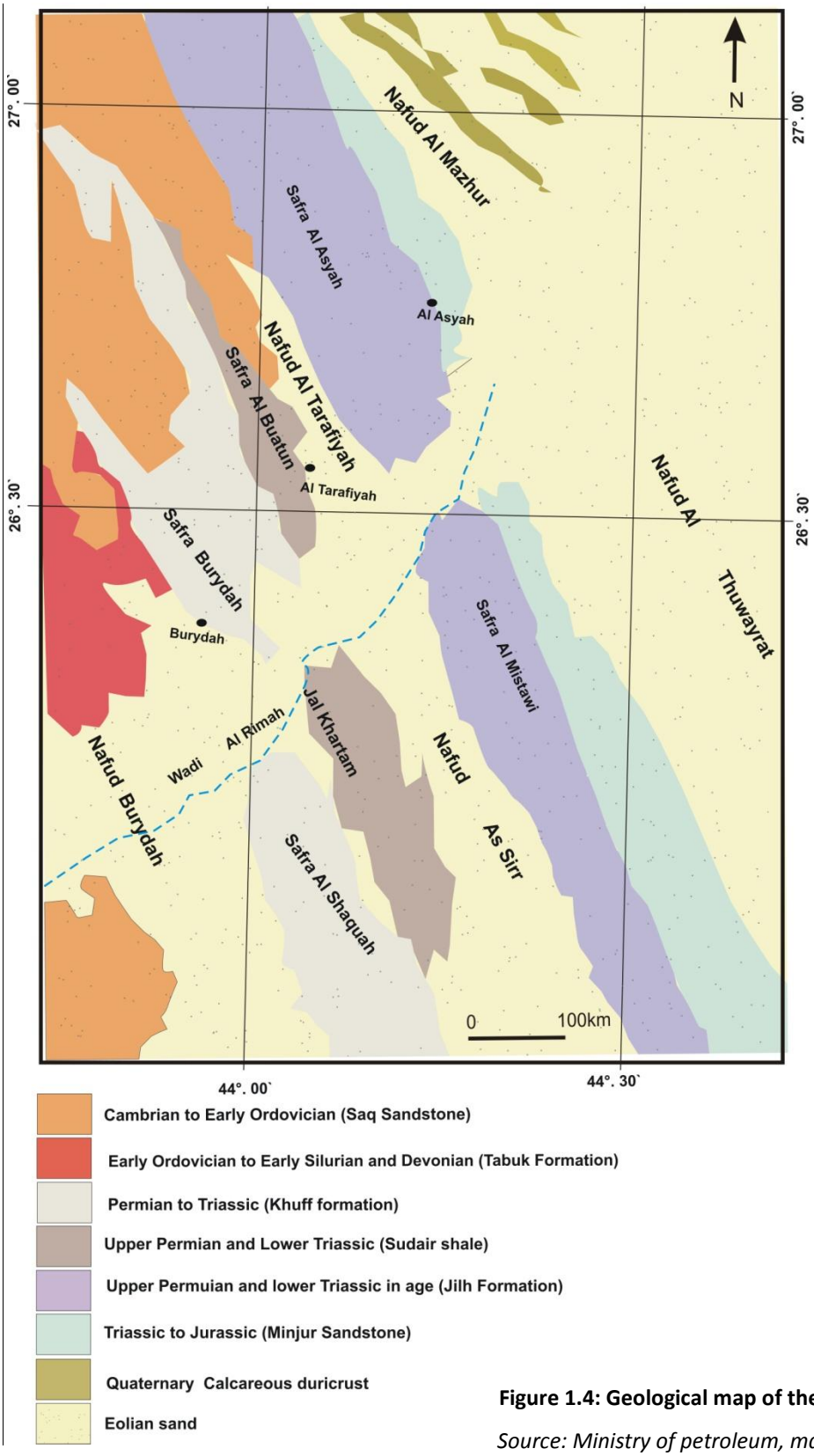

Figure 1.4: Geological map of the study area.

Source: Ministry of petroleum, map206A.1963

1.3.2 The Geomorphological setting

As shown in Figure 1.5 the study area is located in the central core of Saudi Arabia. The landforms of the Burydah area are among the most amazing geomorphic arid systems of Saudi Arabia. Sand dunes and sand sheets are widespread, covering about one-third of the total Burydah area (Manivit et al 1986). The accumulation of sand shows a great variety of dune morphologies accumulated with in depressions and within wadi channels. For examples Linear and dome dunes of Nafud Al Thuwayrat are mostly 50-100 m in height and up to 1-2 km wide. Nafud Al Mazhur, lying to the north of Nafud Al Thuwayrat, extends from north to south, and comprises of linear dunes running from the northeast toward the south near Nafud Al Thuwayrat. Linear dunes run parallel to one another for more than 259 km, and then are joined with Nafud Al Thuwayrat, where the height of the dunes varies between 25 and 50 m, whilst the width may exceed 2 km. Dome dunes are also present in the south. In the middle of the study area is Nafud As Sirr, lying in a depression to the west of Safra Al Mistawi, and the forms are dome dunes. Nafud Burydah is to the west of Wadi al Rimah; here the sands form low linear dunes covering most of the channel of Wadi Al Rimah, and extend 70 km in an ENE-WSW direction, with a width of up to 25 km (Edgell, 2006). Nafud Tarafiyah is situated in the north part of the central study area within the channel of wadi Al Butaun. Nafud is built of linear dune and sand sheets. In the Nafud Al Mazhur there are Lacustrine deposits consisting of 1 m of white to green clay are overlain by intercalated evaporites, carbonate-rich silts and gypsum crusts (Manivit et al., 1986). These deposits are covered by aeolian sands and can be observed at many places within Nafud Al Mazhur in the east of Burydah area.

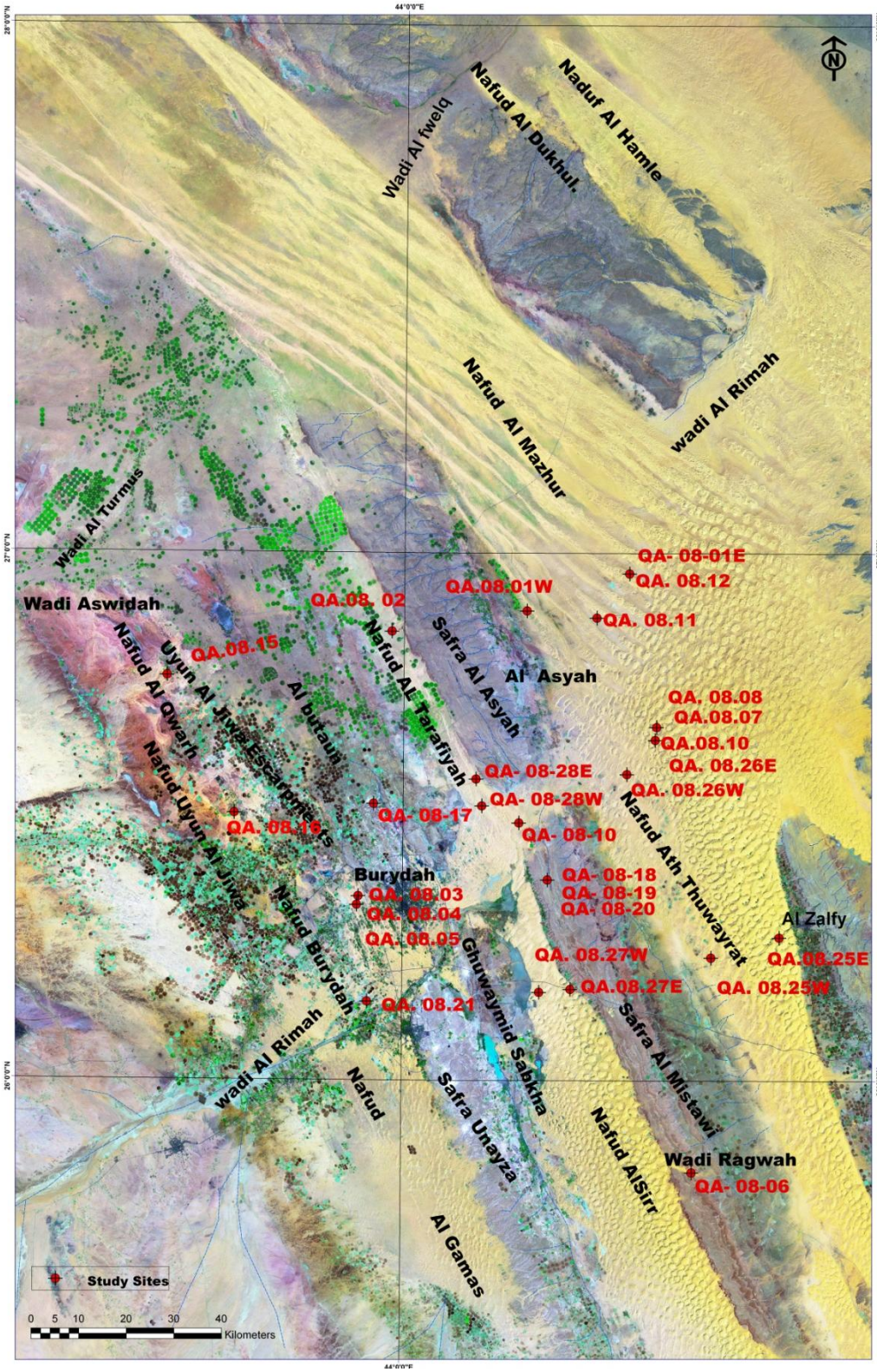

Figure 1.5: Satellite image of the study area with the sample sites shown as red dots. Nafud Burydah (lower centre) and Nafud Tarafiyah (top centre) and Nafud As Sirr (lower centre) Nafud Thuwayrat and Mazhur are seen in the right image. Wadi Al Rimah crosses the area in an eastward direction with little pattern of ancient terraces rising around the channel. (source ETM Image2003)

1.3.3 Climate

The climate of Burydah area is hot and dry and generally classified as arid. Daily temperatures during the summer months (April to October) commonly exceed 40°C in the shade. These temperatures are sometimes accentuated by hot north westerly or westerly winds. Temperatures are low in winter (January and December) and commonly drop to 7°C. The prevailing winds are north easterly in winter, with mean velocities of 6.21 M/h, and north westerly in summer and autumn, when the mean velocities are 8.07 M/h. The wind systems in the study area is clearly shown by the directions of the linear dunes, as seen in table 1.1 and Fig 1.6. The Prevailing wind is N, which transported and loads sand from the northern Great Al Nafud toward central and south Saudi Arabia, according to Edgell (2006). The Shamal wind continues to be the dominant wind. Annual rainfall is only a few centimetres, and mostly occurs between November and March (Annual Climatological Record from 1970 to 2000) (Table 1.1).

Table 1.1: The annual climatological elements in the study area for the period 1970 to 2000.

Month	Temperature		Rain	Relative Humidity	Wind speed	Wind direction
	maximum (°C)	minimum (°C)	(mm)	(%)	(M/h)	
JAN	17	5	19	52	6.21	NE
FEB	19	7	17	43	6.21	N
MAR	25	13	22	38	7.45	N
APR	27	16	30	32	8.0	N E
MAY	37	21	15	22	8.7	N
JUN	40	23	0	12	6.21	N
JUL	40	25	0	10	6.83	NNW
AUG	41	24	0	12	5.59	NNE
SEP	36	21	0	13	4.49	NE
OCT	33	17	4	39	5.59	NE
NOV	25	12	25	43	5.59	E
DEC	20	7	11	46	5.59	NE
Average	30	15	11	30	6.21	-

1.3.4 Natural vegetation and soil

The natural vegetation is restricted to ephemeral and perennial plants, with shrubs and temporary grasses spread such as *Launaea nudicaulis* (Linn.), *Malva parviflora* (cheeseweed mallow) and *Rumex vesicarius* (locally called hummayd) occurring around the Wadi Al Rimah and its tributaries. In addition, *Tamarix, Acacia*, *Ziziphus*, *Amplexicaulis*, *Zygophyllum mandavillei* and *Phragmites* (common reed) appear within the depressions and wadis. There are also *Acacia asak* (Forssk), *Calligonum, Lycium* and *Haloxylon prsicm* on the sand dunes. In addition, palms appear around the main towns of Unayzah and Burydah, and are also found along Wadi Al Rimah, at the foot of Safra Al Ruwayah and within Nafud Al Ghammas.

According to the Atlas Soil Classification Map for Saudi Arabia (1999), the soils of the study area consist of loamy soils, including pale brown silt, yellowish-brown clayey silt and yellowish-brown silty sand. The soils are slightly saline, consisting of 40% silt, 30% sand, and 30% gypsum and calcium carbonate which can be found in the wadis and basins. This soil has been classified as Calciorthids (Saudi Arabia Ministry of Agriculture and Water, 1999).

1.4 Importance of the study

The Burydah area has been selected for the following reasons:

- To date, the Quaternary palaeoenvironmental research conducted in Saudi Arabia in general and in the Burydah in particular has been poorly documented. According to Fleitmann *et al.* (2004), there are vast areas in the central core of Saudi Arabia that have not been explored. In fact there has been a short chronology for the Quaternary period established as a result of work on the neighboring of the area. e.g. Garrard (1981); Hotzl (1978); Whitney (1983); Al Juaidi (2003) and Maclern et al (2009).
- To fill the significant gap in knowledge relating to the late Quaternary history of central Saudi Arabia (McLaren *et al.,* 2008). Numerical chronological detail is

important and will allow for the dating of landforms and sediments.

- Fluvial deposits, aeolian deposits lake and Tufa deposits are well preserved in the Burydah area and represent potential archives for Quaternary times.

1.5 The aims of the research

The principal aim of this research is to examine and reconstruct late Quaternary environmental changes in the area around Burydah, central Saudi Arabia, through studying the physical, chemical and mineralogical deposits preserved in the landscape. This research aims to identify alterations in spatial and temporal patterns of environmental processes resulting from climatic fluctuations between wetter and drier phases during the Quaternary period. The research will assess the impact of environmental change in the past as a way of facilitating modelling of the implications of current and future climatic change in the Burydah area. In particular, the work will focus on the Quaternary landforms of fluvial terraces along the Wadi Al Ramah and its tributaries and the tufa and lake sediments preserved within Nafud Burydah as indicators of wetter phases, and on the dune deposits along Nafud Al Thuwayrat, Al Mazhur and Al Sirr as an indicator of deposition in both drier and wetter phases. Optically Stimulated Luminescence (OSL) and radiocarbon (^{14}C) dating will be used as tools in this research. The chronological findings of this research on the preserved palaeoenvironmental history of the Burydah area will be studied in relation to findings from elsewhere on the Arabian Peninsula (e.g. Al Nafud in the north, Al Quwaiayh in the centre and Rub Al Khali in the south), and in the United Arab Emirates (UAE), the Sultanate of Oman, Yemen and Jordan. The reason for this comparison is that much of Saudi Arabia has not been explored in terms of past climatic changes or well dated using numerical dating techniques, and as a result there is a gap in the Quaternary palaeoclimate archives set in a reliable temporal framework.

A spatial survey using remote sensing techniques and classification methods will also be employed, with the main aim of investigating sand deposits that are present in the

Burydah area, in order to create the best classification for dune redness to bring the study to present environment. The methods selected will be those that best classify and reveal the differentiation and distribution of sand dunes, in order to study the physical properties of each site within the sand dunes and to look at variations in sediment provenance and dune type, building and transportation.

1.6 Research questions

Three key research questions will be addressed to investigate the evidence for climatic changes and to enhance the understanding of the sedimentary evolution of late Pleistocene and Holocene environments in the Burydah area. These questions include:

1. **What evidence of late Quaternary activity of Wadi Al Rimah and its tributaries has been preserved in the Burydah area?**

This will examine the sequences of deposits in three wadis in the Burydah area: the main channel of Wadi Al Rimah, and two of tributaries Wadi Al Butaun and Wadi Al Watah, none of which have been previously examined. Fluvial deposits found are to be studied in terms of the conditions under which they formed and the development of the wadis over time, and changes between fluvial and aeolian regimes. Numerical dating of the wadi deposits will provide information about the past wetter events of these wadi systems and the factors led to evolution such IOM during the late Quaternary (Fleitmann et al., 2007).

2. **How did the sand dunes and sand sheets in the Burydah area evolve during the late Quaternary?**

This question addresses the sand forms and dating of the sand deposits which have not been previously studied. The dune fields in the study area, such as Nafud Uyun Al Jiwa, Nafud Al Qwarh, Nafud Burydah, Nafud Al Thuwayrat, Nafud Al Mazhur and Nafud As Sirr, provide an opportunity to examine the Nafuds' evolution, rates of accumulation and to monitor the changes in the sediment profiles of these Nafuds. The dune forms

and structures provide information about palaeowind directions and dating of Nafud deposits (including the sand sheets) will be used to reconstruct aeolian activity over time. In addition the variations in the sand redness within Nafuds' Al Thuwayrat and Mazhur are used to establish the colour distribution and to inform us on the processes controlling dune formation today.

3. **Do lake and tufa deposits in the Burydah area reflect spatial and temporal patterns of environmental processes resulting from climatic fluctuations between wetter and drier phases during the Quaternary era?**

This question addresses lake deposits which are widespread in the east of Burydah, within the Nafud Al Thuwayrat and Al Mazhur and therefore represent good evidence of wetter phases in this part of Saudi Arabia. The physical and chemical properties of these lake deposits and the mineralogy of the sediments have not been previously examined. The study of these properties should provide a deeper understanding of the humid episodes over the late Quaternary in central Saudi Arabia. Tufa deposits have not been found or studied in central Saudi Arabia. The physical, mineralogical and chemical properties of these deposits will be examined. Dating tufa deposits will enable an understanding to be gleaned of when and under what climatic conditions the tufa formed.

1.7 The structure of thesis

The thesis is divided into six chapters; a brief description of each chapter is included here:

Chapter 1 presents an introduction to the thesis which covers the physical characteristics of the central Saudi Arabia, study area and the physical characteristics of the Burydah area, which include geology, geomorphology, climate, natural vegetation and soil characteristics. Moreover, it justifies the importance of this work, the study's aims, the research questions and the structure of the thesis.

Chapter 2 provides a review of the literature relating to Quaternary climatic changes; the geomorphology and sedimentology of desert deposits; the dating of desert deposits and remote sensing of desert deposits in the Arabian Peninsula.

Chapter 3 provides a review of the research methodology; the aim of this review is to explain how the geomorphological map was created. Remote sensing techniques will be employed as a tool, with the following main techniques: pre-processing, which includes the purpose of the image; geometric corrections and atmospheric corrections; post-processing, which consists of supervised and unsupervised image classification; creating an area of interest (AOI); image analysis using redness rating and spectral redness; Munsell soil colour charts; spectral redness from Landsat ETM images and Milton multiband radiometer (MMR) and magnetic susceptibility (MS). This chapter also explains the field investigation of the study area. Finally, this chapter reviews the laboratory analysis, which includes optically stimulated luminescence dating (OSL), radiocarbon dating (^{14}C), measurement particle size analysis, X-Ray diffraction (XRD) analysis, thin section technique and pollen analysis.

Chapter 4 provides the results of the macromorphological, micro-morphological and morphological characteristics and dating of the desert deposits in the study area, including wadi deposits, dune deposits, lake deposits and geochemical deposits. ***Chapter 5*** presents an interpretation of the outcomes of the empirical work of the study. ***Chapter 6*** presents key findings and summary.

CHAPTER TWO

2 Literature review

This chapter presents a literature review and investigates the geomorphology and sedimentology and the Quaternary climatic changes in the Arabian Peninsula with some examples from other studies conducted around Africa, Jordan, the UAE, Oman and Yemen. It aims to understand the history of the development of late Pleistocene and Holocene environmental changes in these areas.

In doing so, it begins with a brief introduction of the current hydrological systems in the Arabian Peninsula, with, as examples, Wadi Al Rimah, lakes within Rub Al Khali, Jubbah and some lakes in Yemen and UAE. It then examines the winds which influenced past climate in the Arabian Peninsula and some areas in Africa (as examples to give an overview of the environmental changes during the Quaternary period). Examples are then shown of studies which indicate the direction and strength of the monsoon and Shamal winds during various stages throughout the Quaternary period. This is followed by a history of climatic changes in the Arabian Peninsula supported by a literature review conducted around Saudi Arabia (e.g. Jordan, UAE, Oman, Yemen and Africa). In this review where radiocarbon ages in the studies cited are uncalibrated, these age have been calibrated with freely available software INTCAL09 (Reimer et al., 2009) as long we have the site details. A brief summary of the remote sensing applications of desert deposits in the Arabian Peninsula is included to bring the study up to the present day in terms of the environmental situation. The chapter ends with a conclusion.

2.1 Geomorphology and sedimentology of desert deposits in the Arabian Peninsula

2.1.1 Wadi and lake deposits

Lake and Wadi systems in the Arabian Peninsula are thought to be a consequence of increased rainfall associated with variations in moisture during the Quaternary (Zotl, 1984; Parker et al., 2004). McClure (1976) studied lake deposits within the interdunes of Rub Al Khali; the lake contained marls with interbedded alluvial and aeolian sands and gypsum layers increasing towards the top, and beds containing mollusc fossils covered with reddish sands. He suggested that the lakes were active during the late Quaternary, around 31ka (cal BP: 34,832-38,388) and 21ka (cal BP: 24,058-26,293) due to episodes of wet phases in the eastern Sahara desert. Also, McClure (1984) observed lakes occurred roughly simultaneously across the Arabian Peninsula and North Africa. A similar result has been reported by Garrard et al. (1981), with lacustrine deposits containing limestone and marl, covered by evaporites reflecting increased evaporation, under the Nafud Jubbah to the north of the Burydah. The diatomites within the lake indicate high rainfall around the time 25.6 ka (cal BP: 29,573-31,067).

During the Holocene, the lakes along Arabian Peninsula are thought to have been active, and the work conducted by Lezine et al. (1998) distinguished two sections in the lacustrine deposits at Al Hawa lake in Yemen, which is composed of dark-grey unconsolidated abiotic calcareous silts and thin layers of sand, organic matter and shells, ranging in age from 8.7 to 7.2 ka. During this time, the lakes were active and the detrital input of calcareous particles was very low, coeval with the northwards migration of the Indian monsoon (Lezine et al., 2007; Parker et al., 2004). These results are similar to those observed by McClure (1984) at the onset of the Holocene, from 9.3ka (cal BP: 8433-12917) to 6.5 ka (cal BP: 7244- 7611), when the lakes in the south of Saudi Arabia were shallow and playa-like. Others such as, Parker et al. (2006) used mineral magnetic measurements to study Holocene palaeolakes within interdunes areas at Ras Al Khaimah, UAE. They found low mineral magnetic values, corresponding to low levels of magnetic materials (marl and carbonate), and this reflected a period of stability associated with a wet climate, while the high mineral magnetic values related

to aeolian material infilling into the lake indicated a period of intense regional aeolian activity. Parker et al, in this study, linked the lake's development with the domination of the Indian monsoon that brought precipitation into the lake. These studies confirm that the intensified monsoon precipitation fluxes over south Arabia during the Holocene probably played a role in lacustrine development. However, Parker et al (2006) mentioned that the onset of wet conditions was much earlier in south Arabia than in central. This implies need for more investigation of evidence within Burydah in central Saudi Arabia through the analysis and dating of lake deposits in order to reconstruct the lake's history over time.

Wadi Al Rimah and Jubbah Lake represent a palaeo-hydrological system in Saudi Arabia. Unfortunately, there is little information published about these systems; most studies carried out in the wadi region are limited and give general descriptions of the channel and the material within. For example, in central Saudi Arabia, Hotzl et al. (1978) investigated Wadi Al Rimah, which is west of the Burydah area. They argued that the cuestas and escarpments controlled the channel expansion and the accumulation rates; he also concluded that the high percentage of gypsum in the wadi terraces indicates that sedimentation occurred under an arid climate. Also, Hotzl and Maurin (1978) studied wadi deposits at Wadi Birk, located about 400km to the east of Burydah (latitude 23° 20`) in central Saudi Arabia, and found the wadi sediments dominated by silt with a varying percentage of clay and sand with a remarkably high content of gypsum and carbonate calcium which dated to 28.9 ka (cal BP: 35,075-35,630); they described these sediments as products of a period of alternating runoff, dry season and flood. The Hotzl argument is limited and requires further investigation. Also, approximately 400 km to the east of Burydah, Hotzl and Zotl (1978) dated freshwater gastropods within terraces from Wadi Al Luhy ca.8.4 ka (Cal BP 9016-9627), which is evidence of a wet phase prevailing in central Saudi Arabia during Holocene.

On the basis of the above discussion, it appears that there are various lakes in Saudi Arabia which are completely unstudied. Most previous studies have focused on the lake beds, where it is apparent that there are some similarities and differences among

components such as the carbonate, organic materials, fossils and aeolian deposits within the beds. All studies have focused on three lake sites: Al Nafud in northern Saudi Arabia, Rub Al Khali, and Yemen in the south Arabian Peninsula. Most authors supported the argument that the lakes correspond to two major lake periods; the older dated between 37 and 24 ka, and the younger of Holocene age between 9 and 6 ka. However, problems associated with these ages are less reliable (not celebrated) and require further investigation. The lake in the Buraydah area of central Saudi Arabia, has not been explored before and there is a lack of studies relating to lakes in this part of Saudi Arabia.

2.2 Quaternary climatic changes in the Arabian Peninsula

2.2.1 Shamal winds in Saudi Arabia

Today, the current wind system is dominated by the Shamal winds which occur in summer and winter (Fig 2.1). In summer the Shamal wind results from high-pressure cells over northern Arabia: this wind is dry, with velocities of 48km/h; the winter Shamal is less effective but in some periods can produce strong winds of 55km/h (Edgell, 2006; Al welaie, 1985).

There is strong agreement between the studies relating to sand forms, wind direction and strength during various stages throughout the Quaternary period over the Arabian Peninsula; for example, in the south-east Arabian Peninsula, Holm (1960) (Fig2.2) refers to sources of sand in the Rub Al Khali from the Arabian Gulf region under the effect of north winds. Glennie and Singhvi (2002) worked in the eastern Emirates, and found the linear dunes suggested that they were formed by winds blowing from NE. Additionally, studies carried out in northern Saudi Arabia supported the clear effect of the northerly winds: for example, the building of Nafud Al Jafurah in eastern Saudi Arabia is associated with NW to NNW winds. According to Edgell (2006), the sand seas in the Arabian Peninsula (e.g. Great Al Nafud) indicate that they were formed by the trade winds during the last glacial period. This supports Holm's (1960) description, which indicates that the Shamal wind formed these dunes.

From the above discussion, it appears that most authors agree that the longitudinal axes of Nafuds observed in the north, south and east Arabian Peninsula are associated with the Shamal wind, and this wind played a major role in the accumulation and development of dunes in most parts of the Arabian Peninsula, especially in the north. As observed in central Saudi Arabia, the linear dunes and dome dunes are widespread around the Burydah area. This study addresses the sand forms and material properties which no previous studies have dealt with, and environmental change causing sand accumulations.

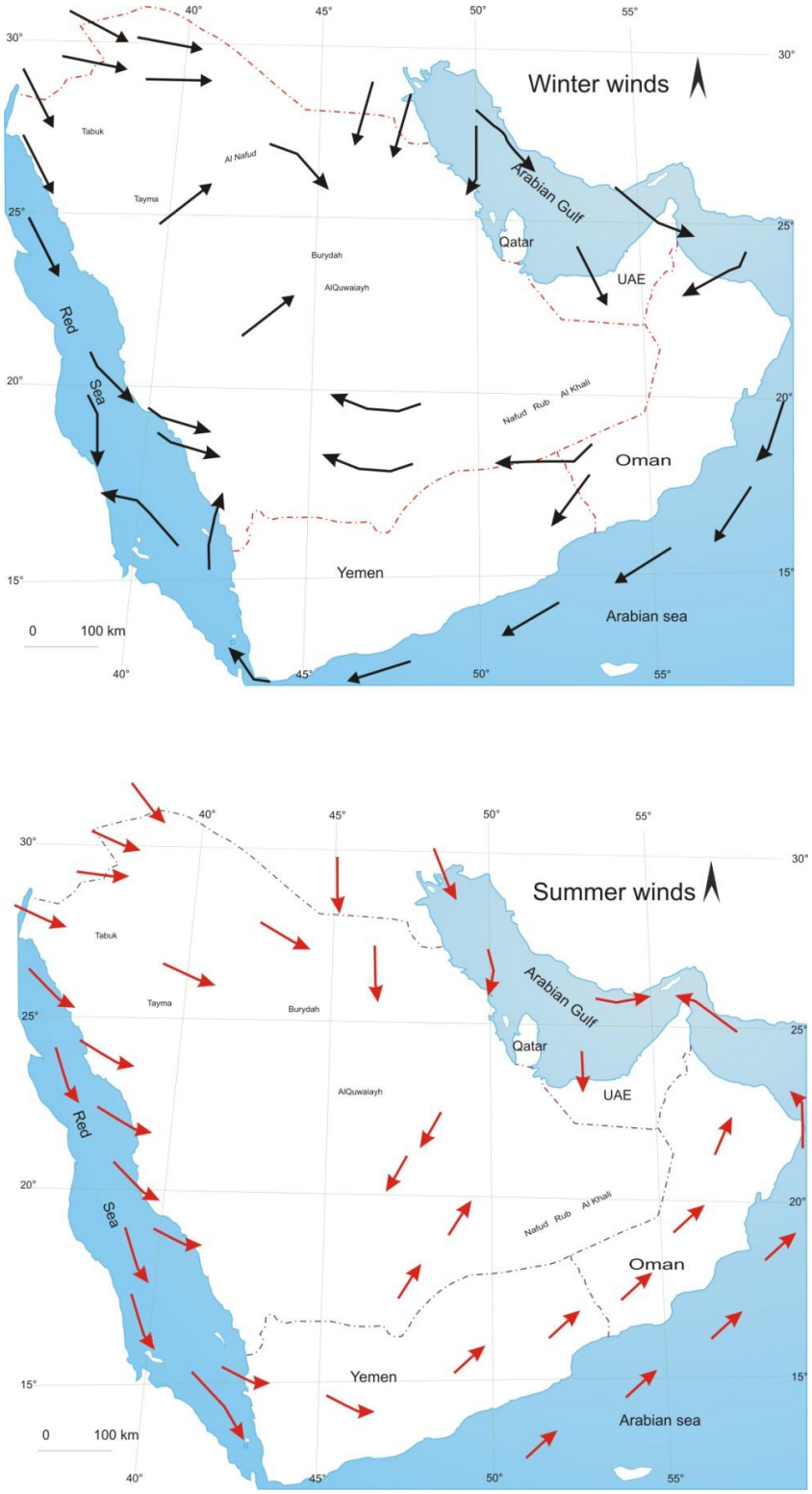

Figure 2.1: Summer and winter winds over Saudi Arabia (Saudi Atlas, 1999)

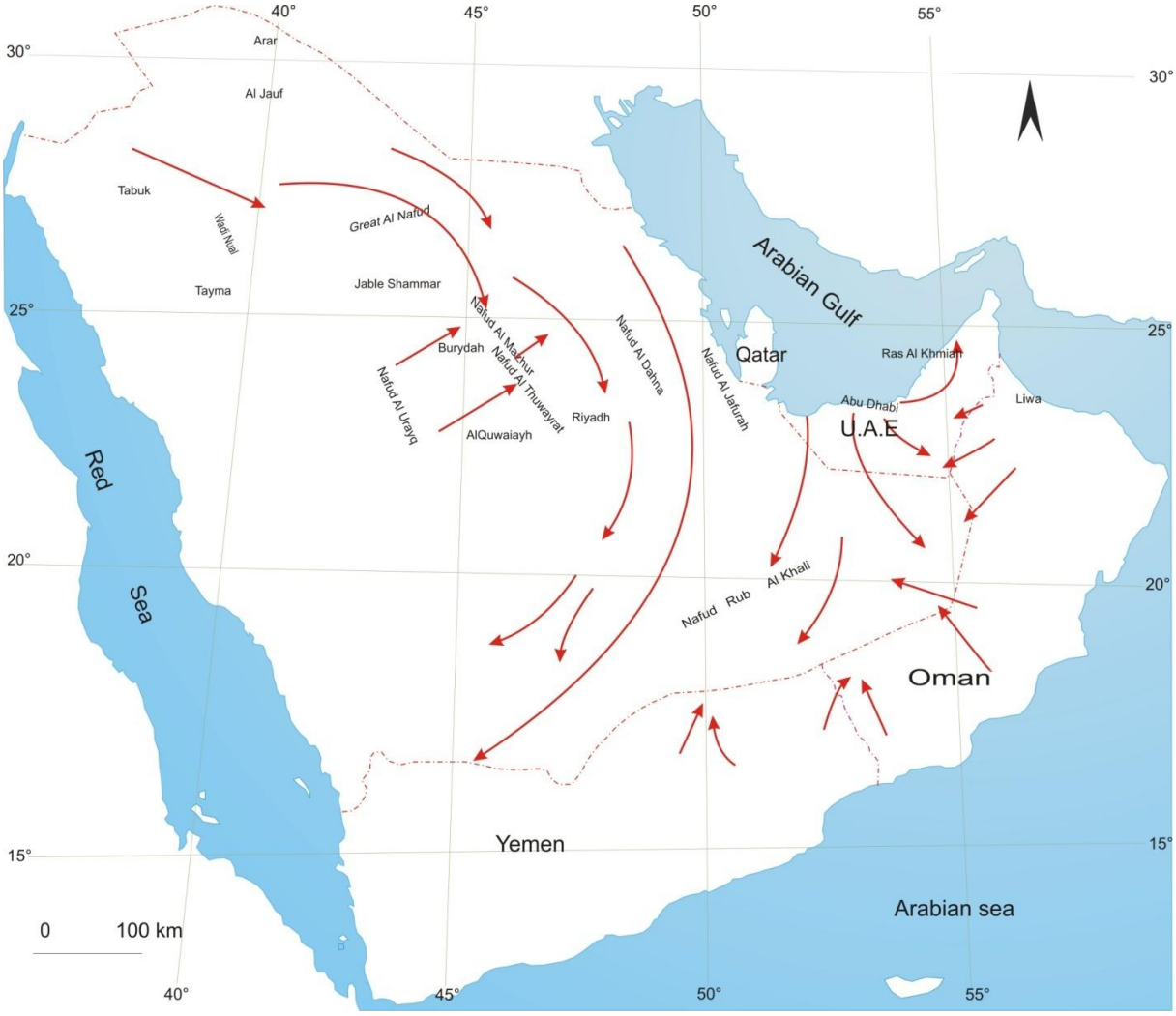

Figure 2.2: Direction of the aeolian sand movements over the Arabian Peninsula, and effect of the Shamal wind (after Holm, 1960, unpublished report) (map re-drawn from Edgell, 2006).

2.2.2 Indian Ocean Monsoon winds

A Quaternary researchers working in the Arabian Peninsula have found evidence that the precipitation is brought by the Indian Ocean Monsoon. The monsoon circulation influenced the past climate of the southeast and north Arabian Peninsula and northeast Africa, which is governed by seasonal migration of the Intertropical Convergence Zone (ITCZ) (Fig 2.3 A and B), and this led to monsoon winds during the interglacial periods being more effective than they are today(Fleitmann et al.,2007). At present they affect the southern coast of the Arabian Peninsula and Africa because the ITCZ position has moved further south, while, in the past, the position of the ITCZ is thought to have moved northward along the Arabian Peninsula and the monsoon rainfall belt lay over the Arabian Peninsula and over north Africa. In the Arabian Peninsula, it reached 23-24°N during the Holocene (Glennie and Singhvi, 2002; McClure, 1984) and in Jordan also (Abed et al., 2008). In contrast, during glacial periods, monsoon intensity was ineffective and weaker over the Arabian Peninsula because the cross-equatorial pressure gradient was weaker due to lower solar insolation and greater snow extent on the Himalayan plateau. The position of the ITCZ and therefore the monsoonal belt was located farther south and arid conditions prevailed on the Arabian Peninsula (Fleitmann et al., 2004, p.23). The monsoon system is associated with two wind systems; the Shamal trade winds and south westerly winds (Stokes and Bray., 2005). Also, due to the northwards movement of monsoon rainfall, Burns et al. (2001) studied speleothem growth at Hoti cave, Oman. Using ^{18}O stable isotopes and U/Th, they found that the growth of speleothem corresponded with wetter interglacial phases during 330-300 ka, 200-180 ka, 130-120 ka and 80-78 ka.

The general picture of the effect of monsoon intensity on Africa, shows that precipitation generally increases and indicators of wet conditions are widespread during interglacial times around 200 ka (Partrige, 1997) and MIS1 and MIS5 (Dupont et al., 2000) and MIS5d, as well as in the Holocene times around 8 ka (Willloghby, 2007). During the early Holocene, the ITCZ appears to have still reached the Tanganyika basin

(Tierney et al., 2010). Also, observations by Johnson et al. (2000), indicate that the lowered Lake Malawi was associated with the southward migration of the position of the ITCZ, which is dominant during the late Holocene over east Africa in response to the Northern Hemisphere cooling and led to high lake levels.

In central Saudi Arabia, Al Juaidi (2003) argued that during interglacial periods monsoon winds may have reached the Al Harmaliah, Uraidan and Nafud Al Sirr Lake, leading to the formation of the majority of the outwash plains and lakes (see Fig 2.4). Fleitmann et al. (2004) concluded that the monsoon precipitation belt was located close to 23-24°N over Saudi Arabia but did not move further, because the sedimentary evidence at Kahf Al Najmah in northern Saudi Arabia did not suggest any of the wet conditions that were found farther north. And during the middle to late Holocene, the summer ITCZ continuously migrated southward and the monsoon precipitation belt decreased gradually in response to decreased solar insolation.

Most authors suggest that the monsoon winds played a major role in the Arabian and African climate during the past, and the Mediterranean winds also played a role in the northern areas of the Arabian Peninsula (Lezine et al., 1998). The Burydah area is located close to 26°N in central Saudi Arabia: no study has examined the effect and extent of the monsoon rains over this part of Saudi Arabia, although evidence of past wetter periods is widespread in this area. The current study focuses on the evidence which was possibly formed and influenced by this monsoon belt in the past, by studying wadi and lake sediments and dating samples. Combined with a review of other research conducted on and around the Arabian Peninsula, this may show differences in the timing and phasing of environmental changes between southern and central/northern parts of the Arabian Peninsula. Evidence should show when, and to what extent, the monsoon system in the Burydah area during the late Quaternary.

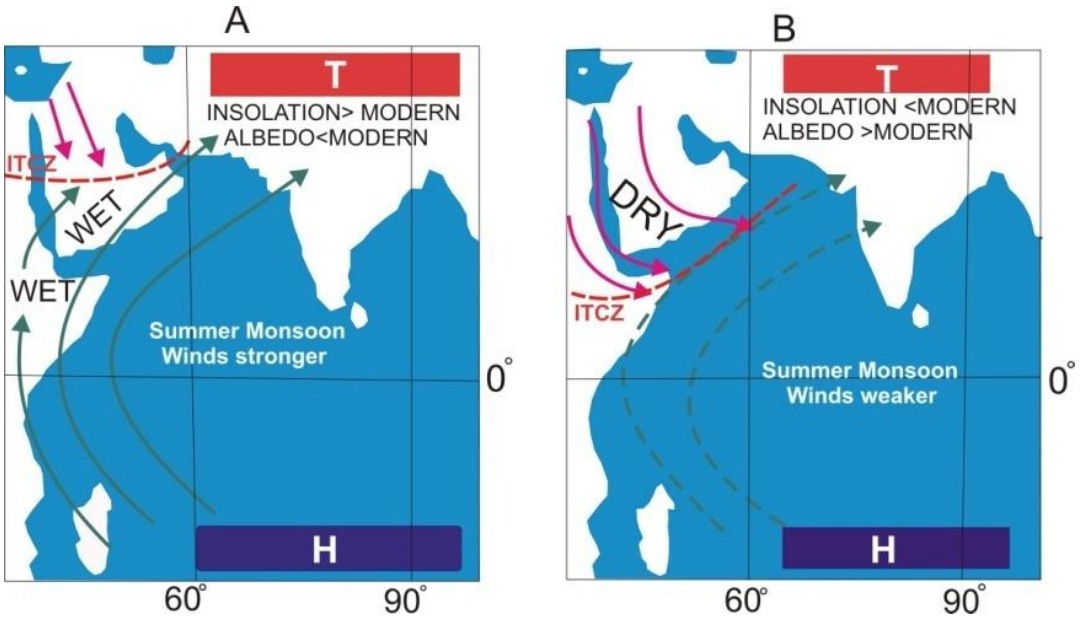

Figure 2.3: The expansion and contraction of Monsoon Circulation over Saudi Arabia 6 ka interglacial (A) and around 18 ka glacial (B) (re-drawn from Fleitmann et al., 2004).

2.3 Pleistocene environmental history of the Arabian Peninsula and surrounding areas

In the Arabian Peninsula, most of the work has been conducted Rub Al Khali, Great Al Nafuds, Emirates and Oman, for example by McClure (1976), Garrad et al (1980), Whitney et al (1983), Burns et al. (2001), Glennie and Singhvi (2002), Prabhu et al. (2004), Preusser et al. (2001, 2005), and Parker (2009). Recent work has been conducted in and around Al Quwaiayh in central Saudi Arabia by McLaren et al. (2009) and Al Juaidi et al. (2003), and some work was carried out in northern Saudi Arabia by Fleitmann et al. (2004) (Fig2.4). The Burydah area has not been previously explored in terms of historic climatic changes, nor has it been well dated using numerical dating techniques; as a result, there is a lack of Quaternary palaeoclimatic information for this part of Saudi Arabia.

The researchers listed above concluded that the Arabian Peninsula was generally wetter during interglacials and drier during glacial: for more discussion of these studies. Parker (2009) published a summary paper for the variable and shifting

landscapes in Arabia. He used 247 absolute ages (U/Th and OSL) compiled from published works dealing with deposits from the Arabian Peninsula, plus samples that he had collected, and he presented evidence which showed that wetter phases had occurred at isotope stages 9 and 7. He concluded in this study that the wetter conditions originated in southern Arabia before reaching central Arabia, due to the influence of the Indian Ocean monsoon (IOM), which took around 1,800 years to move to northern Arabia (25°N) (Parker, 2009), but the problem here is that central Arabia has not been extensively studied in order to accept Parker's argument. This study and OSL dating aim to determine whether or not Parker is correct.

Frumkin et al. (2008) in Jordan, inferred from calcite speleothem, using U-Th dating, that the Mediterranean cyclones influenced the Black Desert during MIS7 ca.250 to 240ka, and from ~230 to ~220 ka. Also, Petit-Maire et al. (2002) reported evidence of the extension of the Mudawwara Lake located between Jordan and the Saudi Arabian border: isotope analysis and U/Th dating of shell deposits show that this lake was active during MIS6 (ca.170 ka, 152 ka, 135 ka) and MIS5e (ca125 ka, 124 ka, 121 ka, 116 ka) under the influence of both Mediterranean and Monsoon rainfall. In general this argument is acceptable and our study will try to highlight this point as much as possible to provide a deeper understanding of the effect of these systems of rainfall on the Burydah area during the late Quaternary. By dating samples from the Burydah area, it should be possible to show if this area was influenced by these systems, as Petit-Maire et al. (2002) and Frumkin et al. (2008) argued.

Glennie and Singhvi (2002) identified that major phases of dune accumulation in the SE Arabian desert occurred during MIS5d (ca110 ka and 115 ka) and MIS4 (ca. 60-50 ka), and they concluded that this reflected the significance of arid glacial conditions leading to exposure of the floor of the Arabian Gulf and the increase of Shamal wind activity transporting sediment from the Gulf to the Emirates and Rub Al Khali. Glennie and Singhvi's study is discussed by Stokes and Bray (2005), who show that many of the ages obtained have large associated errors, which means that it is not possible to identify distinct periods of dune accumulation. In the Wahiba Sands area, Preusser et

al. (2002) used OSL dating to provide a chronostratigraphic framework of aeolian dune formation in the Jafr in Oman, based on 74 samples from three sand cores indicating phases of dune activity occurring around MIS5d (ca120-100 ka), and additional periods of dunes accumulation at MIS4 between (78-65 ka), which seem to be associated with the drop in global sea levels during the glacial cycle, low intensity Monsoons and the increase of north-westerly winds. There is a strong consensus in these studies that the interplay between the Shamal winds and Monsoon winds is a key influence on the Arabian environment, therefore it will be beneficial to examine this interaction in the Burydah area of central Saudi Arabia.

Figure: 2.4 Map showing distribution of Quaternary numerical ages conducted in the Arabian Peninsula. Also the expansion and contraction of Monsoon Circulation over Saudi Arabia, (After McClure, 1984, Petiti –Maire 1994.2002,Glennie and Singhvi and Fleitmann et al., 2004).

From MIS5e to MISb, several wet and dry periods occurred in Southern Africa (evidence from Africa supports this) and the Arabian Peninsula. Telfer and Thomas (2007) argued that the sand accumulation in the Witpan area of South Africa continued accumulating during MIS5c (ca.104ka) and MIS5a to MIS4 (ca.77-76ka). Also, similar dates were found by Bateman et al. (2003) observed the base of linear dunes in the SW Kalahari related to MIS5d (ca113 and 108ka). In the southern Arabian Peninsula, Stokes and Bray (2005), who were working on the sand dunes of Liwa and Al Qafa in the United Arab Emirates in south Rub Al Khali, concluded that the depositional pattern within dunes suggested that dunes were active during MIS5 (ca.75 to 130 ka) and there is limited evidence of aeolian activity during MIS 2-4, which shows a contrast with research undertaken in the Wahiba sands area. In this study, Stokes and Bray argued that the linear dune accumulation at Liwa, UAE, occurred during humid interglacial phases, which were controlled by paleomonsoon and sea level changes as well as variations in the groundwater level; this means that the aeolian deposition is not good evidence of sand accumulations during the dry phases. Juyal et al. (1998) used Infrared Stimulated Luminescence (IRSL) dating and found evidence in Oman that indicates that alluvial fans formed around MS5c (ca.104 ka), and that Wadi Batha was active around MIS5d (ca.117 ka and 110 ka). They concluded that conglomerate sediments were deposited as a response to the SW monsoon which blew strongly over the Rub al Khali during this time.

It appears from the discussion above that the sand dune activity tended towards accumulation in both wet and dry phases and was controlled by different factors, e.g. Monsoon winds and sea level changes and Shamal winds, as well as the water table and sediment supply from sources.

Further evidence provided by Burns et al. (1998, 2001) examined MSI5a in Hoti cave, Oman, and found evidence of speleothem growth corresponding to increases in rainfall during MIS 5a (80-78 ka), due to the northward movement of Monsoon rainfall. Also, Petit-Maire et al. (2002) studied the Mudawwara Lake near the Saudi Arabian border with Jordan, and found that this lake was active during MIS5c (ca.95.4

ka), MIS5b (ca.91.1 ka, 88 ka) and MIS5a (ca.77 ka), under the influence of both Mediterranean and Indian monsoon rainfall. Also Frumkin et al., 2008 in Jordan, argued that the Mediterranean cyclones influenced speleothem growth in the Black Desert between MIS5b and MIS5a (ca.80 and 70ka). Combining these discussions above, there is strong consensus that during the interglacial period during MIS5, wet conditions were more common and lake and cave deposits appear to have developed, the formation of which required considerably higher rainfall, which might have occurred due to the influences of the Indian monsoon rainfall's movement from the south to the north Arabian Peninsula, and the Mediterranean cyclones; both are important in terms of climate change in the Arabian Peninsula (Stoke and Bray, 2005). Issues which require further exploration in the Burydah area are the monsoon rainfall movement northwards over central Saudi Arabia during MIS5, and the effect of the Mediterranean rainfall's extension to the over upper catchments of wadis in central Saudi Arabia during MIS5.

As we move into the MIS3 and MIS2, McLaren et al. (2009) dated a series of outwash plains developing in the centre of Saudi Arabia during the late Quaternary. Their findings showed flood events occurring at 54ka, 53ka and 38ka, associated with phases of increased rainfall and/or decreased evaporation prevailing in central Saudi Arabia. This evidence is consistent with the argument of Preusser (2002), that no dune accumulation has been recorded in the Wahiba sands for the period ca. 64 and 23 ka. Indian Ocean Monsoon activity was reported by Fleitmann et al. (2007), and they suggested that this period was a hyper arid phase until 50ka. Moreover, further evidence for increased sand deposition comes from Liwa sands, where the periods of dune building were ca 45; 51; 54 and 60 under the effect of Shamal winds. Also, researchers in South Africa noted that sand accumulation in the Kalahari was most pronounced in the Witpan sand ca. 57-52ka (Telfer and Thomas, 2007).

McClure (1976) used radiocarbon dating of lake sediments in the interdunes of Rub Al Khali. He suggested that the lake was active during the period 31ka (cal BP: 34,832-38,388) and 21ka (cal BP: 24,058- 26,293) due to an episode associated with enhanced

moisture in the eastern Sahara desert. These dates tie in with ages obtained by Garrard et al. (1981), who argued that lacustrine diatomite under Nafud Jubbah in northern Saudi Arabia, 300 km north of Burydah in central Saudi Arabia, reflected a moist period around 25.6 ka (cal BP: 29,573-31,067) indicating perennial water with less evaporation. In addition, Hotzl et al. (1975) used ^{14}C dating to study Wadi Al Dawasir, 558 km south-west of Riyadh in central Saudi Arabia, and they found calcium carbonate crusts below the surface at Wadi Ranyah, which they dated to 29.8 (cal BP: 29,519- 40,196) and 26.4 ka (cal BP: 26,782-34,981). Similar results were found in the north of Saudi Arabia from radiocarbon dates of lake deposits in Lake Damascus related to ca. 23.6 (cal BP: 26,914-29,537); also, marl within Lake Al Jafr in eastern It appears, from the discussion above, that the dates from Rub Al Khali and Nafud Jubbah, as well as lake Nafud As Sirr, wadi deposits at Wadi Al Dawasir, and the lakes in northern Saudi Arabia, provide good evidence of wetter phases to compared with lakes and wadi deposits in the Burydah area which have not previously been examined and dated, and the ages obtained should provide a deeper understanding of the humid episodes over the late Quaternary in central Saudi Arabia.

From the last 20-14 ka, aridity was more widespread, the evidence of dry conditions in the last glacial has been found in different parts of the Arabian Peninsula (e.g. McClure, 1976; Whitney et al., 1983; Preusser et al., 2002; Juyal et al., 1998 and Glennie et al., 1998) and Africa (Stokes et al., 1998, Telfer and Thomas, 2007). There is strong agreement that during the last glacial maximum (LGM) dry conditions were more common, and dune accumulation appears to have occurred at this time, due to the influence weakened Monsoon system and the southward movement of atmospheric westerly flow, cyclonic activity and subtropical high-pressure cells over the Mediterranean (Pugh, 1997), and the extent of the ice sheets over most northern parts of the world.

In MIS1 in the early Holocene, rainfall shows greatest levels over most parts of Africa and the southern Arabian Peninsula. Early studies of early Holocene in East Africa provide evidence that the moisture and rainfall extent over land, including completely

vegetated land, and freshwater lakes were common during this period (Adams and Faure, 1997; Johnson et al., 2000; Alin and Cohen, 2003). In Nigeria during Holocene, there was a brief moist period ca. 7- 9.9 Ka which corresponds with linear dune activity (Stokes et al., 1997). Water levels rose of Umm Akhtar lake south Egypt was around 9.9 to 9.5cal yr BP and from 7.8 to 6.7 cal yr BP and the enhanced aeolian activity from 6.7 to 6.2 cal yr BP (Nicoll, 1998). The linear dunes in the interior of the central southern Kalahari Sahara, active during 11-13 Ka (Thomas et al., 1998). This evidence of dunes building in the early Holocene shows a strong correlation with Telfer and Thomas (2007), and Bateman et al. (2003) who worked in Kalahari, where the sand dune accumulation continued during Holocene. Stokes et al. (1997), on the other hand, state that dune construction during the Holocene period appears to have been less intensive.

In the southern Arabian Peninsula, the earliest aeolian activity related to 10 ka and 10.5 ka (Juyal et al., 1998). The Awafi linear sand dunes in Ras Al Khaimah (UAE), formed between 9.1 ka and 10.7 ka, and may have accumulated as a response to the low sea level of the Arabian Gulf during the late Pleistocene and the Holocene (Goudie et al., 2000). Also the sand accumulation in Ras Ruways and Qahid in the Sultanate of Oman took place in the Holocene, in approximately 9 to 8 ka, and from ca. 7.8 to 5.4ka (Preusser et al. (2005). Also, Stokes and Bray (2005) argued that the sand dune accumulation at Liwa in the United Arab Emirates occurred during MIS1ca. 6ka and peaked at ca. 2ka, which means that the preserved aeolian deposition is not good evidence of sand accumulation during the dry phases. The dune accumulation in southern Arabia corresponds with the northward movement of the of Monsoon winds, and this is supported by Neff et al. (2001) who used U-Th ages and oxygen isotope studies on speleothems in the northern Hoti cave in Oman, and their ages have suggested a wetter phase related to the early to mid Holocene, around 9.6-6.1 ka. Result of enhanced monsoon precipitation that migrated steadily northwards to the southern shoreline of Oman. According to Fleitmann et al. (2004), Indian monsoon circulation was stronger during the early Holocene, and the mean summer position of

ITCZ was located much farther north than its present position over the Arabian Peninsula.

In central Saudi Arabia, there is some evidence of increased moisture; for example, intensive runoff in the Wadi Ad Dawasir, and increased deposition of the fluvial terraces in the Wadi Al Luhy (Hotzl et al., 1978). Lacustrine deposits comprising limestone, marls and diatomites within Nafud Jubbah dated to 8.5-5 ka BP and 6.5-5.2 ka, reflecting humid climates apparently under the influence of the southward movement of Mediterranean rainfall or an interaction of this with monsoonal air masses (Schulz and Whitney, 1986), which played a role in the climatic evolution of the northern Arabian Peninsula (Whitney et al., 1983). To the north of the Burydah area, the lakes at Nafud Jubbah have been studied by Garrard et al. (1981) and they have argued that the lacustrine deposits under Nafud Jubbah in northern Saudi Arabia relate to a moist period around 6.6 ka (cal BP: 7,465-7,624), during which organic silty sand was deposited, forming a swamp.

In the mid-Holocene, arid conditions prevailed in the Arabian Peninsula (Lezine et al., 1998; McCorriston et al., 2002; Staubwasser and Weiss, 2006) and Africa (Stokes et al., 1998): this related to a weakening of the monsoon precipitation that gradually decreased and migrated southward (Fleitmann et al., 2003; Parker et al., 2004). The evidence of dry phases during the mid Holocene is linked to the weakening of the monsoon. For example, Fleitmann et al. (2007) used isotopes from the cave records on Socotra to demonstrate that variations in monsoon precipitation resulted from the changes in the Indian Summer Monsoon (ISM) circulation during the mid to late Holocene at 5 to 4 ka; the summer ITCZ migrated southward and the precipitation decreased gradually in response to decreasing solar insolation. Lakes at Awafi Ras Al Khaimah (UAE) were related to the mid Holocene around 5.9 – 4 ka: the lake was filled with sand around 4.1 ka (Parker et al., 2004, 2006). Goodall (1995) also studied the sand dunes around Sabkhat Matti in southern Saudi Arabia. Their OSL dating has shown that sand deposits were laid down around 5.9 ka. Also, Hannb (1995), using uranium–thorium and carbon dating in Oman, shows the ages of sand dunes to be around 3.6 ka.

This is consistent with the results of Stokes et al. (1998), who found that the sand-sheet in the Selima sand sea of the Eastern Sahara in Africa had accumulated during a brief moist period in Holocene between ca. 3-4 Ka.

In summary, the studies above illustrate that the Holocene changes in the Arabian Peninsula and Africa are well known, and there is strong agreement that a wet event occurred at the start of the Holocene. Most previous studies related to Quaternary environmental and climate change around the Arabian Peninsula were completed in Africa, with some work in the UAE and Oman, as well as Yemen, Jordan, and a few studies in northern and southern Saudi Arabia; however, no work has been previously conducted in the Burydah area with respect to the Quaternary period. Most of the work done has focused on the influence of the monsoon on the southern Arabian Peninsula and its important effect on global hydrological conditions, while some studies have focussed on the influence of the southward movement of Mediterranean rainfall, especially on the northern border of the Arabian Peninsula (e.g. Jordan lakes); however, no study has focussed on monsoon development and migration over the central Arabian Peninsula.

2.4 Remote sensing of desert deposits in the Arabian Peninsula

This section reviews the use of remote sensing to understand the spatial distribution of the geomorphology of the environment. This research will examine how different researchers have used remote sensing in the Arabian Peninsula in order to monitor and map land forms, as well as to make a distinction between sand forms and various colours using different methods and tools. For example, White et al. (2001) used multispectral remote sensing with reflectance spectra, linear mixture models and geochemistry analysis to classify northern Rub Al Khali. Anton (1983) used the colorimeter to study dune redness in Saudi Arabia and found that the reddest sand appears in eastern Rub Al Khali and Nafud Al Dahnah, with the whitest appearing at Nafud Al Jafurah, where there is a presence of calcite and dolomite with the sand. Bullard and White (2002) estimated reflectance ratings for 15 samples of sand dunes in

Australia. They compared the results of MMR reflectance, which they calibrated to the redness rating derived from the Munsell soil colour chart. Their results showed that simple field spectral measurements provide reliable estimates of iron oxide concentrations and redness, as well as providing redness ratings that are much better than the estimates based on the Munsell soil colour chart used alone.

It appears, from the discussion above, that there is strong consensus that Landsat TM imagery has proved an effective source of information for mapping geomorphological features, and that remote sensing techniques also prove very useful for extracting information for different types of geomorphological phenomena. The spatial distributions of geomorphological phenomena (e.g. sand dunes and wadis) in central Saudi Arabia, especially the area around Burydah, have not been explored or mapped before, and the remote sensing techniques applied in this research will provide valuable information in terms of the spatial distributions of the sand dunes and the regional colour patterns.

2.5 Conclusion

The discussion of the literature review revealed that most of the studies were conducted in Africa, the United Arab Emirates (UAE), the Sultanate of Oman, Yemen and Jordan, with a few in Saudi Arabia; the important part of the available published data was produced 5-10 years ago. This study aims to highlight some of the Quaternary landforms of fluvial terraces along the wadis as indicators of wetter phases, and the dune deposits as indicators of both drier as well as wetter phases, and to determine the gaps in our knowledge. In doing so, it summarizes these studies and presents the future empirical work of the study.

The present study aims to identify the Quaternary deposits and landforms preserved in and around Burydah which have not been studied before, and to interpret the historical accumulation of deposits in the Quaternary succession in central Saudi Arabia as they relate to palaeoclimatic conditions throughout the Arabian Peninsula. The Burydah area has been selected because there is a significant gap in knowledge relating to late

Quaternary history and Quaternary palaeoenvironmental research. The fluvial, aeolian and tufa deposits of the Quaternary landforms are well preserved in the Burydah area, and dating these deposits will provide a better understanding of its origins and evolution during Quaternary times. It is expected that this evidence will confirm the findings of the previous studies in these phenomena (e.g. the effects of monsoon and Shamal winds).

CHAPTER THREE

3 Research methodology and techniques

This chapter aims to describe in detail the research methodology, and to decide the appropriate way to analyse the Quaternary sediments obtained from the study area. The chapter starts with a description of the stages involved in creating the geomorphological map, followed by an explanation of the field techniques. Further, it explains the laboratory analyses and reviews different techniques used in the study.

3.1 Creating geomorphological maps

The following steps are required in order to create a map of the geomorphological features of the Burydah area:

1) Remote sensing methods: supervised image classification, the area of interest (AOI) method, redness rating and spectral redness are the methods applied on the Landsat Enhanced Thematic Mapper (ETM); these methods help to show the differences between sand and other surfaces. According to Abdel Fattah (2006), remote sensing techniques can provide indirect indicators of materials such as rock types.
2) Geometric corrections: the images were geometrically corrected to UTM-WGS 84 zone 38; this was achieved by checking the image using 10 control points in the field (see geometric correction in this chapter).
3) Geological data: the geological map was scanned, transferred to a shapefile and rectified by a GIS technician at the Department of Geography, Qassim University; this transfer helped link the map with satellite images.
4) Arc GIS software was successfully used to create and design a map of the geomorphological features of the Burydah area, with features placed into polygon, line or point files and saved in table attributes.

The actual purpose of creating a geomorphological map is to show the various Quaternary surfaces, including the spatial distribution of alluvial and fluvial terraces

along the Wadi Al Rimah and its tributaries, as well as the materials in the Wadi Al Rimah channel under the Nafud Al Thuwayrat in the east of the study area, and the flood plain in the upper channel within Nafud Burydah. The map also shows the spatial variation of dune colours and formations along the Nafud Al Thuwayrat and Al Mazhur, as well as distinguishing between different types of dune forms, for example linear dunes at Nafud Burydah and domes at Nafud Al Tarafiyah and Nafud Al Mazhur.

3.2 Fieldwork techniques

Field investigation of the study area was undertaken during two field seasons, the first of which took place between 15th July and 15th August 2007. This work involved obtaining satellite images, collecting geological and topographical maps, and general reconnaissance of the study area. Further fieldwork was conducted between mid-February and mid-May 2008. During the period between 16th May and 30th May, the researcher and supervisor, as well as a field assistant, were working and collecting samples. Fieldwork included the following steps:

3.2.1 Ground verification

Prior to visiting the sampling sites, the first stage involved preparing maps and a hard copy of the Landsat image covering the area. The second stage entailed using the GPS to determine the location of the geomorphic features. Additionally, ten ground control points (GCPs) were chosen as reference points, including crossroads, roundabouts, small isolated hills and circular irrigated farms. Study sites were surveyed during an intensive 30-day period during mid-February and mid-May 2008. Ground verification was conducted by visiting each study site and comparing these with maps and images.

3.2.2 Identification of study sites

The next stage was to identify suitable landforms and sections for research purposes. Different sections were chosen along the study area, with some sites located within sand dunes, others within interdunes and some located within wadi channels (see Fig 1.6). A mechanical digger was used to clear some sites, while other sections were exposed by wadi incision or natural erosion. At each site the process consisted of cleaning the section, recording the code and numbers of each unit, recording latitude/longitude, drawing the section on graph paper and photographing it. Detailed measurements were taken and stratigraphic logging of the preserved deposits carried out, including the thickness of the deposit, bedding, structures and the nature of the boundaries, as well as the presence/absence of fossils. Samples of the sediments were taken for different analyses (e.g. OSL, ^{14}C dating, XRD, thin section analysis and particle size analysis).

Some of the study sites were chosen to represent aeolian processes, so an overview could be obtained of the patterns of environmental processes resulting from climatic fluctuations during the late Quaternary. There were three representative sections in the northwest of the study area: small linear dunes, section QA.08.15 within Nafud Al Qwarh, linear dunes, section QA.08.16 within Nafud Uyun Al Jiwa and large linear dunes, section QA.08.05 within Nafud Burydah. Two sections were in the east of the study area at interdune areas in the Nafud Al Thuwayrat, one located at the foot of the dome dune named Nafud Dasmah QA.08.07, and the other being section QA.08.08. Two sections were located in the south of the study area: Nabkh sand within Wadi Ragwah QA.08.06 and the sand sheets sections QA.08.18, QA.08.19 and QA.08.20, preserved under Al Mastwe plateau in the east of the study area (Fig 1.5).

Some of the sections were chosen to study fluvial terraces along the Wadi Al Ramah and its tributaries; these land forms resulted from the wetter phases during the late Quaternary. Two sections were located in the northern study area; the first represented the palaeochannel in the distal region of the Nafud Al Tarafiyah, section QA.08.02, which was named wadi Wadi Al Butaun, and the second section was also a palaeochannel: a

tributary to Wadi Al Rimah, named Wadi Al Watah QA.08.17. The third section was in the west of the study area in the upper wadi, Wadi Al Rimah QA.08.21; this section represented a floodplain around the wadi. Finally two sections were in the east of the study area, located in the main channel of Wadi Al Rimah. Section QA.08.10 was within the interdunes of Nafud Al Thuwayrat, showing alternation between fluvial and aeolian deposits, and section QA.08.14 was located in the interdunes of Nafud Al Rubayiyah, showing good evidence of wadi activity (Fig 1.5).

The sections representing geochemical deposits, including evaporite and lake deposits, were located in the east of the study area. Section QA.08.11 had evaporite deposits located in the interdune areas within Nafud Al Mazhur and lake deposits in section QA.08.12, in the east within the interdunes of Nafud Al Thuwayrat. Two sections were located in the interdunes of Nafud Burydah: the tufa deposits sections QA.08.03 and QA.08.04; these tufas represented an evolution of the tufa lake in this part of study area during the late Quaternary.

3.2.3 Sampling for dating

Sections with suitable deposits for Optically Stimulated Luminescence (OSL) dating had to be determined, as well as suitable units and sections where organic matter was found in the tufa and in some wadi units to be collected for ^{14}C dating. For OSL sampling the process involved hammering plastic tubes (35cm long, 5mm in diameter) into a vertical section. When the tubes were full of sediment, they were kept out of the light, sealed up and marked at both ends prior to being placed in black bags. A part of each sample was collected in a plastic bag (13×21cm), sealed in the field to prevent water loss, then stored in plastic containers with a cover. The intention was to measure background dose rates in the field, but this was not possible as a calibrated gamma spectrometer was unavailable. Instead, background dose rates were based on sub-samples of the material collected for dating. For radiocarbon dating ^{14}C profile, sampling the process involved a clean metal knife was wrapped in thick aluminium foil before being placed in thick black plastic. All samples were then stored before being

transported to the UK (see Chapter 4 for sample locations and unit numbers collected for OSL and ^{14}C).

3.3 Laboratory analyses

Samples were prepared and analysed at the University of Leicester laboratories, the Sheffield Centre for International Drylands Research and the laboratories of the British Geological Survey.

3.3.1 Optically stimulated luminescence (OSL) dating

All samples were prepared following the guidelines of Boulter and Bateman (2009) and Duller (2008). 12 samples were prepared and analysed during 2009 by a researcher under Mark Bateman's supervision, and the 13 samples were dealt with primarily by Bateman during 2010. The tubes were opened in the laboratory under subdued red-orange light, and the material in the central part of the tube, which had not been exposed to light during sampling, was used to measure the equivalent dose (D_e). Samples were washed with hydrochloric acid (1M HCl) over a three-week period to remove any carbonates and then treated with hydrogen peroxide (30% H_20_2) over a two-week period to remove any organic matter. Each sample was then dry-sieved for thirty minutes to obtain the 125-250µm size fractions. Heavy mineral fractions with a higher specific gravity than quartz were separated with the use of sodium polytungstate at a specific gravity of 2.70. Following this, each sample was etched in 40% hydrofluoric acid (HF) for a period of 60 minutes to remove any minerals lighter than quartz, such as feldspars, as well as to remove the outer layer from the remaining quartz grains. The samples were then washed in HCl (1M) for a further 40 minutes to remove any acid-soluble fluorides and after a final drying, were re-sieved between 125 and 250µm to remove any residual non-quartz grains.

The water content for each sample was determined using the moisture value of the sub-samples in the tube or from the samples that were collected in plastic bags in the field. Water content is determined because the water between grains in the

environment absorbs some of the radiation, which affects the dose rate and hence the age (Duller, 2008).

The annual radiation dose for samples is derived from naturally occurring concentrations of uranium (U), thorium (Th) and potassium (K). It was intended to measure gamma dose rates in the field which is increasies date quality especially in cases where the samples are very close to stratigraphic breaks, but it was not possible to measure this as gamma spectrometry was unavailable. This will therefore be based on subsamples of the material collected for dating by inductively coupled plasma mass spectrometry (ICP-MS), using a conversion from an elemental concentration to the effective dose rates, and calculated using a formula from Aitken (1985). For these analyses, 5g were milled to get representative samples. The dose received from cosmic rays was calculated using the formulae of Prescott and Hutton (1994) and Grun (1994, 2009).

3.3.2 OSL Measurements

For measurement, samples were mounted as a monolayer onto 9.8mm stainless steel discs using silicon oil. Sample measurements were carried out using a RisøTL-DA-15 SG (Scooby) (Fig 3.1), the resultant luminescence was measured through a Hoya U-340 filter, which transmits emissions from c280nm to 380nm, and a strontium 90 beta source was used for irradiation.

The Single Aliquot Regeneration protocol (SAR) (see Murray and Wintle, 2000, 2003 for details) was used to determine D_e. Before D_e can be examined, dose recovery, a preheat test, infrared stimulation (IRSL) and a range finder must be completed (see Appendix 5.1). An infrared IRSL check for feldspar contamination was made (for details see Aitken, 1998). The infrared stimulation showed no feldspar contamination, certifying that all samples were suitable for measurement. Finally, the range finder was used to measure the correct regeneration points for the growth curve, and to determine the approximate preheat of either 200°C or 180°C for 10s, prior to each OSL measurement

being adopted (See table, Appendix 5.1). All samples were analysed using a conventional five-point dose to determine D_e (see Appendix 5, Table 5.2).

SAR data were analysed using Analyst software developed by G.A.T. Duller. The quality of the data from each aliquot was checked to ascertain whether growth curves fitted through all regeneration points. Most samples showed a good decay curve and growth curve as well as an acceptable histogram resulting from accepting aliquot points and the recycling values, which were between 0.90 and 1.10 (see Appendix 5.4). In respect to the reliability of the OSL data, fluvial samples (e.g. Shfd09138; 09137 and Shfd09142) are potentially problematic due to reworking with partial bleaching prior to deposition as a result of water turbidity and sediment movement. Some grains may contain an antecedent OSL signal, which will result in an overestimation of the burial age. A series of studies dating fluvial sediments focused on the problems associated with partial bleaching (e.g. Olley et al., 1994; Rodnight et al., 2006 and Thomsen et al., 2007).

The SA-SG spreadsheet (Unweighted; Weighted; Probability; Central Age Model and Common Age Model) was used to establish burial De. Some samples showed a normal distribution with low scatter, in which case the mean was used, and some showed large scatter, in which case the finite mixture model was used to establish burial De. In the case of samples where D_e was greater than 200 Gy (e.g. Shfd10112), these may give a minimum age due to the luminescence signal being close to quartz saturation by radiation. In these cases of saturation, the minimum age can be determined (see tables in Chapter 4 and Appendix 5.2 for more clarity and to aid understanding of this calculation).

Figure 3.1: Luminescence measurements were made on TL-DA-15 fitted with a single grain attachment (Scooby).

3.3.3 Radiocarbon Dating (^{14}C)

The availability of organic matter and inorganic carbonate in some sections and units in the study area, such as tufa, lakes and wadis, made them suitable for radiocarbon analysis. Samples were refrigerated during storage, then transported via a depot in London to Florida for analysis with Beta Analytic. Accelerator mass spectrometry (AMS) dating and Radiometric-Standard delivery were undertaken on selected organic materials.

The tufa carbonate and organic materials obtained that were suitable for calibration were calibrated using the INTCAL04 (Reimer et al., 2004). The samples had more than one calibration age; in these cases the calibration age used the circa oldest-end limit age to youngest-end limit age (see tables in Chapter 4). The samples which were out of the upper limit of INTCAL04 were calibrated using INTCAL04 (Reimer et al., 2009), which goes back much further.

3.3.4 Particle size analysis

A representative number of sub-samples were measured within the units of sand dunes and fluvial deposits in the study area. The light-diffraction technique is one of the most

widely used methods for measuring particles in the size range of 0.1 to 2000µm. The Coulter LS TM running under Windows™ software consists of three instruments, LAS100Q, LS200 and LS230, whose job it is to measure particle size distribution. When employing this method, the first step is to remove carbonates, if they are found (samples are boiled in 10ml HCl until the reaction is complete, then washed in distilled water and finally dried), remove the roots, and dry the sample in an oven at 110°C for 1-2 hours or overnight. Next, 1-2g are placed into a beaker and mixed with Calogen Dispersant. The samples are then placed in the sample cup and then in a Coulter LS TM cylinder. The Beckman Coulter LS software depicts the samples and grain size results statistically. Grain size analysis calculates mean grain size, and can generally be understood as reflecting the average energy of the depositional environment where standard deviation is used as a measure of sorting by comparing the samples to Friedman and Sanders classes (Maurice, 1988).

3.3.5 X- ray diffraction analysis (XRD)

The XRD was used to examine sediments and compounds in the rocks and sediments to identify their mineral components. There is a whole range of applications for the various components of sediments (Maurice, 1988).

3.3.6 Preparation for whole-rock analysis

Approximately 15g of each sample were removed and crushed in a grinder to achieve a fine, uniform particle size. For XRD analysis, approximately 3g of the material was micronised under acetone for 10 minutes and then sprayed on the dry chamber at approx 150°C, following the method described by Hillier (1999). The aim of use this method is to produce a sample which can be handled in a way that does not affect the results of the X-ray powder diffraction analysis (Hillier, 1999).

3.3.7 Preparation for clay mineral analysis

A reciprocal shaker and ultrasound treatment was used on the material (about 15g sub-samples) after they had been first crushed and mixed with distilled water. The suspension was then sieved at 63µm and the fine material of <63µm was placed in a measuring cylinder and added to about 1ml of 0.1M 'Calgon' sodium hexametaphosphate to prevent flocculation of the clay. After that, the fine material of fraction <2µm was removed and dried at 55°C. Approximately 100mg of this material was placed in distilled water and then pippetted onto a ceramic tile in a vacuum pump. The mounts were Ca-saturated using 0.1M CaCl2.6H2O solution and washed twice to remove excess reagent (Kemp and Wagner, 2009) (Fig 3.2).

3.3.8 Whole-rock and clay mineral analysis

Whole-rock XRD was analysed under the PANalytical X'Pert Pro series diffractometer, equipped with a cobalt-target tube and X'Celerator detector and operated at 45kV and 40mA. The samples were scanned from 4.5-85°2 theta at 2.76°2 theta/minute. The diffraction data were initially analysed using PANalytical X'Pert Highscore Plus (version 2.2a) software, together with the latest version of the International Centre for Diffraction Data (ICDD) database. Less than 2µm oriented mounts were scanned from 2-40°2 theta at a rate of 1.02°2theta/minute after air-drying, then subjected to an ethylene glycol solvent and heated at 550°C for 2 hours. Clay mineral species were then identified according to their characteristic peak positions and their reaction to the diagnostic testing program (Kemp and Wagner, 2006).

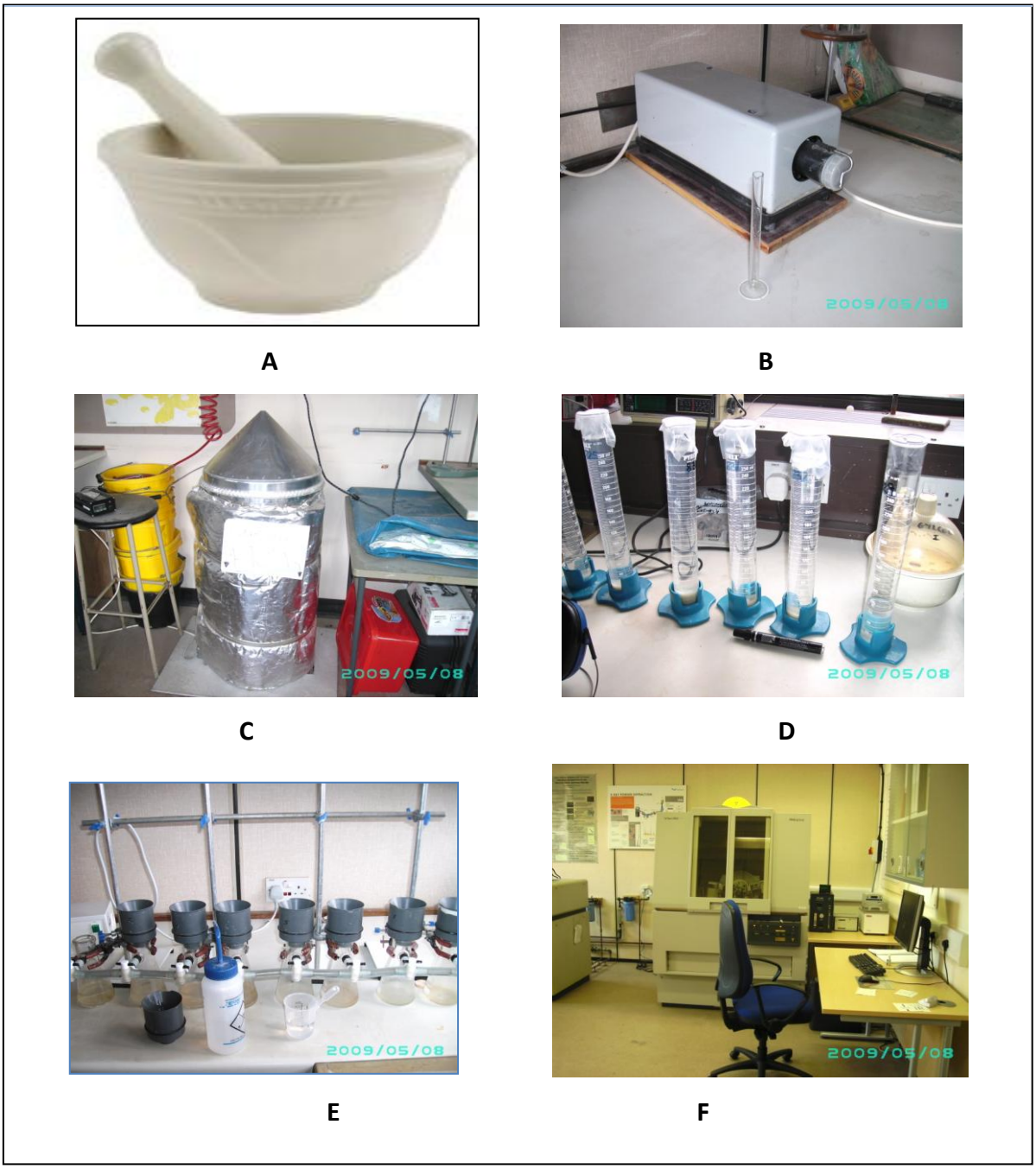

Figure 3.2: The stages for whole-rock and clay analyses at British Geological Survey (A) crushed, mortar samples; (B) micronising the samples in acetone for 10 minutes; (C) spray–drying the samples at 150°C in a drying chamber; (D) standing the clay samples in a cylinder; (E) producing an oriented mount for analysis by pipetting onto a ceramic tile and (F) finally scanning the samples under a PANalytical X'Pert Pro series diffractometer.

3.3.9 Thin sectioning

The preparation of thin sections of loose materials such as sand and clay is done in order to determine the mineralogy of the samples. These were prepared using the standard techniques outlined by John Miller (1988) (Fig 3.3). Samples were impregnated with resin and Araldite XD716 hardener (weight use: 100g of Araldite DBF resin to 33g of XD716 hardener). The samples were then placed in a sample cup and then onto a flat surface in the oven at approx 80°C for a minimum of 2 hours. After drying, the samples were ground until they had a smooth flat surface to ensure the best possible contact with the slide. The samples were ground on a Metaserv 2000 grinder to remove any rough surfaces. Slides for the samples were from a glass sheet frosted with a paste of black silicon carbide 600 grit and water to ensure that a flat, even surface was achieved. The samples and slides were marked and put on the hotplate to warm, then pasted with Araldite 2020; following this, the samples were placed on a hotplate and exposed to a pressure of about 1kG cm^{-2} overnight. The samples were then ready to be cut; several sizes of thin sections were made, with the sizes dependent on the available equipment and the area required for examination - the normal size is 25 × 76mm (Maurice, 1988). Samples were then ready for cutting down with a Petro thin saw. Then the samples were ground down using a diamond wheel on the Petro Thin; further grinding was achieved by hand on a glass using black silicon carbide 600 grit. The thickness was then checked under the low-powered microscope to a thickness of 0.03 mm (Miller, 1988; Perkins & Henke, 2004).

The thin sections were then examined using a petrographic microscope at magnifications of up to 400x; polarised light was used to identify the mineral compositions, and unpolarised light was used to examine cemented, film coating grains, surface characteristics and porosity, plus some mineral identification.

Figure 3.3: The stages of preparation for thin sections. (A) Araldite DBF resin and Araldite XD716 hardener used to impregnate the samples; (B) samples put on the hotplate to warm; (C) cutting the samples slowly for standard thin sections; (D) Metaserv 2000 grinder to grind down the samples; (E) glass slides ground down by hand on a flat glass using black silicon carbide 600 grit and checked under a low-powered microscope.

3.4 Remote sensing methods

Landsat Enhanced Thematic Mapping Imagery (ETM) for the Burydah area in central Saudi Arabia indicates a series of sand dunes covering this area. The imagery shows this sand with different morphology in different colours. A total of 10 control points were chosen within Nafuds and sand samples collected from different parts in the east and west (see Appendix 6.1 for the sample locations). The aim of using this imagery was to apply the remote sensing methods to extrapolate and understand what information could get from sand dunes, in order to infer the physical properties such as redness and reflectance from different sites and how they changed across the whole study area. These could be linked to the results of Munsell colour, magnetic susceptibility and sand redness. In order to achieve this, the image went through three stages (See Fig 3.4.

The purpose of using remote sensing methods was to examine spatial variation in dune colours and dune forms within Nafud Al Thuwayrat, Nafud Al Sirr and Nafud Al Tarafiyah, where the field observation showed that these Nafuds are redder toward the eastern parts. The colour property and sand morphology can provide information about the environmental history of Nafud. For example the processes that influence dune colours, sources of the sand and the regional processes effective on the sand such as geology, geomorphology and chemical weathering. Finally the remote sensing methods applied in this research have the ability to map the sand sea. Additionally, as previously mentioned, these can bring the environmental information provided by this study up to the present day.

3.4.1 Image pre-processing techniques

This stage involved different steps, the purpose of which was to increase the image quality and image resolution. These steps included:

3.4.1.1 Geometric corrections

Correction of the Burydah ETM Landsat 7 image UTM-WGS 1984 Zone 38N had already been done by the Saudi Centre of Remote Sensing (SCRS), but to ensure that the image geometric correction was made correctly, the image required a selection of ground control points (GCPs). It is usual to choose reference points such as crossroads, roundabouts, small isolated hills and mountains, and more than 5 points need to be entered. This method uses points that have been extracted from a GPS (Garmin 278c) to identify the land features outlined above.

The ERDAS program was then utilised to ensure that the coordinates of the ground control points were identical to the same geographic points in the images of Burydah, resulting in an accurately corrected image. Image correction was used in this research to improve the quality and appearance of the image. This procedure allows for both visual interpretation and the extraction of quantitative information such as redness rating and reflectance.

3.4.1.2 Atmospheric correction

There are a series of methods for atmospheric correction, such as radiometric correction models; apparent reflectance model, Moran models and improved image-based models. One of the most popular approaches is based Cost model combined with dark pixel subtraction and is a technique that determines the value of the pixel in the image with the lowest brightness value. This pixel is presumed to have zero ground reflectance such that its radiometric value represents the additive effect of the atmosphere (Chavez, 1996). The basic assumption is that within the image some pixels are in complete shadow and their radiation received at the satellite is due to atmospheric scattering (Moran et al., 1992). The dark pixel subtraction is applied to take band ratios of the large water treatment reservoirs to the east of Burydah. To generated Cost Model, ERDAS program required and the data from header file was used (see Appendix 7).

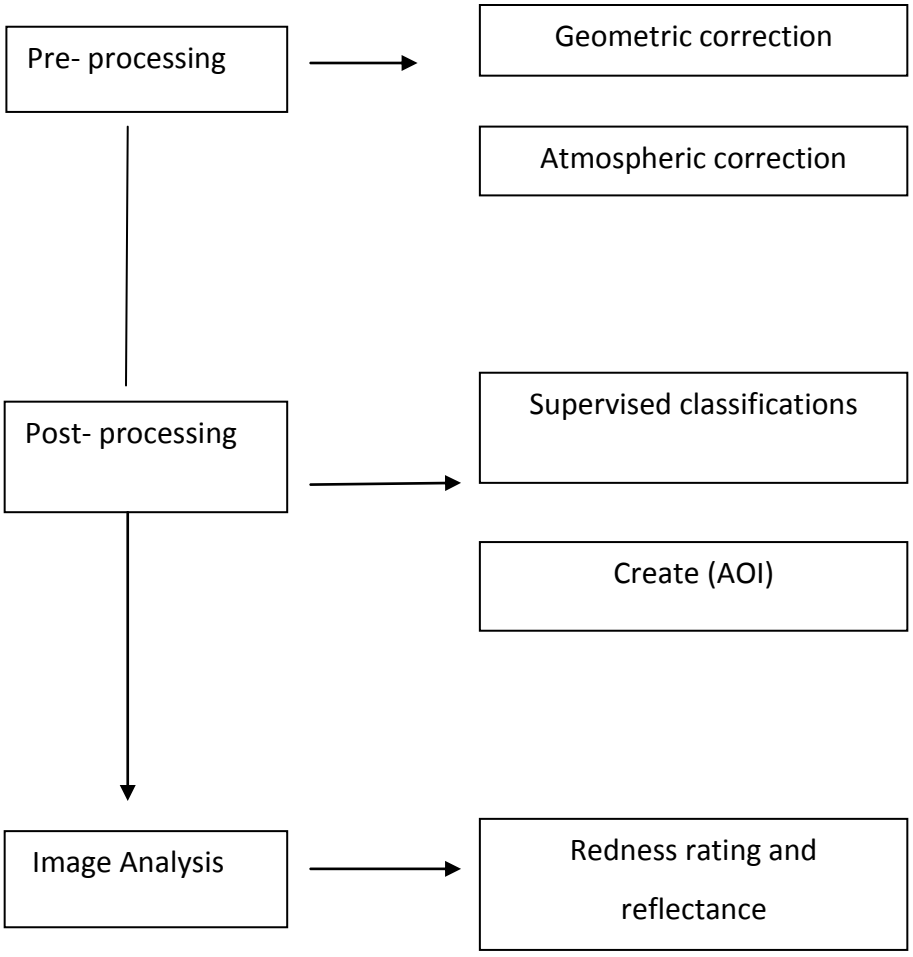

Figure 3.4: Layout of the Remote Sensing Methods.

3.4.2 Image post-processing

3.4.2.1 Supervised image classification

The supervised classification is defined as a procedure for identifying spectrally similar areas on an image by identifying 'training' sites of known targets and then computing those spectral signatures to other areas of unknown identity. The training sites are essential for setting the supervised classification. The recommended size of the training areas selected was about 3x3 pixels (Joyce, 1978). It is important to note that spectral

data computes the average for the nine pixels and then compares with the spectral signatures derived from MMR and Munsell colour. Each area is determined from maps and ground data. Ten training location areas were used to represent the accuracy of sand colour for each site, as well as representing the sites where the samples were collected in the field (See map in Appendix 6.1). To create the classification, ERDAS Imagine 2010 software was used on the Landsat ETM image. The reason for applying this method in this research was to extrapolate the field results on the sand to estimate the sand colour changes across the study area, due to the variation in red iron oxide (Hematite oxides) and/or other components such as carbonates.

3.4.2.2 Definition of an area of interest (AOI)

An Area of Interest (AOI) was created around the sand areas. This method was applied on the ETM image that was classified by supervised classification methods. The three sand classes were recorded by AOI and excluded all the non-sand areas, including bedrock and vegetation areas outside and within the sand region, and the predicted image only showed the sand class. As a result of AOI, the image was suitable for further processing.

3.4.3 Image analysis

3.4.3.1 Establishing dune redness

Redness rating can be expressed as reflectance in the visible red part of the spectrum divided by the sum of visible blue, green and red reflectance. Spectral redness using model building by ERDAS Imagine 2010 was achieved for the images in this study using the following formula:

$$R = BRF_r / (BRF_r + BRF_g + BRF_b)$$

where:

R = spectral redness

BRF_r = bidirectional reflectance in visible blue part of spectrum (400-500nm)

BRF_g = bidirectional reflectance in visible green part of spectrum (500-600nm)

BRF_b = bidirectional reflectance in visible red part of spectrum (600-700nm). Bullard and White (2002) refer to this formula on page 5, but they used it in the wrong context

The purpose of using the redness rating (RR) from the ETM image was to determine what the redness value is and how this redness changes over the sand dunes; these redness values were correlated with the redness rating derived by the Munsell colour charts, and these results were then calibrated to the image with a regression equation. The reason for this method being applied in this research was to examine spatial variation in dune colours, and the redness rating can provide reliable estimates of the concentration of the Hematite oxides.

3.4.4 Munsell soil colour charts

To determine sand colour in the study area and achieve a redness rating, samples were collected from different locations in the dune field (see Chapter 4 for the sand colour and locations); the colours were determined by comparing the sand sample with the Munsell soil chart, 1998 edition (Fig 3.5). The redness rating (RR) was calculated using the equation used by Torrent et al. (1980):

R= HC/V

R = redness rating

H = a hue value derived from the Munsell hue where 7.5 for 2.5 YR; 5 for 5 YR; 2.5 for 7.5 YR, and 0 for 10 YR (Torrent et al., 1980)

C = the Munsell chroma

V = the Munsell value.

The aim of using this method was to estimate a Munsell colour value via redness rating to extrapolate how this redness changes along the sand dunes in the study area; the redness results were correlated to spectral measurements from the ETM Image and then calibrated to the image with a regression equation to find out how they were correlated.

Figure 3.5: Examples of determining the colour by comparing the sand sample (e.g. QA .08.25E)

3.4.5 Milton Multiband Radiometer (MMR)

Radiance measurements of different sand samples were taken in the laboratory using an MMR. All measurements were taken between the hours of 10:30 and 17:00 on 24th September 2009, and samples were re-measured between the hours of 10:30 and 17:00 on 28th September 2009. It is normally advisable to take more than one measurement of the reflectance (Milton, 1980*).* Each sand sample was placed in a black plastic dish and illuminated by a 1000w lamp at a distance of 50cm and at an angle of 45° (see Bullard and White, 2002, for more detail). The sensor head was positioned overhead at 90° to the sand samples and a Kodak gray card was used as a standard reference panel; the sensor head was 20cm above the card (Milton and Rollin*,* 2003), (Fig 3.6).

Reflectance was calculated using the formula:

$$\textbf{Reflectance factor} = \frac{(S_\lambda - VS_\lambda)}{(R_\lambda - VR_\lambda)}(k_\lambda)$$

S_λ = digital number from surface in band λ

R_λ = digital number from the reference panel in band λ

VS_λ = dark level offset from buffers 1-4 (surface, bands 1-4)

VR_λ = dark level offset from buffers 5-8 (reference panel, bands 1-4)

k_λ = absolute reflectance of the reference panel in band λ.

The next stage was to create a redness rating from the results obtained from the MMR: the equation:

$$\mathbf{R = BRF_r / (BRF_r + BRF_g + BRF_b)}$$

where:

R = spectral redness

BRF_r = bidirectional reflectance in visible blue part of spectrum (400-500nm)

BRF_g = bidirectional reflectance in visible green part of spectrum (500-600nm)

BRF_b = bidirectional reflectance in visible red part of spectrum (600-700nm)

The redness obtained was compared with the redness rating obtained from the image as well as the redness rating derived from the Munsell soil colour chart, and the results were calibrated with a regression equation. The aim in using this method was to find out whether or not reflectance reflects the changes in the redness value and thus changes in the sand minerals e.g. Hematite oxides and carbonates.

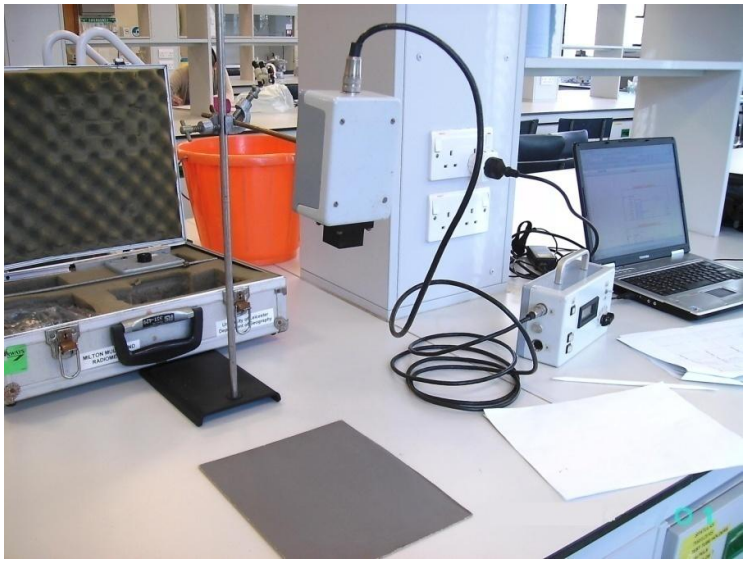

Figure 3.6: Measurement of sand samples was carried out in the laboratory using a Milton multiband radiometer.

3.4.6 Magnetic susceptibility (MS)

The Bartington MS2 System is one of the most popular methods that indicate the magnetic susceptibility of the material. This system consists of a meter and ten sensor heads; each sensor has been designed for a specific purpose (Dearing, 1994, 1999). In this research the Bartington MS2 system was applied to measure the magnetic susceptibility of ten samples collected from the sand dunes across the study area (see Chapter 4 for sample locations). The meter (MS2) operates at low frequency and is linked to a sensor (MS2B); both are controlled by Windows software (Fig 3.7). To start the measurements, the first step is to obtain readings from ambient air before placing the sample in the sample holder. Measurements are taken from the sample prior to obtaining the last air readings, before removing the sample and saving the values.

The susceptibility obtained was correlated with the redness rating obtained from the image as well as the redness rating derived from the Munsell soil colour chart and MMR, and the results were then calibrated with a regression equation to the image.

The reason for using this technique was that estimates of the magnetic susceptibility in the samples might reflect chemical variations in the sand, which are related to the spatial variability of iron oxides present in these sands in relation to the bedrock around the sands as well as the sand sources.

Figure 3.7: The MS2 meter and the MS2B Dual Frequency sensor; unit SI x10^-8, range x1.0 and Container volume 10ml.

CHAPTER FOUR

4 Results

4.1 Introduction

The aim of this chapter is to describe the main physical characteristics of the study sites and to present an explanation of the physical, chemical and mineralogical deposits preserved in the sections studied. This was achieved by using the results of field descriptions with X-ray diffraction (XRD) (see appendix 3) and thin section analyses, and then linking these findings with the dates obtained by OSL and radiocarbon dating. For consistency, this thesis will use Willoughby's (2007) classification of MIS ages, this not means this is best classification, but this study used this just to be consistency and most of the evidence that Willoughby used for past environmental and climatic change were from Africa which is close the environmental in the Arabian Peninsula. Radiocarbon samples are all calculated and calibrated using INTCAL 04 radiocarbon age calibration (Reimer et al., 2004) with a upper age limit is about 20 ka and a lower ages is about 250 years(report by Tamers and Hood., 2010) (see Appendix 4), also some samples are calibrated using INTCAL09 which goes much back further(Reimer et al., 2009). This chapter investigates the physical characteristics of the wadi deposits, also sand deposits (Nafud) and spatial variation in dunes redness and sand form and redness by remote sensing methods to bring the study to the present environment. Finally the chapter discusses palaeolake deposits and tufas deposits discovered in study area.

4.2 Wadi Deposits

4.2.1 Fluvial deposits at Wadi Al Butaun QA.08.02

The Wadi Al Butaun is a fluvial system located to the north of the Burydah area (26°50′58″N - 43°56′03″E**)** (Fig. 4.1). The wadi is a tributary channel of Wadi Al Rimah and is one of the longest wadi systems in the study area running NW to SE for at least 150 km through the Burydah area. At present it is blocked by sand accumulated from the linear dunes of the Nafud Al Tarafiyah (Fig 4.1). The section studied is 5 meters

thick, and comprises 10 sedimentary units. There is evidence of sedimentary, pedogenic and diagenetic processes that have been in operation. Unit 1 is made up of 30 cm of low-angled, cross-bedded, moderately sorted sands that indicate fluvial deposition under moderate energy conditions. An OSL of 85.5 ka (Table 4.1), which falls into MIS stage 5a-5b of the last interglacial according to Willoughby's (2007) definition. Deposited unconformably above Unit 1 is 5cm of indurated sands. This massive, calcium carbonate enriched and hardened layer represents a break in fluvial activity. The cemented sediments at the eroded surface indicate conditions that resulted in the drying out of the wadi and cementation at a palaeo surface. Following on there is the deposition of 40 cm of cross bedded (Unit 3) sands and gravels followed by 30cm of planar bedded sands (Unit 4). These two Units, along with Unit 1 are suggestive of wetter conditions with a perennial flow rather than the typical flash-flood ephemeral wadis that exist under arid conditions today because most grains appear to be well rounded and polished surface with a less amounts carbonate deposition. Unit 5 is 45cm thick, it is similar to Unit 4 in terms of sand grain size and sorting (Fig 4.3) but it contains evidence (along with the uppermost part of unit 4) of post-depositional carbonate nodules that extend up toward another unconformity that separates Unit 5 from 6. Units 6 and 7 comprise a sequence of interbedded indurated and non-indurated sand beds, all separated by unconformities. The three indurated sand layers are similar in nature to Unit 2. These surface sands are likely to represent localised reworking of sediments of the exposure that have subsequently become cemented. The unlithified sands in between the cemented units are of similar grain size and sorting to each other but show no sedimentary structures that would help to distinguish the depositional environment (ie either small-scale aeolian or fluvial activity). Post-depositional carbonate root structures nodules and a burrow are present in Unit 7 but not 6. These structures provide clear evidence of pedogenic carbonate accumulation beneath a palaeosurface. There is then a return to moderate energy fluvial conditions in Unit 8 with 85 cm of interbedded planar cross-bedded sands. This unit is very similar in nature to the fluvial unit below.

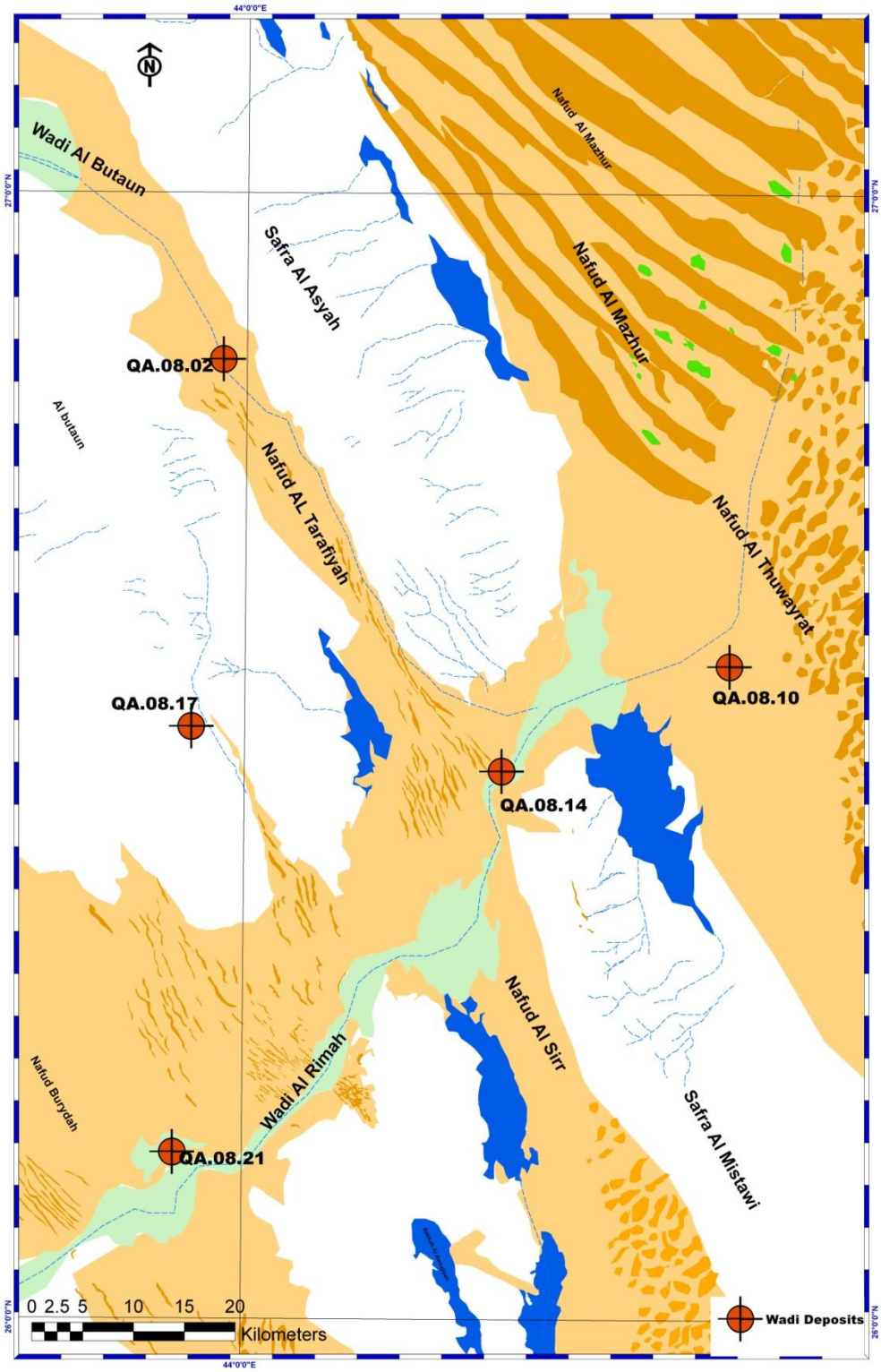

Figure 4.1: The study area with the wadi sites shown as red dots.

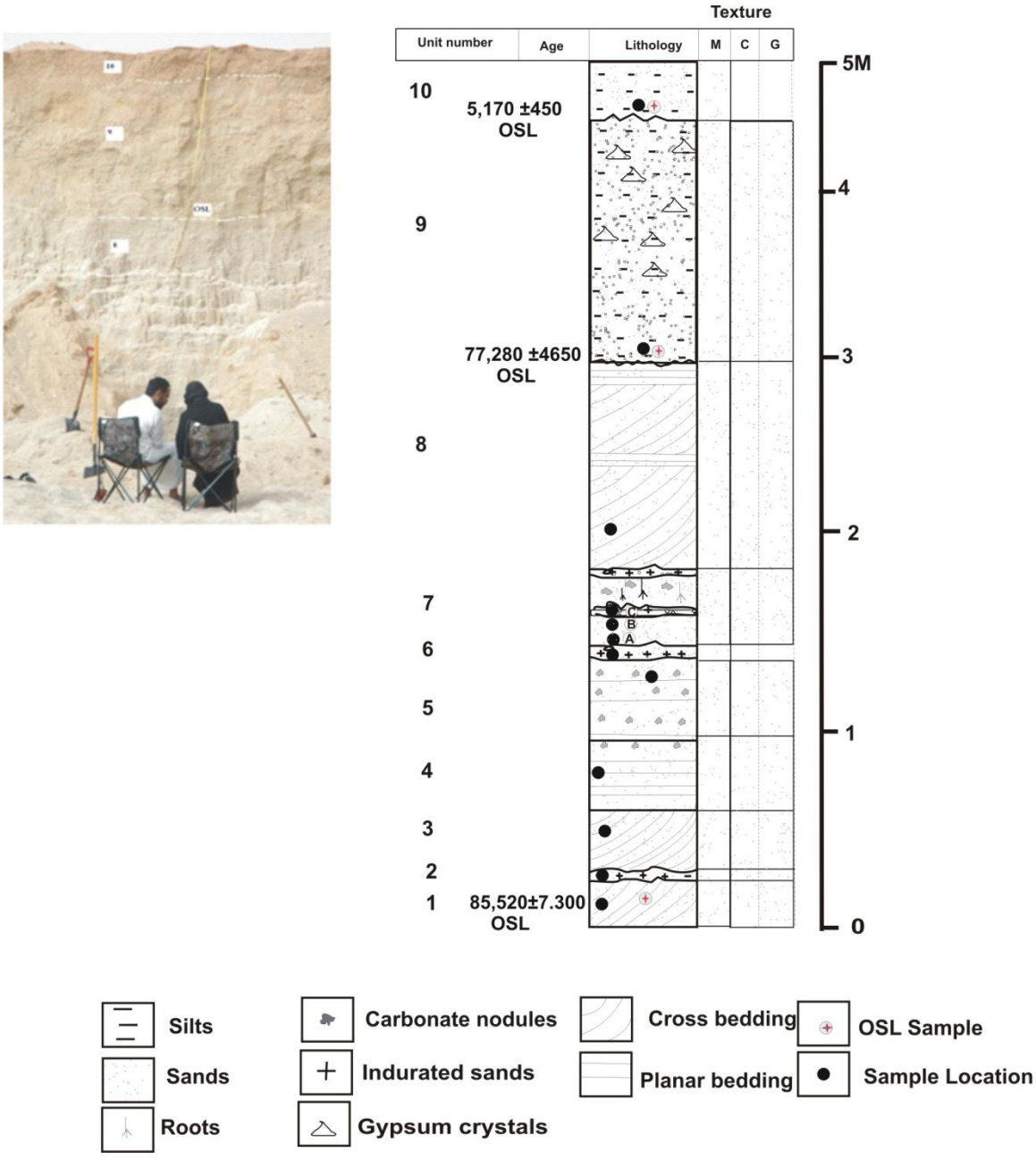

Figure 4.2: Schematic sedimentary log of section QA.08.02 comprising the fluvial sands of Wadi Al Butaun. On the stratigraphic log (M) medium sand, (C) is coarse sands and (G) is gravels

At a height of 3 m above the base of the section there is another major unconformity, which has cut into the top of Unit 8 and a palaeochannel has been infilled with medium to coarse grained sands that are moderately sorted. There is no clear evidence of bedding in this palaeochannel**,** although post depositionally formed gypsum crystals

that increase in abundance towards the top of this unit have been identified. The presence of the gypsum crystals indicate that upon drying out of this palaeochannel arid condition with high evaporation rates must have existed.

The base of this palaeochannel has been OSL dated to 77 ka (Table 4.2) which still falls into MIS5a of the last interglacial when conditions were thought to have been warmer and wetter than today (Willoughby, 2007). The contact between Unit 9 and 10 is an erosional feature. Unit 10 is 25cm thick, and comprises of largely fine-grained sands. This unit is more orange in colour than the lower units (7.5 YR6/6 orange). In addition, mineralogically the sands contain 83.6% quartz (making up the percent of the whole rock mineralogy) in comparison, for example, to Unit 8 that contains 66.5% and unit 9 that contains 66.6%. Thus on mineralogical, granulometic and colour evidence it is argued that unit 10 represents a windblown sand sheet deposit. This deposit has been dated to 5.1ka, thus represents the loss of evidence of a wadi in this location and drier conditions by the mid Holocene.

Sample	Lab- ID Shfd09	Depth (m)	De (Gy)	Dose (µGy a-1)	Model used to establish De	Age		Alpha (µGy/ka)	Beta (µGy/ka)	Gamma (µGy/ka)	Cosmic (µGy/ka)
						(a)	±				
QA.08.02.01	135	4.3	169.12±10.86	1978±111	Finte component1	**85,520**	**7,300**	9 ±2	13.04±108	537±27	127±6
QA.08.02.09	136	1.25	173.98±4.21	2251±124	Central age	**77,280**	**4,650**	10±3	1453±120	602±31	186±9
QA.08.02.10	120	0.2	10.71±.79	2071±96	Central age	**5,170**	**0,450**	22±6	1204±91	631±29	214±11

Table 4.1: OSL dates obtained from the sedimentary section QA.08.02

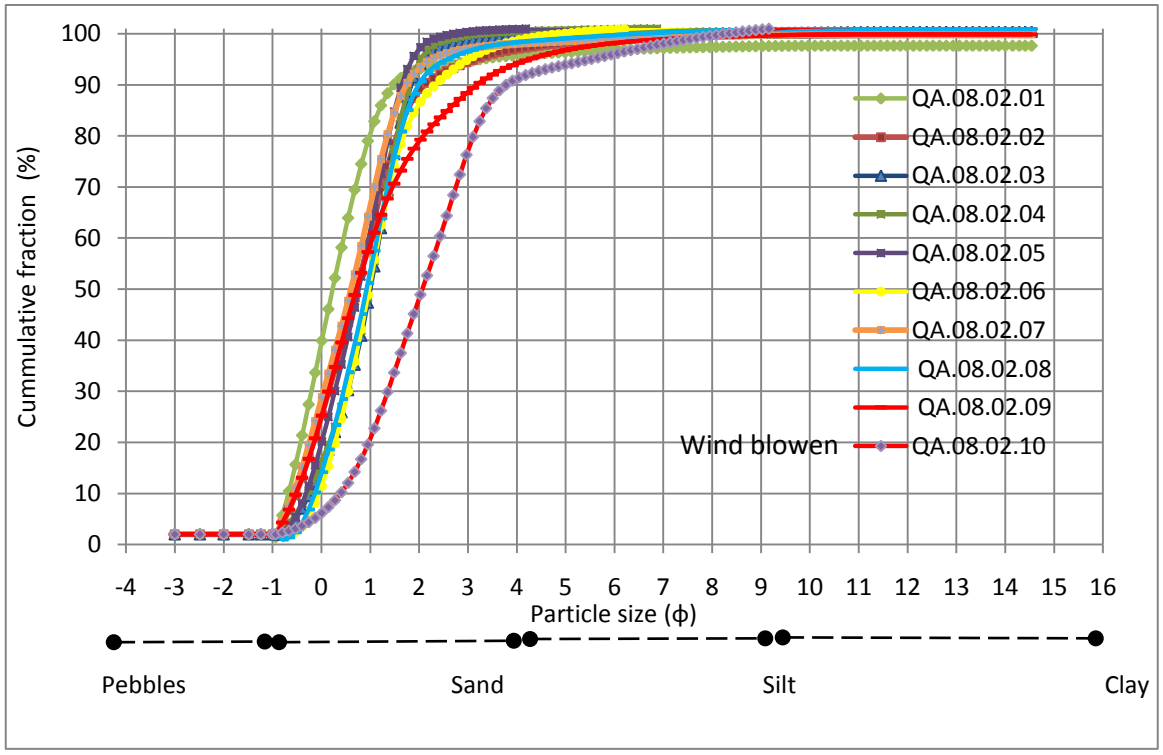

Figure 4.3: Cumulative percentage of the grain size composition from section QA.08.02 at Wadi Al Butaun.

4.2.2 Fluvial deposits at Wadi Al Watah QA.08.17

The Wadi Al Watah is a tributary channel of the Wadi Al Rimah. It runs parallel to Wadi Al Butaun, from the north-west to the south-east for at least 120 km through the Burydah area (26°50′59″N-43°56′06″E). At present, the wadi is blocked by sand accumulated to form the linear dunes of Nafud Burydah (Fig 4.1). This exposure is 3 m thick, comprises 10 Units that can be distinguished on the basis of variations in sedimentation, particle size analysis and post-depositional processes. Unit 1 is 46 cm thick, contains flat bedded silty sands (Fig 4.4). This Unit comprises 67.9% quartz (making up the whole rock mineralogy), 10% feldspars, 5.8% calcite. The particle size range (Fig 4.5) and bedding is indicate a moderate to low energy flowing river. Following on is Unit 2, which is 45 cm thick and has a similar particle size distribution to Unit 1 but is now displaying low angled planar laminations. The whole rock mineralogy percentage distribution is very similar to unit 1 (see Appendix 3), it is proposed that Unit 2 formed under similar environmental conditions to Unit 1. However the presence of carbonate nodules in Unit 2 distinguishes it from Unit 1 below. An OSL dated sample near to the top of Unit 2 gives an age of early Holocene ages (10 ka), which indicates evidence of fluvial activity prior to and at this time. The upper boundary of Unit 2 is unconformable and contains desiccation cracks. This evidence plus the carbonate nodules suggest the end of fluvial activity, exposure, drying out of the wadi resulting in a subaerial surface perhaps with some plants present on the sand due to the evidence of pedogenic carbonate nodules that formed around roots.

In general terms, Units 4-9 can be grouped into a series of massive beds of quartz-rich silty sands containing varying amounts of carbonate nodules. Each of the Units is separated by erosional surfaces. In particular, Unit 6, contains a significant number of carbonate nodules (calcite nodules up to 13.3% of the whole rock mineralogy)(see Appendix 3) representing root nodules, in addition there are desiccation cracks present at the upper erosion surface (Fig 4.4).

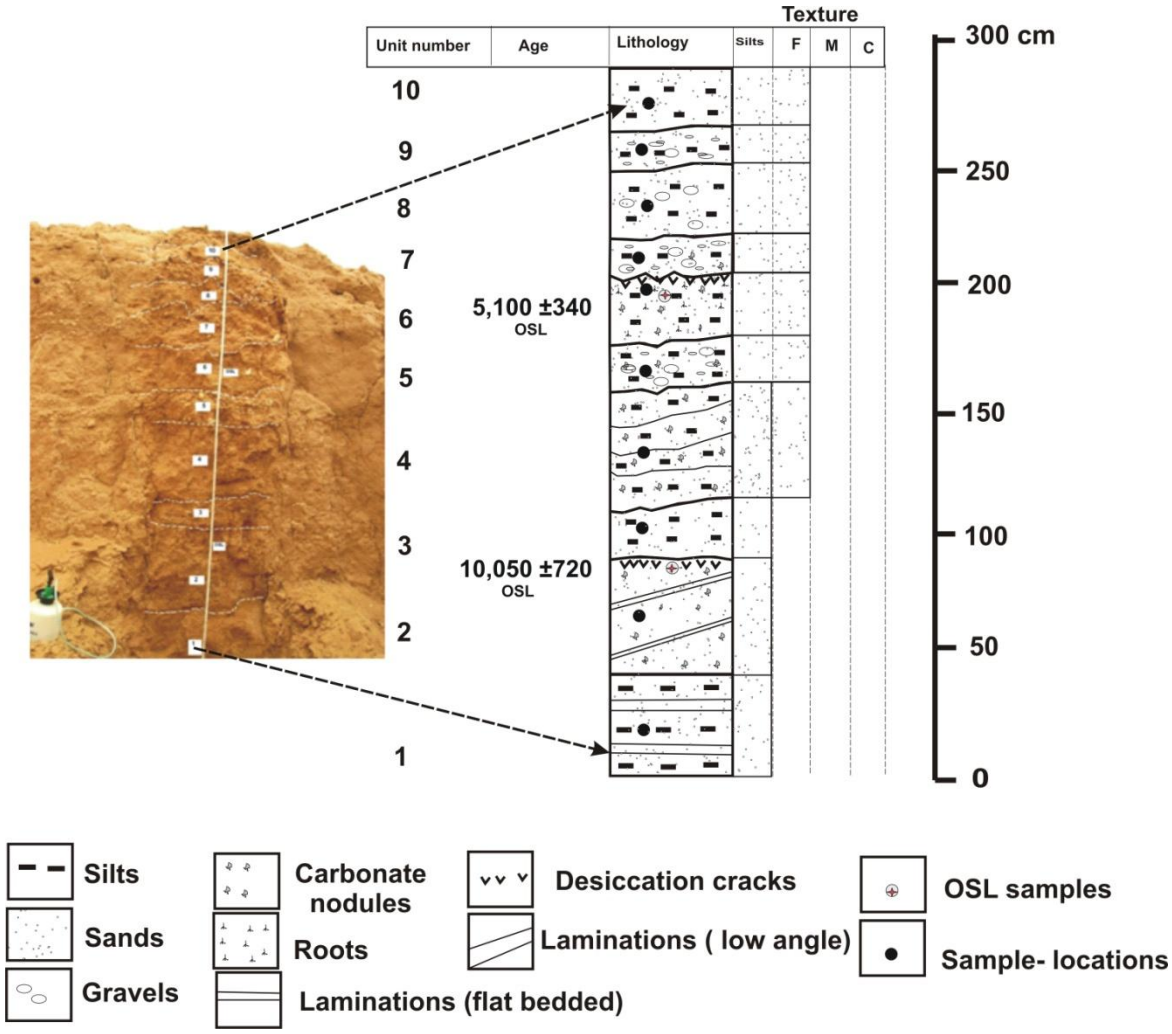

Figure 4.4: Schematic sedimentary log and view of section QA.08.17 of the fluvial sands at Wadi Al Watah. On the stratigraphic log (F) is fine sand (M) medium sand, (C) is coarse sands.

Similar to the unconformity at the top of Unit 2, this unit is indicative of drying out of the low energy river below (Unit 3-6), with the formation of a palaeosurface with vegetation present. An OSL age from near the top of Unit 6 gives age of 5.1 ka. Units 7-9 preserve a record of the return of fluvial conditions as described below, but the presence of gravels suggest that energy conditions may have been slightly higher. Unit 10 comprises the best sorted unit of sands in this section; there is a significant increase in the amount of quartz present compared to the lower beds (see Appendix 3). Unit 10 consists of 77.9 % quartz 4.3 %, feldspar 11%, calcite, plus clays making up the whole rock mineralogy, No clear bedding is evident. On the basis of grain size, sorting and

mineralogy it is argued that unit 10 is an aeolian sand cover that is evident on the top of this river cutting exposure today.

Sample	Lab- ID	Depth (m)	De (Gy)	Dose (µGy a-1)	Model used to establish (De)	Age		Alpha (µGy/ka)	Beta (µGy/ka)	Gamma (µGy/ka)	Cosmic (µGy/ka)
						(a)	±				
QA.08. 17.02	Shfe09142	2.3	28.9 ±1.7	2877 ±116	Finte component1	**10,050**	**720**	38 ±10	1658 ±110	1020 ±35	161 ±8
QA.08.17.06	She10113	0.7	13.54 ±0.67	2654 ±121	Finte component 1	**5,100**	**340**	33 ±9	1552 ±114	869 ±39	199 ±10

Table 4.2: OSL date obtained from the sedimentary section QA.08.17

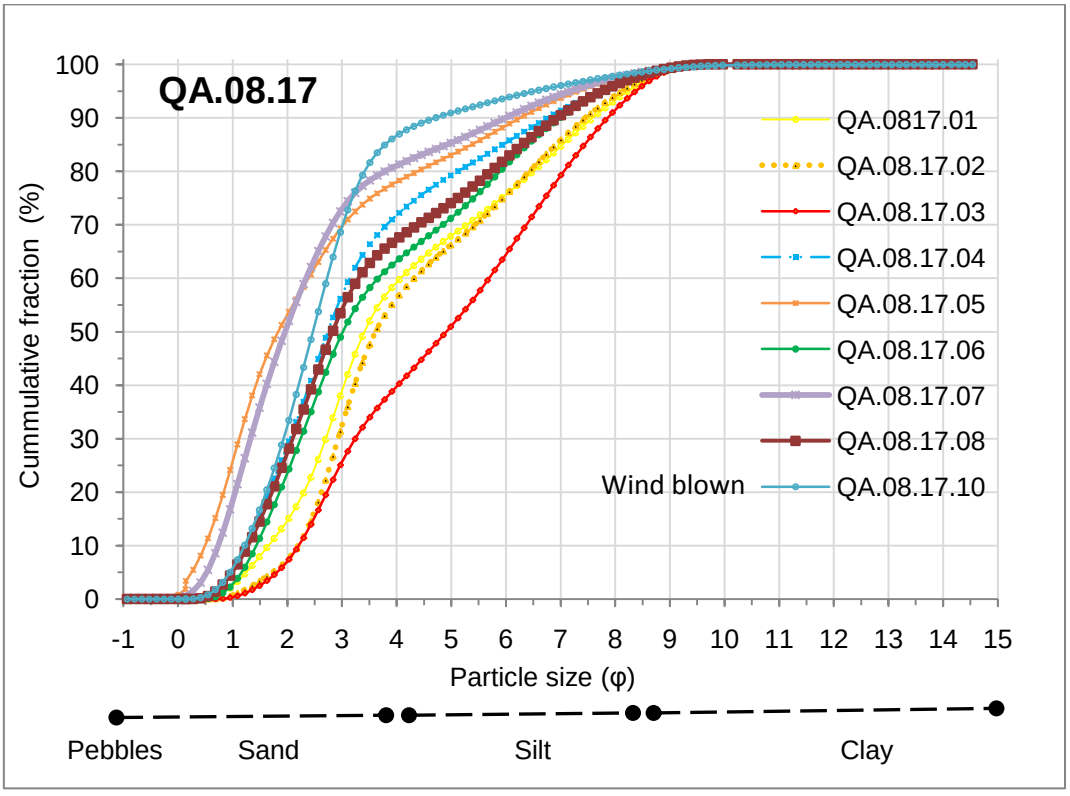

Figure 4.5: Cumulative percentage of the grains size composition at section QA.08.17 at Wadi Al Watah.

4.2.3 Wadi Rimah deposits within Nafud Al Gamas QA.08.21

This site is located in the upper part of Wadi Al Rimah (26°08′71″N- 44°53′45″E) (Fig 4.1). The quarry is located about 3km from the modern day channel. Twenty three sedimentary Units within a 3.5 m thick section have been distinguished on the basis largely of post-depositional processes including precipitation of carbonates, gypsum crystals, as well as organic feature such as macrofossil moulds, roots and burrows. In addition there are slight variations in colour and granulometic properties throughout the section. The junctions between all the units are unconformable.

Unit 1 is 6 cm thick, consists of dark, reddish-brown (2.5 YR 3/4) very fine silts and clays. XRD analysis (see Appendix 3) shows that the deposit is low in quartz (9.9%) feldspars (6.1%) but is rich in clays (palygorskite-9.5%; smectit-3.4%; chlorite-4.8% and kaolinite-2.9%) and undifferentiated mica species (15%). On the <2 µm clay fraction, smectite, illite, kaolinite, and chlorite dominate, perhaps indicating that a significant part of the mica species group could be illite. In addition, the XRD data shows a significant contribution from the post-depositional introduction of calcite (25.6%) and gypsum (22.8%). This unit also contains evidence of roots along with unidentified macrofossils. The contact between Units 1 and 2 is wavy and the unit above is more poorly sorted and contains a coarse sand-sized fraction (suggesting slightly higher energy conditions) than that which resulted in the deposition of Unit 1. The deposit is bright reddish-brown in colour (5YR 5/6) and shows a similar mineralogy to Unit 1 (see Appendix 3) in terms of amounts of quartz, feldspars and clays. However, this unit contains lower amounts of carbonate (13.1%) but significantly higher gypsum values in comparison to Unit 1(50.7%). There is also some evidence of organic matter.

Unit 3 comprises pale reddish-brown (5 YR 5/4) fine silts and clays with a similar mineralogy to Unit 1 (Appendix 3). Post-depositional carbonate nodules (24.6%), gypsum crystals (20.5%) along with roots and macrofossil moulds are all present.

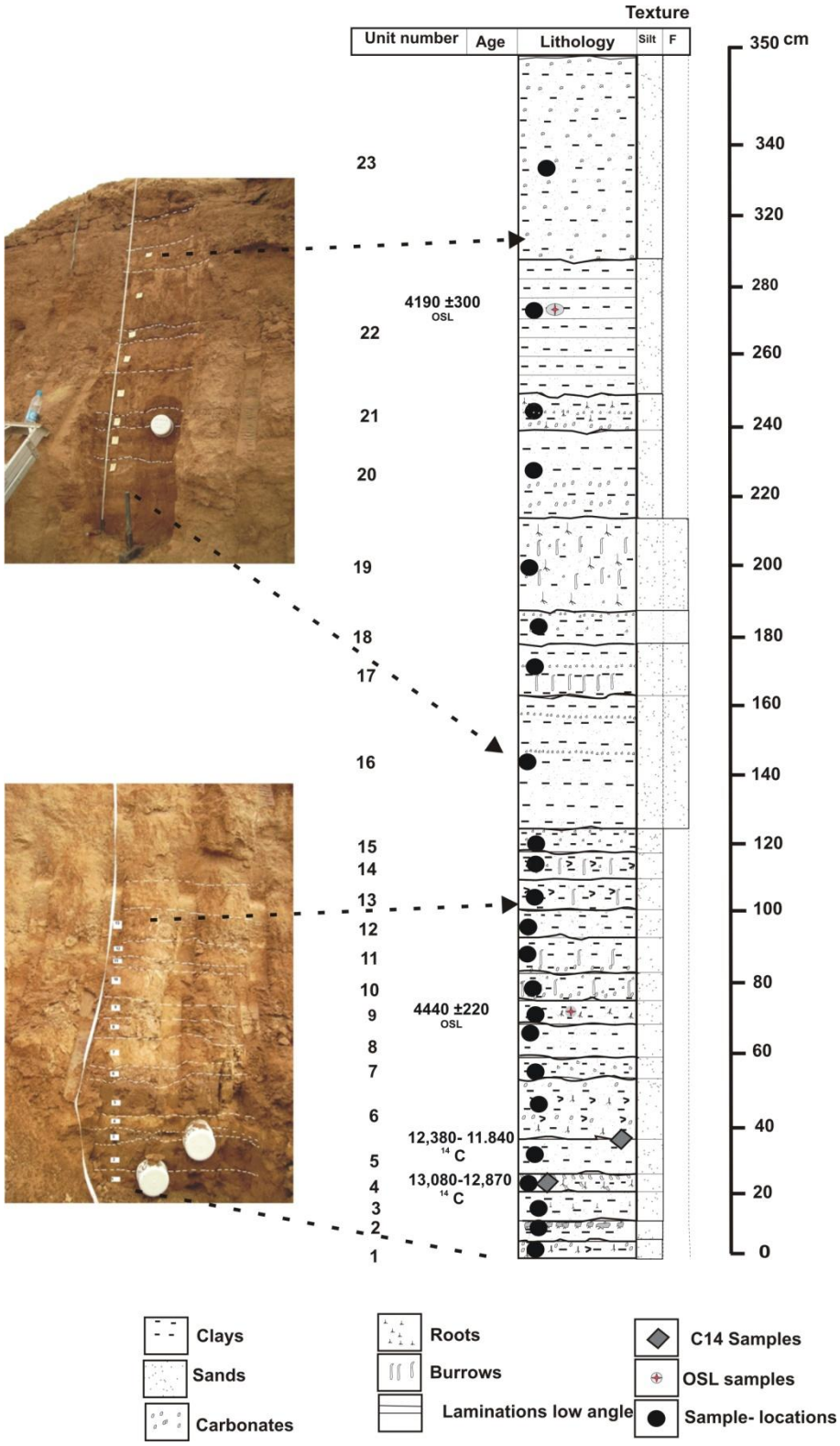

Figure 4.6: Schematic sedimentary log and view of section QA.08.21 of Wadi Rimah deposits within Nafud Burydah. On the stratigraphic log (F) is fine sand

Unit 4 is very similar in nature to Unit 3 and a calibrated radiocarbon age of (cal BP 13,080 to 12,870) (Table 4.4 and Appendix 4.1) and has been obtained, indicating an early Holocene age according to (Willoughby, 2007). Unconformably overlying Unit 4 is Unit 5, which is an orange bed of sandy silts (7.5 YR6/6) that has an early Holocene calibrated radiocarbon age of 12,380 to 11,840 cal BP. This sample has more than one calibrated age (Table 4.4 and Appendix 4.2). Mineralogically this deposit is similar to the lower beds and it also contains post-depositional carbonate nodules (17.5%) and abundant gypsum (22.6%). Units 6-15 are all similar deposits texturally, lacking clear sedimentary structures but they vary in terms of their abundance in post- depositional roots, carbonate nodules and gypsum crystals and are all separated by erosional contacts. Unit 9 has a mid Holocene, OSL age of 4.4 ka.

From Unit 16 and above the individual units became much thicker, perhaps indicating that flood events are occuring over longer periods of time. As below, each unit is separated by erosional contacts. Units 16-19 are largely coarse grained silts XRD analysis on Unit 19 shows evidences of post depositional gypsum crystals (16.3%) and carbonate nodules (13.6%) (Appendix 3). The dominant clays are montmorillonite, chlorite and illite that are indicative of weathering of granite in the upper catchment area of the Arabian Shield.

Units 20-23 are fine grained silts than those in the bed below. Unit 21 contains a high amount of evidence of post-depositional roots, gypsum (28.5%) as well as carbonate (16.6%) (See Appendix 3). Unit 22 is similar unit 21 and has an OSL age of 4.1ka which shows evidence of periodic wet activity in Wadi Al Rimah.

The interpretation of this section is one of periodic flooding of Wadi Al Rimah onto the floodplain of the study area allowing the settling out of silts and clays (and during larger flood events some sands). These wet events are separated by phases of gradual drying out, the establishment of vegetation on the floodplain and the gradual formation of carbonate nodules. Then with further evaporation, during the final drying out stages, gypsum crystals precipitated out. The cementation of carbonate deposits at palaeosurfaces stopped infiltration of water during subsequent flood events which

preserved the gypsum crystals. Thus Wadi Al Rimah was periodically flooding throughout the early and mid Holocene.

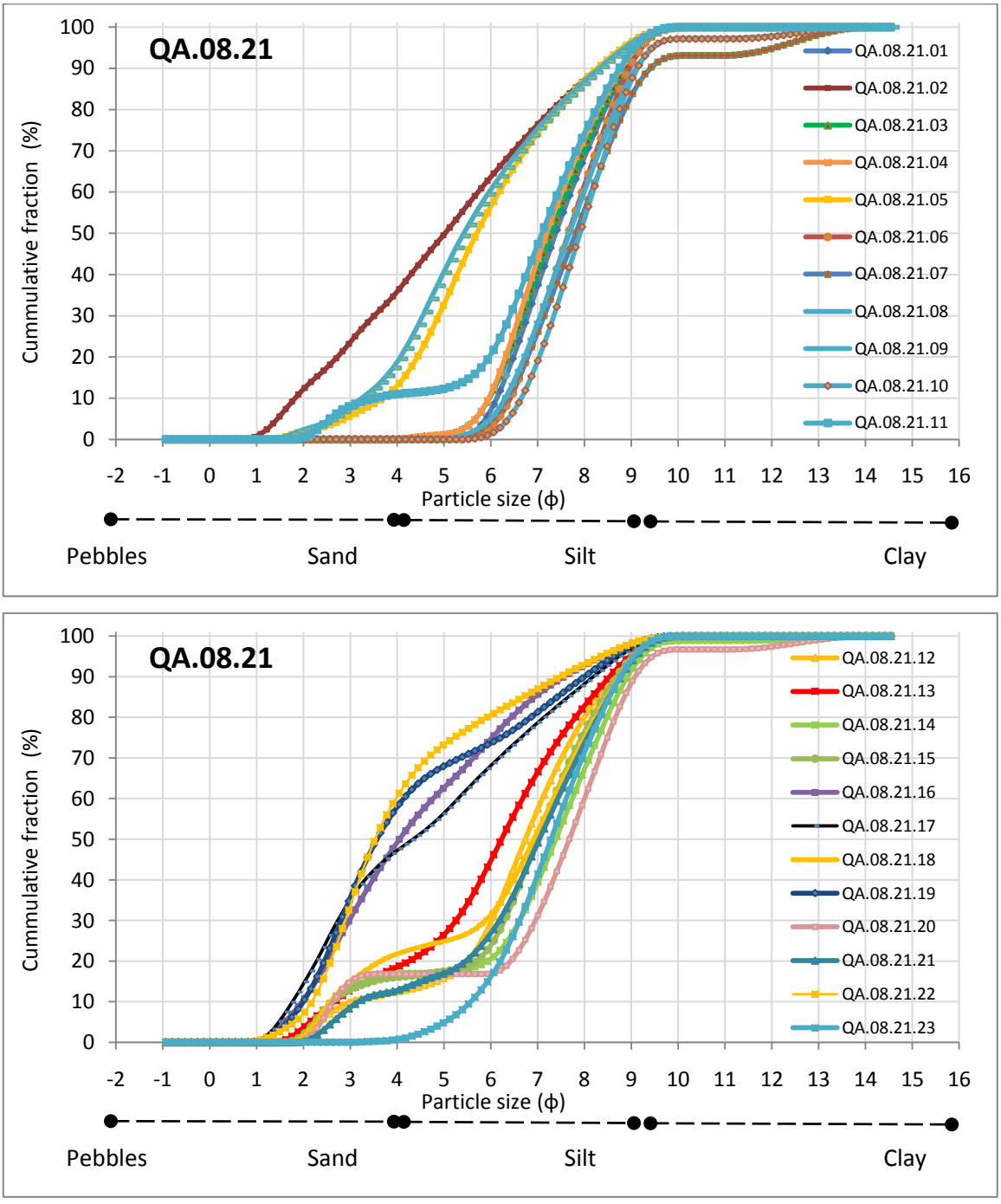

Figure 4.7: Cumulative percentage of the grains size composition at section QA.08.21 of Wadi Rimah deposits within Nafud Burydah the upper Figure represents the lower units from (1 to 11) and the lower Figure represents the upper units (12- to23).

Sample	Lab- ID	Depth (m)	De (Gy)	Dose (µGy a-1)	Model used to establish (De)	Age		Alpha (µGy/ka)	Beta (µGy/ka)	Gamma (µGy/ka)	Cosmic (µGy/ka)
						(a)	±				
Qa.08.21.09	Shfd09143	2.9	14.06±0.52	3166±107	Central age	**4,440**	**0.200**	56±14	1753±98	1208±41	150±7
QA.08.21.22	Shfd10114	0.70	12.56±.68	3000±137	Central age	**4,190**	**0.300**	35±9	1764±129	1002±45	200±10

Table 4.3: OSL dates obtained from the sedimentary section QA.08.21

Sample	Depth	Material	Technique	Lab code	Measured		Convential		Calibration source	Calibrated age (BP) 95% 2 sigma ¤
					(age)	±	(age)	±		
QA. 08.21.04	3.46	Organic matter	AMS	Beta 279237	11,090	60	**11,030**	**60**	**INTCAL 04**	**13,080 to 12,870**
QA.08 .21.06	3.21	Organic matter	AMS	Beta 279238	10,270	60	**10,310**	**60**	**INTCAL 04**	**12,380 to11.970** **11,870 to 11840**

¤ See Appendix 4

Table 4.4: Radiocarbon dates obtained from the sedimentary section QA.08.21. The ages in this section celebrated by INTCAL04. Reference is: Reimer, P. J., Baillie, M. G. L., Bard, E., Bayliss, A., Beck, J. W., Bertrand, C. J. H., Blackwell, P. G., Buck, C. E., Burr, G. S., Cutler, K. B., Damon, P. E., Edwards, R. L., Fairbanks, R. G., Friedrich, M., Guilderson, T. P., Hogg, A. G., Hughen, K. A., Kromer, B., McCormac, F. G., Manning, S. W., Ramsey, C. B., Reimer, R. W., Remmele, S., Southon, J. R., Stuiver, M., Talamo, S., Taylor, F. W., van der Plicht, J., and Weyhenmeyer, C. E. 2004a. IntCal04 Terrestrial radiocarbon age calibration, 26 - 0 ka BP. Radiocarbon 46, 1029-1058.

4.2.4 Wadi Rimah deposits within Nafud Al Rubayiyah QA.08.14

This site is located where Wadi Al Rimah channel traverses the sand dunes of Nafud Rubayiyah, in the centre of the study area (26°28′95″N - 44°12′01″E) (Fig 4.1). This section exposes inter-bedded medium fine grained sands through to clays. Unit 1 is a clay dominated reddish-brown (2.5YR 4/6) deposit. There is no evidence of any sedimentary structures in this massive deposit. In the base unit there is post depositional carbonate nodules and animal burrows are evident. An OSL age of 110 ka (Table 4.5) was obtained from a height of 90 cm from the base of section, which indicates a MIS 5d age according to Willoughby (2007). Regarding to the age reliability, it should be note that there are no indicators of the post-depositional carbonate nodule formation and animal burrows wich may influence the reliability of the age, although their concentration increased in the base of unit. The equivalent dose rate of 127 Gy is still under the estimate of quartz saturation. An erosional contact separates this bed from the overlying Unit 2, which is a poorly sorted of silty sand that is reddish-brown (2.5YR 5/3). This bed lacks any significant evidence of post-depositional processes. Unit 3 is a massive, weak red (2.5 YR 5/2) silt-rich deposit that contains evidence of roots running throughout and an associated higher carbonate percentage 7.2% compared to Unit 1 (Appendix 3). On top there are recent moderately sorted medium sand sheet deposits.

Thus this sequence shows evidence of fluvial activity in Wadi Al Rimah during the last interglacial resulting in 1.5m of sediment accumulation followed by a phase of drying out and precipitation of carbonate nodules. It is unknown whether burrows were syn-depositinal or post-depositional. Above the erosional contact there has been a phase of aeolian accumulation, as a sand sheet (no bedding is evident). There is another major wet phase evident in Unit 3 that is texturally more similar to fluvial Unit 1 rather than the coarser grained sediments of Unit 2 and 4 which clearly now need to be dated. Finally the upper Unit is the modern aeolian sand sheet.

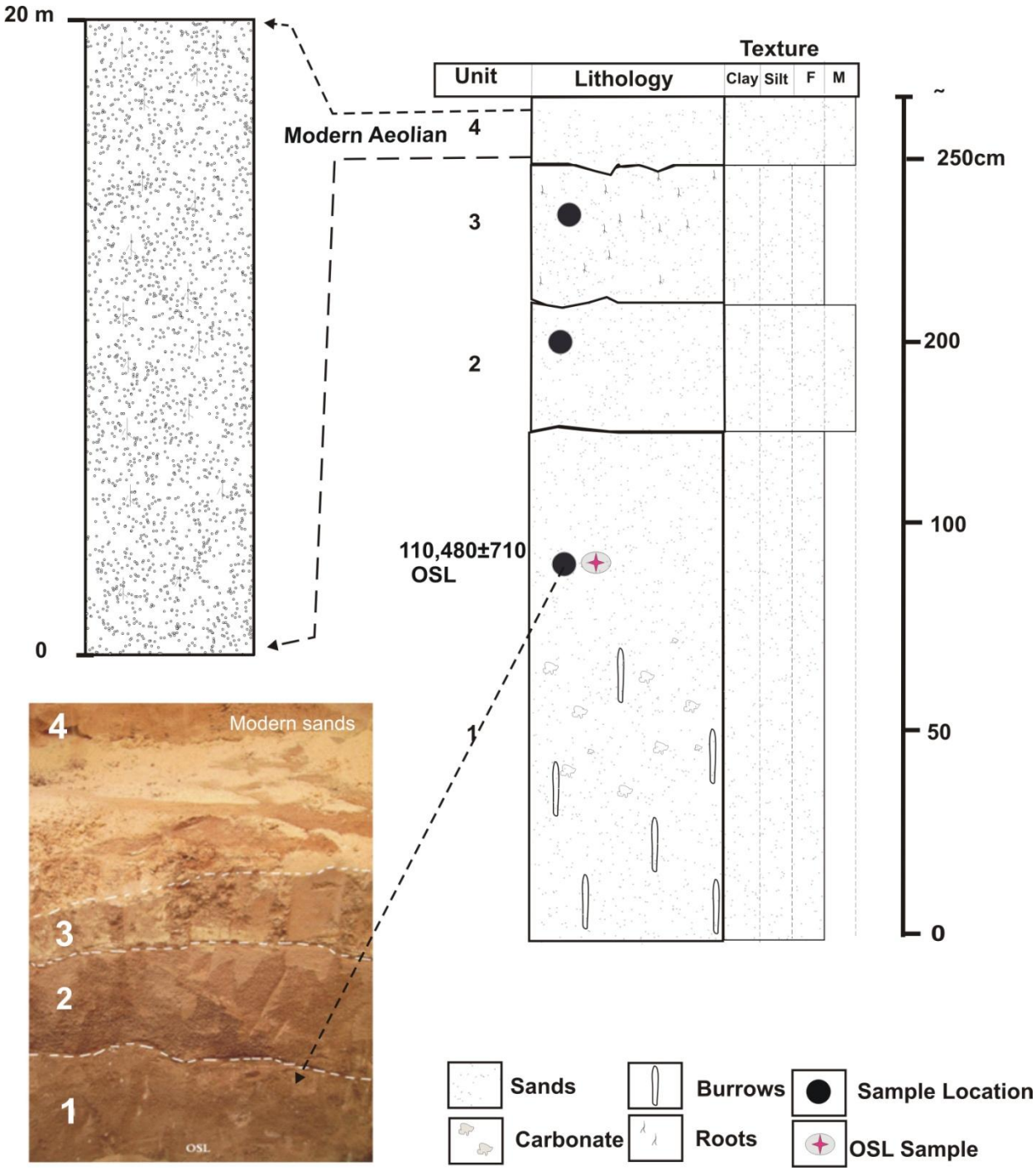

Figure 4.8: Schematic sedimentary log and view of section QA.08.14 within Wadi Rimah deposits in Nafud Al Rubayiyah. On the stratigraphic log (F) is fine sand, (M) is medium sand. The upper unit is the modern aeolian sand which is varies in thickness between dune crests and interdunes.

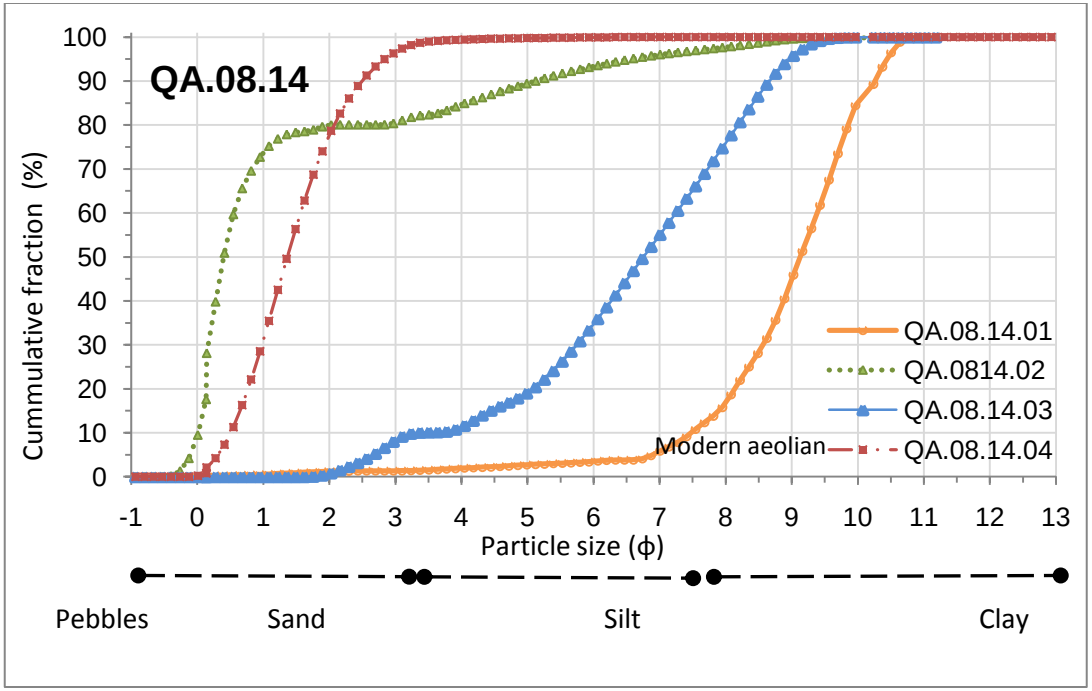

Figure 4.9: Cumulative percentage of the grains size composition at section QA.08.14 of Wadi Al Rimah deposits

Sample	Lab- ID	Depth (m)	De (Gy)	Dose (µGy a-1)	Model used to establish (De)	Age		Alpha (µGy/ka)	Beta (µGy/ka)	Gamma (µGy/ka)	Cosmic (µGy/ka)
						(a)	±				
Qa.08.14.01	Shfd09134	1	127.8±5.6	1157±48	Finte component 1	**110,480**	**6,700**	12±3	610±45	343±16	192±10

Table 4.5: OSL dates obtained from the sedimentary section QA.08.14

4.2.5 Wadi Rimah deposits within Nafud Thuwayrat QA.08.10

Section QA.08.10 is located within the Wadi Al Rimah channel on the eastern margin of the study area (26°34′86″N., 44°26′24″E), where the Wadi Al Rimah channel runs through the Nafud Al Thuwayrat (Fig 4.1). The section is up to 130 cm thick and is composed of four Units (Fig 4.10). At the lowest position in the section, Unit 1 is made up of 40 cm of low-angled laminated medium grained sand that are orange in colour (7.5 YR 6/6). There is an unconformable contact with the upper bed. XRD analysis of Unit 1 shows high amounts of quartz (86%) (Appendix 3). An OSL sample provides age of 11.9 ka. The sediments represent evidence of windblown activity due to the grains size properties, dominance of quartz grains of orange colour. Above this unit there is a massive Unit 2 which is much finer grained than the unit below, with quartz amounts of 71.8% and more clays are present (palygorskite-2.2%; chlorite-1.7%, kaolin-1% and mica species-3.3%), indicative of a weathering source from upper Wadi Al Rimah. Burrows and roots are present with post-depositional carbonate nodules (7%). The colour is a pale brown (7.5 YR 5/4), which could be related to the clays present (Appendix 3), which may have been a result of wadi activity. In the middle section, Unit 3 is aeolian sand dated at 4.8 ka (Table 4.6). It consists of medium sized sand (Fig 4.11), with minor numbers of burrows and roots found. There is no clear bedding in this unit and it has an unconformable upper contact. The colour is bright brown (7.5 YR 5/6). The upper unit bed has a thickness of 40 cm and is made up of poorly sorted fine grained sands. The unit has abundant burrows which increase in frequency towards the top. The bed has a wavy basal contact and the top is a flat palaeosurface rich in Bulrush. The wadi at this stage perhaps looks like shallow ponded body of water in an interdune location.

The key findings of section QA.08.10 is that the wadi Al Rimah was covered by phases of sand accumulation by Nafud Al Thuwayrat. The wadi terraces show alternation between fluvial and aeolian deposits, with evidence of periodic wadi activity in the early Holocene at C. 11.9 ka followed by low activity and ponding during the mid Holocene at about 4.8 ka.

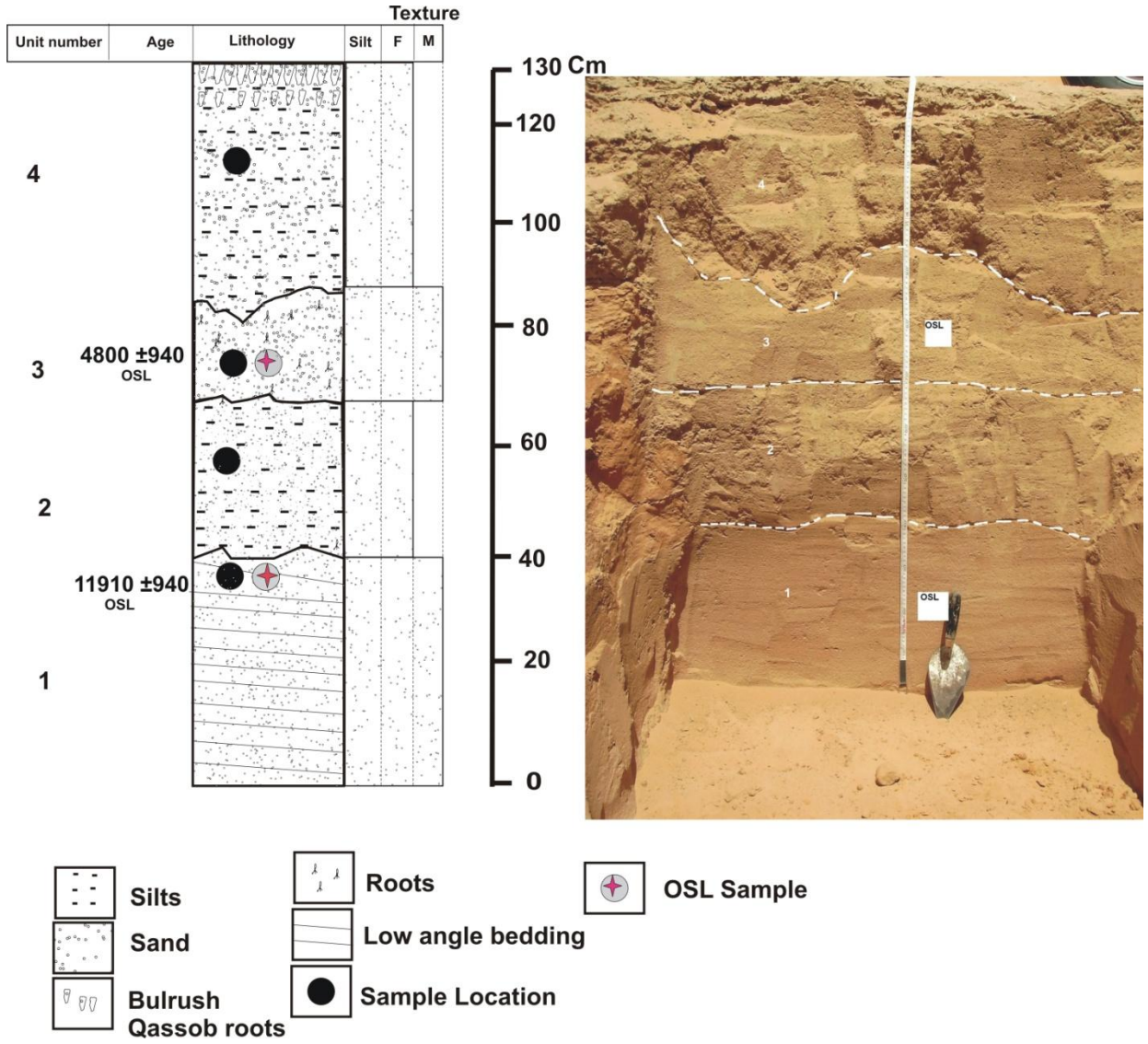

Figure 4.10: Schematic sedimentary log and view of section QA.08.10 on the Eastern margin of the study area, where the Wadi Al Rimah channel runs through the Nafud Al Thuwayrat. On the stratigraphic log (F) is fine sand and (M) is medium sands

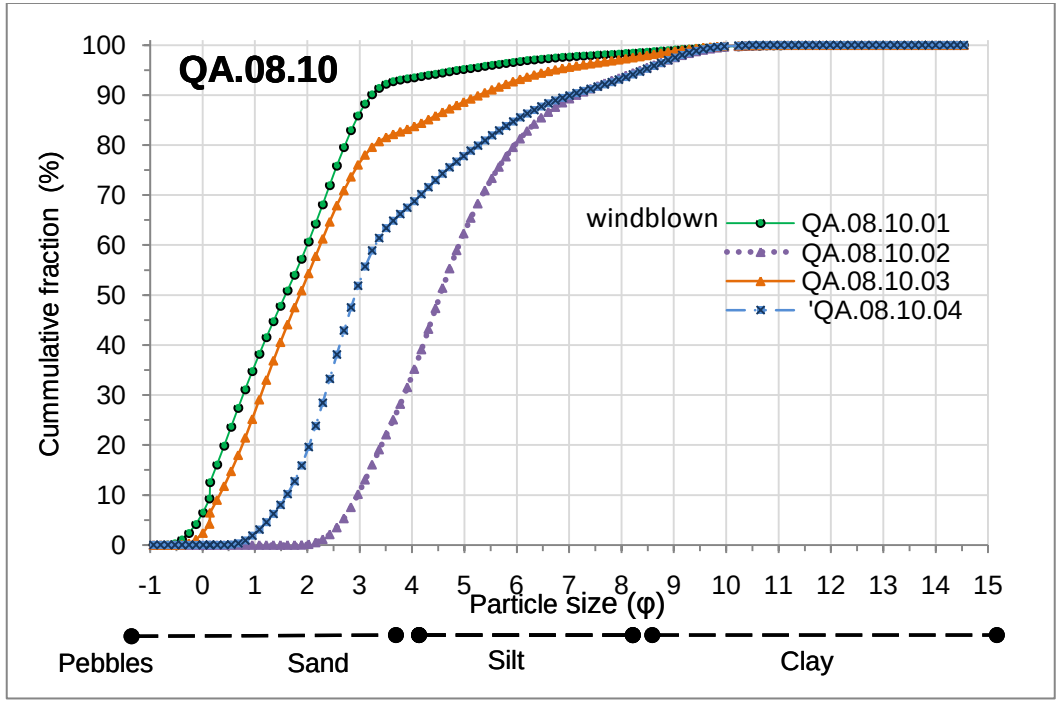

Figure 4.11: Cumulative percentage of the grains size composition at section QA.08.10 of Wadi Al Rimah deposits

Sample	Lab- ID	Depth (m)	De (Gy)	Dose (µGy a-1)	Model used to establish (De)	Age		Alpha (µGy/ka)	Beta (µGy/ka)	Gamma (µGy/ka)	Cosmic (µGy/ka)
						(a)	±				
QA.08.10.01	Shfd09137	1	17.52 ±1.135	1471 ±66	Finte component 1	**11,910**	**0,940**	14 ±4	823 ±62	438 ±20	197 ±10
QA.08.10.03	Shfd09138	.35	8.155 ±0.291	1698 ±74	Finte component 1	**4,800**	**0,270**	19 ±5	938 ±69	533 ±24	209 ±10

Table 4.6: OSL dates obtained from the sedimentary section QA.08.10

4.3 Dune Deposits

4.3.1 Nafud Al Qwarh QA.08.15

Nafud Al Qwarh is located on the western outskirts of the town of Al Qwarh (26°46′12″N - 43°27′97″ E).The Nafud is flanked by Al Qwarh escarpment in the north-west and extends for 10 km from Wadi Al Makhrim to Al Qwarh village (Fig 4.14). Section QA.05.15 is an aeolian deposit that has been exposed as a transverse section through a linear dune. It comprises 10 m of flat low angle curved beds (Fig 4.12) that can be distinguished on the basis of small variations in particle size analysis (Fig 4.13). The sand in the lower Nafud consists of orange (7.5 YR 6/6) fine sands with a small amount of silt. The upper surface in Unit 1 has a thin (< 8 mm) crust-like surface that has dried out; suggesting that sand accumulation stopped for a short a period. Unit 1 gives an age of mid Holocene 3.5 ka (table 4.7). Unit 2 initially starts as low-angled beds that become steeper towards the top. The particles are moderately-sorted fine to medium sands; there is evidence of roots and some specks of charcoal suggesting either naturally burning vegetation or some human activity. An OSL date from a depth 9 m from the top of sand dunes gives an age of 200 year (Table 4.7).

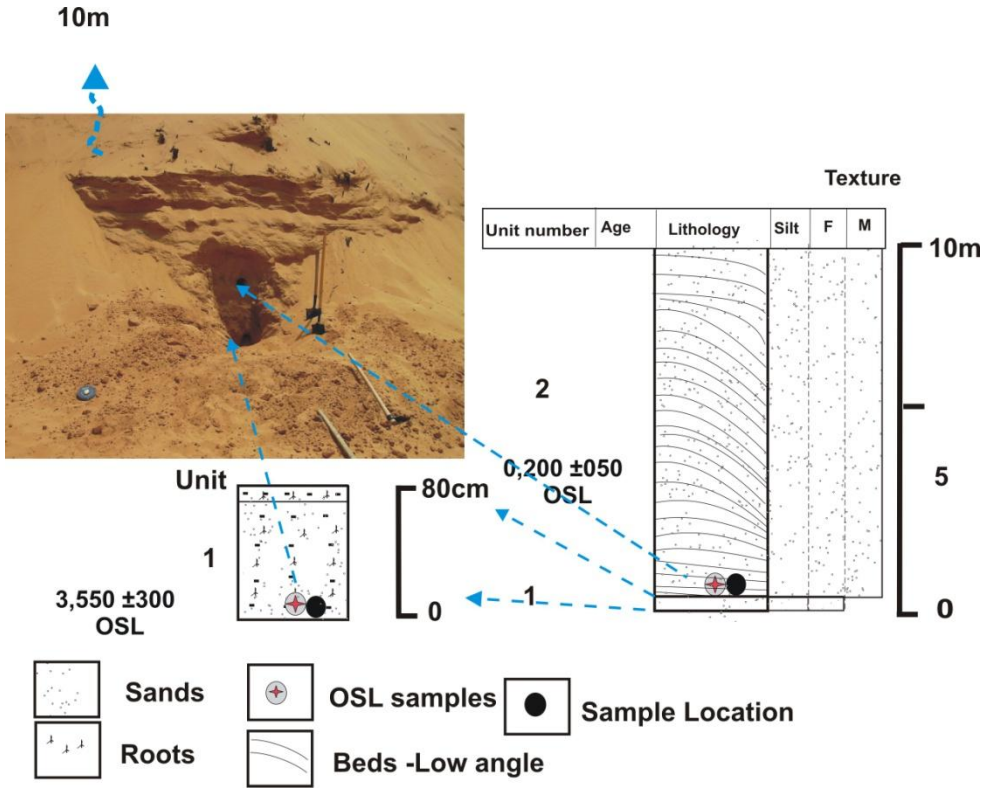

Figure 4.12: Schematic sedimentary log and view of section QA.08.15 where Nafud Al Qwarh lies in the North-west Burydah area. On the stratigraphic log (F) is fine sand, (M) is medium sand.

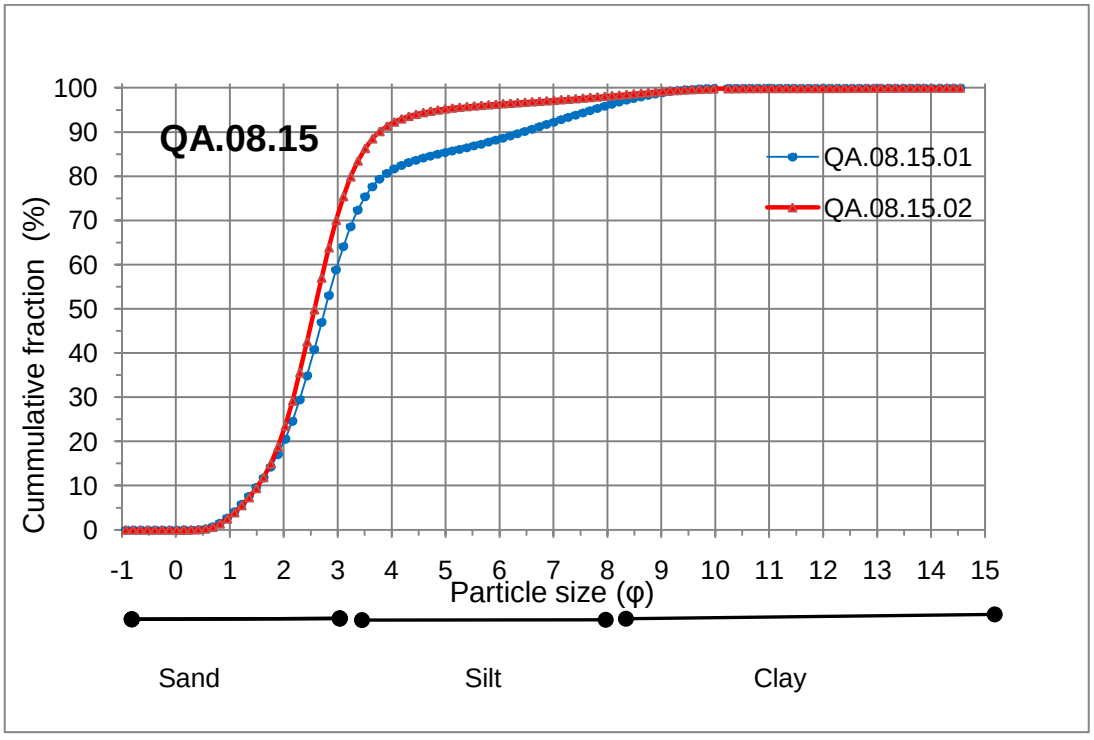

Figure 4.13: Cumulative percentage of the grains size composition at section QA.08.15

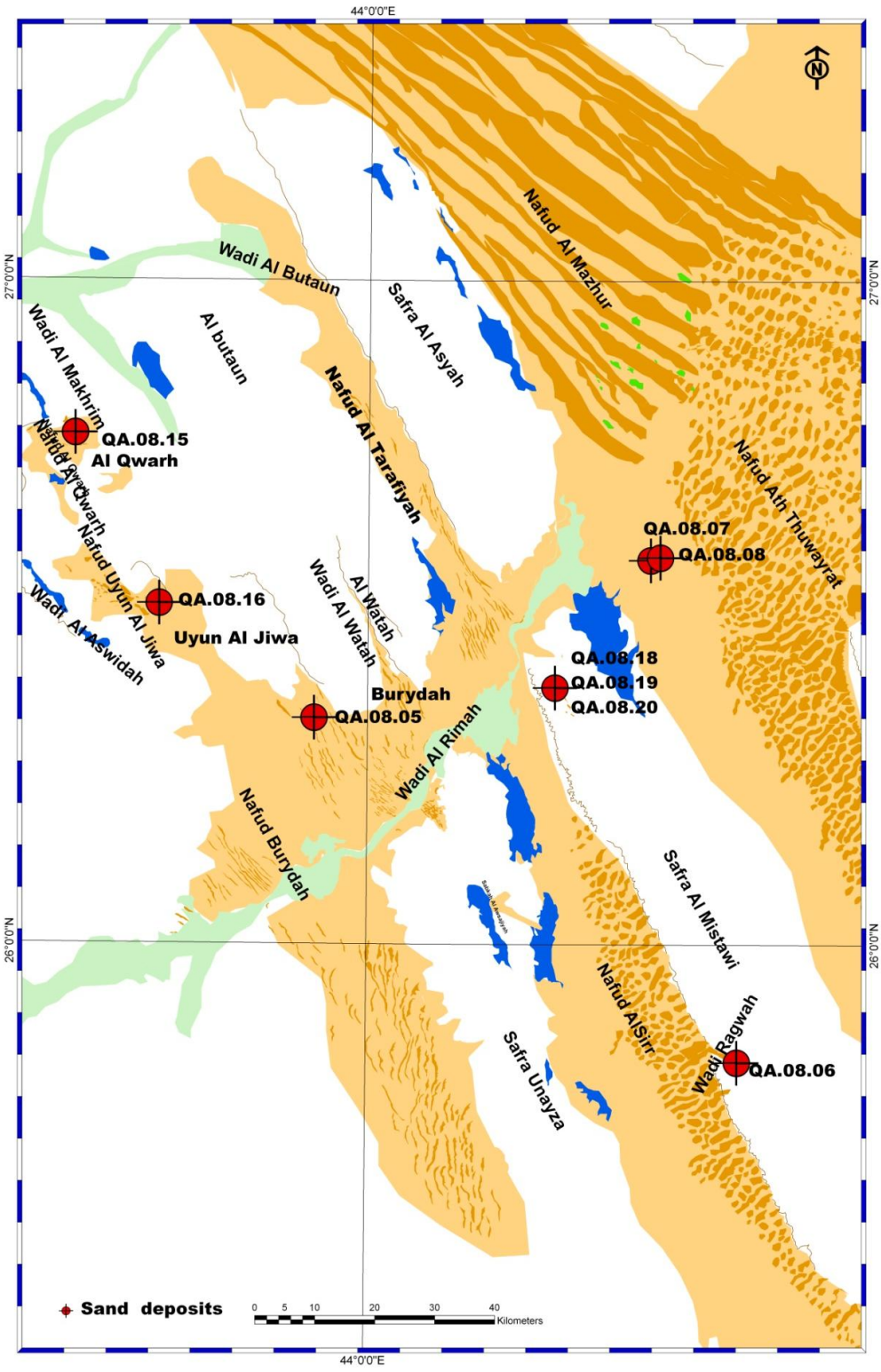

Figure 4.14: The study area, the sample sites of dune deposits are shown as red dots.

Sample	Lab- ID Shfd	Depth (m)	De (Gy)	Dose (µGy a-1)	Model used to establish (De)	Age		Alpha (µGy/ka)	Beta (µGy/ka)	Gamma (µGy/ka)	Cosmic (µGy/ka)
						(a)	±				
QA.08.15.01	10118	10.80	9.57±.66	2696±133	Finte component 1	**3,550**	**300**	27±7	1677±125	925±42	66±3
QA.08.15.02	10115	10	0.48±.12	2387±113	Finte component 1	**0,200**	**050**	26±7	1454±107	840±38	67±3

Table 4.7: OSL dates obtained from the sedimentary sections QA.08.15 in west of study area.

4.3.2 Nafud Uyun Al Jiwa QA.08.16

This Nafud (Fig 4.14) is part of a dune field to the west of Uyun Al Jiwa village (26°30′52″N - 43°36′60″E). Extending for 10 km from Wadi Al Aswidah to the upper flanks of Nafud Burydah. The Nafud form is a small linear dune with an overall east-southerly drift direction (average about 147°) (Fig 4.15). This indicates that most of the sand formed parallel to the usual wind transport direction. The lower sample was collected at a depth of 40 m, (Fig 4.16) and it consists of fine-grained sands, displaying moderate-sorting (Fig 4.17). There are fine laminae in this depth containing fine grains which is indicate the different sorting of grains with a range of mineral types (Fig 4.18). An OSL age from a height of 10m from the base of the section gives an age 9.8 ka indicating an early Holocene age (table 4.8). An age of 4.7 ka was obtained from a height of 40 m from the base of the section which is related to the middle Holocene; this indicates a rough rate of accumulation of sand in this linear dune of 30 m over 5 ka which means about 60 cm per one hundred year. For future research clearly now need more samples between these two ages and may deeper than 40m to examined the sand evolution during the time and investigated if there evidence of LGM.

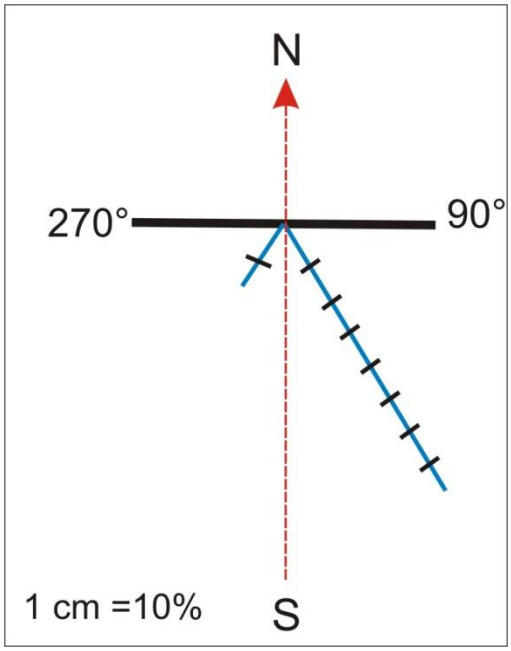

Figure 4.15: The Directions of the dunes' axes in the Nafud Uyun Al Jiwa. The dune axis measured by a random selection of dune direction along Nafud extended and then computed the average of direction as well as the percent of each direction. This methods of data represented in adopted from Mohamed 2002, Al dughairi 2003. (see Appendix 2 to show how the direction computed)

Sample	Lab- ID Shfd	Depth (m)	De (Gy)	Dose (µGy a-1)	Model used to establish (De)	Age		Alpha (µGy/ka)	Beta (µGy/ka)	Gamma (µGy/ka)	Cosmic (µGy/ka)
						(a)	±				
QA.08.16.01	09140	40	9.86±.46	1004±53	Central age	**9,820**	**690**	11±3	635±50	339±16	20±1
QA.08.16.02	09141	10	8.44±.35	1763±81	Central age	**4,790**	**0,300**	23±6	1042±76	632±29	67±3

Table 4.8: OSL dates obtained from the sedimentary sections QA.08.16 in west of study area.

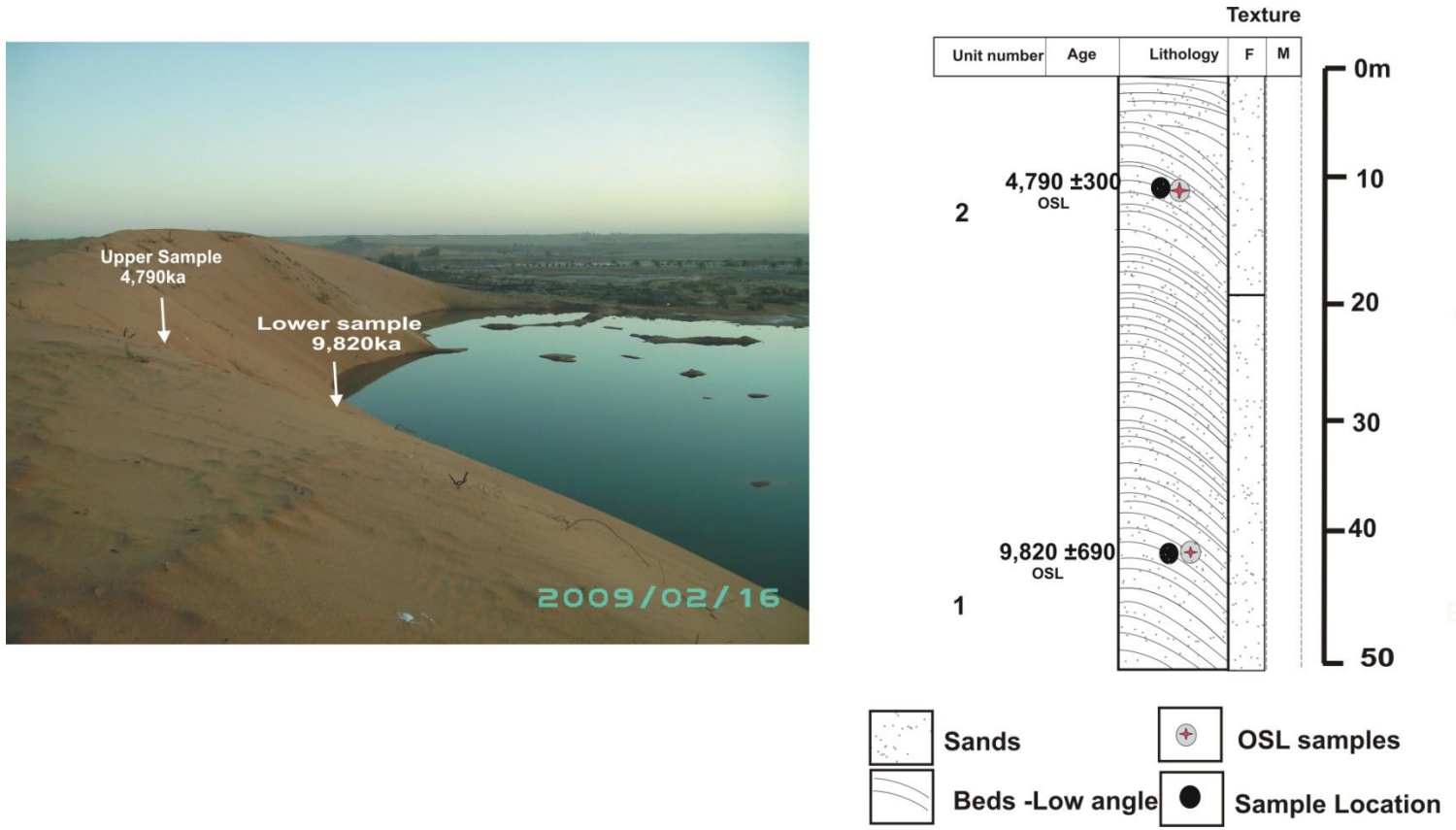

Figure 4.16: Schematic sedimentary log of section QA.08.16 at Nafud Uyun Al Jiwa. On the stratigraphic log (F) is fine sand, (M) is medium sand. In the photo, white arrows show the units location.

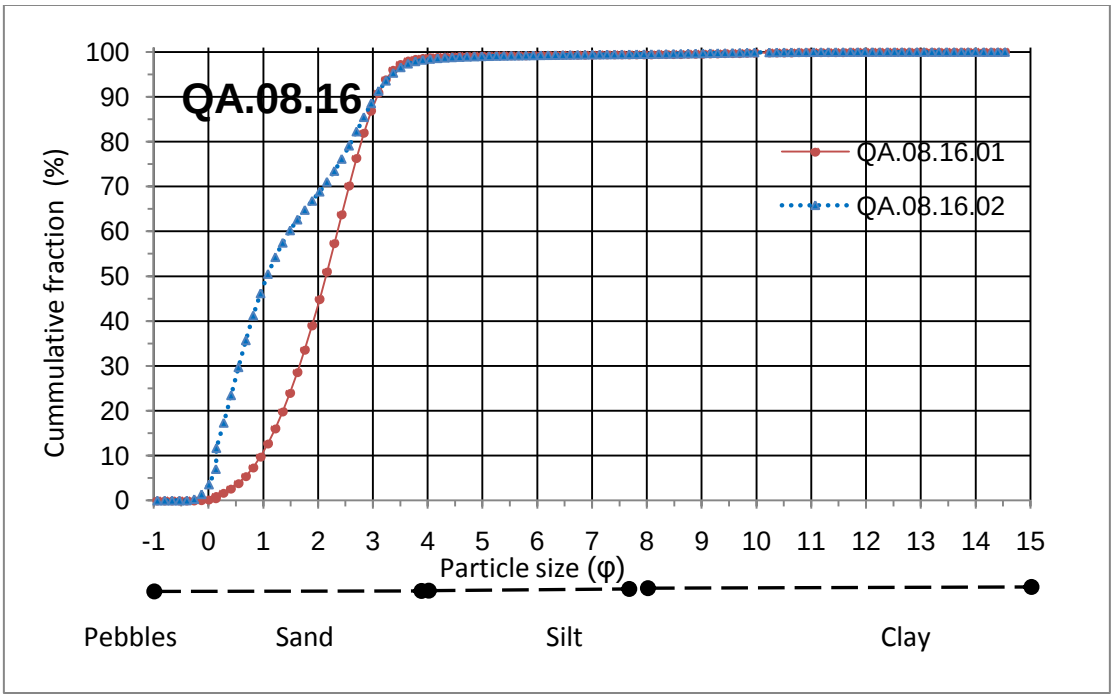

Figure 4.17: Cumulative percentage of the grains size composition at section QA.08.16

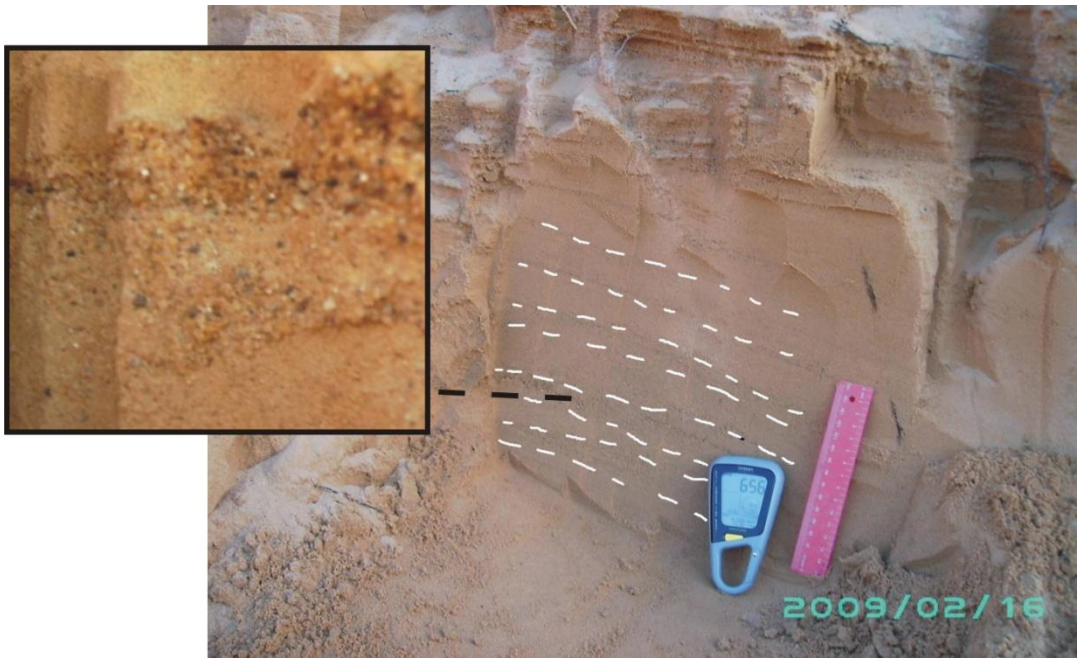

Figure 4.18: View of the sand beds at lower of Nafud Uyun Al Jiwa

4.3.3 Nafud Burydah QA.08.05

The dune field to the west of Burydah city (26°20′33″N - 43°56′03″E), extends for 40 km, from Wadi Al Rimah in the south until it joins the Nafud Uyun Al Jiwa in the North (Fig 4.14). The predominant dune morphology is linear, the axis drift is predominantly towards the south east and south west (direction rose 175° and 210°) (Fig 4.19) which suggests that dunes form in bidirectional winds, at present winds coming from north-westerly in summer (NW) but in winter winds come from the north- east.

The lowermost part of Nafud (Fig 4.20), comprises an aeolianite containing varying amounts of carbonate nodules and abundant rhizoliths running throughout the unit. Grain size analysis shows that this deposit is very fine sand (Fig 4.21). The sands are indurated with increasing levels of cementation towards the top of unit 1B. The cementation pattern suggests that they formed in the capillary fringe above the groundwater table with rapid evaporation at the surface. The age of this deposit is 99.5 ka (table 4.9), and falls into MIS stage 5d according to Willoughby's (2007) definition. Two issues should be note in this unit, dose rats could be changes due to carbonate nodules and rhizoliths and equivalent dos estimates of 157Gy which generlly is still lie close to the estimate of quartz saturation (Table 4.9). Overlying the aeolianite are loose aeolian sands that are laminated with low angle bedding, at the base and the angle increase towards the top. The deposit is dominated by moderately sorted medium sands. An OSL age from the base of the section gives an age of 9.4 ka. This sample was taken just to the east of where 2B & 2C were sampled. This was because workmen had been removing sand from beneath where we sampled and it had slumped. Above the former deposits sample 2B around at a depth of 20m from the base of the section was sampled, it has a Holocene age, of 10.8 ka. An OSL age of 9.5 ka from a height 40 m. The ages from 20m to 40 m suggest that there has been significant aeolian activity in the early Holocene. The dune has accumulated about 20 metres of sand during 1,290 ka, which means 1.55 m per 100 year that suggests high rates of sand accumulation.

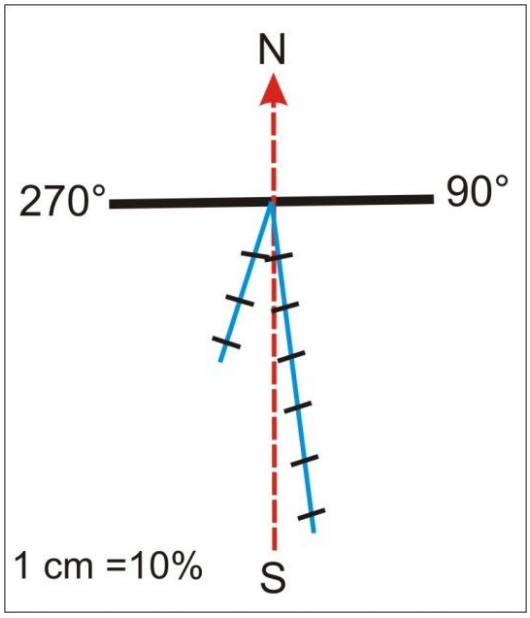

Figure 4.19: The Directions of the dunes' axis in the Nafud Burydah. The dune axis measured by a random selection of Nafud direction along Nafud extended and then computed the average of direction as well as the percent of each direction. This methods of data represented in adopted from Mohamed 2002, Al dughairi 2003. (see Appendix 2 to show how the direction computed)

Sample	Lab- ID Shfd	Depth (m)	De (Gy)	Dose (µGy a-1)	Model used to establish (De)	Age		Alpha (µGy/ka)	Beta (µGy/ka)	Gamma (µGy/ka)	Cosmic (µGy/ka)
						(a)	±				
QA.08.05.01A	10116	53	157,47±9.18	1582±80	Finte component2	**99,520**	**7,690**	18±5	1011±76	534±25	19±1
QA.08.05.02A	09132	51	8.79±.39	936±49	Central age	**9,390**	**650**	9±2	590±47	305±14	32±2
QA.08.05.02B	09133	30	9.526±.377	884±46	Central age	**10,780**	**710**	10±2	555±44	298±14	22±1
QA.08.05.02C	09134	10	10.15±.66	1070±54	Finte component1	**9,490**	**780**	9±2	661±52	333±15	67±3

Table 4.9: OSL dates obtained from the sedimentary sections QA.08.05 in west of study area.

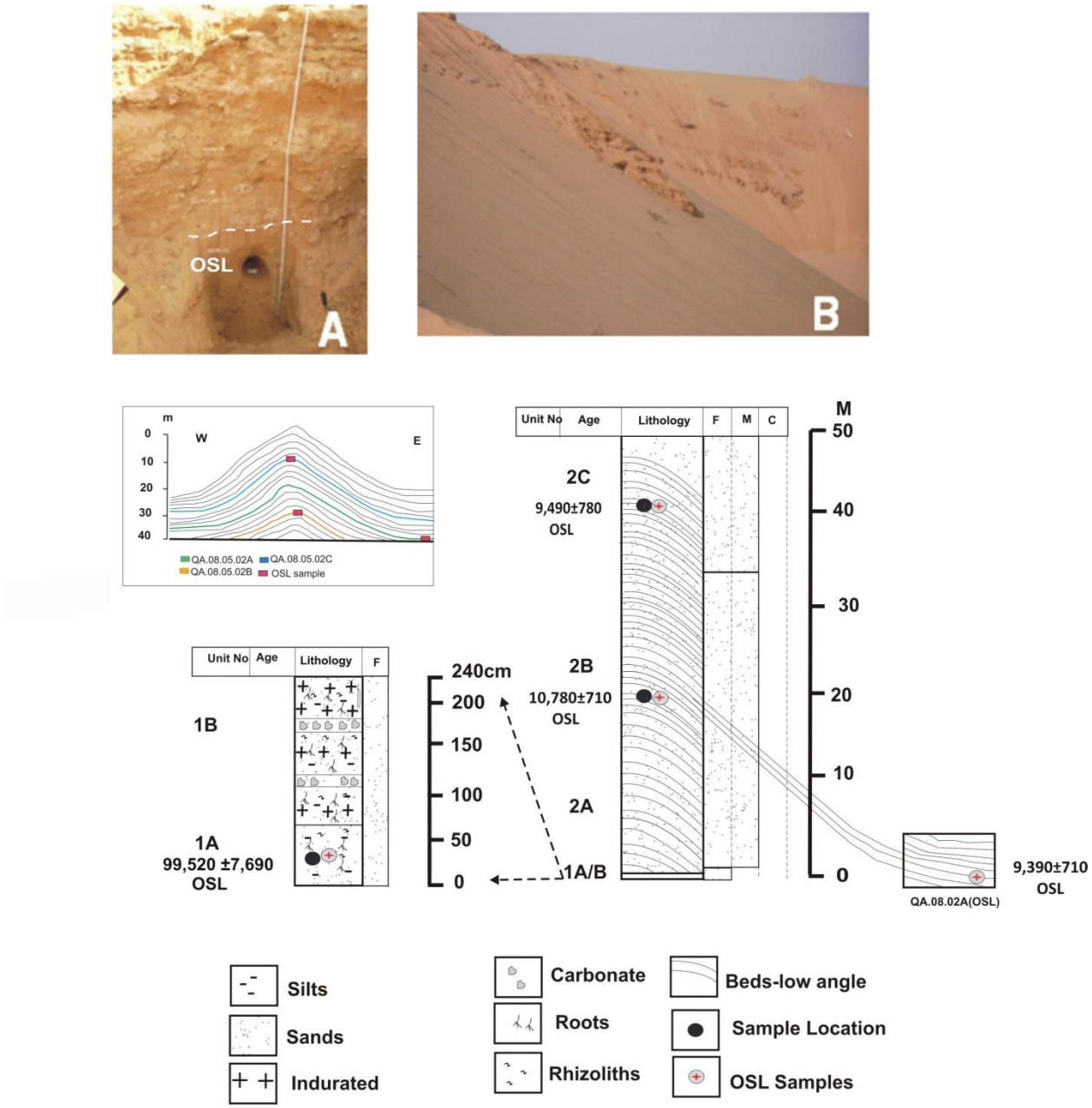

Figure 4.20: Schematic sedimentary log of section QA.08.05 on the Nafud Burydah. (B) is of uppermost Units from QA.08.05.02A; QA.08.05.02B and QA.08.05.02C. (A) is of the lowermost units from QA.08.05.01A and QA.08.05.01B. On the stratigraphic log (F) is fine sand, (M) is medium sand and (C) is coarse sand.

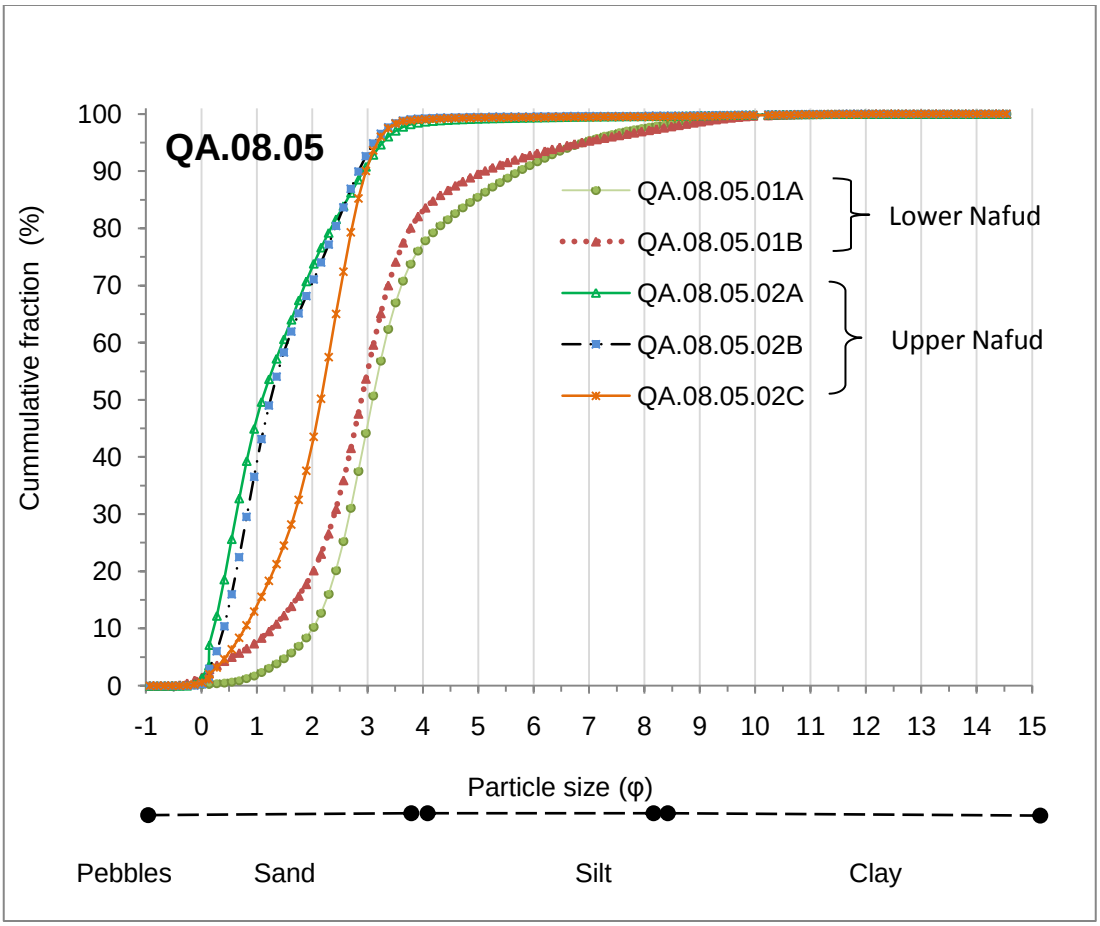

Figure 4.21: Cumulative percentage of the grains size composition at section QA.08.05

4.3.4 Nafud Dasmah within the Nafud Al Thuwayrat site QA.08.07

Section QA.08.07 is situated in the interdunes at the foot of the Nafud Dasmah at the east of the Burydah area within Nafud Al Thuwayrat (26°40′56″N - 44°29′496″E) (Fig 4.14). Two Units have been excavated in the base of the Nafud that can be distinguished on the basis of variation in colour and in amounts of post-depositional carbonate (Fig 4.22). The lower unit is 30 cm thick, contains moderately sorted medium grained sands (Fig 4.23). XRD analysis shows that the deposits is high in quartz (91.4%) with feldspars (4.3%) and a small number of carbonate nodules (<5%) (Appendix 3), but in the field it could be seen that the amounts of carbonate appear to increase in abundance towards the top of the unit. The colour of the sand is light yellow (2.5 YR 7/4). The carbonate nodules perhaps suggest that the water table was close to the surface during sand accumulation as no roots were found in association. The bed above is Unit 2, it shows similar sand size and sorting characteristics but the unit is weakly-cemented. Unit 2 is a sand light grey colour (5 YR 8/2), and in the upper surface of this bed there are rhizoliths, some of which can reach 7 cm in diameter which indicates established vegetation. The abundance of post-depositional carbonate nodules and roots possibly is a result of a rise in regional groundwater levels or slightly higher levels of rainfall.

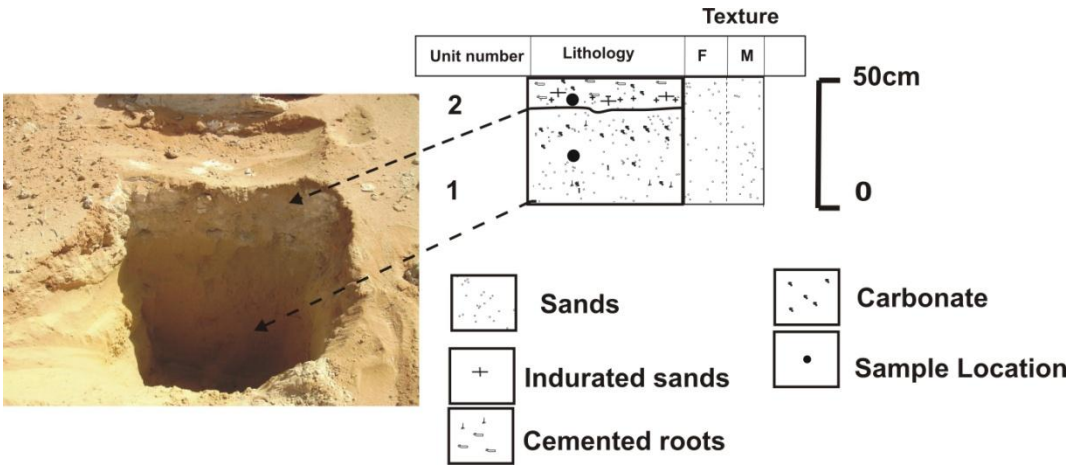

Figure 4.22: Schematic sedimentary log of section QA.08.07 of Nafud Al Thuwayrat. On the stratigraphic log (F) is fine sand, (M) is medium sand.

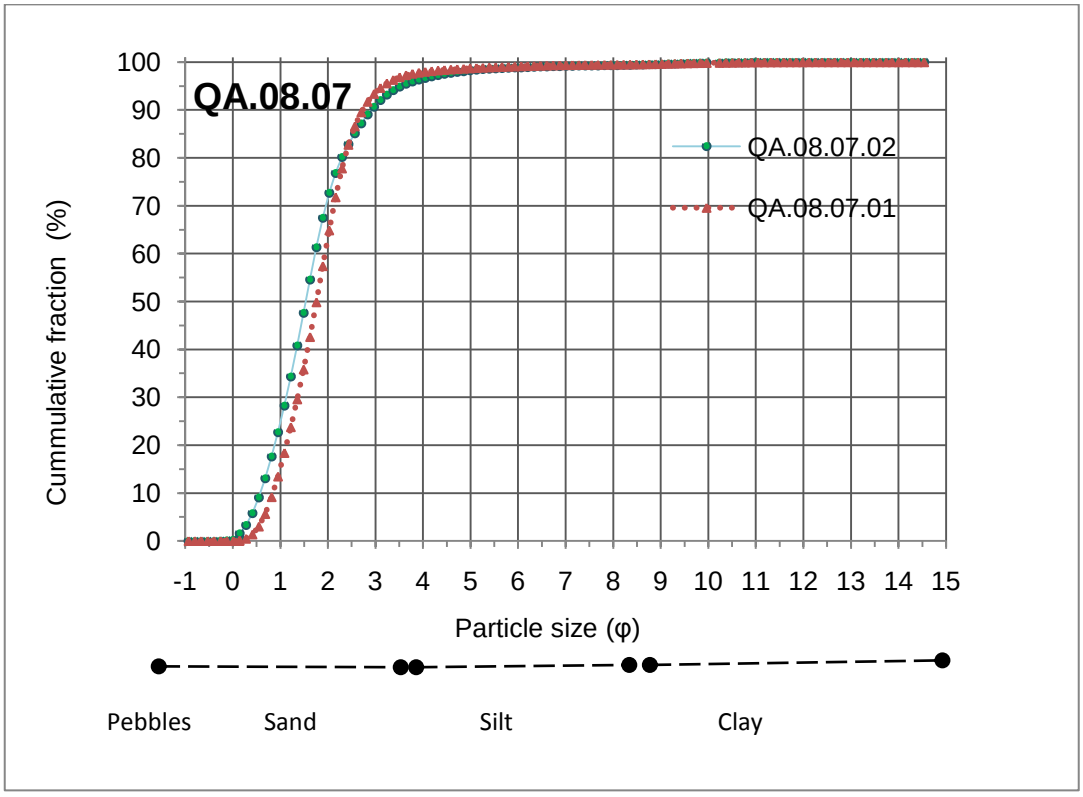

Figure 4.23: Cumulative percentage of the grains size composition at section QA.08.07

4.3.5 Nafud Dasmah within Nafud Al Thuwayrat site QA.08.08

This Nafud is a dune field located in the east of the Burydah area (26°40′49″N - 44°30′26″E). It extends for 180 km from Nafud Al Mazhur, and covers up to 60 km until it joins the Urayq Al Bldan to the south (See Fig 4.14). The width of the vertical sedimentary section is 120 cm and six Units have been identified that can be distinguished on the basis of variations in colour and in post-depositional processes as well as the vegetation features such as roots (Fig. 4.24 & 4.25). All Units contain medium sand-sized grains, except Unit 4 which contains finer grained sands. Unit 1 has a light yellow (2.5 YR 7/4) sand. XRD analysis show most sand grains are quartz (90.7%) and feldspars (4.2%) (making up the whole-rock mineralogy) (Appendix 3). Unit 1 gives an age related to MIS 3 ca. 49.1 ka, according to Willoughby's (2007) definition. Unit 2 is similar to the Unit 1, but here roots and post-depositional carbonate nodules are more abundant. The thin section data show significant increase of post-depositional carbonate development, perhaps associated with a rising water table. Unit 3 is composed of pale orange medium-grained sands with a similar mineralogy to Unit 1. The top of Unit 3 gives a Holocene age of 11.3 ka, (Table 4.10). Unit 4, is pale brown colour (7.5 YR 5/3) and made up of fine-grained sands. Unit 5, is similar to Unit 1 but here there is more evidence of post-depositional carbonate nodules (7%). At the top is Unit 6, which is a layer composed of fine sand, pebbles, and rubble with roots sitting on orangey-yellow sand. The rubble layer comprises cemented indurated lake deposits indicating that the modern day interdunes occasionally get flooded due to changes in the groundwater table.

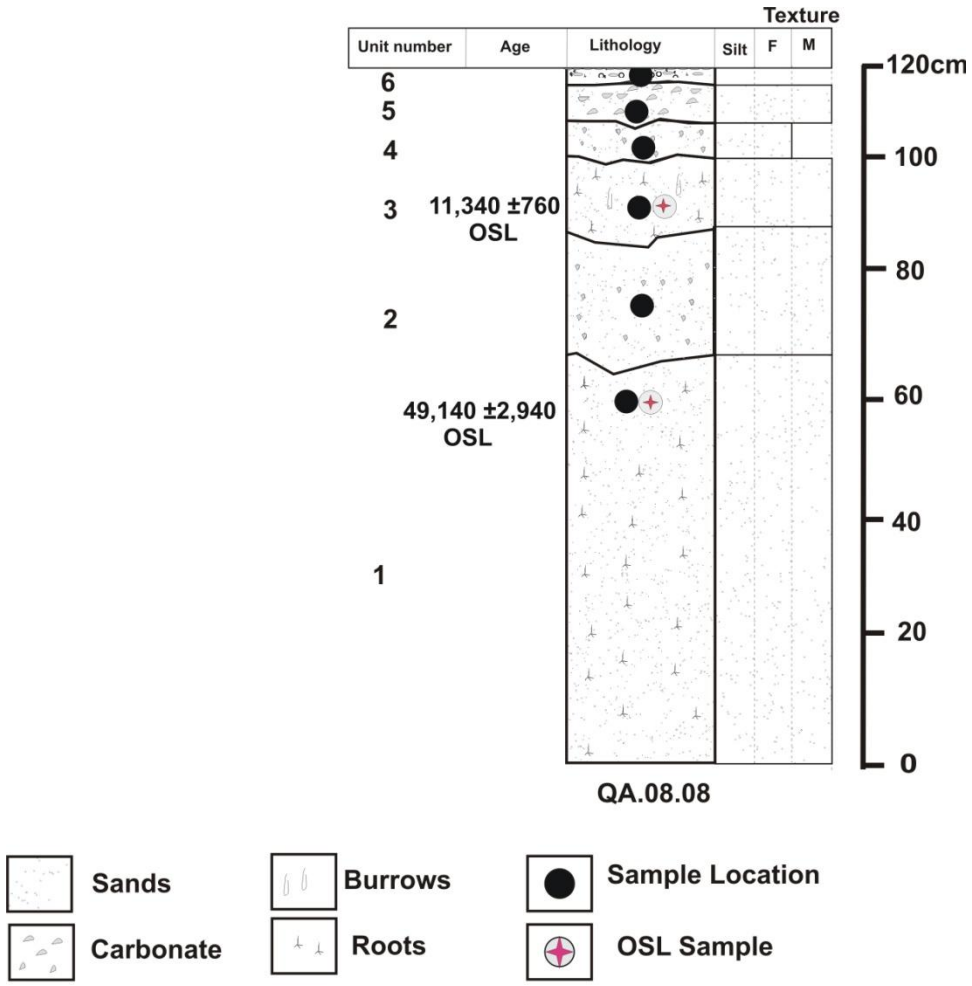

Figure 4.24: Schematic sedimentary log of section QA.08.08 close to Nafud Dasmah in Nafud Thuwayrat. On the stratigraphic log (F) is fine sand, (M) is medium sand.

Sample	Lab- ID	Depth (m)	De (Gy)	Dose (µGy a-1)	Model used to establish (De)	Age		Alpha (µGy/ka)	Beta (µGy/ka)	Gamma (µGy/ka)	Cosmic (µGy/ka)
						(a)	±				
QA.08.08.01	Shfd10111	0.54	52.64±2.2	1071±46	Finte component1	**49,140**	**2,940**	8±2	564±43	297±14	202±10
QA.08.08.03	Shfd10123	0.29	15.62±.79	1377±60	Finte component2	**11,340**	**±0,760**	11±3	748±56	409±19	209±10

Table 4.10: OSL dates obtained from the sedimentary section QA.08.08.

Figure 4.25: View at QA.08.08 01 Nafud Dasmah in Nafud Thuwayrat

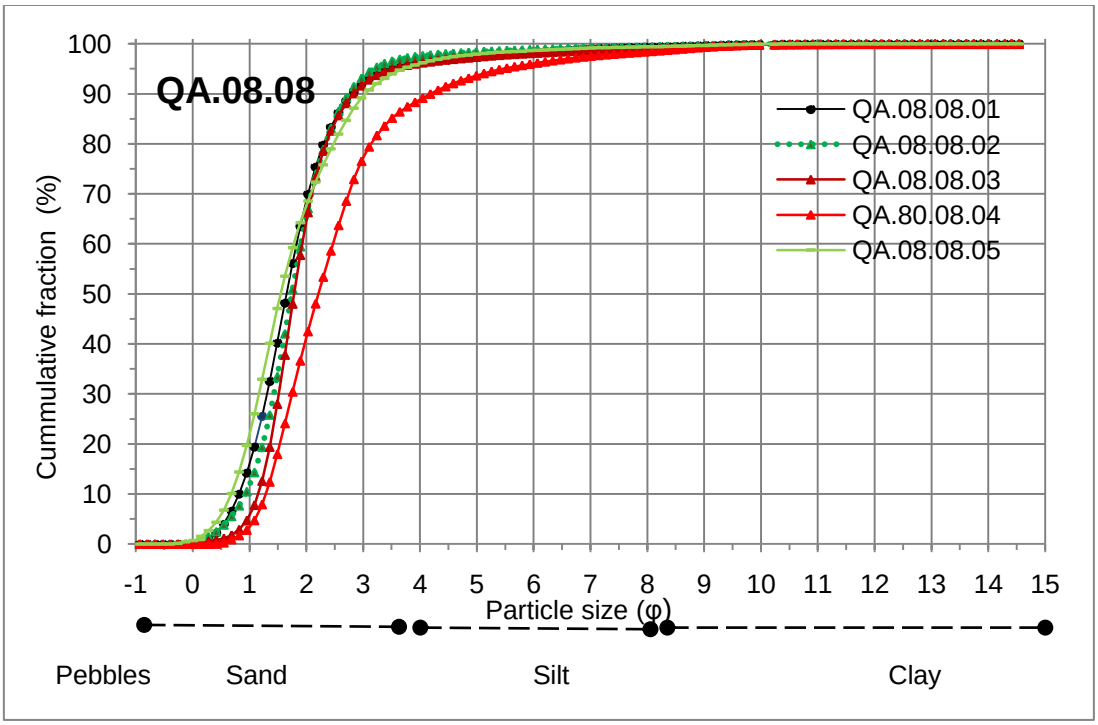

Figure 4.26: Cumulative percentage of the grain size composition at section QA.08.08

4.3.6 Nabkah in the Wadi Ragwah QA.08.06

This Nabkah is located in the south eastern part of the study area at the eastern edge of the Nafud As Sirr (25°49′34″N - 44°34′35E). It is a finger of sand that juts out into the surface of the Safra Al Mistawi. At the end of the finger there is Wadi Ragwah on the eastern margin, by the Am-Hazam village (Fig 4.14). The section is comprised of five units (Fig 4.27).

The Units can be distinguished on the basis of variations in grain size and sorting (Fig 4.28). At the bottom of the section, there is Unit 1, it is a sandy unit consisting of reddish-brown, (5 YR 4/6) poorly-sorted material as some boulders are present on top of the bedrock surface. Unit 2 is similar to the unit described previously but here the colour is pale reddish-brown (5 YR 4/4) and the grains are poorly sorted (when some gravelly horizontal layers are taken into consideration). The XRD analysis data shows an abundance of quartz (68.7%) with feldspars (3.7%), and about (20 %) of post-depositional carbonate (Appendix 3). Unit 3 consists of laminae of sand, with some dispersed carbonate nodules increasing toward the top. An OSL age of this deposit was dated to 5.3 ka, (mid Holocene) (Table 4.11). Unit 4, consists of moderately-sorted medium sands. In Unit 5 the sands are coarse grained and are moderately-sorted. Clear low angled bedding characterises the upper 1.5 m. There are some visible roots in this unit, particularly in the upper 1.2m. An OSL date obtained from the middle unit gives an age of late Holocene (2.1 ka) (Table 4.11).

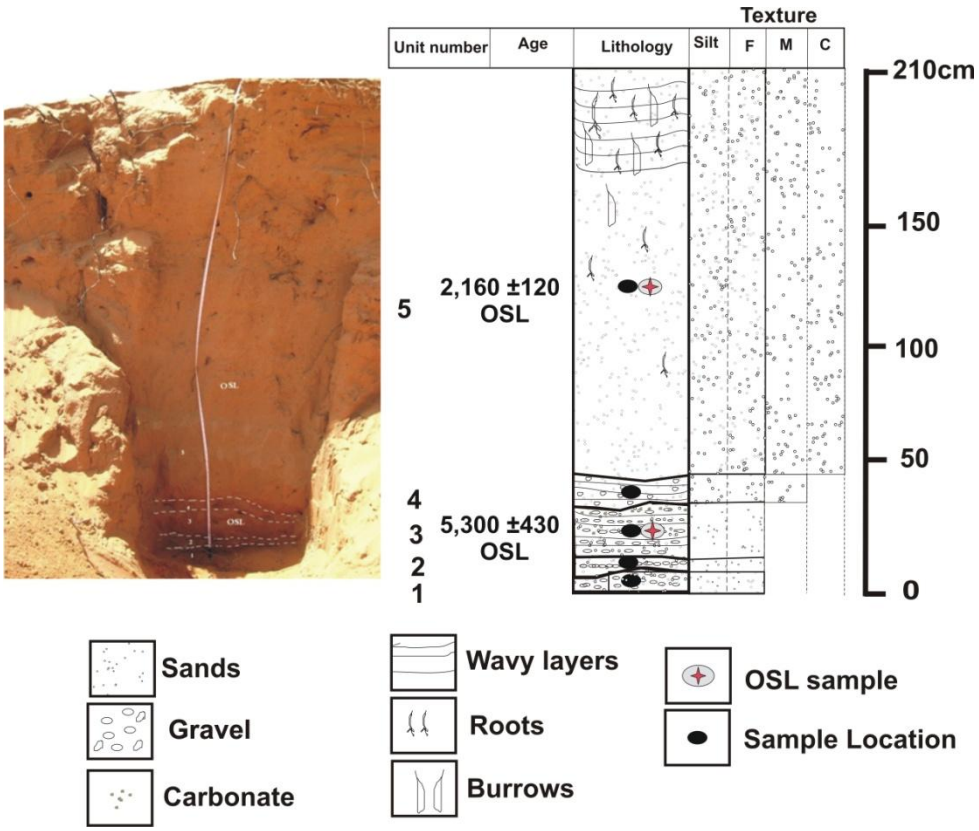

Figure 4.27: Schematic sedimentary log of section QA.08.06 Nabkah in the Wadi Ragwah deposit within Nafud As Sirr. On the stratigraphic log (F) is fine sand, (M) is medium sand and (C) is coarse sand.

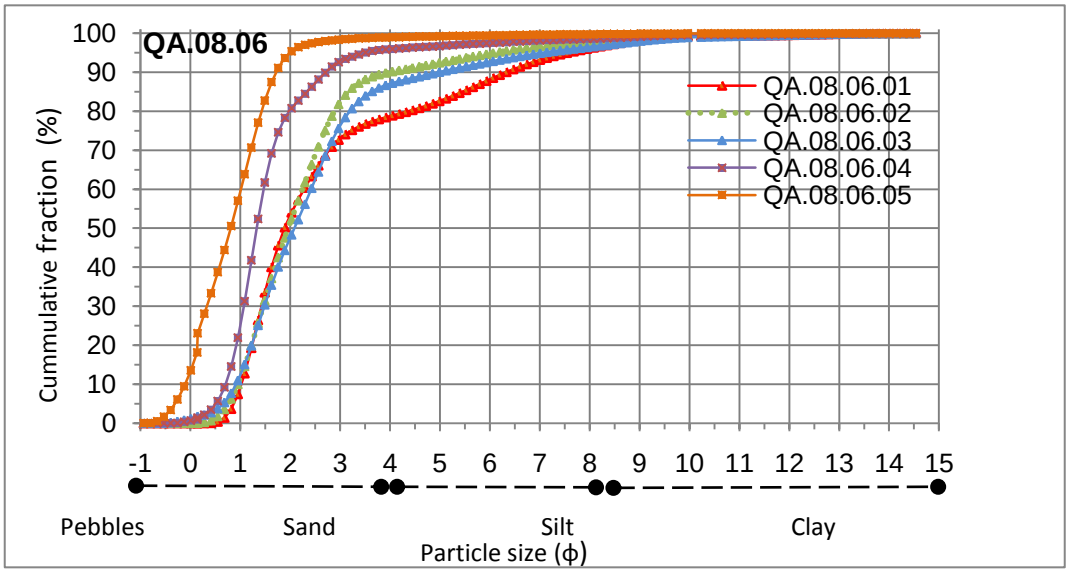

Figure 4.28: Cumulative percentage of the grain size composition at section QA.08.06

Sample	Lab- ID	Depth (m)	De (Gy)	Dose (µGy a-1)	Model used to establish (De)	Age		Alpha (µGy/ka)	Beta (µGy/ka)	Gamma (µGy/ka)	Cosmic (µGy/ka)
						(a)	±				
QA.08.06.03	Shfd10122	2.9	8.37±0.58	1578±68	Finte component2	**5,300**	**0.430**	16±4	880±64	531±24	150±8
QA.08.06.05	Shfd10119	1.4	2.79±.08	1290±59	Finte component1	**2,160**	**0.120**	10±3	724±56	372±17	183±9

Table 4.11: OSL dates obtained from the sedimentary section QA.08.06

4.3.7 Red weathered deposit at Al Mistawi Plateau

Three sedimentary sections located on the east of study area, consist of red sand beds preserved under the surface of the Al Mistawi Plateau. First section QA.08.18 (26°23′18″N - 44°16′30″E) (Fig 4.14) shows a sequence comprising of three units (Fig 4.29 &4.30). In the lower section, Unit 1 is 42cm thick, of bright reddish-brown colour (5 YR 4/8), fine sand moderately-sorted. XRD analysis shows that the deposits are high in quartz (80.1%) as well as rich in post-depositional carbonate (10.8%) may derived run off on the Safra Al Mistawi. The top unconformable contact demonstrates evidence of desiccation cracks. Overlying, is Unit 2, which has a thickness of 40 cm. It is similar to unit below but here the colour is bright reddish-brown (5 YR 6/6) and there is an increase in the clay minerals compared to the unit below (palygorskite-4.2%, chlorite-1.0, kaolin-0.5% and mica species 1.2%). The deposit is very poorly sorted and contains some boulders that are irregularly distributed within the unit and do not seem to display any clear fabric. XRD data shows that the deposits contain less quartz than the unit below (47.1%) and is rich in powdery carbonate (20.9%) as well as gypsum (17.4%), which seems to increase towards the top of the bed. Unit 3 is similar to unit 2, but contains clays (palygorskite-6.2%, chlorite-1.5, kaolinite-1.0% and sub species mica1.8%) (see Appendix 3), perhaps indicating that they are weathering products from nearby Nafud and the wadis in the Safra Al Mistawi.

The second section QA.08.19 is just 30 m to the south of section QA.08.18. It is composed of four sedimentary Units (Fig 4.29 and 4.30). Unit 1, has an average thickness of 10 cm of red (10 R 4/8) colour silts that appear to be very poorly sorted. XRD data shows quartz is the dominant mineral (63.4%) and significant carbonate nodules (calcite-11.9% and dolomite-14.2%), with slight amounts of gypsum (5.2%). Unit 2, is slightly redder than unit below (10 Y 4/6) consisting of fine sands, that are inter-bedded with broken-up few boulders. XRD analysis shows a similar composition to the unit below with a slight increase in the amount of gypsum (18.2%). Unit 3, is reddish-brown (2.5 YR 4/6), and consists of broken-up bedrock with silts and fine-grained sands, poorly-sorted texture. This unit contains of post-depositional carbonate (23%) and bundles of palygorskite clay (6.7%), perhaps a result of weathering of wadi deposit in the Safra Al Mistawi. Unit 4, is

composed of fine sands, silts and clay interbedded with broken-up few boulders. The minerals are similar to the unit below with significant increase in the amount of gypsum (28.8%) (see Appendix 3).

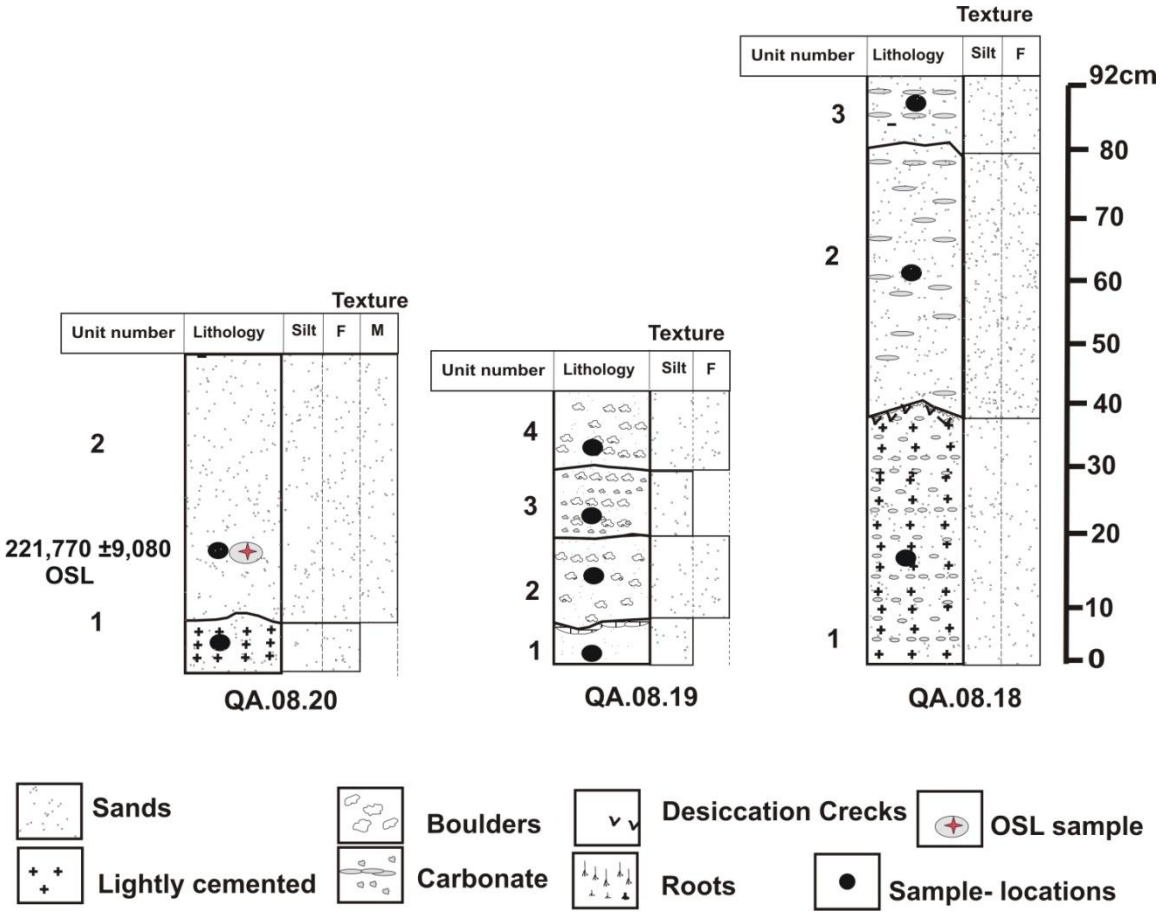

Figure 4.29: Schematic sedimentary log of section QA.08.18; 19 and 20 of the red beds were preserved under the surface of the Al Mistawi Plateau in the east Burydah. On the stratigraphic log (F) is fine sand, (M) is medium sand

Third section QA.08.20, is composed of two sedimentary Units (Fig 4.30B/D). Unit 1 is bright brown colour (5 YR 5/8), consists of lightly-cemented fine-grained sand, and may present the top of the bedrock surface. XRD analysis shows that quartz (55.4%) dominates with post-depositional carbonate nodules of calcite (7.1%) and more dolomite (32.4%). The deposit above is Unit 2, comprising 40 cm of red medium-grained sands (10 R 5/6) (Fig 4.31). XRD analysis shows the dominate mineral is quartz (76.1%) with post-depositional carbonate nodules of calcite (4.3%) and dolomite (13.1%) (see Appendix 3).

An OSL date obtained is 221ka (Table 4.12) MIS stage 7 according to Willoughby's (2007) definition, The equivalent dose of this sample is 207Gy, this rate is high but sill under the eastmite of quartz saturation. The upper surface consist of reg surface (Fig 4.30D). The sand in these sections looks like windblown deposited from nearest linear dunes of Nafuds Al Mazhur and Nafud As Sirr, with l little contribution from the wadis cross the Safra Al Mistawi.

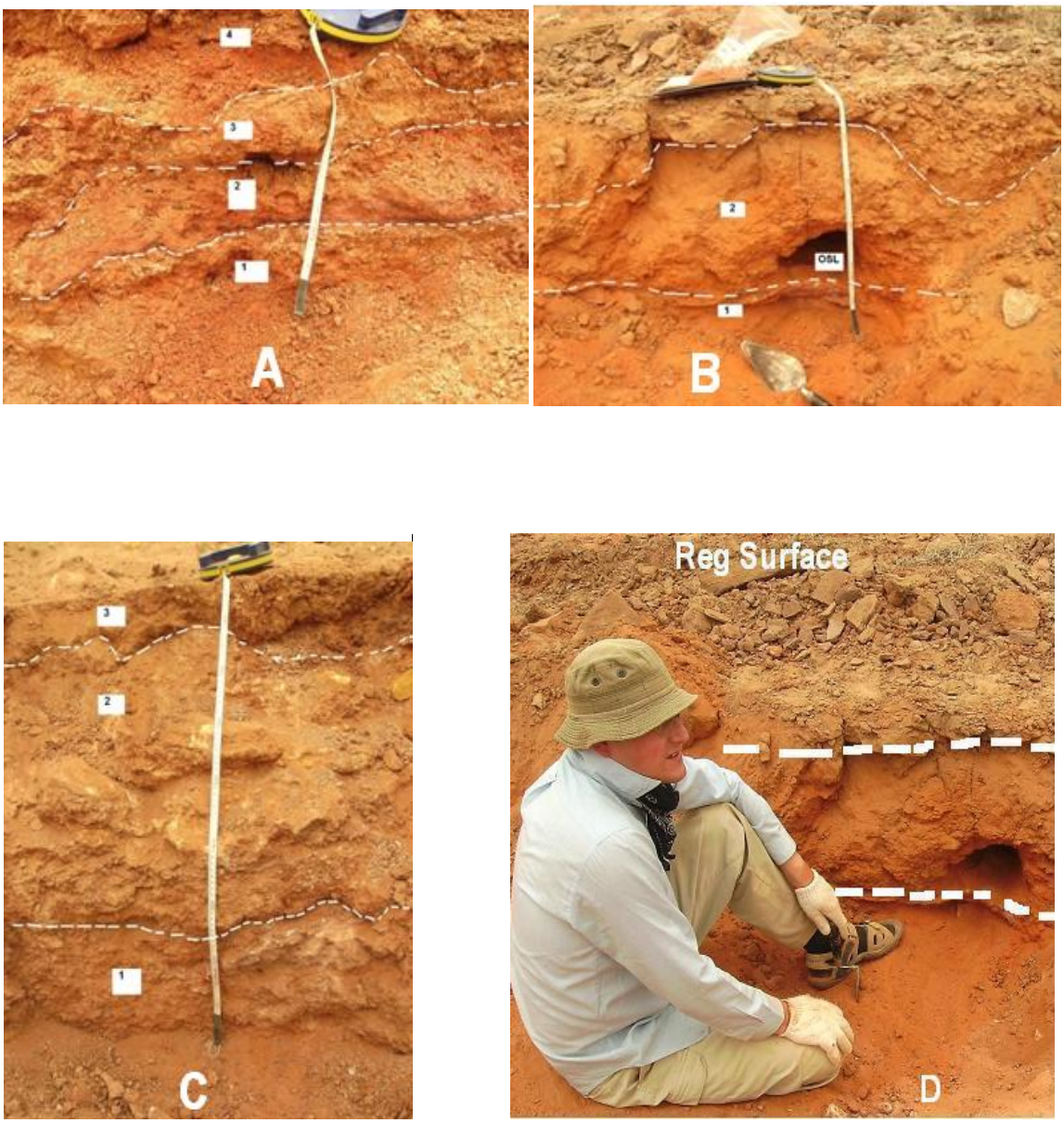

Figure 4.30: View of deposits preserved under the surface of the Al Mistawi Plateau the upper-left A is section QA.08.19 and the upper right B QA.08.20 and the lower C is QA.08.18 and D the Reg surface on the upper unit at section number QA.08.20

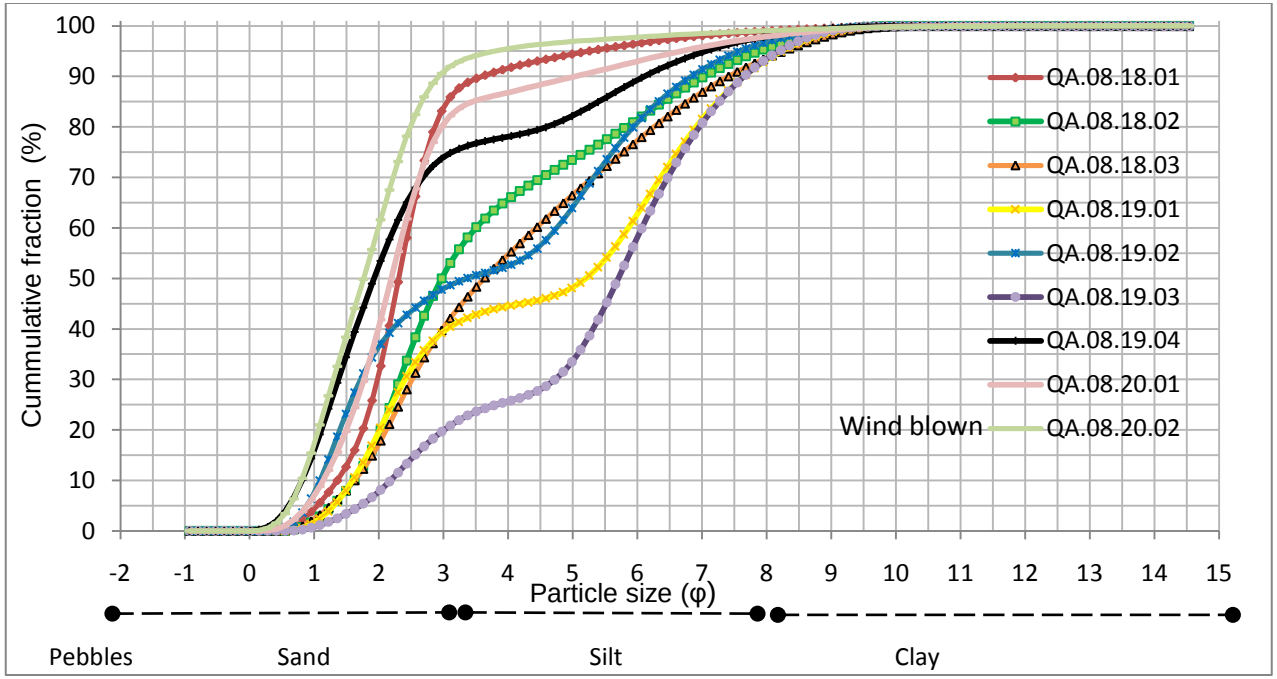

Figure 4.31: Cumulative percentage of the grains size composition at section QA.08.19,18 and 20

Sample	Lab- ID	Depth (m)	De (µGy a^{-1})	Dose (uGy/ka)	Model used to establish (De)	Age		Alpha (µGy/ka)	Beta (µGy/ka)	Gamma (µGy/ka)	Cosmic (µGy/ka)
						(Ka)	±				
QA.08.20.02	Shfd10112	0.40	207.72±3.19	937±36	Central age	**221,770**	**9,0800**	10±3	439±32	278±12	209±10

Table 4.12: OSL dates obtained from the sedimentary section QA.08.20 in west of study area. the mean De is hight but still under the eastmite age.

4.3.8 Dune redness

The examination of redness patterns shows spatial variation in dune colours across the study area, and this method can provide reliable estimates of the concentration of Hematite oxides and other components. The red color appearing in the sand dunes across the Burydah area can be used to infer information about the sand development, evolution of the sand forms and the environmental history; using this method will enable this study to be brought up–to-date, showing the current situation of the Burydah environment.

4.3.8.1 Image classification

The samples collected from linear dunes and dome dunes through the field work showed a random range of colours from each Nafud. The extent of the three dune colour classes derived from the ETM, along with class 4 which is merged from two separate classes (namely exposed bedrock and vegetation) are shown in Figure 4.32.

The strong brown colour, Class1, as represented by training sites at QA.08.25E and the surrounding area, covered the eastern and most south-easterly and northern parts of the Nafud Al Thuwayrat. The dune forms here are considered to be dome dunes. In addition to appearing in parts of the middle linear dunes of the Al Mazhur, strong brown sands also occured in the Nafud As Sirr, in parts of the middle and eastern Nafud (see Fig 4.32). However, strong brown sands also appear to correspond with the upper crest of the narrowing linear dunes in Nafud Al Mazhur. The reddish-yellow colour, class 2, as repersented by sites QA.08.27E and QA.08.27W, are dome and linear dunes and are situated closest to the Wadi Al Rimah channel, as it crosses Nafud Al Thuwaryate and sabkah skirting the western Nafud Al Thuwaryate, As Sirr and Al Mazhur. This class occured in the central and north-eastern Nafud and interdune area within the Nafud Al Mazhur. Class 3, pale yellow sand colour, represented by traning sites at and around QA.08.28E and QA.08.28W, cover the most northerly parts of the Nafud As Sirr and are

linear and dome dunes. In addition the pale yellow sand covers the majority of the parts of the Nafud Al Tarfiyah site, which are linear dunes.

4.3.8.2 Creating the area of interest (AOI)

Classes I, 2 and 3 of the image classification were merged to identify areas that are dunes defining an area of interest (AOI), which has been represented by the Nafud only. This AOI then underwent subsequent image analysis for redness, potential Munsell colour zone and magnetic susceptibility.

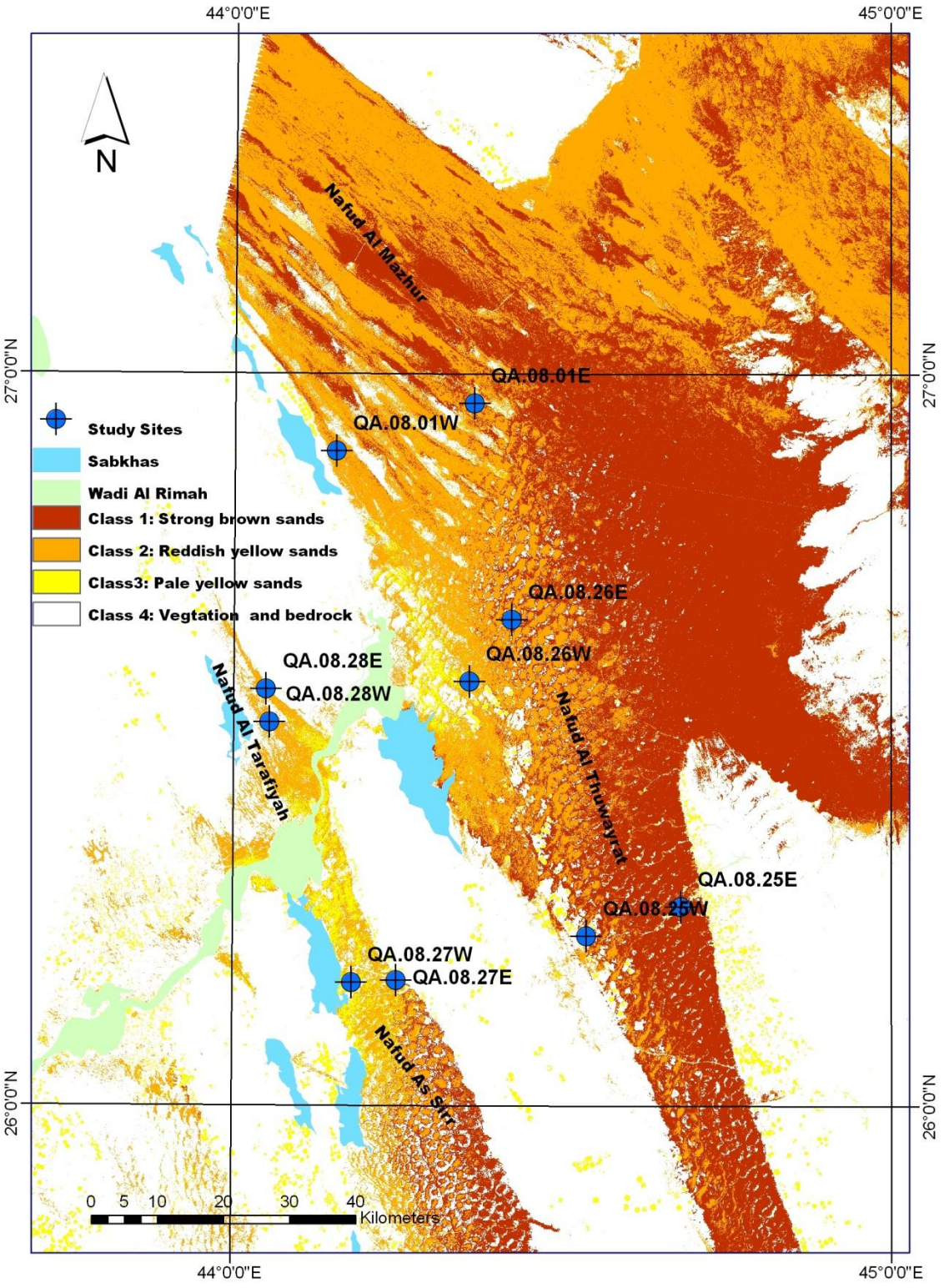

Figure 4.32: The Supervised image classification showing sand colours (classes 1-3) and bedrock plus vegetation (class 4).The area of interest was made from classes1-3.

Nafud	Site	Latitude	Longitude	Munsell Colour chart	Munsell Color	Munsell Redness	ETM Redness	Milton redness		Supervised classes
Al Mazhur	QA.08.01W	26°. 53'.38"N	44°. 26'.07" E	7.5 YR 6/8	Reddish yellow	3.3	0.59	0.54	L	2
	QA.08.01E	26°.57'.34" N	44°. 26'.16"E	7.5 YR 6 /6	Reddish yellow	2.5	0.63	0.68	M	2
Thuwayrat	QA.08.25W	26°.34'.33" N	44°. 30'.11"E	7.5 YR 6/8	Reddish yellow	3.3	0. 63	0.71	M	2
	QA.08.25E	26°.39'.49" N	44°. 29'.32"E	7.5 YR 5/8	Strong brown	4	0.66	0.77	M	1
Thuwayrat	QA.08.26W	26°.13'.54" N	44°. 36'.26"E	7.5 YR 6/6	Reddish yellow	2.5	0.59	0.39	L	2
	QA.08.26E	26°.16'.18" N	44°. 45'.23"E	7.5 YR 6/6	Reddish yellow	2.5	0.63	0.51	L	2
As Sirr	QA.08.27W	26°.10'.06" N	44°. 15'.22"E	7.5 YR 6/6	Reddish yellow	2.5	0.57	0.55	L	2
	QA.08.27E	26°. 10'.15 N	44°. 19'.18"E	7.5 YR 6/6	Reddish yellow	2.5	0.59	0.49	L	2
Al Tarafiyah	QA.08.28W	26°.31'.23" N	44°. 7'.39"E	2.5 YR 7/4	Pale yellow	4.29	0.55	0.86	H	3
	QA.08.28E	26°. 34'.9" N	44°. 7'.33"E	2.5 YR 7/ 4	Pale yellow	4.29	0.55	0.73	M	3

Table 4.13: Summary of: Munsell colour estimates and calculated Munsell redness rating; ETM redness estimates from satellite imagery; Milton Multiband Rediometer redness rating and classification (L: Low redness; M:Medium redness and H:High redness); and the traning class each sample was used for the supervised classification;for all 10 sand sample sites used in the dune redness study.

4.3.8.3 Image redness

The ETM Image redness ratings in the whole study area range between 0.52 and 0.73. The redness rating was greatest to the east of the Nafud Al Thuwayrat, in particular the central Nafud. The redness was found to be least towards the south-west, including Nafud Al Tarafiyah, northern Nafud As Sirr and south-west Nafud Al Mazhur. There is a general gradation in concentration of redness between these two extremes, however dune morphology may control some local redness, such as dome dunes, where the redness appears more concentrated, while the linear dunes appear less concentrated.

ETM Redness values collected from the 10 sample sites ranged between 0.55 and 0.66 (see Table 4.13), and the concentration of redness is greater generally at the eastern sites of Nafud Al Thuwayrat, Al Mazhur and Nafud As Sirr; while the redness rating is generally least at the western sites due to a lower hematite concentration and/or its mixing with some calcite and gypsum. The lowest concentration of redness was associated with the Nafud Al Tarafiyah, as well as in the samples of the eastern Nafud Al Mazhur and northern Nafud As Sirr. This may have been related to an increase in the amount of calcite and gypsum within Nafud and the interdune areas (see Fig 4.33), due to nearby wadi channels and sabkha areas.

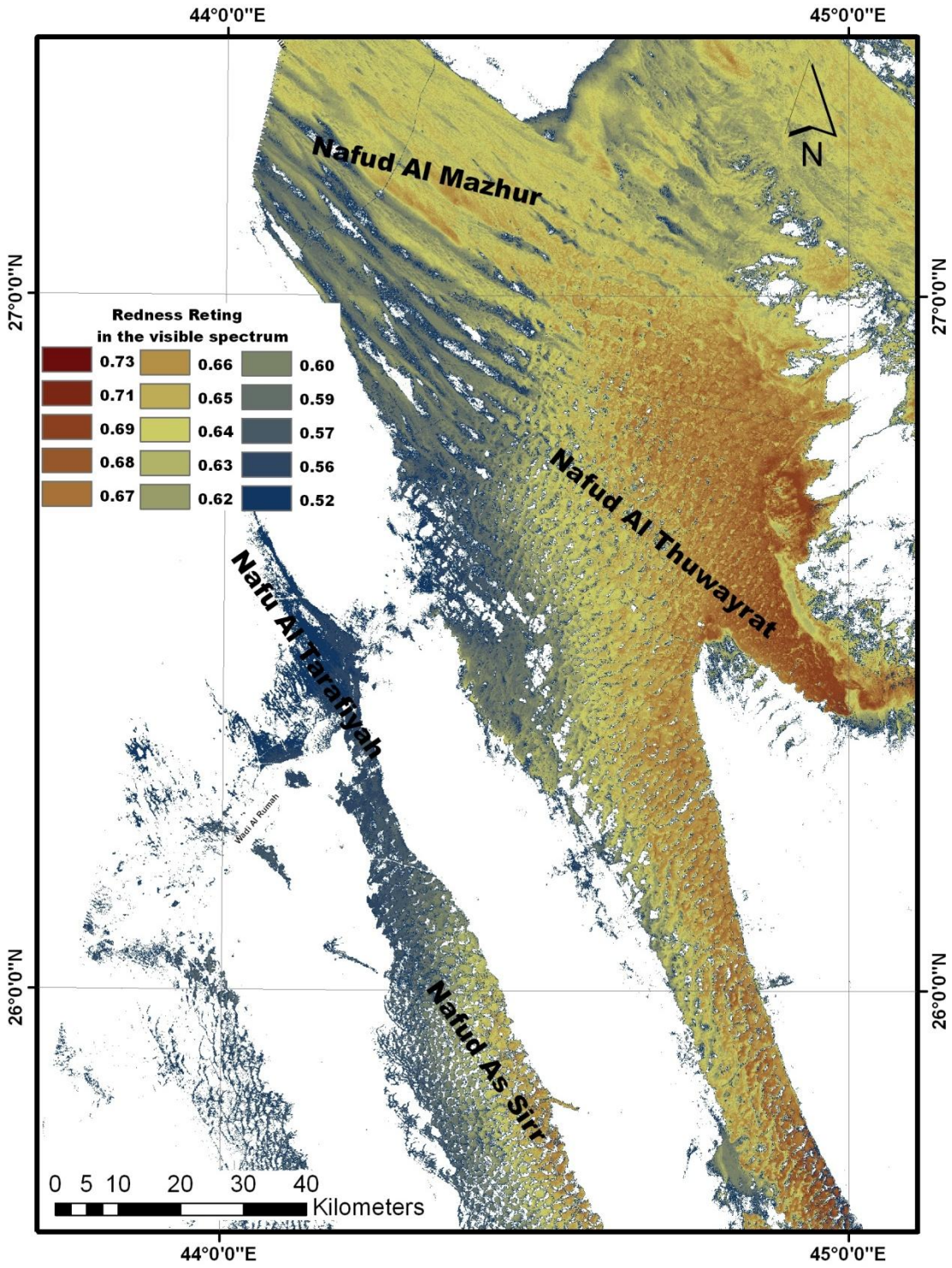

Figure 4.33: Estimate of sand redness derived from the ETM image.

4.3.8.4 Laboratory spectral redness

The redness ratings calculated from the Milton Multiband Radiometer (MMR) instrument showed three levels of spectral redness (see Table 4.13). Low spectral redness ratings of <0.56 were shown in samples QA.08.01W, QA.08.26W, QA.08.26E, QA.08.27W and QA.0827E. Medium spectral redness ratings of 0.56-0.80 were shown in samples QA.08.01E, QA.08.25W, QA.08.25E and QA.08.28E. High spectral redness ratings of >0.80 were found in the QA.08.28W sample. The low spectral redness ratings occurred in the samples from the north-east and west of Nafud Al Thuwayrat and east of Nafud Al Mazhur, as well as in both samples collected from the upper crest of the north-east and north-west of Sirr, which probably correspond to the high levels of hematite. The highest spectral redness ratings occurred in the west of Nafud Al Tarafiyah, which correspond to low levels of hematite. The medium redness rating occurred in the sample sites south-east and south-west of Nafud Al Thuwayrat, the eastern sample of Nafud Al Mazhur and south-east of Nafud Al Tarafiyah. These samples correspond to the intermediate levels of hematite oxides.

The correlation between the Munsell redness ratings and redness derived from the Milton multiband radiometer (MMR) measured in the lab shows good confidence: R^2= 0.65. This relationship can be described by equation 1:

Y= 4.2616 x + 0.519 (1)

Where:
Y = MMR redness
X = Image redness

Generally as Milton redness increases, Munsell colour also increases (see Fig. 4.34). However the interval between Munsell colours is poor and a wide range of Milton redness values can both correspond to the same Munsell colour rating and overlap different Munsell colour ratings; this means that the correlation is not very reliable. Similar results (R^2= 0.88) were found by Bullard and White (2002). They used Munsell redness and MMR redness to estimate the sand colour of the Australia Desert, finding that the Munsell colour estimate is less precise in differentiating between sand colours and that the Milton multiband showed a reliable estimate of sand colour.

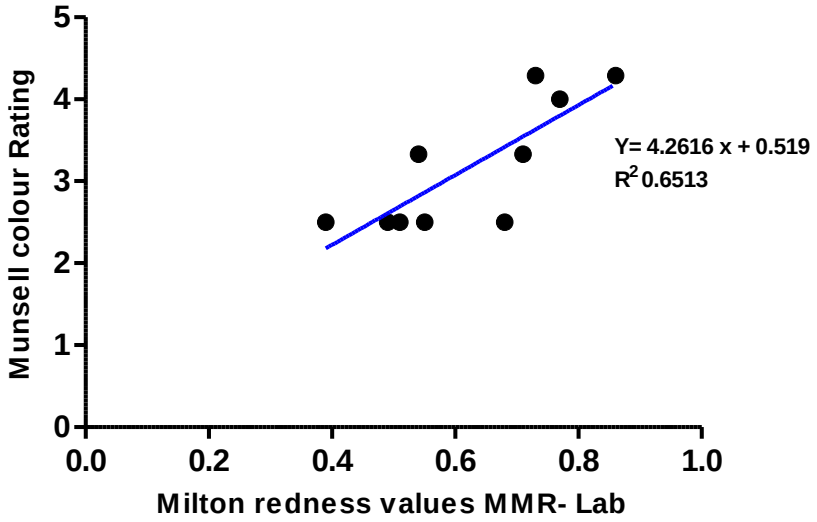

Figure 4.34: Correlation of Munsell redness rating recorded in the field with the sample redness rating derived from (MMR) reflectance values.

The correlation between the redness ratings derived from the Milton radiometer and Landsat ETM redness for the 10 sites showed no correlation: R^2= 0.0006 (see Fig 4.35). Their relationship can be described by equation 2:

Y= 0.0997 x + 0.5629 (2)

Where:

Y = MMR redness

X = Image redness

The low number of sample sites probably contributed to the weak correlation. This lack of correlation was too weak to calibrate the ETM image with laboratory ratings, so the original redness image was used to estimate the Munsell colour and Magnetic Susceptibility. The reason why the correlation is weak may be related to the low number of samples selected, and it is possible that the addition of a greater number of samples from new sample sites would have strengthened this relationship.

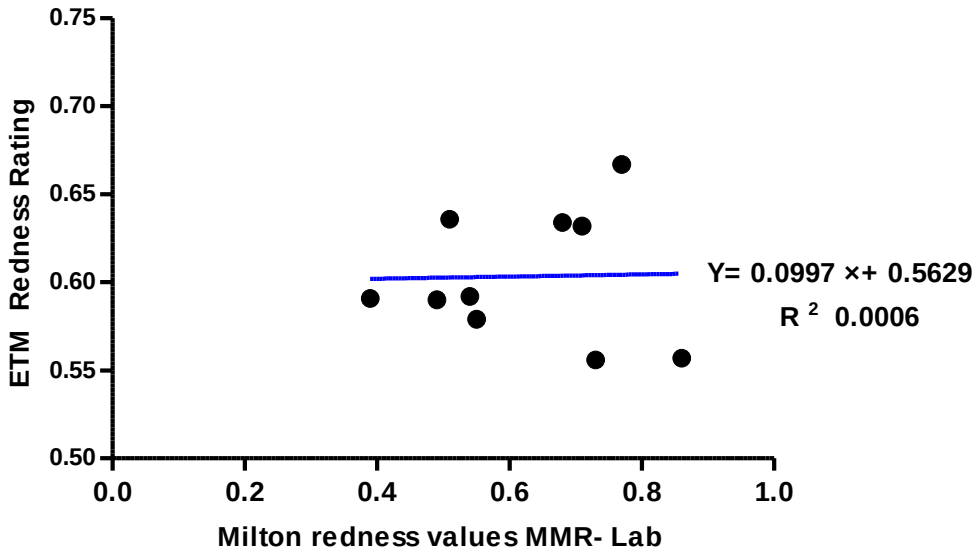

Figure 4.35: Correlation of ETM redness rating with the sample redness calculated from the MMR reflectance values.

4.3.8.5 Potential Munsell colour zones

The results of the conversion of the Munsell colour to the redness rating are presented in Table 4.11 and Figure 3.36. The range extended from 2.5 to 4.9, and the high range occurred in sample QA.08.25E, to the east of the Nafud Al Thuwayrat, along with samples at both sites associated with the Nafud Al Tarafiyah. The low redness rating occurred in the samples to the west of Al Mazhur (QA.08.01W), those to the north-east and west of the Nafud Al Thuwayrat (QA.08.26E, QA.08.26W and QA.08.25W) and the Nafud As Sirr in both sites (QA.08.27E and QA.08.27W).

The colours obtained from the ten field samples are presented in Table 4.13. The reddish-yellow colour occurred in the west and east of the Nafud Al Mazhur; in the south-west of the Nafud Al Thuwayrat and in both the west and north-eastern area of the Nafud Al Thuwayrat. With the exception of the south-east of Nafud Thuwayrat, the colour appeared a strong brown, while in the Nafud As Sirr at both the western and eastern

sites; the reddish colour was shown to be evident. The sand in the Nafud Al Tarafiyah displayed a pale yellow colour.

The correlation between the Munsell colour redness and image redness is described in equation 3 and shown in Fig 4.36; this relationship was used to predict the sand colour (see Fig 3.37):

Y= -4.726 x + 6.0257 (3)

Where:
Y = Munsell redness
X = Image redness

This relationship was used to predict potential Munsell redness in the sand seas. To do this the redness rating was grouped into three colour zones in accordance with the results of the ten sample sites and field knowledge.

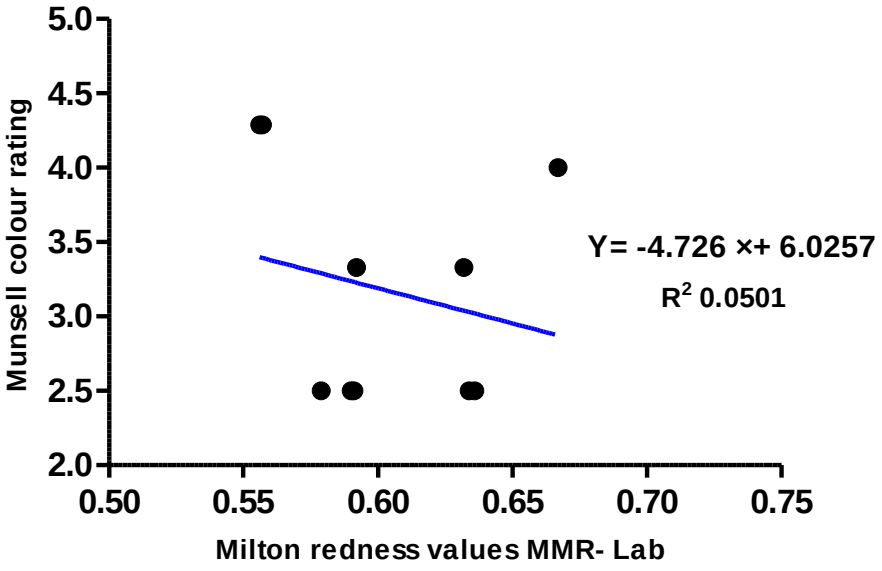

Figure 4.36: Correlation of ETM redness rating with the sample redness calculated from the Munsell colour.

There are three Munsell colours: strong brown, reddish-yellow and pale yellow (see Table 4.11), and colours were allocated to 3 zones. The first zone, a strong brown colour, was only present in one sample, QA.08.25E, which yielded a Munsell redness rating of 4 in accordance to colour class, 7.5 YR 5/8: strong brown colour, located along the eastern end of the Nafud Thuwayrat. The second zone is a reddish-yellow colour that appeared in seven of the samples, yielding a Munsell redness rating of 2.50 and 3.3 (see Table 4.13). These samples were assigned to the colour class 7.5 YR 6/6 and 6/8 in the same chroma, in the Nafud Thuwayrat QA.08.25W, QA.08.26W and QA.08.26E, Nafud As Sirr QA.08.27W and QA.08.27E, and in the Nafud Al Mazhur QA.08.01W and QA.08.01E. The third zone was pale yellow in colour, and there were two samples at the Nafud Al Tarafiyah which yielded a Munsell redness rating of 4.29, assigned to colour class 2.5 YR 7/4.

The potential Munsell colour zone map is represented in Figure 4.37. In general, Zone 1 has shown high concentrations of the strong brown colour which occurred towards the most eastern part of the Nafud, and decreased towards the most western part. The Nafud Al Thuwayrat has associated strong brown coloured sands along both its eastern and southern margins, where they are near to bordered areas of red sandstone rich in oxides (hematite). The Middle Nafud is predominantly strong brown in colour, as such formations contain a greater amount of oxides, with the exception of the interdune areas.

Zone 2 occured in the west Nafud Al Mazhur site and presented a reddish-yellow colour, with the exception of the upper linear dunes along the eastern Nafud where the colour was similar to the Nafud Al Thuwerat as a consequence of border formation. In addition the most easternly margin of the Nafud As Sirr appeared reddish-yellow in colour, while the dunes were less red towards the west. The bordered Sabkah areas were mostly yellow towards the north where dunes contained a greater carbonate content, where the Nafud developed around the wadi Al Rimah channel. Zone 3 occured in most of the Nafud Al Tarafyah and was therefore classifed as a pale yellow colour due to the presence of carbonate-coated quartz grains.

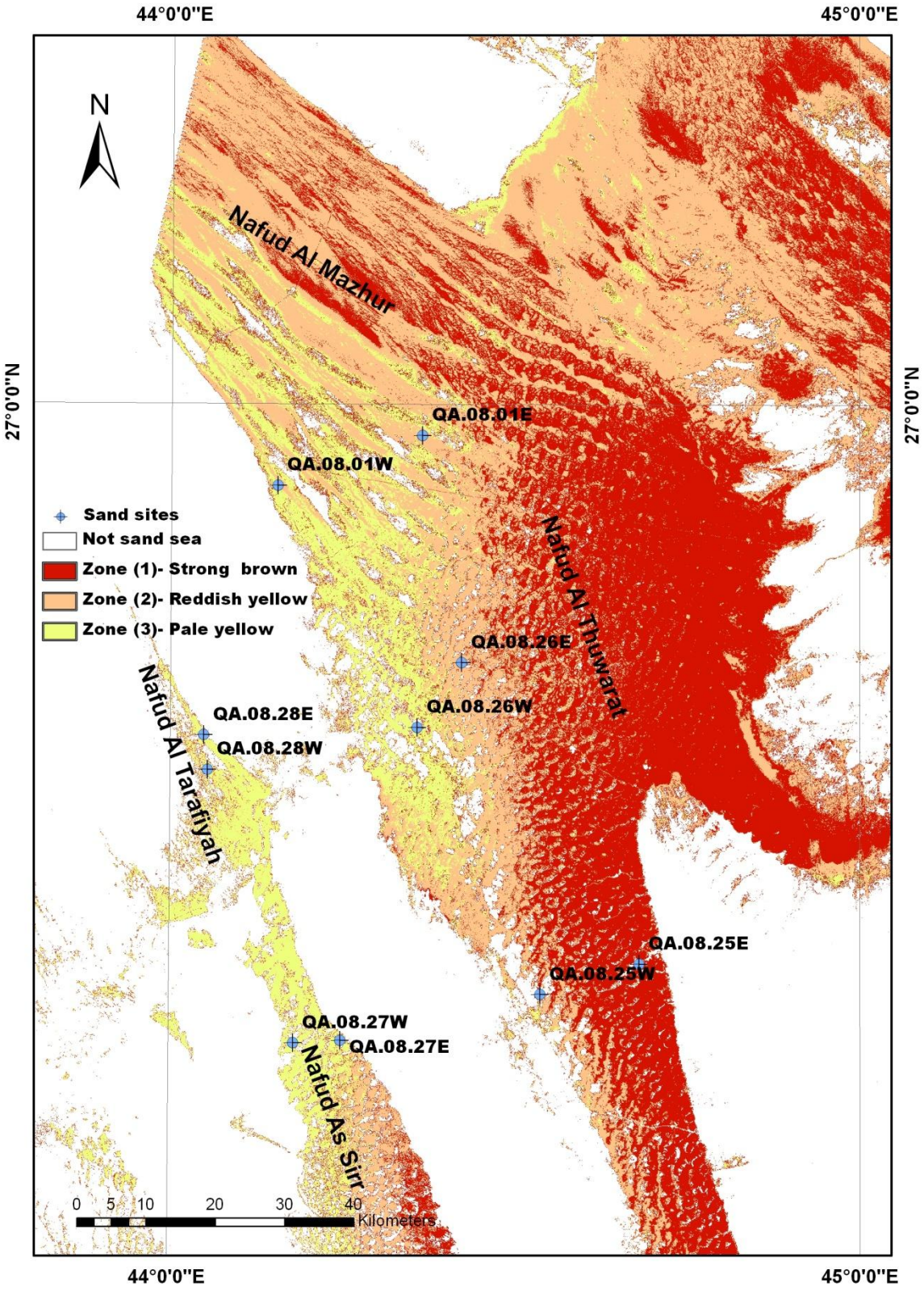

Figure 4.37: The potential munsell colour zones redness. The three zones are: Zone (1) Munsell Hue 7.5 YR 5/8; Zone (2) Munsell Hue 7.5 YR 6/6; Zone (3) Munsell Hue 7.5 YR 7/4. The non-sand areas are excluded using the AOI (e.g. vegetation, water bodies and geological features).

4.3.8.6 Magnetic susceptibility

The magnetic susceptibility results obtained from the ten samples in the sand sea are presented in Table 4.14. Magnetic susceptibility could be grouped into three levels: higher susceptibility between 33 and 52, medium values between 21 and 32 and low values less than 20. The correlation between magnetic susceptibility and ETM redness is described in equation 4. This relationship was used to predict the potential values of magnetic susceptibility in the Nafuds. It is possible that the addition of a greater number of samples from new sample sites would have strengthened this relationship (see Fig 4.38 and Fig 4.39).

y= 81.994x + 16.275 (4)

Where:

Y = magnetic susceptibility.

X = Image redness.

When ETM image redness ratings were high, magnetic susceptibility increased. High values of magnetic susceptibility occurred from the middle to the most easterly part of the Nafud Al Thuwayrat (see Fig 4.38) towards the Jabal Tuwayq. There were high magnetic values (33-55) along the eastern edges of Nafud As Sirr towards the Safra Al Mistawi, which decreased towards the northern end of the Nafud. The medium values (21-32) of magnetic susceptibility were generally graded between the extremes of high and low values; however, there was some influence of dune morphology which presented small transition values of magnetic susceptibility. The low magnetic susceptibility values (less than 20) generally occurred in the Nafud Al Tarafiyah and in some parts of the western margin of the Nafud Al Mazhur, as well as in the north-western part of the Nafud As Sirr. These magnetic values were low because the sand contained few iron oxides. The Nafud Al Tarafiyah was located within and near to the sabkhah, which meant that the sand contained more carbonate and fewer iron oxides.

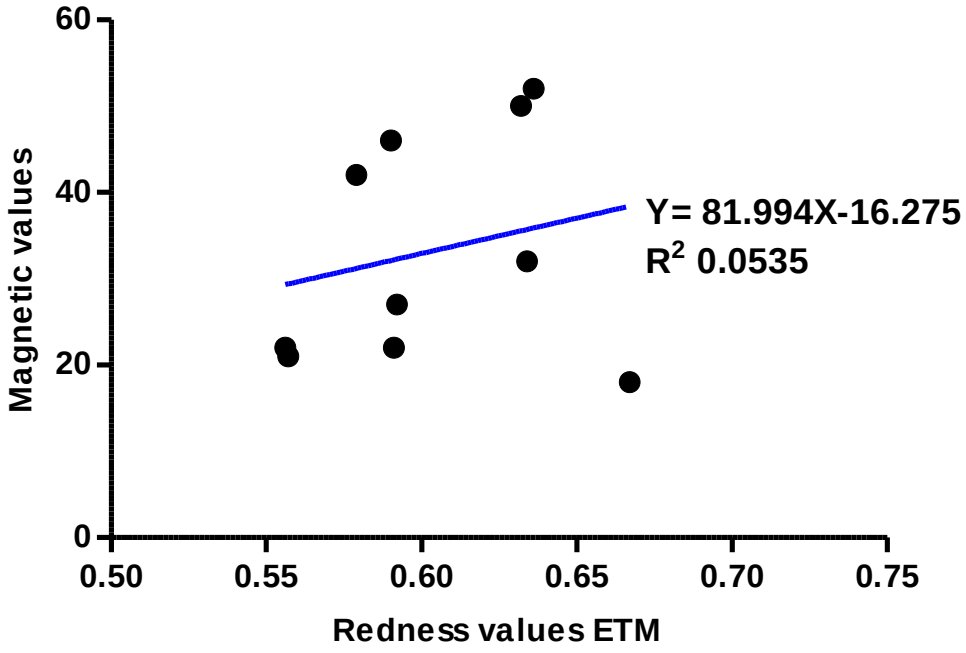

Figure 4.38: Correlation of ETM redness rating with magnetic susceptibility in the sand seas.

Lab- ID	Sites ID	LFsus	Category
Leice1.2008	QA.08.01 E	32	M
Leice 2.2008	QA.08.01 W	27	M
Leice 3.2008	QA.08.25 E	18	L
Leice 4.2008	QA.08.25 W	50	H
Leice 5.2008	QA.08.26E	52	H
Leice 6.2008	QA.08.26W	22	M
Leice 7.2008	QA 08 27E	46	H
Leice 8.2008	QA 08 27W	42	H
Leice 9.2008	QA.08.28E	22	M
Leice 10.2008	QA.08.28W	21	M

Table 4.14: Results of the magnetic susceptibility tests, using a sensor MS2B with a range of x10, in container volume 10ml. LFsus=unit SI x10-8.

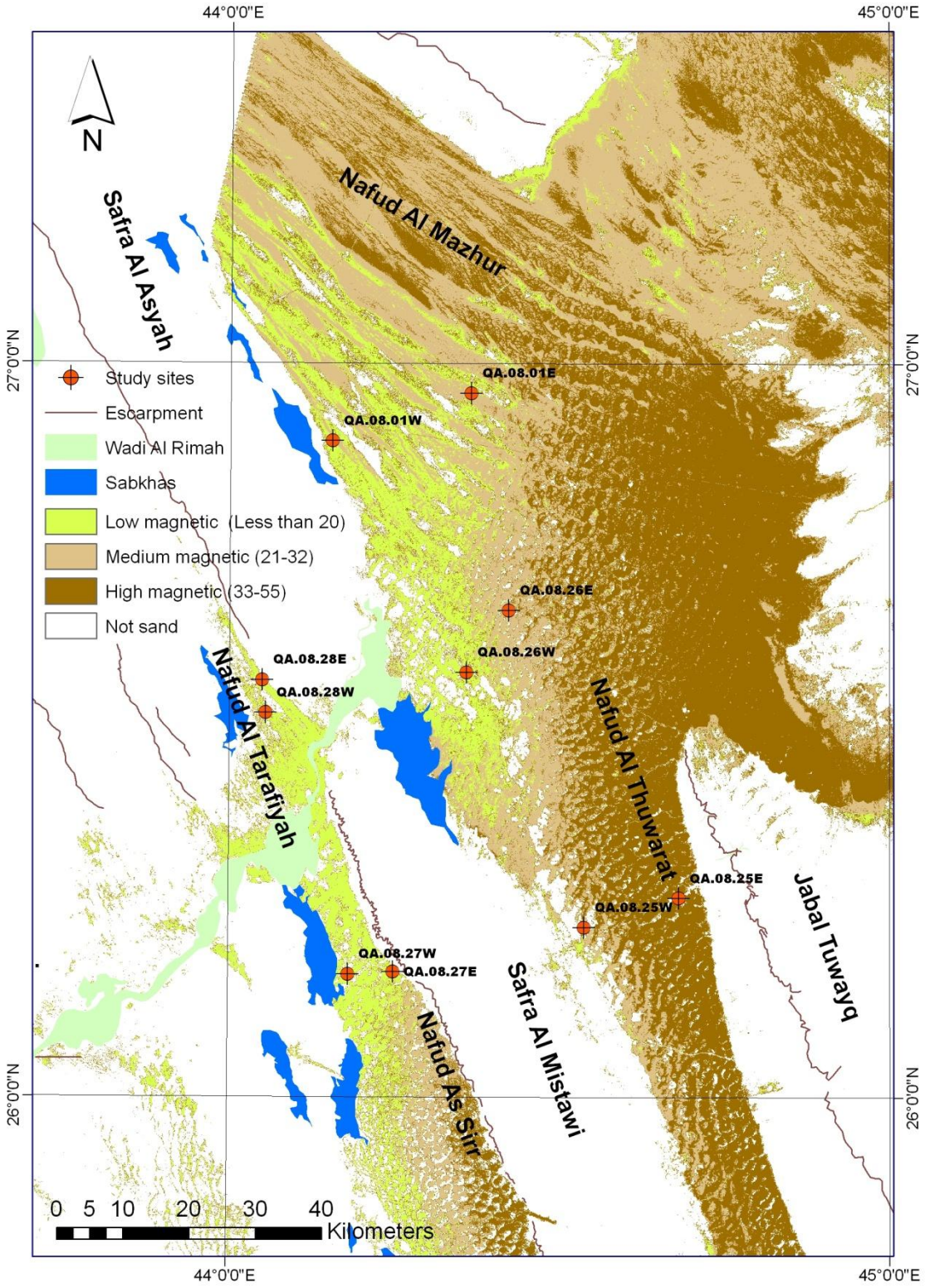

Figure 4.39: Estimate of magnetic susceptibility values in the sand seas, using regression analysis between magnetic susceptibility of samples and image redness (3x3windows) on the sample sites. Low, medium and high magnetic susceptibility limits were chosen to match sand colour classes in Figure 4.32

4.4 Lake Deposits

Lake deposits were located in the interdune area within the Nafud Al Mazhur, close to the city of Al Asyah (Fig 4.40). Two sections have been excavated:

4.4.1 Evaporite deposits within Nafud Al Thuwayrat site QA.08.11

Section QA.08.11 was located under a linear dune of the Nafud Al Mazhur (26°52′48″N – 44°22′25″E) (Fig 4.41) and was exposed in an interdune. The section was composed of 4 sedimentary Units (Fig 4.40). Unit 1 measured 15 cm and consisted clays comprised of palygorskite (14.7%) which forms under arid conditions, mica species (18%) with minor amounts of smectite (2.6%); chlorite (4.2%) and kaolinite (2%). Gypsum nodules (43.1%) dominate (Appendix 3). There was evidence of minor root development and the colour was greenish grey (10 Y 5/1) as result of the mix of the minerals present. Overlying this Unit 2, was another evaporite deposit, white in colour (2.5 Y 8/1), and consisted of vertical columns of celestine crystals. Throughout these vertical columns there were minor amounts of windblown fine sands that increased in abundance towards the top.

Unit 3 represented a change in facies with an increase in the amount of sand in the interdune area. There was an interruption in the evaporite formation and 3cm of aeolian sands were deposited. Unit 4 represented a return to gypsum precipitation and evaporation processes in the interdune area of the Nafud al Mazhur dominating over wind activity.

The geochemical date from the evaporite indicates that there was a change in the abundance from calcium in the waters to form gypsum in Units 1 and 4 to strontium in Unit 2 to allow the precipitation of celestine.

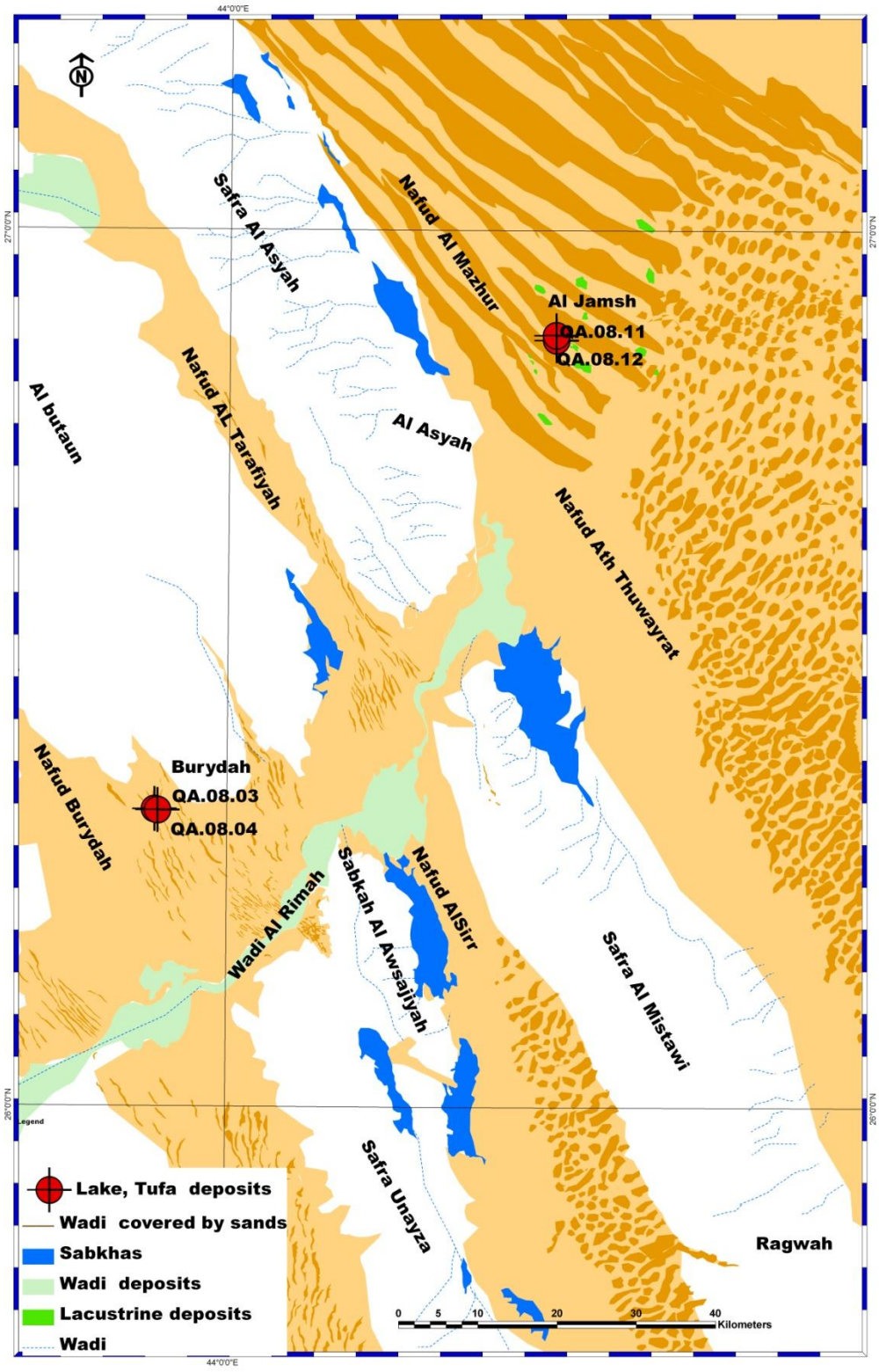

Figure 4.40: Lake localities in the context of the whole study area. Sampling points shown as red dots.

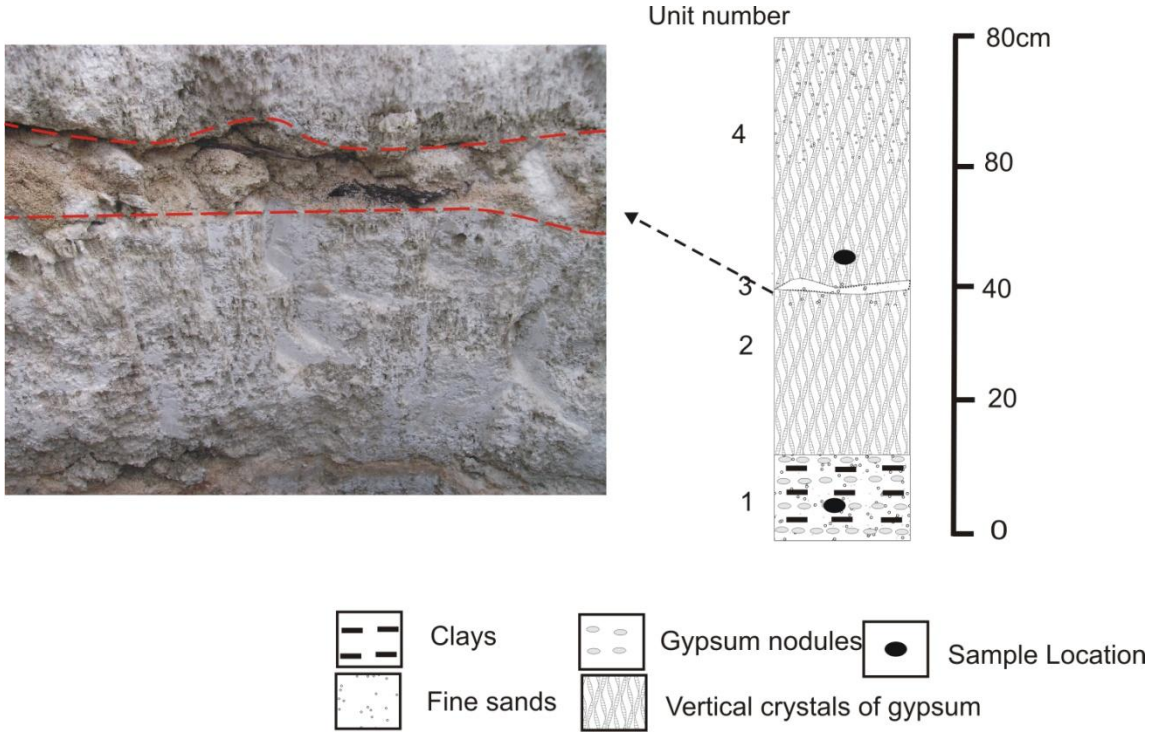

Figure 4.41: A schematic sedimentary log and view of section QA.08.11 in the Nafud Mazhur. The image shows the vertical columns of gypsum and the aeolian sand were deposited.

4.4.2 Lake deposits within the Nafud Al Thuwayrat site QA.08.12

The sedimentary section QA.08.12, was located in the south west of the Nafud Al Mazhur (26°20′19″N - 43°51′50″E), and was exposed within an interdune (Fig 4.40). The basal Unit QA.08.12.00, (Fig 4.42) was a pale yellow colour (2.5 Y 8/3), and contained abundant post-depositional carbonate nodules (63.1%), mixed with sands (quartz-20.9 %). The clay minerals were dominated by palygorskite- 3.7%; smectite- 1.1%; chlorite- 2.2%; kaolinite - 1% and mica species- 3.5% (Appendix 3). A radiocarbon age obtained from the carbonate sediment related to MIS3 (32,138-34,453 cal BP). This unit lay to the north of the main section at a distance of 0.5 -1.0 m, and was situated towards the centre of the interdune (Fig 4.42 and 4.43). Above is Unit 1, it had a thickness of 15 cm consists of sands with post-depositional carbonate laminae present at the lower junction. XRD analysis showed that this unit contained more quartz (75.6%), and less carbonate (8.1%), with similar amounts of clay to the Unit below (see Appendix 3). An unconformable junction with the upper bed could be found and the colour was presented as a dull yellow colour (2.5 Y 6/3).

This Unit was overlain by Unit 2, which has been dated 40,624-43,223 cal BP and has consisted of finely laminated carbonate deposits. Unit 3, presented with a bed thickness of 25 cm, and appeared to have laminar bedding similar to Unit 2 but has been broken up, perhaps as a result of surface desiccation. The colour was light grey in presentation (2.5 Y 8/2). The XRD date showed that the Unit was dominated by calcite, (80.4 %) (Appendix 3). Unit 4, has been dated 33211-34570 cal BP (Table 4.15), and was a light-grey colour (2.5 Y 8/1) and consisted of massive horizontal post-depositional carbonate. The Unit showed an unconformable junction with the upper bed. Unit 5, consisted of laminated calcite with post-depositional carbonate. The colour was pale yellow (2.5 Y 8/3), and was also dominated by calcite (93.4%) plus low amounts of quartz (5.9%). The upper most bed was 6; with a thickness of 4 cm. It consisted of a cap of reg (rocks and sand).

Sample	depth	Material	Technique	Lab-code	Measured (age)	(±)	Conventional (age)	(±)	Calibration source	Calibrated age-BP ¤	probability distribution
QA. 08.12.04	0.20	Tufa carbonates	Radiometric	Beta 279236	28,830	240	29,200	250	ANTCAL09	**33211-34570**	1
QA.08 .12.02	0.70	Tufa carbonates	Radiometric	Beta 282897	36,840	800	37,200	830	ANTCAL09	**40624-43223**	1
QA.08 .12.00	1.40	Tufa carbonates	Radiometric	Beta 279235	28,360	300	28,710	320	ANTCAL09	**32138-34453**	1

¤ See Appendix 4

Table 4.15: Radiocarbon dates obtained from the sedimentary section QA.08.12, all ages in this section celebrated by INTCAL09. Reference is: Reimer PJ, Baillie MGL, Bard E, Bayliss A, Beck JW, Blackwell PG, Bronk Ramsey C, Buck CE, Burr GS, Edwards RL, Friedrich M, Grootes PM, Guilderson TP, Hajdas I, Heaton TJ, Hogg AG, Hughen KA, Kaiser KF, Kromer B, McCormac FG, Manning SW, Reimer RW, Richards DA, Southon JR, Talamo S, Turney CSM, van der Plicht J, Weyhenmeyer CE (2009) IntCal09 and Marine09 Radiocarbon Age Calibration Curves, 0–50,000 Years cal BP. Radiocarbon 51: 1111-1150

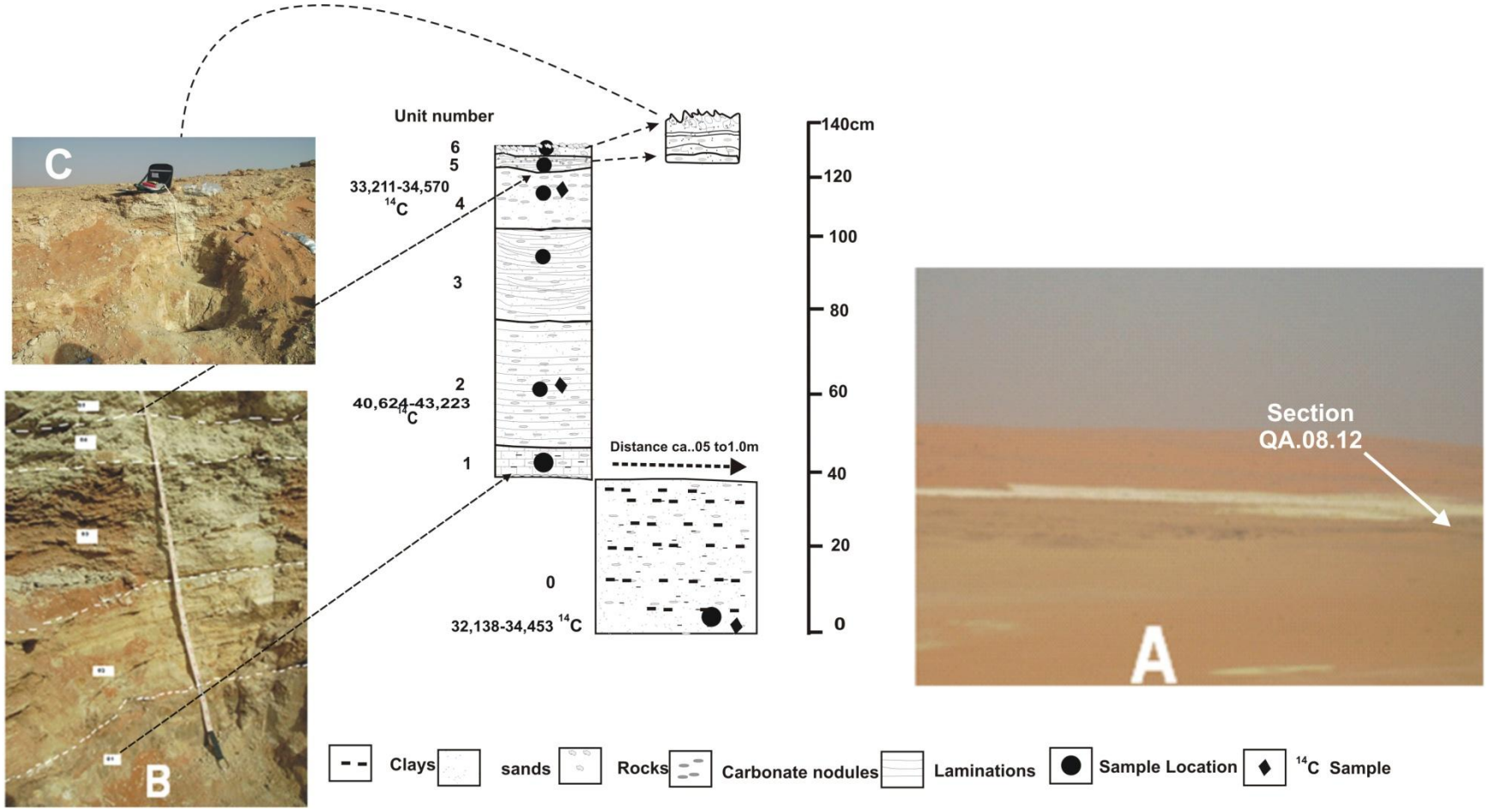

Figure 4.42: View and schematic sedimentary logs of section QA.08.12, photo A shows the interdunal lakes, B photo shows the section of the lake beds (1 to 6) and C shows the upper most bed 6 (cap of reg).

4.5 Geochemical Deposits

4.5.1 Tufa deposits within Nafud Burydah section QA.08.03

Tufa deposits are located to the north of the main channel of the Wadi Al Rimah, in an interdune between the linear dunes of the Nafud Burydah (26°20′20″N - 43°51′33″E) (Fig 4.40). The section QA.08.03 measured 214 cm thick and was composed of 16 sedimentary units (Fig 4.43).

In the tufa sections, All samples in this section had one calibrated age except for samples QA.08.03.10 and QA.08.03.04 which had more than one calibration age due to the imprecise relationship between radiocarbon and calendar years. The calibration age used was the circa oldest-end limit age to youngest-end limit age. The calibration source was (INTCAL04) (Appendix 4).The lowermost Unit 1 (thickness 6 cm), was made up of fine sands with silt and clay (39 % chlorite). Fine fragments of bone were observed. There was also evidence of burrows and mottling. The overall colour was a pale yellow orange (10 YR 7/2). Unit 2 was approximately 16 cm thick, with wavy laminated layers. The ^{14}C age 9790±70 years BP of the deposits in this Unit corresponded to a calibrated age range of 11,300 to 11,120 cal B.P (Table 4.16 and Appendix 4.3). Unit 3 was similar to Unit 2, but was separated by unconformities above and below. Unit 4 was about 37 cm thick comprised fine sand and silts that appeared as wavy laminae. There were also indicators of small amount of post- depositional carbonate nodules, roots and mottling. There was abundant evidence of organic activity with calcified filaments and leaf moulds, this unit corresponded to a calibrated age range between 11,610 to 11,240 cal B.P (early Holocene) (table 4.16 and Appendix 4.4). There was a 20 cm deposit above which showed a massive nature, (Unit 5), and consisted mainly of small carbonate nodules and greater evidence of organic activity than any other unit of this section. Overlying this was a Unit that was 40 cm thick (Unit 6). This was a wavy Unit and contained rhizoliths. An age 8,280±50 BP in the lower part of Unit 6 corresponded to a calibrated age range from 9,440 to 9,120 cal B.P

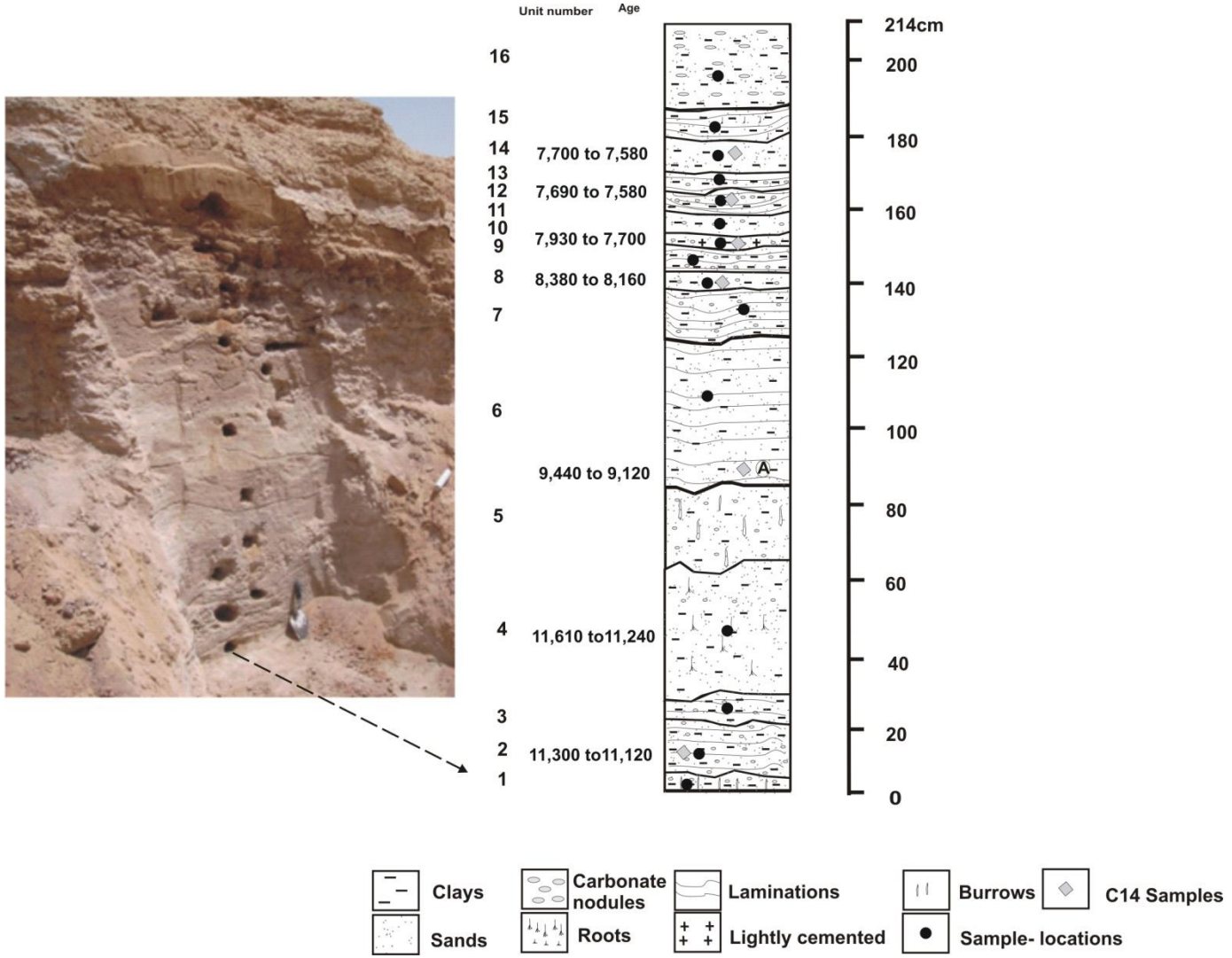

Figure 4.43: Schematic sedimentary log and view of section QA.08.03 of tufa deposit within Nafud Burydah.

(Holocene)(Table 4.16 and Appendix 4.5). Unit 7 contained fine sands with darker organic mottled horizons, and the colour was pale orange (7.5 HR 6.4). Unit 8 was made up of abundant calcified filaments and lightly cemented tufa. XRD analysis showed detection of the following minerals: Mg calcite (39.6%) dominated along with small amounts of quartz (37.1%); feldspar (8.7%); palygorskite (3.4%) and mica species (4.7%) (see Appendix 3). The age 7430±60 BP of the tufa in this unit corresponded to a calibrated age range between 8,380 to 8,160 cal B.P. (table 4.16 and Appendix 4.6) Unconformable above was Unit 9, and this was 11 cm thick, wavy and laminated, comprised of fine sand. This Unit was similar in nature and appearance to Unit 7. Overlying this was Unit 10, which presented with a thickness of approximately 2-3 cm and contained lightly cemented carbonate nodules. This Unit was similar in nature to Unit 8; but this bed had laterally extensive cemented layers which were not considered common features. The tufa age was about 6980±40 BP in Unit 10; a date which corresponded to the calibrated age range between 7,930 to 7,700 cal B.P (table 4.16 and Appendix 4.7). Unit 11 was of a similar nature to Unit 7. Unit 12 presented with a similar texture to Unit 8, but contained dark brown organic patches rich in calcified filaments. There was a flat contact with the upper bed. The tufa in this Unit had a calibrated age range of 7,690 to 7,580 cal B.P (table 4.16 and Appendix 4.8)**.** Unit 14 was calibrated age c. 7,700 to 7,580 cal B.P (table 4.14 and Appendix 4.9), and was approximately 9 cm thick, and made up of fibrous crystals. The XRD data showed this unit was dominated by high quantities of aragonite, whose value was (88.8%) and perhaps indicative of evidence of saline water deposits with small amounts of calcite (5.6%) (see Appendix 3). Unit 15 consisted of laminated fine sands with minor amounts of clay and silt. There was also evidence of roots and organic matter. The upper section was Unit 16, a massive unit made of very fine sand with small amounts of clay and silt. It presented with a mottled appearance, possibly due to some minor root developments. There was a small amount of Fe mottling, and a few carbonate nodules present. The colour was pale reddish-brown, (5 RY 5/4). The composition of this unit were mainly silicates, quartz (62.5%), feldspars (13.9%), with minor amounts of mg calcite (5.1%).(seeAppendix.3).

Sample	Material	Depth	Technique	Lab-code	Measured (age)	(±)	Conventional (age BP)	(±)	Calibration source	Calibrated age (BP) 95% 2 sigma ¤
QA. 08.03.02	Tufa carbonates	0.200	Radiometric	Beta 279229	9,410	70	9,790	70	INTCAL 04	**11,300 11,120**
QA.08.03.04	Tufa carbonates	0.160	AMS	Beta 282891	9,570	50	9,940	50	INTCAL 04	**11,610 -11520 11,500- 11,240**
QA.08.03.06A	Tufa carbonates	0.120	AMS	Beta 282892	7,950	50	8280	50	INTCAL 04	**9,440 9,120**
QA.08.03.08	Tufa carbonates	0.07	Radiometric	Beta 279230	7,120	60	7430	60	INTCAL 04	**8,380 8,160**
QA.08.03.10	Tufa carbonates	0.60	AMS	Beta 282893	6,670	40	6,980	40	INTCAL 04	**7,930 –7890 7,880- 7,700**
QA.08.03.12	Tufa carbonates	0.50	AMS	Beta 282894	6,450	40	6,800	40	INTCAL 04	**7,690 7580**
QA.08.03.14	Tufa carbonates	0.45	Radiometric	Beta 279231	6440	50	6800	50	INTCAL 04	**7,700 7,580**

¤ See Appendix 4

Table 4.16: Radiocarbon dates obtained from the sedimentary section QA.08.03 all ages in this section celebrated by INTCAL04. Reference is: Reimer, P. J., Baillie, M. G. L., Bard, E., Bayliss, A., Beck, J. W., Bertrand, C. J. H., Blackwell, P. G., Buck, C. E., Burr, G. S., Cutler, K. B., Damon, P. E., Edwards, R. L., Fairbanks, R. G., Friedrich, M., Guilderson, T. P., Hogg, A. G., Hughen, K. A., Kromer, B., McCormac, F. G., Manning, S. W., Ramsey, C. B., Reimer, R. W., Remmele, S., Southon, J. R., Stuiver, M., Talamo, S., Taylor, F. W., van der Plicht, J., and Weyhenmeyer, C. E. 2004a. IntCal04 Terrestrial radiocarbon age calibration, 26 - 0 ka BP. Radiocarbon 46, 1029-1058.

4.5.2 Tufa deposits within Nafud Burydah section QA.08.04

This section was located about 40 m to the west of section QA.08.03 in the linear dunes of the Nafud Burydah, in the interdune of the Nafud (26°20′20″N - 43°51′33E) (Fig 4.40). The section composed of seven tufa beds that presented with an overall thickness of 2.60 m (Fig 4.44).

In this tufa section all samples were considered to be of one calibrated age, except sample QA.08.04.06D which had two calibration ages due to the imprecise relationship between radiocarbon years and calendar years. In addition the perturbations on the curve due to the variations in long time of radiocarbon activity were also considered (see Appendix 4). The ages used were the circa oldest-end limit to youngest-end limit.

The basal Unit, QA.08.04.00 was located 20 m to the south of the main section. It was 20 cm thick, and the base showed a hardened layer of cemented fragments that contained poorly-sorted very fine sand with carbonate nodules and minor amounts of organic material. The colour was pale yellowish brown (10 YR 5/3). The upper part of this unit graded up into a dark soil–like layer. It consisted of very coarse silt with small quantities of fine sand. The colour was a greyish yellow-brown, (10 YR 4/2). The mineral composition contained quartz (41.1%); high-Mg calcite (39.1%) and gypsum (4.7%). The clay minerals were dominated by palygorskite, smectite, chlorite, kaolinite and mica species (Appendix 3). The tufa in this unit corresponded to the calibrated age range 10,230 to 9,900 cal B.P (table 4.17 and Appendix 4.10). This Unit was located at a greater depth compared to the main section. Unit 1 was about 20 m to the north of Unit QA.08.04.00; 30 cm thick of moderately sorted fine sand, rich in organics with abundant root casts running through out. There was a lack of carbonate and no evidence of bedding due to bioturbation. Overlying this was a 70 cm thick deposit (Unit 2), which was poorly sorted medium sand with abundant roots. The roots could be identified by their form and brown-red colour. In this Unit there was no evidence of bedding due to bioturbation; but there was a small amount of carbonates. The colour was pale yellow-orange (10 YR 6/3). This Unit had the highest percentage of sand which suggested a greater aeolian contribution at this time.

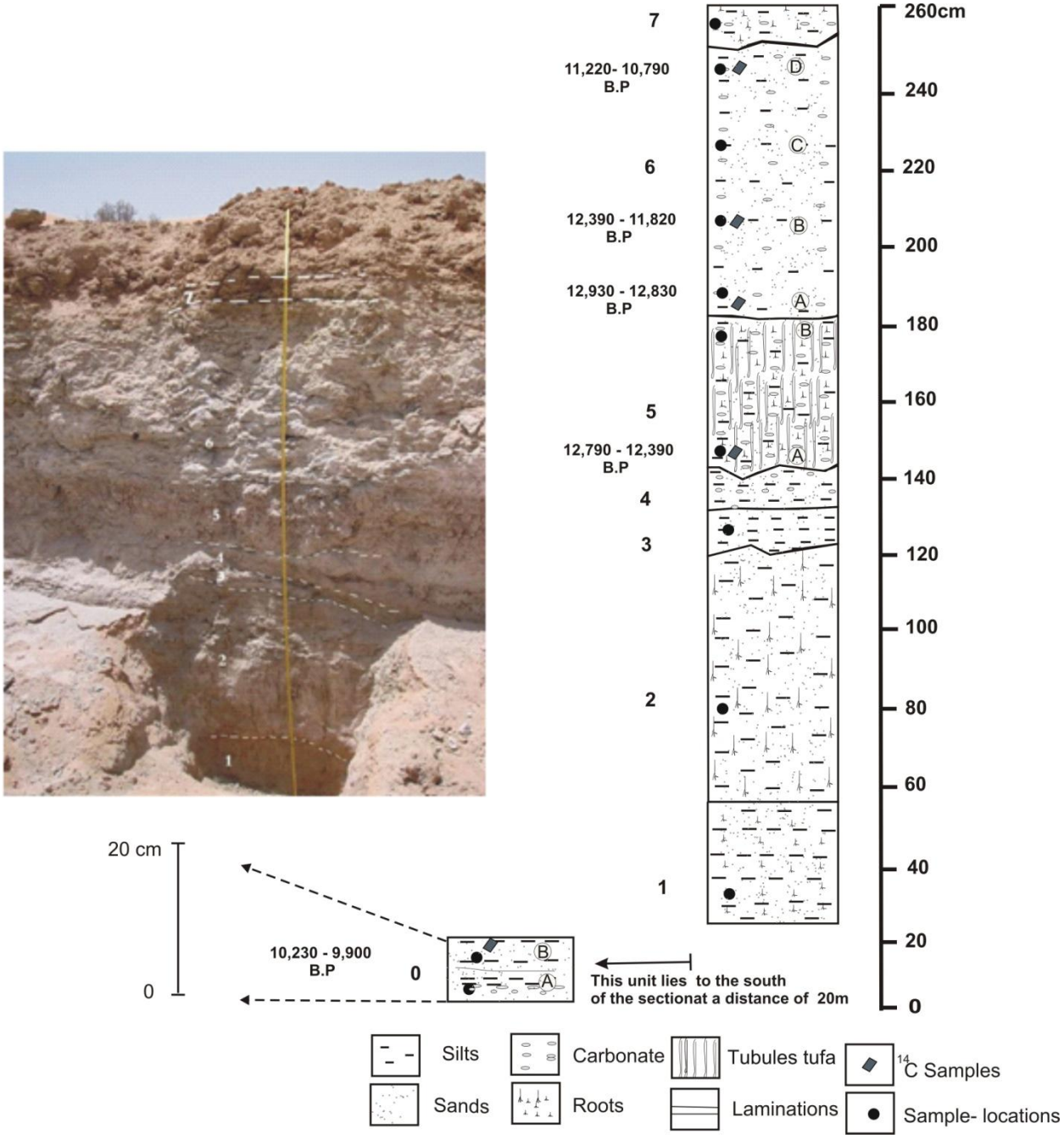

Figure 4.44: Schematic sedimentary log and view of section QA.08.04 of tufa deposit within Nafud Burydah.

Unit 3 was a 6 cm thick massive unit, of very fine sand with minor quantities of clay. The colour was a greyish yellow-brown (10 YR 6/2). Unit 4 was similar to Unit 3 but it had a pale yellow-orange colouring (10 YR 7/2) and the mineral composition was dominated by calcite (40%), quartz (37.1%) and feldspars (8.5%) (Appendix 3). Overlying this was Unit 5, which comprised carbonate nodules and roots, with calcite filaments of a light grey colour (10 YR 8/2) and high-mg calcite (69.1%) (Appendix 3). This deposit provided an age which corresponded to the calibrated age range 12,790 to 12,390 cal B.P (table 4.17 and Appendix 4.11). The upper part of this bed was similar to the lower Unit 5; but there was abundant evidence of organics in the form of numerous tubules filled with bright orange red Fe- oxide powder. Four samples were collected from (Unit 6), 6A, which consisted of poorly-sorted, very fine sand. Carbonate nodules were present and organic material found. The colour was pale yellow (2.5 Y 7/3). The calibrated age from tufa was dated 12,930 to 12,830 cal B.P (table 4.17 and Appendix 4.12). 6B, was similar, but contained high carbonate nodules as well as organic material and the calibrated age from tufa was dated 12,390 to 12,820 cal B.P (table 4.17 and Appendix 4.13). The upper-most layer was 6D, and its structure resembled a stromatolite as it contained black organic layers in between white layers, heavier in weight than the lower tufa deposits. The age from this tufa corresponded to a calibrated age range from 11,220 to 10,790 cal B.P (table 4.17 and Appendix 4.14). The upper most bed (Unit 7) measured 10 cm in thickness and contained poorly-sorted fine sand. Organic algal matter was present and carbonate nodules were also found. Red stains from oxidation surrounded the roots. This resembled the top of unit 6 but red silt infiltrated down into it. The mineralogical composition of this unit was predominantly calcite (83.5%) the quartz appeared to drop in this unit (11.3%). To explain why age at unit 04 are old than units below are perhaps additional old carbonate within interdunes may be blown to the tufa and deposited in the water.

Sample	Depth c m	Material	Technique	Lab-code	Measured (age-BP)	(±)	Conventional (age-BP)	(±)	Calibration source	Calibrated age (BP) 95% 2 sigma ¤
QA. 08.04.00	240	Tufa carbonates	Radiometric	Beta 279232	8,650	60	8,950	60	INTCAL 04	**10,230 - 9,900**
QA.08.04.05A	110	Tufa carbonates	Radiometric	Beta 282895	10,280	60	10,580	60	INTCAL 04	**12,790 - 12390**
QA.08.04.06A	80	Tufa carbonates	Radiometric	Beta 279233	10,570	60	10,910	50	INTCAL 04	**12,930 -12,830**
QA.08.04.06B	50	Tufa carbonates	Radiometric	Beta 282896	9,980	60	10,300	40	INTCAL 04	**12,390 -11820**
QA.08.04.06D	10	Tufa carbonates	Radiometric	Beta 279234	9,350	60	9,680	60	INTCAL 04	**11,220- 11,060** **11,030-11,000** **10,970-10,790**

¤ See Appendix 4

Table 4.17: Radiocarbon dates obtained from the sedimentary section QA.08.04.

4.6 Summary of findings

The findings of this research have shown evidence for significant wet phases reflected increased activity of Wadi Al Rimah during the Marine Isotope Stage (MIS) 7. Subsequently there was also evidence of fluvial activity in the Wadi Al Rimah and its tributaries during the last interglacial period in MIS 5d, 5b and 5a. After these events, the palaeolakes reached their highest levels at ca.30 to 40 ka. There has been no evidence of climatic conditions during the Last Glacial Maximum (LGM) perhaps suggesting that conditions were hyper-arid with an environment that was erosive rather than depositional.

During the Holocene, the majority of the wadis in Burydah continued to be active; and in the inter-dune lake tufa deposits formed at ca.12-7 ka. Linear dunes were forming at the same time as were the wadis, and tufa was therefore active. Moving through to the mid-Holocene towards the present day, there has been evidence for a drying out of the majority of the Wadi Al Rimah and its tributaries; and the establishment and growth of sand sheets covering the wadi and the lowlands.

By ca.5 ka onwards the Burydah area which became arid, with similar conditions that persist today. These results are similar to those observed elsewhere on the Arabian Peninsula and other areas in Africa, Oman, The United Arab Emirates, Yemen and Jordon.

CHAPTER FIVE

5 Discussion

5.1 Interpretation of the Wadi deposits in the Burydah area

The stratigraphic sections studied provide evidence for the late Pleistocene and Holocene palaeo-environments in the Burydah area (see Fig 5.1 and Fig 5.2). The fluvial terraces located in the main channel of Wadi Al Rimah (QA.08.14.01), where the wadi runs through the middle study area, reflects evidence of a flood deposits of poorly sorted clays with silts and sands. The sample has provided good evidence to suggest that the wadi Al Rimah extended into the linear dunes and the linear formed in response to enhanced shamal winds during this time (Fig 5.3 shows an example of the type of flood which has been suggested).

The OSL age obtained from the wadi deposits was 110 ka, which coincided with MIS 5d as proposed by Willoughby (2007). As previously mentioned, information prior to this age needs to be supported by other age data from the units above, as well from other sites in the Burydah area. It has been argued that at this time the upper catchment of the Wadi Al Rimah was supplied by rainfalls as significant transportation was required for this sand-rich site, in order to receive fine grained silts and clays.

The apparent fluvial and sand deposits of these ages would suggest that they have been formed during increased humidity; perhaps as a result of the southward Mediterranean rainfall penetration over northwest Saudi Arabia – the upper catchment of the Wadi Al Rimah. In addition deposits support a significant increase in the winter shamal winds in the Burydah area. This age fits with evidence from findings of lake sediments from Jordan which indicated that the lake was active during ca. 116 to 95 ka (Abed et al., 2008) due to the intense Mediterranean rainfall.

Other previous work has found that dry phases in the SE Arabian desert and the major phases of dune accumulation which occurred during ca 110 ka and 115 ka were due to an increase of shamal wind activity which transported sediment from the Gulf to the Emirates and Rub Al Khali (Glennie and Singhvi., 2002). In addition aeolian dune

formation in the Jafr in Oman, has indicated phases of dune activity occurring between ca 120-100 ka and has been associated with the drop in global sea levels during the glacial cycle, low intensity monsoons and the increase of north-westerly winds (Preusser et al., 2002). In Africa, Bateman et al. (2003) observed the base of linear dunes in the SW Kalahari related to ca 113 and 108 ka.

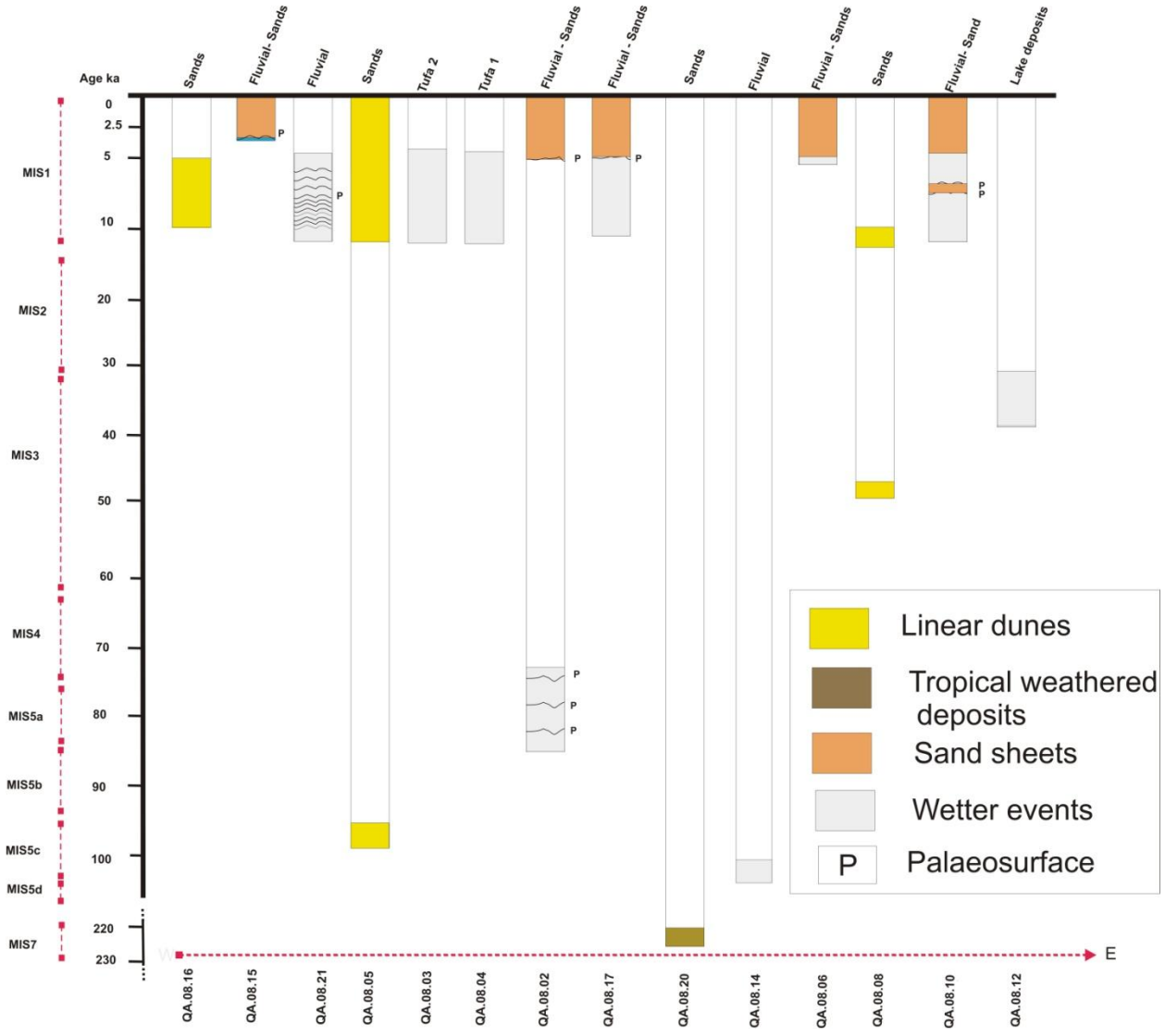

Figure 5.1: Summary of the findings of this research. The marine oxygen isotope records according to Willoughby (2007).

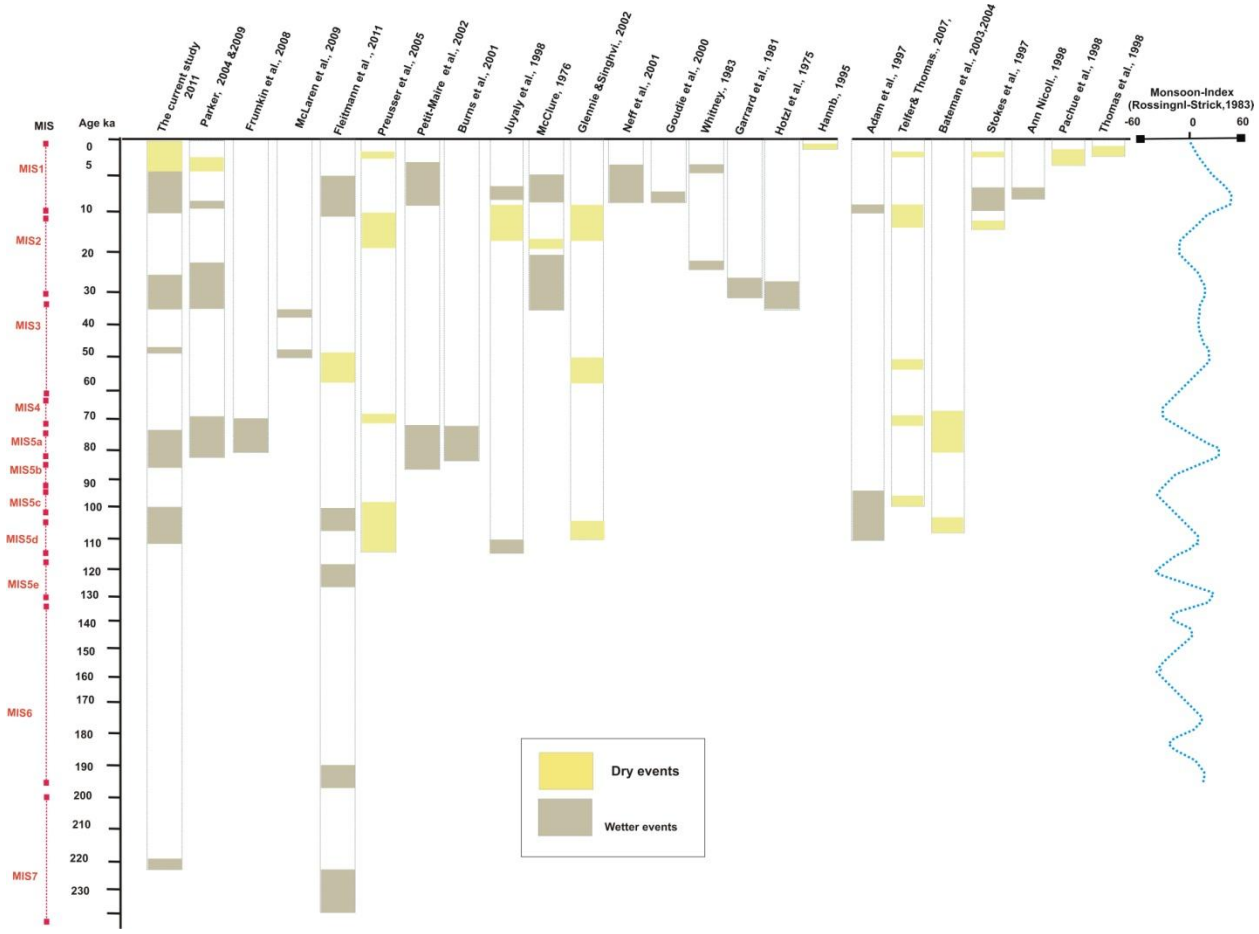

Figure 5.2: Summary of the findings of this research and others worked in the Arabian Peninsula and surrounding areas.

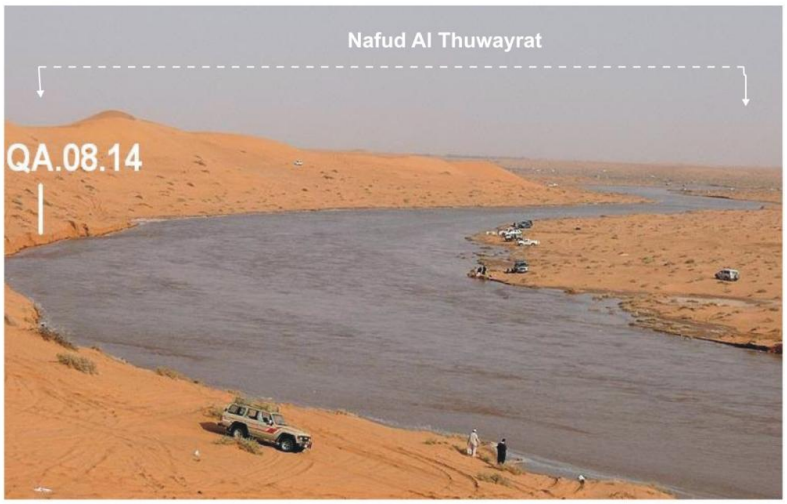

Figure 5.3: View in the Wadi Al Rimah, show the recent flow during 2009.

In the Wadi Al Butuan, section QA.08.02, fluvial activity would suggest that there were significant wet phases in the last interglacial period, ca. 77 ka to 85 ka yrs BP which correspond with stages MIS 5b and 5a. Wadis during this period of time reflected rhythmic cycles of sedimentation separated by breaks in fluvial activity and exposure of palaeosurfaces.

During this time, the wadi deposited about 3 metres of fluvial sand over a period lasting approximately 8240 years. Conditions at the time for depositions appeared to have humid period; and there has been other evidence for a humid period around this time (see Fig 5.1 and 5.2).

However, in Jordon, Petit-Maire *et al*. (2002, 2010) argued in favour of the theory of an extension of freshwater bodies in the Mudawwara Lake, southern Jordan (29° N), between 88 ka and 77 ka; whereby the shells have formed an extensive and thick bed associated with fine quartz sand, gravel and coquina resting on marls. These deposits appear to have been formed under the influence of both Mediterranean and Indian monsoon rainfall. Moreover, this date corresponds with other dates by Frumkin et al. (2008) from calcite speleothems in Jordan which were related to excessive water periods with high vegetation between ~ 80 and 70 ka under the effect of migration of the Mediterranean systems and Indian monsoon rainfall.

Further evidence in Oman, as argued by Burns *et al* (1998, 2002) at the Hoti cave, has claimed that the growth of a speleothem corresponded to increases in rainfall during 80-78 ka, and thus has been associated with migration of the Mediterranean systems and Indian monsoon rainfall.

Paleosol strata were found by Anton, (1984) with regards to the Al Dahna dunes in central Saudi which indicated that dunes stabilised with vegetation cover during marine isotopes stage 5. It could be suggested that, during the last interglacial period Wadi Al Butaun developed from the upper catchment of the wadi and its tributaries which were Jabal Shammer (27°N) in the north west of central Saudi Arabia (Figure 1.4). These areas could have been supplied by additional rainfall derived from cyclones responsible for the Mediterranean rainfall system; and/or Indian monsoon rainfall that migrated northward to (29° N), as Petit-Maire *et al*. (2002) argued in Jordan. It also corresponds with the rains over the Burydah area (26°N) in central Saudi Arabia. This evidence has provided a contrast with research undertaken in Africa conducted by Telfer & Thomas (2007) and Bateman et al., (2003) whereby sands in the Witpan area of South Africa continued to accumulate during MIS5a to MIS4.

The upper Wadi Al Rimah QA.08.21 was periodically flooded throughout the early and mid-Holocene. The lower section deposits indicate relatively humid climatic conditions from 13 to 11 ka. During this period the Wadi Al Rimah experienced larger and more frequent flood events with sediment being distributed on the floodplains of the study area. These wet events were separated by phases of gradual drying out (desiccation); indicated by the formation of carbonate nodules and the establishment of vegetation on the floodplains. This has been indicated by the fragments of plant material and tree leaves that have been found within the sediment. With further evaporation, during the final drying out stages, gypsum crystals precipitated out. The cementation of carbonate deposits at the palaeosurfaces prevented the infiltration of water during subsequent flood events and preserved the underlying gypsum crystals.

It could be suggested that during this period these areas appear to have been supplied by additional rainfall derived from cyclones responsible for the intensity of the Mediterranean rains; and/or penetration of monsoon rains in central Saudi Arabia.

In addition in the early Holocene period around 12 ka, the lower channel of the Wadi Al Rimah, (QA.08.10), was covered by sand accumulation in Nafud Al Thuwayrat. The wadi terraces showed alternations between fluvial and aeolian deposits. This site thus shows clear evidence of Wadi Al Rimah deposits extending into Nafud Al Thuwayrat. It has been argued that at certain points in the past this wadi cut though the sand sea; or possibly prior to the evolution of the Nafud in this location. The satellite imagery suggests that the wadi extended much further to the north east toward Iraq; and this is therefore an area for future research.

No evidence found in the central Saudi has supported a wet phase around this period; and the evidence obtained coincides with the period of a slight rise in the sea level within the Arabian Gulf (Goudie et al., 2000). It also coincides with lacustrine deposits developed around 11 ka in Yemen (Parker et al., 2006 and Lezine et al., 1998). The view provided by Fuchs and Buerkert, (2007), has shown a period characterised by high sand accumulations at 12 ka, associated with the low intensity of the summer Indian monsoon around the oasis of Maqta in northern Oman; and also with an absence of speleothem growth in Oman (Fleitmann et al., 2003).

With regards to Africa, similar evidence to that described for the Holocene conditions have been identified on Lake Victoria which was an open basin in ca.11.2 ka (Johnson, 2000). In addition fluvial runoff increased during ca 13 ka -11 ka, as well as the savannah which reached its northernmost position during this period (Hooghiemstra, 1987). During 13-11 ka temperature and moisture increased throughout most parts of Africa (Adams et al., 1997 and Gasse, 2000) In addition in western Nigeria the growth of linear dunes and the loss of sediment occurred during ca 12 ka (Stokes et al., 1998). At Witpan in southern Africa, sand continued to accumulate during 15-9 ka under the effects of reducing soil moisture, greater sediment availability and a greater frequency of sand-transporting

winds (Telfer and Thomas, 2007). Linear dunes in the interior of the central southern Kalahari Sahara, were active during 11-13 ka (Thomas et al., 1998).

In the early Holocene around 10 ka, the Wadi Al Watah (26°N) was a tributary palaeochannel system which led to the Wadi Al Rimah channel. This wadi deposited moderate to low energy fluvial deposits. The fluvial sands in the lower two units of this section has suggested wetter phases around 10 ka. The wadi during this period reflected rhythmic cycles of sedimentation and alternations between quiet and high wadi activity supporting the flat bedded and low angled planar laminations.

Following this phase there was a period of lower wadi activity with a short drying out and desiccation stage with the development of carbonate nodules. There is evidence of wet phases in the far west of the study area in the upper catchment of the Wadi Al Rimah section QA.08.21; at the same time as the downstream site QA.08.10. This would indicate that there was a significant wet event during this period, due rainfall derived from cyclones responsible for the intensity of the Mediterranean rains; and/or penetration of monsoon rains in central Saudi Arabia

These results show that the wetter conditions in central Saudi Arabia started ~12 ka, and do not therefore concur with results published by Parker (2009). He concluded that a wetter phase occurred around 10 ka in southern Arabia before reaching central Arabia, due to the influence of the Indian Ocean monsoon (IOM), which he suggested took around 1,800 years to move to northern Arabia (25°N). However others believe that the monsoon precipitation belt was located close to 23-24°N over Saudi Arabia, but did not move further. Whereas the evidence at Kahf Al Najmah (30°N) has not suggested any of the wet conditions that were found further north (Fleitmann et al., 2004).

In the southen Arabian Peninsula the Hoti cave in Oman evidence shown in the speleothems has indicated a wetter phase between 9.6-6.1 ka. This was related to enhanced monsoon precipitation that migrated steadily northwards during the Holocene to the southern shoreline of Oman (Neff et al., 2001).The findings of this study (in the Burydah area) (Fig 5.0 and 5.2) have indicated that the monsoon probably migrated much further north than previous work has suggested.

In Africa a similar result was found during the early Holocene whereby the monsoon appeared to have reached the Tanganyika basin (Tierney et al., 2010). The majority of Africa saw wet and warm conditions during ca13-11 ka (Adams et al., 1997; Gasse, 2000); and the land was completely vegetated (Adams and Faure, 1997; Johnson et al., 2000 and Alin and Cohen, 2003). This moved further to the Umm Akhtar lake in southern Egypt (22°N) where there was a standing water body during 9.9 to 9.5 cal yr BP and from 7.8 to 6.7 cal yr BP, which corresponded with the greatest frequency of African lake high stands (Kathleen, 2001).

By the middle of the Holocene, the Wadi Al Butaun was covered by windblown orange sand sheets, named Nafud Al Tarafiyah; around ca 5 ka. These dates have concurred with other evidence found in this study which has shows significant sand sheet development elsewhere after the mid Holocene, such as the Wadi Al Watah. The upper section of the Wadi Al Watah (QA.08.17.06), would suggest that this wadi was still active with a contribution from aeolian sand sheet activity in the mid Holocene at about 5.1 ka. This was associated with dry conditions which have been supported by the presence of a slight increase in the amounts of calcite and palygorskite minerals. The formation of palygorskite usually occurs in arid conditions meaning that the annual rainfall is between 50-100 mm (Jimenez-Espinose & Jimenez-Millan., 2002).

Similarly the Wadi Al Rimah (section QA.08.10.02) deposits suggest slightly higher abundances of silt and fine sand, which may have been the result of low runoff and high sand input; where the wadi was shallow and the wadi environment was enriched with vegetation.

A present-day comparison can be made with the channel vegetation, which is called in Arabic 'Qassob' (Bulrush) (Fig 5.4). The Qassob plants have been referred to by Aldughairi (2003) as being widespread around the Wadi Al Rimah and within the depressions where most of the records by Arab historians have described the wadi environment (in the last 100 years) as being swampy.

In addition the upper channel of the Wadi Al Rimah section (QA.08.21.08) periodically experienced flooding throughout the mid Holocene between 4.4 to 4.1 ka. The wadi

during this time was exposed to big flood events, and these events were separated by drying out phases with high evaporation rates. This supported the increase in amounts of gypsum and palygorskite which usually occurred in drier conditions as reported by Jimenez-Espinosa & Jimenez-Millan (2002).

These events discussed above, can be related to the high effectiveness of the shamal winds which played a major role in central Saudi during the mid-Holocene (Holm, 1960; Edgell 2006). As well as the southward migration of IOM wind during the mid to late Holocene ca 5-4 ka, in southern Arabia which led to a gradual decrease in precipitation in response to decreasing solar insolation.

The movement of IOM during the mid-Holocene corresponded with the low level of different lakes in Arabia such as those at Awafi Ras Al Khaimah (UAE) ca 5.9 – 4 ka which were filled with sand around 4.1 ka (Parker et al., 2004). There was also sand dune accumulation around Sabkhat Matti in southern Saudi Arabia around 5.9 ka (Hannb, 1995). This was consistent with the sand-sheet in the Selima sand sea of the Eastern Sahara in Africa which accumulated during a brief moist period in the Holocene between ca. 3-4 ka (Stokes et al., 1998). In addition the sand dunes in Inner Mongolia, indicated aeolian activity with a long-term oscillation trend towards arid conditions 5 ka (Pachur et al., 1995).

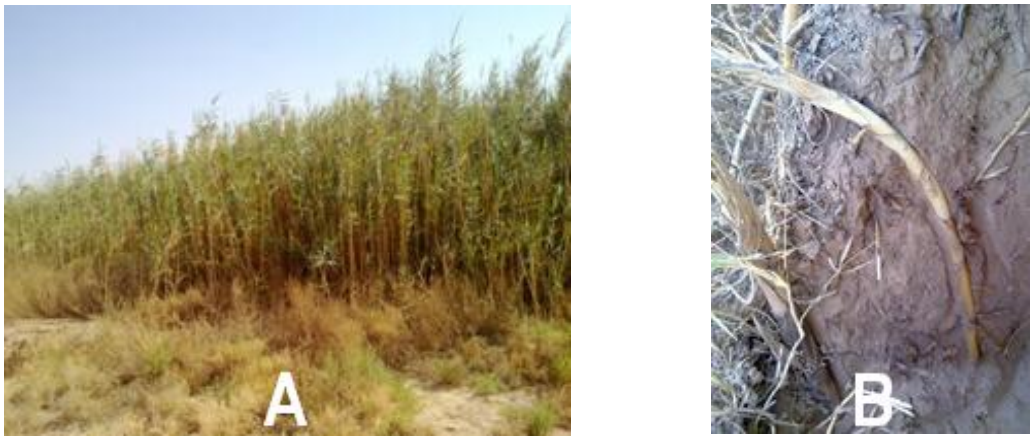

Figure 5.4: The Qassob plants in the Wadi Al Rimah: (A) showing the leaves and stalks and (B) the roots; similar to the remaining roots in section QA.08.10.

5.2 Interpretation of the dune deposits in the Burydah area

The western belts of the linear dune system in the study area have indicated a general southerly drift direction, which would suggest that most sand formed parallel to the usual wind transport direction from north-westerly winds. This would appear to agree with Holm (1960), whereby maps of the direction of the aeolian sand movements over the Arabian Peninsula showed the sand dunes in central Saudi Arabia to appear in a circular arc with a NW direction (Fig 1.2).

Additionally, the dunes on the North Emirates coast were formed under NNW winds (Glennie, 1995), and the building of Nafud Al Jafurah in eastern Saudi Arabia was associated with NW to NNW winds (Edgell, 2006). OSL dating has shown different periods of sand accumulation ca. 99.5 ka to 200 years ago. The oldest sand age has been obtained from the lower parts of Nafud Burydah and has indicated that these sands which have become cemented by $CaCO_3$ formed about 99.5 ka. This has occurred under the effects of rising water tables and strong Shamal winds which have played a major role in the preservation and development of these dunes.

This aeolianite is the only one that has been found so far in the study area. It has displayed all the classical characteristics of aeoliantes as described in McLaren (2007). The age of this aeolianite would appear to be close to the ages obtained by Preusser et al. (2002) for aeolian dune formation in Al Jafr in Oman, indicating phases of dune activity occurrence around 120-100 ka. In addition the age obtained was close to the sand accumulation in the Witpan area of South Africa (ca.26°N) which continued accumulating during MIS5c (ca.92 to 104ka) due to differing factors such as: less rain and lower temperatures; no rainfall reduction and higher temperatures; low soil moisture and greater sediment availability and greater frequency of sand transporting winds (Telfer & Thomas, 2007)

In the MIS3 ca. 49 ka the sand dunes in the Dasmah within Nafud Al Thuwayrat, (QA.08.08.01) were active under the effect of Shamal winds, with the water table availability which was an important control of sand accumulations(Stokes and Bray., 2005). This date is consistent with the argument put forward by Fleitmann et al. (2007),

who suggested that this period at 50 ka was a hyper arid phase; and dune accumulation had thus been active in the Wahiba sands.

Moreover, there has been further evidence for increased sand dune building at Liwa sands, during ca 45; 51; 54 and 60 under the effect of Shamal winds (Stokes and Bray, 2005). Linear dunes in the Witpan area of South Africa also accumulated during ca. 57-52 ka (Telfer and Thomas, 2007).

The date 49 ka is not in accordance with the findings of McLaren et al. (2009) and Al Juaidi (2003), who provided evidence of wetter events in the outwash plains that occurred at 54 ka and 53.9 ka; which they argued were associated with phases of increased rainfall and/or decreased evaporation that prevailed in central Saudi Arabia. Again if the dunes and outwash fans formed around the same time this may indicate that either the dunes were not a good indicator of aridity and/or the wet events identified by McLaren et al. (2009) and Al Juaidi (2003) were small-scale localised events.

In the early Holocene, around 11.3 ka, Nafud Dasmah within Nafud Al Thuwayrat, (section QA.08.08), showed high levels of roots and burrows and some carbonate development. This would suggest that such sand accumulation corresponded with a rise in the water table and a slightly wetter phase.

In addition, sand deposits at Nafud Burydah showed indications that dunes were still active and the water table was an important control of sand stabilisation. The subsequent accumulation which coincided with lacustrine tufa developed in the interdunes areas. The units QA.08.05.02A to QA.08.05.02C, are both Holocene with estimated OSL ages of 9.5-10.5 ka respectively.

The vertical accumulation rate between Units QA.08.05.02B and QA.08.05.02C has been 15.5m ka^{-1} which would suggest extremely high levels of sand accumulation, with rates that are about five times faster than the linear dunes in Rub Al Khali (UAE) studied by Goudie et al., (2000). In this study, Holocene dunes from Awafi accumulated at a vertical rate of 3.3m ka^{-1} which they argued, “accumulated very rapidly ~10,000 years ago’’ (pg. 1001).This is very interesting as it implies a large sediment source and very high sediment transport rate from the Great Al Nafud to Nafud Burydah.

An age obtained from the lower Nafud Uyun Al Jiwa is close to the age of Nafud Burydah. This Nafud was deposited around 9.8 ka. These ages support the argument that indicates that aeolian deposition is not a direct indication of arid conditions in the Arabian Peninsula. For example, Stokes and Bray (2005) argued that the sand dune preservation at Liwa in the United Arab Emirates occurred during wetter phases which were controlled by the sea level and precipitation that coincided with global climate variations. Goudie *et al*. (2000), in the Awafi linear (25°N) sand dunes in Ras Al Khaimah (UAE), showed that dunes developed between 9.1-10.7 ka and concluded that aridity could not be considered the critical factor of sand accumulation and may have accumulated as a response to sediment supply and vegetation destabilisation by expanding humans during the late Pleistocene and the early Holocene.

In addition in the Wahiba sands, aeolianites representing the aeolian activity related to 10 ka and 10.5 ka (Juyal *et al.,* 1998). The dune accumulation in southern Arabia corresponded with the northward movement of the monsoon winds (Neff et al., 2001 and Fleitmann et al., 2004).The migration of humans into inner Arabian Peninsula has been influenced by the monsoon moisture during the early Holocene (Parker., 2009).

Comparable evidence of dunes building in the early Holocene in Africa showed agreement with dunes building in the Arabian Peninsula; for example the linear dunes in the interior of the central southern Kalahari Sahara were active during 11-13 ka (Thomas et al., 1998). In addition the dunes building in Kalahari, where the sand dune accumulation continued during ca.10 to 8 ka (Telfer and Thomas, 2007 and Bateman et al., 2003).

In the mid Holocene, Nabkah in the Wadi Ragwah (QA.08.06), deposited around 5.3 ka, which showed that they were formed under the influence of slight wadi activity which coincided with strong shamal winds (NW) across the wadi via Nafud Al Sirr. Similar sand accumulation was found during ca. 4.7 ka, in the upper parts of linear dunes named the Nafud Uyun Al Jiwa. The ages obtained have agreed with the hypothesis that in the mid-Holocene, arid conditions prevailed in the Arabian Peninsula; and that the shamal winds played a major role in the sand deflation (Lezine *et al*., 1998; McCorriston *et al*., 2002 and Staubwasser and Weiss, 2006). This results from high-pressure cells over northern Arabia

(Edgell, 2006), which also withdraw of the monsoon precipitation. Were decreased gradually in response to changing northern hemisphere summer solar insolation; with decadal to multi-decadal variations in monsoon precipitation being linked to solar activity (Neff et al., 2001, Fleitmann *et al*., 2003; Parker *et al.*, 2006).

The records relating to the Awafi Lake at Ras Al Khaimah (UAE) showed that Awafi filled with red sands and fine carbonate was blown into the lake around ca. 4.1 ka. This may have been related to more than one factor, and weakened the influence of the IOM that retreated southwards, and human activity (Parker, *et al*., 2004, 2006). In addition the sand dunes around Sabkhat Matti in southern Saudi Arabia have shown that sand accumulation was related to ca. 5.9 ka (Goodall, 1995).

This evidence is consistent with the mid-Holocene, arid conditions in Africa, where most of the studies have interpreted sand building as equating to arid periods (Telfer &Thomas., 2007). For instance, in Inner Mongolia aeolian activity prevailed with a long-term oscillation trend towards arid conditions between 6.5–5.5 ka. The dunes migration and deflection in Umm Akhtar playa in southern Egypt was also around 6.7 ka. In addition, a sand-sheet in the Selima Sand Sea accumulated during a brief moist period in the Holocene between ca. 3-4 ka (Stokes et al., 1998); and upper linear dunes in Witpan aeolian sand deposition continued to accumulate during ca 4.9 to 3.1 ka (Telfer &Thomas., 2007).

By the late Holocene, around 3.5 ka, the sand sheet continued its developments in Nafud Al Qwarh, evidence of weathering predictions from nearby areas via Wadi Aswidah and correspond with drier conditions. The evidence of roots and the presence of silt would suggest that the first stage of the sand accumulation was a result of stabilisation by vegetative cover. According to Preusser et al (2005) with regards to the Khuwaymah sands in Oman, such aeolian sand contained paleosol layers with fauna and roots and coincided with the end of the Holocene around ca.3.6. They assumed that this represented arid climatic conditions and the paleosol horizons and roots implied moist conditions due to the special setting near the coastal area and slight increase of the water table.

The latter date of Nabkah on the wadi Rghwah developed around ca. 2.1 ka. The sand formation has usually been associated with wind deflection from the nearby Nafud Al Sirr under the effectiveness of the shamal winds. By the last 200 hundred years, the upper sand sheet at section (QA.08.15.02) within the Nafud Al Qwarh would suggest that these sands accumulated over a short time frame as a result of increased wind intensity and associated human activity.

The sand formation in the Rghwah Nabkah has coincided with peaking of aeolian reworkings from the Liwa area in the southern Arabia at ca 2.8 ka. In addition it coincided with linear dune formation in the Witpan area whereby their formation continued during the late Holocene ca 2.8 ka to 500 years

In the Burydah area the historical records have described the Burydah area being around 100-200 years of age, with localised wadi flow and heavy rain during winter and a long, hot dusty season over consecutive years (Aldughairi, 2003). Comparable results were observed by (Telfer & Thomas., 2007) in the upper dunes in the northern Witpin area where their accumulations have been sporadically active for much of the Holocene between ca. 840 to150 years ago.

A red weathered deposit has been estimated as interglacial during MIS7ca. 221ka. The grain size distribution and red coating has suggested that they were derived from the adjacent Nafud. The red stain around the sand grains may have been weathered out from the sandstone bedrock of the Jillh Formation that contained Hematite; perhaps under the influence of increased moisture levels.

Schwertmann (1993) argued that the formation of Hematite requires enough moisture with high temperatures to form. No correlation supported this period (221 ka) in central Saudi or even in the south and east; except the period mentioned by archaeological observations by Petraglia et al., (2009) They cited that stone tools were found by Whalen et al., (1980) in the Dawadmi area which related to 200 to 204 ka; and during this time Acheulean hominines were present around lakes, and the environment was thought to be wet with a complement of plants and animals.

Additionally, Frumkin et al (2008) found evidence in the Black Desert on the north Arabian Desert in Jordan (32°N) for moist episodes between ~230 to ~220 ka due to the effect of Mediterranean cyclonic systems in the area; which received moisture from the warm Mediterranean sea.

5.3 Interpretation of the Lake deposits in the Burydah area

The lake deposits (QA.08.12) recovered from the lowland interdunes area of the Nafud Al Thuwayrat; were found to be in an interstadial phase between ca. (33, 138-34, 453 cal year BP to 40,624-43,223 cal year BP). This lake was carbonate-rich and was thought to have been sourced largely from run-off received from wadis and gullies on the Safra Al Asyah. This gently sloped to the east with an average gradient of about 1.5° and flowed into the Nafud Al Mazhur. The interpretation of section QA.08.12 is thus as follows:

The deepest unit was sampled at a distance of 0.5 to1.0 metres from the interdune (Fig 5.5). This unit has provided the youngest age of (32,138-34,453 cal year BP). The unit has been dominated by reworked aeolian sands from the base of the interdune and a mix of clays. In the main section unit (1), it has been proposed that this unit formed the junction of the edge of the limb of one of the dune sands with the palaeolake; an age of unit 2 comprised lake carbonates and Unit 3 showed a continuation of carbonates, but with evidence of desiccation structures at the top.

Unit 2 was (40,624-43,223 cal year BP) which was older than unit 0. However it has been argued that unit (0) was located in the deepest part of the palaeolake with clays being deposited. Unit (4) which lay unconformable on unit (3), also represented lake carbonate and this deposit would appear to be roughly contemporaneous (same age as) with Unit 0 (Unit 4 is 33,211-34,570 cal year BP). Thus, at about 33-34 BP there were clays being deposited in the centre of the palaeolake and carbonates were further out. Unit 5 represents a continuation of Unit 4 but then the lake dried out and in doing so carbonate nodules formed. This was also an occurrence in the centre of the lake, which led to 63.1% secondary carbonates in unit (0).

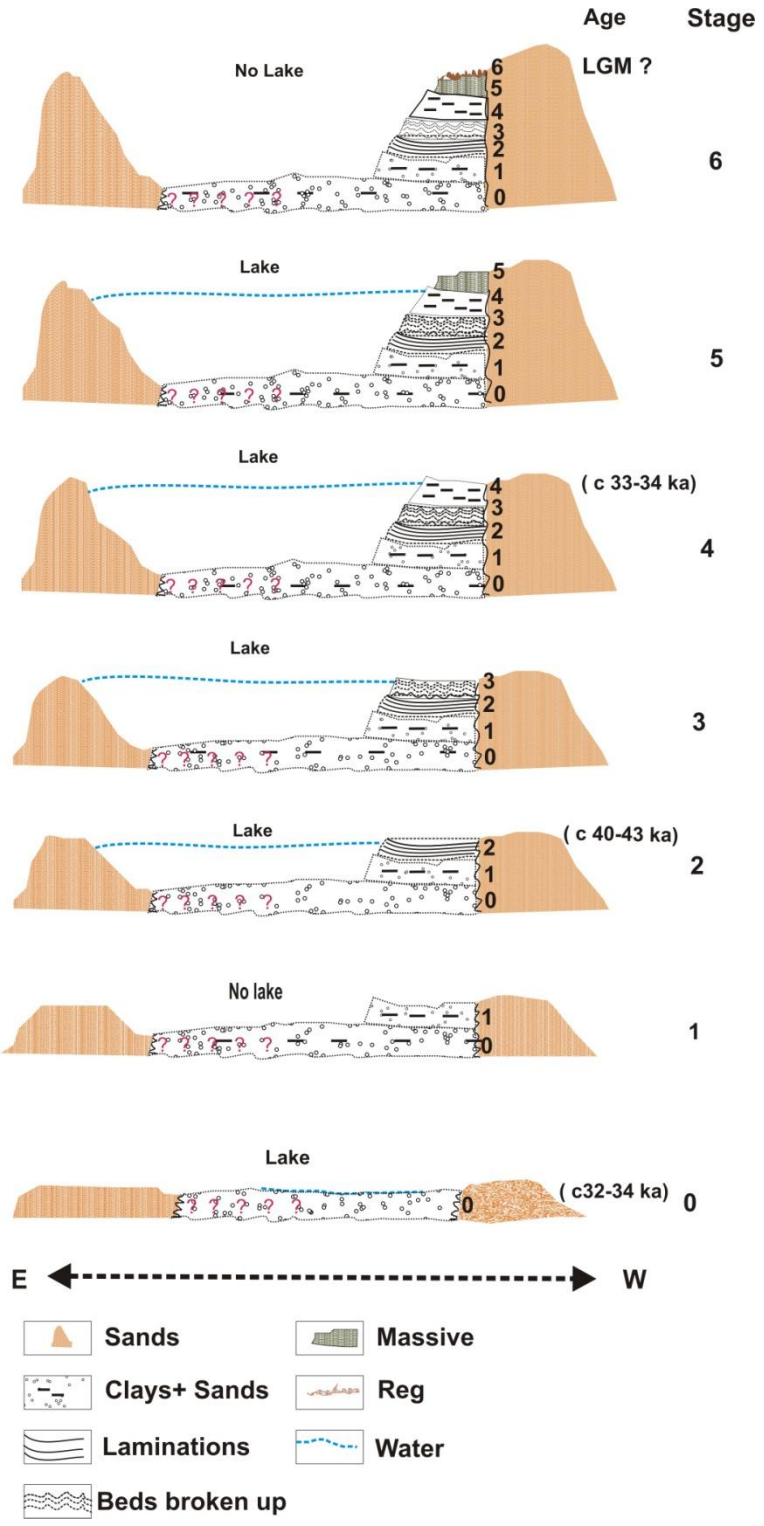

Figure 5.5: schematic shows the evaluation of the Lake at section QA.08.12.

The lake at QA.08.11, appeared in the north edge of the lake and provided evidence for significant evaporation, explaining the high amounts of gypsum (84%). This has been followed by increased amounts of sand and with increasing sand deposition, marking the end of the lake period; and was followed by sands and then the development of a reg surface (desert pavement).

Studies based on records of lake sediments in the Rub Al Khali and Great Al Nafud have indicated that conditions were relatively humid during 26-40 ka. For example, the carbonate deposits within the lakes in Rub Al Khali related to the period ca. 34,832 - 38,388 cal year BP to 24,058 - 26,293 cal year BP, due to an episode associated with moisture in the eastern Sahara desert (McClure, 1976).

In addition, the lakes within the Great Al Nafud in North Saudi Arabia have been related to wetter phases around 34-24 ka and 27.8-25.5 ka (uncalibrated) (Schulz and Whitney, 1986). Garrard et al., (1981) found lacustrine diatomite under the Nafud Jubbah in northern Saudi Arabia ca. 29,573-31,067 cal year BP, which reflected perennial water with less evaporation. Moreover, the calcium carbonate crusts below the surface at Wadi Ranyah have dated to 29,519 - 40,196 cal year BP.

Evidence from carbonate deposits in Lake Damascus have been related to ca. 26,914 - 29,537 cal year BP. In addition Huckried and Wieseman, (1968) provided evidence for a large lake to the north of Saudi Arabia within Lake Al Jafr in eastern Jordan, in which the marl within the Lake dated back to 29,393-32,775 cal year BP.

Additionally, towards the west of the Maryut Lake in the Alexandria region, Egypt, the Lake was active around ca ~35 ka (Warne and Stanley 1993). The similarities between the records from the Lake in the Burydah area, other records from those in the southern and northern Arabian Peninsula, and results from lakes in north Africa, have provided some confidence in our ages and that the Lake in the Burydah area could have received rainfall, when the ITCZ reached its northernmost position and Monsoon winds brought moisture from the Indian Ocean.

5.4 Interpretation of tufa deposits within Burydah section QA.08.04 and QA.08.03

Overall, the tufas have range in age from 12.7 ka cal BP through to 7.5 ka cal BP i.e. from the early through to the mid-Holocene in age. The initial evidence has indicated that due to the presence of high Mg calcite and or aragonite in many of the samples, the existence of a stromatolite dated to 11.2-10.7 ka cal BP. The presence of evidence of grasses, algal mats, algae and cyanobacteria, with evidence of both horizontal and vertical carbonate structures, has indicated that these deposits are lacustrine tufa (It is acknowledged that there are a wide range of further analyses e.g. SEM that need to be conducted on these sediments which will be completed in the near future).

It has been argued that these meteogene tufas formed in the shallow marginal zone of an interdune lake with the stromatolites forming as a direct result of algae forming algal mats (producing the dark bands); and the other organisms along with precipitate of carbonate (forming the lighter bands).

The high amount of aragonite and Mg calcite in some of layers (e.g. Unit QA.08.03.14, QA.08.03.08, QA.08.04.04, QA.08.04.07 and QA.08.04. 05A) may suggest that at these stages the water forming in the tufas was more saline compared to the units where low Mg calcite dominated. The higher concentrations of sand in some units may also be indicative of higher levels of activity on the dunes next to the tufa deposits and the growth of the tufa was corresponding with sand building (see Fig 5.6).

These deposits thus support evidence for wetter conditions during the early to mid-Holocene found in the Burydah area (26°N); and elsewhere in Africa and the Arabian Peninsula (Fig 5.1 and 5.2) as outlined in Fleitmann et al. (2004).

The Indian monsoon circulation was stronger during the early Holocene, and the mean summer position of ITCZ was located much farther north than its present position over the Arabian Peninsula. Lake deposits in Jubbah, North Saudi Arabia (28°N) developed around ca. 7.4-7.6 ka cal BP (Garrard et al., 1981). In addition, gastropods found in shell deposits within terraces of the Wadi Al Luhy (21°N) were widespread around ca. (9 - 9.5 ka cal BP) (Hotzl and Zotl and Al Sayari, 1978).

These dates match with the similarly aged lacustrine sediments found at the south Arabian peninsula around Awafi at Ras Al Khaimah (UAE) relating to the period (8.5 ka cal BP) as a result of the variation in monsoon intensity (Parker, *et al*., 2004). There are also ages from lacustrine deposits at Hawa which range in age between 8.7 to 7.2 ka cal BP (Lezine et al.1998). In the northern Hoti cave in Oman, speleothems have suggested a wetter phase related to the early to mid-Holocene, around 9.6-6.1 ka, due to enhanced monsoon precipitation that migrated steadily northwards during the Holocene to the southern shoreline of Oman (Neff et al., 2001).

All the evidence from tufas has support the fact that during the early Holocene the IOM was located over the Burydah and perhaps much farther north over the Nafud Jubbah (28°N); and not as Parker argued whereby IOM started in south Arabia before reaching the central area.

These results are similar to those observed in Africa, whereby the rainfall showed greatest levels over most parts of Africa, that the land was completely vegetated; and that lakes in northern Africa were widespread during this period (Adams and Faure, 1997; Johnson et al., 2000 and Alin and Cohen, 2003). The rise up of the Umm Akhtar lake in southern Egypt was around 9.9 to 9.5 cal yr BP and from 7.8 to 6.7 cal yr BP due to enhanced Monsson winds (Kathleen, 2001), and in Nigeria the briefest moist period was between ca. 9.9-7- ka (Stokes et al., 1997).

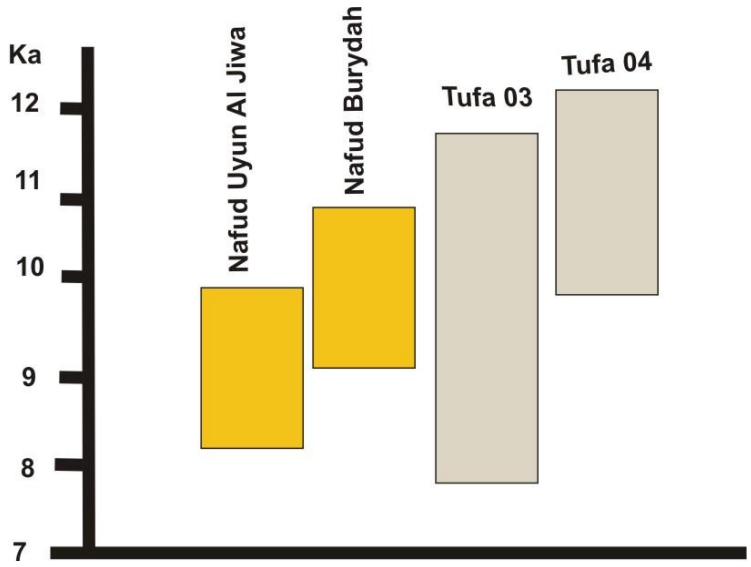

Figure 5.6: Summary diagram which shows the evaluation of the age overlaps of the tufa and dunes in the Burydah area. This would indicate that there was a significant wet event during this period.

5.5 Factors influencing the redness of the Nafud

In terms of the present Burydah environmental and more recent processes, spatial variation in dune redness patterns can be informative. When comparing Figure 4.37 with Figure 5.7, the dunes redness rating derived from the ETM image within the Nafud Al Mazhur, Al Thuwayrat, Al Tarafiyah and As Sirr show that the sand colour in the Al Nafuds ranges between reddish to reddish-yellow (7.5 YR 6/8) and pale-yellow (2.5YR 7/4) in colour.

Most of the sand in the eastern margins of the Nafud Al Thuwayrat is strong brown in colour 7.5 YR 5/8. There are lower values of sand redness in most of the eastern parts of the Nafud Al Mazhur and the western Nafud As Sirr but there is a gradation towards the west of the Nafud.

The colour in the east is reddish–yellow (7.5 YR 6/8), whilst the western parts of the Nafud are more reddish–yellow (7.5 YR 6/6). The least red sand dunes are found in the most northerly parts of Nafud As Sirr and Nafud Al Tarafiyah where the sands are pale-yellow (2.5YR 7/4).

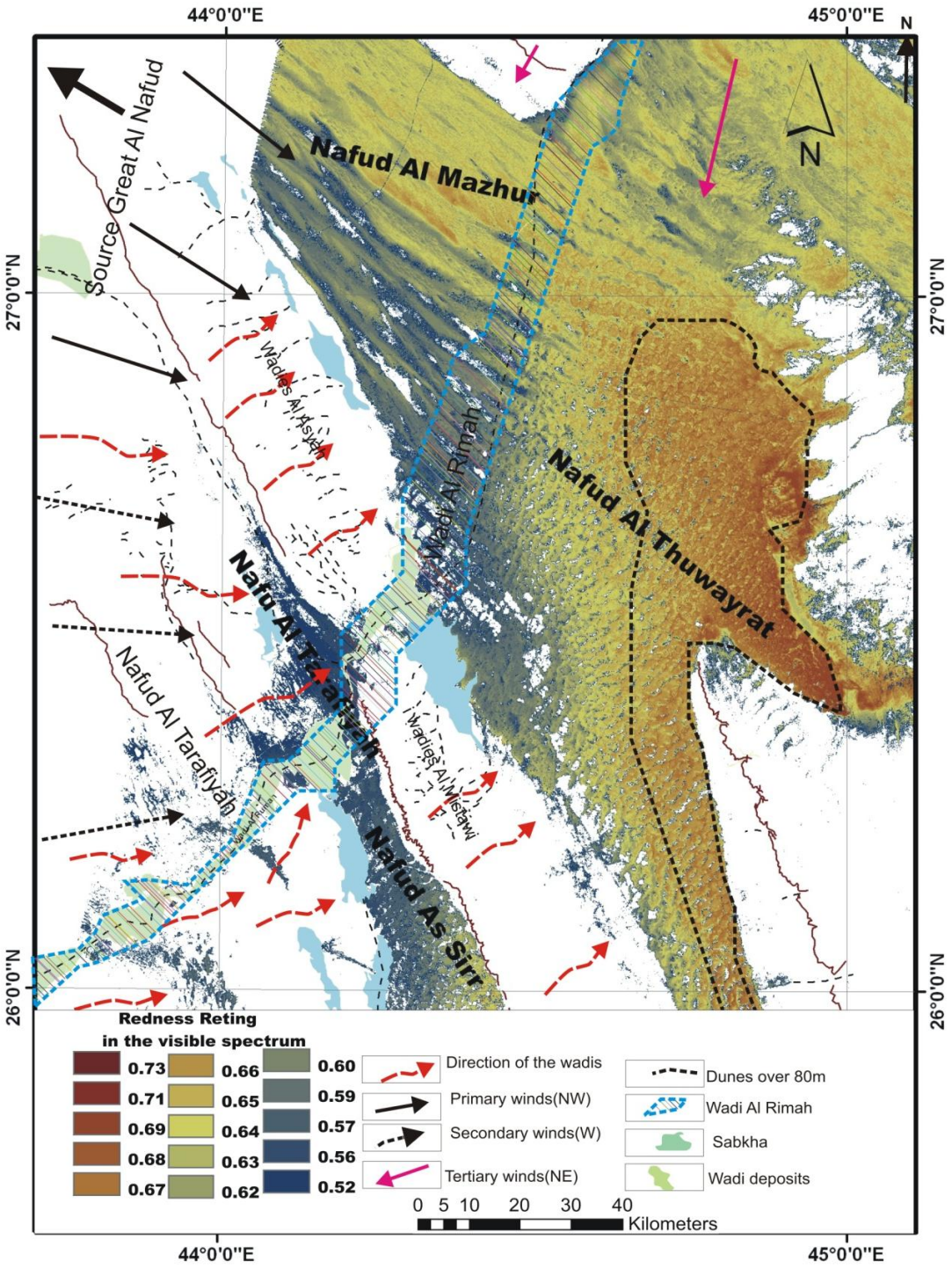

Figure 5.7: Schematic diagram of potential processes controlling dune redness. The black arrows show the direction of the west winds. The red arrows show the direction of the wadis channel. The green area is the Sabkhah which extend as a belt along the west Nafuds, wadis and gullies and are marked by thin black dotted lines e.g., wadis in the Safra Al Asyah and to the west of Nafud Al Mazhur and wadis in the Safra Al Mistawi to the west of Nafud Al Thuwayrat. Palaeo channels of Wadi Al Rimah covered by sands have been marked by a blue dotted line. The dotted black line marks the high dunes over 80m.

The processes that influence dune redness in the landscape are:

- Primary processes/sources.
  - The first process that needs to be considered is erosion and entrainment of sand-sized grains. In order for sand to be entrained and transported from the source area, there needs to be enough wind energy to allow these processes to occur. The main source area where these processes operate is in the Great Nafud to the north-west of the study area (Al Sayari and Zotl., 1978; Al welaie, 1985 and Edgell, 2006); and where the shamal wind systems dominate. Edgell (2006) identified that the primary source of sand for the Nafud Al Thuwayrat was the great Al Nafud, via Al Mazhur.
  - The sands have been transported in a south-easterly direction through the linear dune system of Nafud Al Mazhur and towards Nafud Al Thuwayrat. There must then have been a lowering of the sediment transport rate, which allowed the sands to be deposited to allow the build-up of dome dunes in Nafud Al Thuwayrat.
- Secondary Processes/sources.

  Secondary sources of sediment into the Nafuds come from the west and include the Wadi Al Rimah and its tributaries, the sabkhas as well as bedrock located on the western margins of the Nafuds. Edgell (2006) has also argued that a secondary sand source is most likely the Wadi Al Rimah and Wadi Al Batin. In addition, White et al (2001) working in the northern Rub Al Khali found reductions in dune redness in the proximity of adjacent coastal sabkhah and interdune pans. The dome dunes of Nafud Al Thuwayrat cap the hills of the Minjur Formation, and this evidence is supported by many farmers who drill wells in the area, and they have reported bedrock at a depth of about 50-60 metres.

  Bedrock has also been observed in the field, where it has been seen to be extracted for road aggregates (Fig 5.8). This bedrock under the Nafud has been dominated by iron-enriched sandstones (Manivit et al., 1986). It is likely that the haematite from the bedrock was eroded and transported to the Nafud under the winds that had blown predominantly from N and NW and/or the formation of hematite developed under sand

moisture and the oxides minerals may have been filtered into sand that was carried up. Edgell (2006) also referred to Minjur sandstone being exposed in the interdunes of Nafud Al Thuwayrat. The influence of geology has also been suggested as an influence on sand redness by White et al., (2001), who concluded that one of the main controls on sand colour in Rub Al Khali was the geology of the adjacent Oman Mountain.

Other factors influential for dune redness are the dune form (type) in particular those dunes which build up and are relatively stationary (e.g. the dome dunes) and are far redder than the more active linear dunes, which extend downwind. The dune type also affects dune thickness/sediment build up (Fig. 5.7). The areas where sediment thickness is greatest are also the reddest as there is not enough sand movement for the clays and haematite on the grains to be knocked off (Gardner and Pye 1981).

Finally, dune moisture is an important variable. If the environment is too wet then the clays and haematite weather, and are subsequently removed (Gardner and Pye 1981). Equally, the formation of haematite requires enough moisture to enable chemical weathering of primary minerals (Jimenez-Espinosa & Jimenez-Millan, 2002); water activity was an important factor in controlling sand colour (Schwertmann, 1993). Moreover, haematite formation is significantly reduced when there is active water in the sand system (Jimenez-Espinose & Jimenez-Millan., 2002). Folk (1976) also observed that sand reddening was a product of moisture availability with high temperature and time.

All of these factors play a role in affecting dune redness with a decrease in sand reddening and magnetic susceptibility along the middle and west Nafud Al Mazhur, most of west Nafud As Sirr and all parts of Nafud Al Tarafiyah. In these locations the sands contain increased amounts of carbonates from the wadis and sabkhah to the west of the Nafuds (Fig 5.9).

In terms of the amounts of haematite present in the sands, the ETM redness results have shown a low redness concentration in the western Nafud Al Thuwayrat, Nafud Al Mazhur and Nafud As Sirr, indicating low levels of haematite. In terms of dune form, it is interesting to note that the spatial distribution of redness in the ETM image (Fig 5.7),

has shown redness increasing towards the eastern parts of Nafud Al Thuwayrat and As Sirr; with high magnetic components and a strong brown colour along the middle of the Nafud, with an increase towards the most eastern parts.

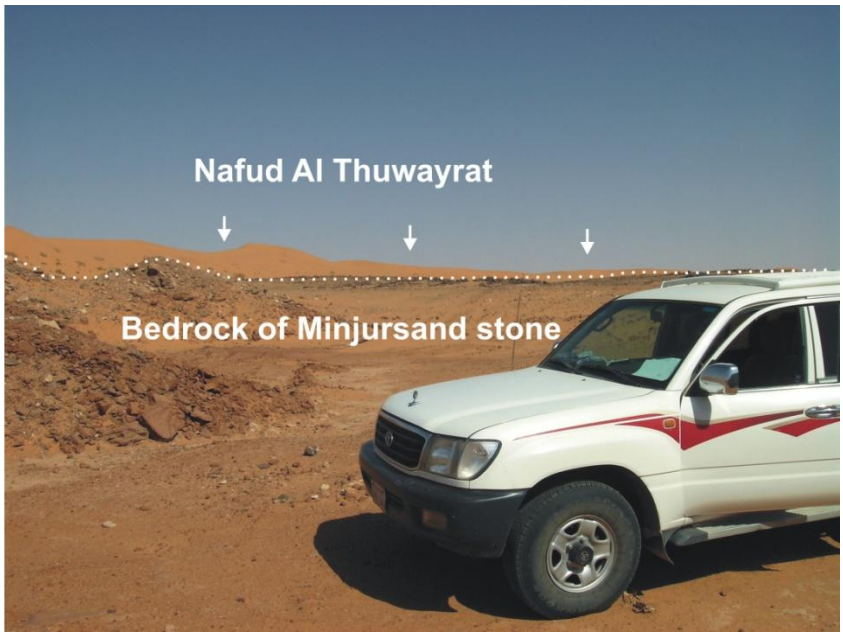

Figure 5.8: The bedrock of Minjur sandstone, frequently exposed in the interdune of the Nafud Al Thuwayrat. In the white dashed-dotted line the dunes cap the hills of the Minjur Formation.

Figure 5.9: The sabkhah commonly found along the west of Nafud As Sirr. Such sabkhah represent a potential source for some Nafud deposits.

CHAPTER SIX

6 Conclusion

6.1 Introduction

The purpose of this research has been to study the environmental changes in the Burydah area in central Saudi Arabia. The first step has involved the implementation of an extensive literature review to derive relevant evidence related to past environmental changes; since this environment has not been well explored in terms of the Quaternary period.

During the second stage there has been the formation of a geomorphological map based on satellite images. The third stage has investigated the study area through fieldwork previously conducted during 2008 to delineate the Quaternary deposits. During this time 25 sections were investigated and samples taken from wadi terraces, aeolian deposits and lake sediments as well as tufa.

The next stage involved dating representative samples using OSL (25 samples) and ^{14}C dating (17 samples). These numerical ages have thus represented one of the first attempts to develop a geochronology in the Burydah area in central Saudi Arabia. Sedimentalogical and geochemical studies have involved:

1) Particle size analysis conducted on 148 sediment samples and has thus provided a good indicator for highlighting environment processes. 2) XRD has been used to examine 75 samples and identify their mineral components. 3) Thin section studies have been applied to 148 sediment samples using a petrographic microscope. The micro scale features and minerals presented in the samples were thus examined. Finally, the use of remote sensing was found to bring study to the present environment and has been successful for the establishment and mapping of the forms and colour of the dunes in various Nafuds.

6.2 Key Findings

This study has shown evidence of wet and dry events at various points in time over the last 221 ka, which has been identified through the analysis of the sedimentological, geochemical and petrological properties of a range of sediments sampled from the study area and numerical dating of a subset of them.

The oldest red weathered deposits preserved in the east of Burydah area have shown that there was significant evidence for intense Shamal winds with a slightly moister period during MIS7. The findings of the deposition of fluvial and aeolian sediments which occurred in the Burydah area within the lower Wadi Al Rimah, showed there were significant moister phases in the last interglacial period especially in MIS 5d (~110 ka). This was represented by slightly increased fluvial activity in the wadi which also coincided with sand dune preservation. To date there has been no evidence for a wet period around 110 ka in Saudi Arabia. The Burydah area, during this phase, showed an increase of wadi activity; whereby the upper wadi possibly received increased rainfall over the west of Saudi Arabia and was therefore active and fed down to the study area where sand dunes were forming in response to the enhanced Shamal winds.

The lower Nafud Burydah indicates that dunes formed in the warmer period MIS 5c (99 ka). Evidence from the paleo-channel represented by the Wadi Al Butaun at the northern edge of the Burydah area, reflected wetter phases again related to MIS 5b and 5a (77 ka to 85 ka). Fluvial activity in the Burydah area during the last interglacial period probably formed under the effectiveness of high rainfall, when the ITCZ reached its northernmost position and Monsoon winds brought moisture from the Indian Ocean. In addition there was perhaps some contribution of north westerly Mediterranean systems with winter rainfall received within northern Saudi Arabia during MIS5, supporting evidence of an extension of the Mudawwara lake between 88 ka and 77 ka (Petit-Maire *et al*., 2002) (that located about 300km to the north of the upper Wadi Al Butaun catchment). Moreover, there was also growth of calcite speleothems in Jordan between 80 and 70 ka (Frumkin et al., 2008). Further evidence argued by Burns *et al*. (1988, 2002)

at the Hoti cave, Oman, has claimed that the growth of speleothems corresponded to increases in rainfall during 80-78 ka. All this evidence has indicated that the upper catchment of the wadi Al Butaun, and its tributaries in the northern parts of central Saudi Arabia reserved Monsoon rainfall, due to northernmost position of ITCZ, that brought moister from the Indian Ocean. In addition perhaps winter Mediterranean systems rainfall as well reached the northern parts of central Saudi Arabia and brought moister from the warm Mediterranean Sea.

The next major geomorphological event was related to sand deposition in Nafud Al Thuwayrat at about 49 ka. As shown from earlier evidence these dunes provided information to support Shamal wind activity; and their formation often coincided with evidence of water table activity.

The next wet phase has been represented by lake deposits in the eastern edge of Burydah within Nafud Al Thuwayrat at about 30 to 40 cal BP. The Al Mazhur lake possibly benefited from runoff from the west wadis crossing Safra Al Asyah with some contribution from Wadi Al Rima. This date could be linked with evidence of lacustrine sediments dated to a similar age such as those of Rub Al Khali, Nafud Jubbah, Lake Nafud As Sirr and wadi deposits at Wadi Al Dawasir and the Al Sulb Plateau. Additionally, similar North Africa lakes such as the Maryut Lake in Egypt, were active during ca ~35 cal BP (Warne and Stanley 1993).

Following on from this are the well-known wet events between 12 ka to 7 years ago represented by tufa deposits and the establishment and growth of large sand dunes, thus supporting evidence for wetter conditions during the early to mid-Holocene. This which could also be linked with evidence from, Africa e.g. rise up of the Umm Akhtar lake in northern Africa (Karhleen, 2001); also a brief moist period in the Nigeria lake between ca. 9.9-7 ka (Stokes et al., 1997).

Similar evidence has also been provided from the Arabian Peninsula such as of runoff of Wadi Ad Dawasir and Wadi Al Luhy (Hotzl *et al*., 1978); As Sirr palaeolakes (Garrard *et al*., 1981; McCorriston *et al*., 2002); southern point of Al Rub al Khali (McClure, 1967); Nafud Jubbah (Whitney *et al.,*1983) speleothems in the northern Hoti cave (Neff, *et al.,*

2001) and lacustrine sediments at Awafi at Ras Al Khaimah (Parker, *et al.,* 2004). This wet evidence may support Monsoon activity during the Holocene with some contribution being made from winter Mediterranean rainfall systems in the study area.

By 5 ka and towards the present day the dominant deposits are sand sheets in the Burydah area indicating that it has become relatively arid, i.e. similar to present day conditions with short wet events. This has been linked to decreased monsoon precipitation, which has decreased gradually in response to the changing northern hemisphere summer solar insolation. The ITCZ position was northward in the early Holocene and from 7.8 ka the ITCZ has continuously migrated southward away from Saudi Arabia. Sands with marl beds at Awafi and Ras Al Khaimah lakes were related to the mid-Holocene around 5.9 – 4 ka and were followed by arid phases when lakes were filled by sands ages 4 ka (Parker, *et al., 2004,* 2006). Further north around Sabkhat Matti, OSL dating has shown aeolian sand deposition occurring around 5.9 ka (Goodall, 1995). Similar dunes building found in Africa, related to the mid-Holocene, such as sand in Inner Mongolia, dunes in Umm Akhtar southern Egypt; and additionally, linear dunes in Witpan sands (Telfer & Thomas., 2007).

Bringing the study up to the modern day, the remotely sensed data has shown increased dune reddening towards the east and less reddening toward the west at Nafud Al Thuwayrat and Al Mazhur and As Sirr. The major direction of the systems of linear dunes, whereby axes are towards the south east in most dunes, have been controlled mostly by the effect of the Shamal winds. The geological and morphological characteristics around and within sand dunes are extremely important factors that are controlled by sand accumulation.

The main controls on recent sand accumulation in the Nafuds affecting sands colouration are:

1) Aeolian sands being blown by the Shamal winds from the North West;
2) Great Al Nafud sources zones supplying sand to the shamal winds system;
3) The wadis and sabkha deposits bringing in sediments via fluvial and occasional aeolian activity;

4) Dune form and sand thickness (i.e. dom dunes in the Nafud Al Thuwayrat more redder than liner dunes in the Nafud Al Mazhur);

5) Trapped depressions and Questas; Wadi Al Rimah and its tributaries.

6.3 Summary

To summarise, there is clear evidence of wetter events during MIS7 and MIS5d, MIS5b and MIS5a with linear dunes also developing around MIS5C (Fig 6.1). During glacials, there has been evidence of linear dune formation at MIS4 followed by palaeolake development at MIS3 (Fig 6.1). No preserved evidence of these conditions that existed at the peak of the last glacial period was found as part of this study. This may suggest that conditions at this time were hyper-arid and the erosive more rather than depositional, which thus concurs with the findings of many studies over this period in the Arabian Peninsula such as McClure, (1976); Whitney et al., (1983); Preusser et al., (2002); Juyal et al., (1998) and Glennie et al., (1998); and with regards to Africa such as Stokes et al., (1998), Telfer and Thomas, (2007). There is clear evidence of wetter conditions during early to mid-Holocene (Fig 6.2) associated with latitudinal expansion of the monsoon rains (see Tuenter et al., 2003).

Following on from this the tufa and many of the fluvial deposits in the study area became buried under sand sheets, indicating a movement towards the arid conditions of today (Fig 6.3) associated with ITCZ migration southward and monsoon precipitation decreasing gradually in response to decreasing solar insolation (Fleitmann et al., 2006). In the modern environment we can see evidence of large-scale linear dunes, widespread sand sheets lying next to ephemeral wadi channels that flood occasionally. In addition, information has been gained from studies of dune colouration about the influence of a range of processes operating on the landscape today.

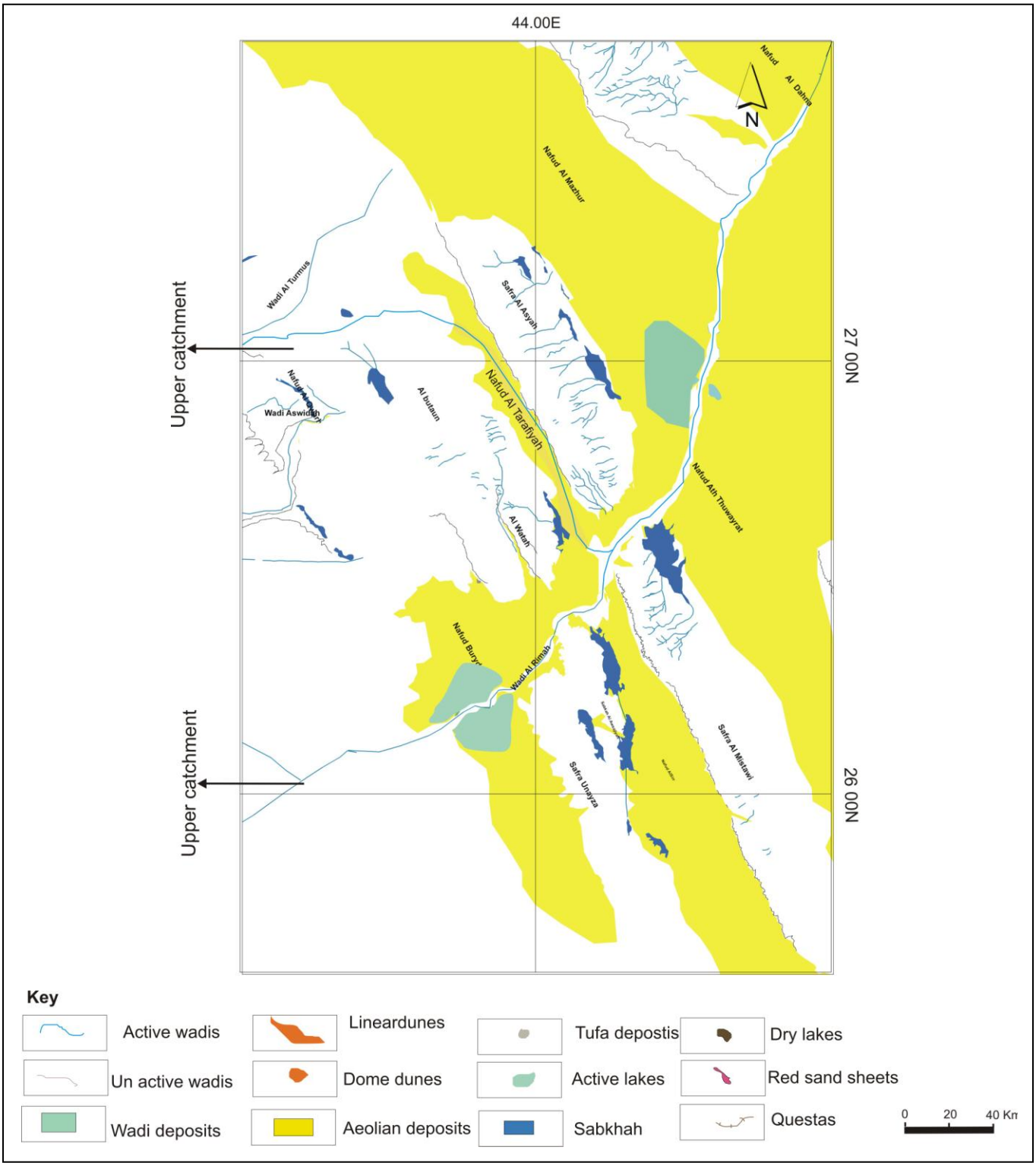

Figure 6.1: Palaeogeographic map of the study area. Last interglacial (MIS3 toMIS5) the marine oxygen isotope records according to Willoughby, (2007).

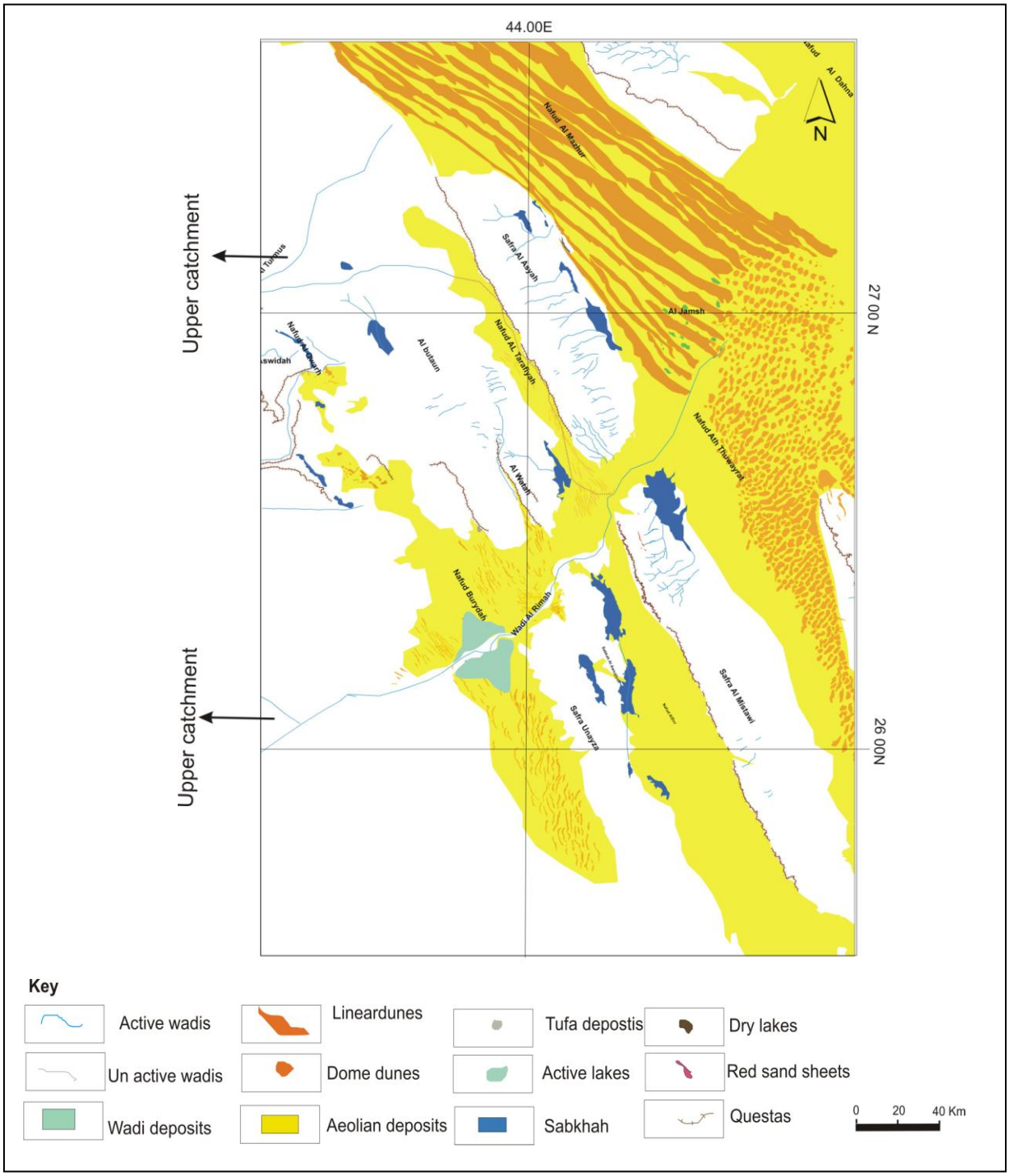

Figure 6.2: Palaeogeographic map of the study area during the early Holocene (12-5 ka). Most wadi in the Burydah was active and Linear dune still building

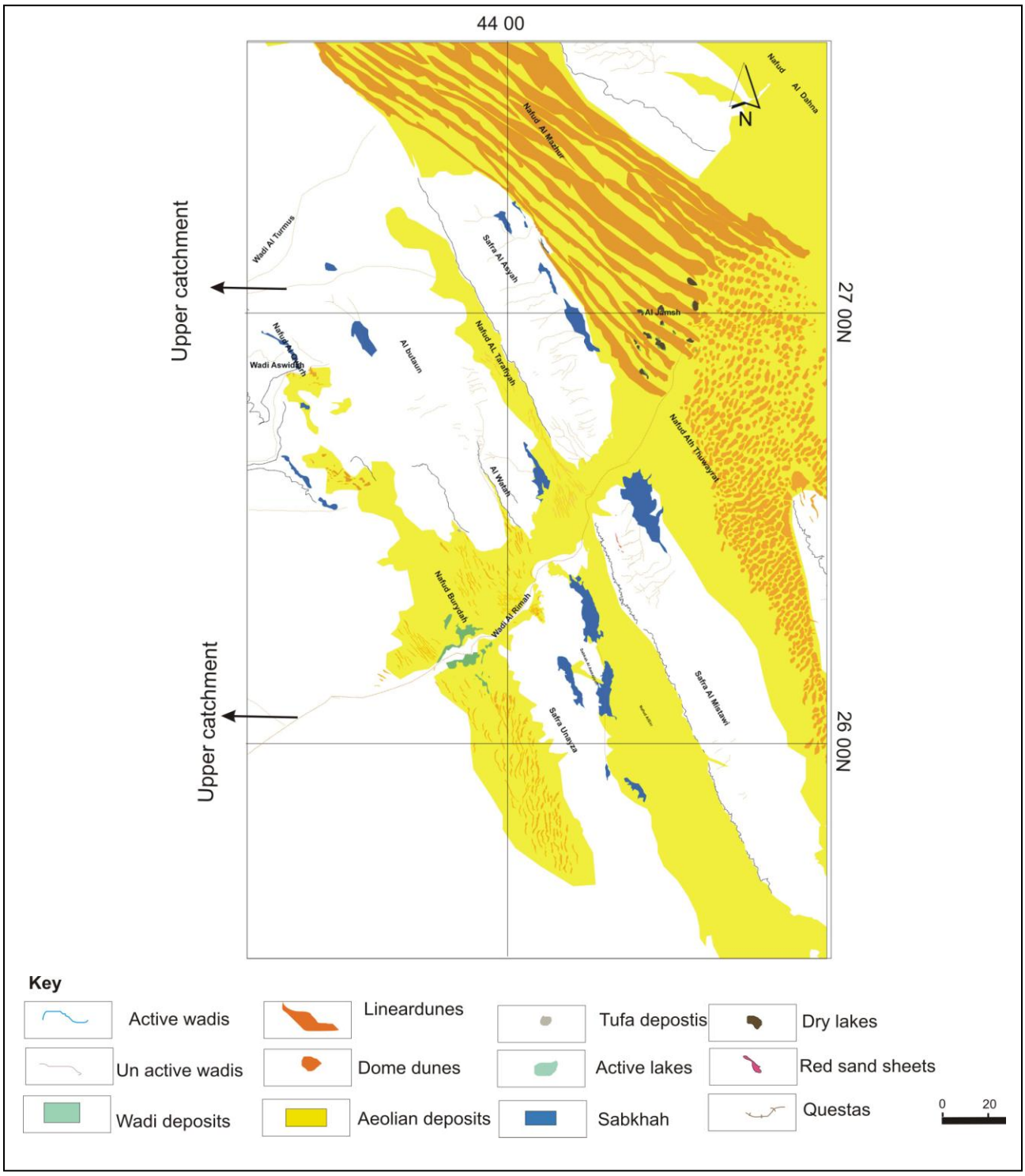

Figure 6.3: Palaeogeographic map of the study area during the mid-Holocene (5 ka – Present). Burydah became more arid , the Linear dune and sand sheets were common.

Bibliography

Abdel Fattah, 2006. Basic foundations of remote sensing and images. Airashe Library, Saudi Arabia.

Abed A. M., Yasin S., Sadaqaa R., Al Hawari., 2008. The paleoclimate of the eastern desert of Jordan during marine isotope stage 9. Quaternary research. vol. 69, pp. 458-468.

Adams J. M., Faure H., (1997) (ed.s), QEN members. Review and Atlas of Palaeovegetation. Preliminary land ecosystem maps of the world since the Last Glacial Maximum. Oak Ridge National Laboratory, TN, USA. http://www.esd.ornl.gov/projects/qen/adams1.html

Aitken, M., 1998. An Introduction to Optical Dating. The Dating of Quaternary sediments by the use of photon-stimulated luminescence. Oxford, UK.

Alin, S., Cohen, A., 2003. Lake-level history of Lake Tanganyika, East Africa, for the past 2500 years based on ostracode-inferred water-depth reconstruction. Palaeogeography, palaeoclimatology, palaeoecology 199, pp. 31-49.

Al Dughairi, A., 2003. Geomorphologic Al Watah in Saudi Arabia. Masters thesis, King Saud University, Riyadh Saudi Arabia.

Al Juaidi, F., 2003. The utilisation of merged remotely sensed data from geomorphological investigation in the Desert of Central Saudi Arabia, PhD. thesis submitted to University of Leicester. UK.

Al Juaidi, F., Millington, A., McLaren, S., 2003. Evaluating image fusion techniques for mapping geomorphological features on the eastern edge of the Arabian shield Central Saudi Arabia. Geographical Journal, vol. 169, pp. 117-131.

Al Sayari, S. and Zlotl, J., 1978: Quaternary period in Saudi Arabia 1: Sedimentological, Hydrogeological, Hydrochemical, Geomorphological and Climatological Investigations in central and Eastern Saudi Arabia. Springer- Verlag, Vienna.

Al Welaie, A. 1985. Geomorphology and Geomorphology of Saudi Arabia. Al Obeikan Library. Riyadh, Saudi Arabia.

Anton, D., 1983. Modern aeolian deposits of the Eastern Province of Saudi Arabia. 365-378.In: Brookfield, M E., Ahlbrand, T, S. (eds.) Advances in sedimentlogy, Amsterdam, Elsevier.

Anton, D., 1984. Aspects of geomorphological evolution, In: Jado, A., Zötl, J. (eds) Quaternary Period in Saudi Arabia, Springer-Verlag, Vienna, vol. 2, pp. 275-296.

Bateman, M.D., Thomas, D.S.G. and Singhvi, A.K. 2003. Extending the aridity record of the Southwest Kalahari: current problems and future perspectives. Quaternary International 111, 37-49.

Bailey, G., Al Sharekh, A., Flemming, N., Lambeck, K., 2007. Coastal prehistory in the Red Sea Basin underwater archaeology, and the Farasan Islands. Proceedings of the seminar for Arabian studies, p.37.

Boulter, C., Bateman. M., 2009. Guidelines for optically-stimulated luminescence dating of sediment. Sheffield Centre for International Drylands Research, University of Sheffield. U.K.

Bray, H. E., Stephen, S., 2004. Temporal patterns of arid-humid transitions in the South-Eastern Arabian Peninsula based on optical dating. Geomorphology, vol. 59, pp. 1-4.

Brown, G., Schmidt, D., Huffman, A., 1989. Geology of the Arabian Peninsula: Shield area of Western Saudi Arabia. U. S. Geological Survey professional paper 560-A.

Bullard, J., White, K., 2002. Quantifying iron oxide coatings on dune sands using spectrometric measurements: An example from the Simpson-Strzelecki Desert, Australia. Journal of geophysical research, vol.107, vol B6, p. 2125.

Burns, J., Fleitmann. D., Mudelsee, M., Neff, U., Matter, A., Mangini, A., 2002. A 780 year annually resolved record of Indian Ocean monsoon precipitation from a speleothem from south Oman. Journal of geophysical research, p. 107.

Burns, S., Matter, A., Mangini, A., Mudelsee, M., 1998. The history of the monsoon in Southern Arabia results based on stable isotopes and U/Th dating of speleothems. Mineralogical Magazine 62A, pp. 261-262.

Chapman, R., 1978. Geology. In AL Sayari, S. and Zotl, J. (eds), Quaternary Period in Saudi Arabia, Springer-Verlag, Vienna, 4-8.

Campbell, J., 2002. Introduction to remote sensing. Third edition, Taylor and Francis, New York.

Chavez, P., 1996. Image based atmospheric correction revisited and improved. Photogrammetric engineering and remote sensing, vol. 62, pp. 1025-1036.

Dearing, J., 1999. Environmental magnetic susceptibility using the Bartington MS2 system. ISBN British Library.

Duller, G. A. T., 2008. Single grain optical dating of Quaternary sediments: why aliquot size matters in luminescence dating. Boreas, vol. 37, p589-612.

Dupont, L., Jahns, F., Marret, and Shi Nig., 2000. Vegetation changes in equatorial West Africa: Time-slices for the last 150 ka Palaeogeography, Palaeoclimatology palaeoecology 150:95-122.

Edgell, H., 2006. Arabian Desert nature, origin and evolution. Springer, Netherlands.

Fleitmann, D., Burns, S., Mudelsee, M., Neff, U., Mangini, A., Matter, A., 2003. Palaeoclimatic interpretation of high-resolution oxygen isotope profiles derived from annually laminated speleothems from Southern Oman. Quaternary Science Reviews. vol. 23, pp. 935-945.

Fleitmann, D., Matter, A., Pint, J., Al Ahanti, M., 2004. The speleothem record of climate change in Saudi Arabia. Suadi Geological survey. Riyadh.

Fleitmann, D., Burns, S., Mangini, A., Mudelsee, M., Kramers, J., Villa, L., Neff, H., Al Subbary, A., Buettner, A., Hippler, D., Matter, A., 2007. Holocene ITCZ and Indian monsoon dynamics recorded in stalagmites from Oman and Yemen (Socatra). Quaternary Science Reviews, vol. 26, pp. 170-188.

Folk, R., 1976. Reddening of desert sands. Simpson Desert, NT Australia. Jrnl. Sed. Petr.,

Frumkin, A., Miryah, B., Vaks, A., 2008. Paleoenvironment of Jawa basalt plateau, Jordan, inferred from calcite spekeothems from a lava tube. Science Direct. vol 70, pp. 358-367.

Fuchs, M., Bürkert, A., 2007. A20 ka sediment record from the Hajar Mountain range in N-Oman and its implication for detecting arid humid periods on the southeastern Arabian Peninsula. Earth Pcanetary Science Letter, vol. 256, pp. 546-558.

Gardner, R., Pye, K., 1981. Nature, origin and paleoenvironmental significance of red coastal and desert dune sands: Prog. Phys. Geog., vol. 5, pp. 514-534.

Garrard, A., Harvey, C., Switzer, V., 1981. Environment and settlement during the upper pleistocene and holocene at Jubbah in the Great Nefud, Northern Arabia. Riyadh. Atlal 5, pp. 137-148.

Gasse, F. 2000. Hydrological changes in the African tropics since the last glacial maximum. Quaternary Science Reviews, vol. 19, pp. 189-211.

Glennie, K., Singhvi, A., 2002. Event stratigraph, paleoenvironment and chronology of SE Arabian deserts. Quaternary Science Reviews, vol. 21, pp. 853-869.

Glennie, K., 1995. The desert Southeast Arabia: A product of Quaternary climatic change. Geology of Quaternary desert margins, Balkema. Rotterdam, pp. 279-291.

Glennie, K., Belushi, J., Maskery, S., 1998. The inland Sabkhahs of the Huqf, Oman: A product of past extremes of humidity and aridity. Geology of Quaternary Desert Margins, Balkema. Rotterdam, pp. 117-122.

Goodall, T., 1995. The geology and geomorphology of the sabkhat Matti region (United Arab Emirates): a modern analogue for ancient desert sediments from north-west Europe. PhD thesis, University of Aberdeen, UK.

Johnson. T., Keits, K., Odada, E., 2000. The Holocene history of Lake Victoria. Amnbio, Royalswedish Academy of Sciences.113-135.

Goudie, A., Golis, A., Stokes, S., Parker, A., White, K., Al Farrajs, A., 2000. Latest pleistocene and holocene dune construction at the North Eastern edge of the Rub al Khali, United Arab Emirates. International association of sedimentolgists, vol. 47, pp. 1001-1021.

Grun, R. 1994. A Cautionary Note: Use of 'water content' and 'depth for cosmic dose rate' in the AGE and DATA programs. Ancient TL 12, p. 50.

Hannb, C., 1995. Predominant features of the Quaternary relief development seaward of the Oman Mountains as reflected in Wadi and coastal terraces. Conference on Quaternary desert and climatic change, Al-Ain, United Arab Emirates.

Hillier, S., 1999. Use of an air-brush to spray dry samples for X-ray powder diffraction. Clay Minerals, vol. 34, pp. 127-135.

Holm, A., 1960. Desert geomorphological in the Arabian Peninsula. Science, pp.123, 1369-1370.

Hötzl, H., Maurin, V., 1978. Wadi Birk, In Al Sayari, S.; Zötl, J., (eds): Quaternary period in Saudi Arabia, Springer-Verlag, Vienna, pp. 209-216.

Hötzl, H., Jado, A., Moser, H., Rauert, W., Zötl, J., 1984. The youngest Plestocene, In Jado, A., Zötl, J., (eds) Quaternary period in Saudi Arabia Sptinger-Verlag, Vienna.

Hötzl, H., Job, C., Moser, H., Rauert, W., Stichler, W., 1984. Hydrogeological and hydrochemical investigation in the upper part of Wadi Al Rimah. Quaternary period in Saudi Arabia, Springer-Verlag, Vienna, pp. 182-193.

Hooghiemstra, H., 1987: Changes of major wind belts and vegetation zones in NW Africa 20.000-5000yr B.P., as deduced from a marina pollen record near cap blanc. Elsevier Science B.V.vol 55, 1-3.

Jimenez-Espinosa, R., Jimenez-Millam. J., 2002. Calcrete development in Mediterranean colluvial carbonate systems from SE Spain. Journal of Arid Environments, vol. 53. pp. 479-489.

Johnson, T., Keits, K., Odada, E., 2000. The holocene history of Lake Victoria. Amnbio, Royal Swedish Academy of Sciences.

Joyce, A., 1978. Procedure for gathering ground truth information for a supervised approach to computer implemented land cover classification of Landsat-TM multispectral scanner date. NASA reference publication 1015. Houston.

Juyal, N., Singhvi, A., Glennie, K., 1998. Chronology and palaeoenvieonmental significance of Quaternary desert sediment in South-Eastern Arabia. Geology of Quaternary desert margins, Balkema. Rotterdam, pp. 315-325.

Kassler, P., 1973. The structural and geomorphic evolution of the Persian Gulf. In: Purser (Editor), The Persian Gulf. Springer, New York, N.Y., pp. 11-32.

Kathleen, N., 2001. Geoarchaeology of Umm Akhtar playa: early holocene palaeoenvironments of South Egypt. Archaeological Geology NO125. (Abstract).

Kemp, S.J., Wagner, D., 2009. Mineralogical analysis of Quaternary rock from Saudi Arabia England. Nottingham, UK, British Geological Survey, 81pp. (CR/09/093) (Report).

Lancaster, N., 2003. Aeolian Chronology and Paleowind vectors in Northern Rub al Khali, United Arab Emirates. XVI INQUA Congress (Abstracts), p. 141.

Lezine, A-M., Salieg, J., Inizan, M., 1998. Holocene Lake from Ramlate As Sab Atayn Yemen. lllustrate the impact of monsoon activity in Southern Arabia. Quaternary research. Paris, France, vol 50, pp. 290-299.

Manivit, J., Denis, V., Alain, B., Paul, L. and Jackie, F., 1986. Explanatory notes to the geologic map of the Burydah Quadrangle, sheet 26G. Kingdom of Saudi Arabia, ministry of petroleum and mineral resources Saudi Arabia.

Maurice. E., 1988. Techniques in sedimentary, Blackwell Publishing, London.

Maurice. E., 2001. Sedimentary petrology. Blackwell Publishing, Oxford, London. (Third edition).

McClure, H., 1967. Radiocarbon chronology of late Quaternary lakes in the Arabian desert. Nature, vol 263, pp. 755-756.

McClure, H., 1984. Late Quaternary palaeoenvironments of the Rub al Khali. PhD thesis, University College London, U.K.

McCorriston, J., Oches, A., Walter, D., Cole, L., 2002. Holocene palaeoecology and prehistory in highland southern Arabia. Pale´orient 28: 61–88.

McLaren, S., Al Juaidi, F., Millington, A., Bateman, M., 2009. Evidence for episodic humidity in the arid interior of Central Saudi Arabia over the last 60 ka, Journal of Quaternary science. U.K.

McLaren, S., Gilbertson, D., Grattan, J., Hunt, C., Duller, G., Barker, G., 2004. Quaternary palaeogeomorphologic evolution of the Wadi Faynan area Southern Jordan. Palaeogeography, palaeoclimatology, palaeoecology, vol. 205, pp. 131-154.

Milton, E. J., 1980. A portable multiband radiometer for ground data collection in remote sensing. International Journal of Remote Sensing, vol 1, no. 2, pp. 153-165.

Milton, E. J., Rollin, E M., 2003. Estimating irradiance spectrum from measurements in a limited number of spectral bands. School of geography, University of Southampton, Highfield, UK.

Ministry of Agriculture and Water, 1999. The soils atlas of Saudi Arabia, Ministry of Agriculture and Water, Saudi Arabia.

Ministry of Agriculture and Water, 1988. Climate atlas of Saudi Arabia, Ministry of Agriculture and Water, Saudi Arabia.

Moran, M.S., Jackson, R.D., Slater, P.N., Teillet, P.M., 1992. Evaluation of simplified procedures for retrieval of land surface reflectance factors from satellite sensor output, Remote sensing of environment, 41, pp. 169-184.

Murray, A. S., Wintle, A. G., 2003. The single aliquot regenerative dose protocol: potential for improvements in reliability. Radiation Measurements, vol. 37, pp. 377-381.

Neff, U., Burns, S. J., Mangini, A., Mudelsee, M., Fleitmann, D., Matter, A., 2001. Strong coherence between solar variability and the monsoon in Oman between 9 and 6 kyr ago. Nature, vol. 411 pp. 290-293.

Nicoll, A., 1998. Holocene playas as sedimentary evidence for recent climate change in the presently hyperarid Western Desrt, Egypt, Doctoral dissertation. Tucson: The University of Arizona (unpub-lished).

Olley, J.M., Pietsch, T., Roberts, R. G., 2004. Optical dating of Holocene sediments from a variety of geomorphic settings using single grains of quartz. Geomorphology 60, 337–358.

Pachur, H. J., Wunnemann, B., Zhang, H.C., 1995. Lake evolution in the Tengger Desert, Northwestern China, during the last 40,000 years. Quaternary Research, 44, 171 – 180.

Parker, A., Eckersleyl, L., Smith, M., Goudie, A., Stokes, S., Ward, S., White, K. , Hodson, J., 2004. Holocene vegetation dynamics in the North-Eastern Rub al-Khali desert, Arabian Peninsula. A phytolith, pollen and carbon isotope study, John Wiley, pp. 19, 655-676.

Parker, A., Preston, G., Walkington, H., Hodson, M., 2006. Developing a framework of holocene climatic change and landscape archaeology for the lower Gulf region, South-Eastern Arabia. Blackwell Publishing, vol. 17, pp. 125-130.

Parker, A., 2009. Pleistocene climate change in Arabia. Developing a framework for Hominin dispersal over the last 350 kyr. Springer Science +Business Media, pp. 39-49.

Partrige, T. 1997. Cainozoic environmental change in Southern Africa, with special emphasis on the last 200 ka. Progress in Physical Geography21, 3-22.

Pedley, H., 2000. Ambient temperature freshwater microbial tufa. In: Riding, R. E., Awramik, S. M., Microbial sediments Berlin. Springer-Verlage pp. 179-186.

Perkins, D., Henke, K. R., 2004. Minerals in thin section. Pearson Prentice Hall. U.S.A.

Petit-Maire, N., Carbonel, P., Reyss, J., Sanlaville, A., Abed E., Bourrouilh, R., Fontugne, M., Yasin, S., 2002. A vast Eemian palaeolake in Southern Jordan. Global and planetary change. Science Direct. pp. 1-6.

Petraglia, D., Drake, N., Alsharekh, A., 2009. Acheulean landscapes and large cutting tools assemblages in the Arabian Peninsula. Springer Science, pp. 103-116.

Powers, R., Ramirez, L., Redmond, C., Elberg, J., 1966. Geology of the Arabian Peninsula sedimentary geology of Saudi Arabia, geological survey professional. United States government printing office, Washington, D. C., pp. 147.

Prabhu, C., Shankar, R., Anupama, K., Taieb, M., Bonnefille, R., Vidal, L., Prasad, S., 2004. A 200 Ka pollen and oxygen isotopic record from two sediment cores from the Eastern Arabian Sea. Palaeogeography, palaeoclimatology, palaeoecology, pp. 214, 309-321.

Preusser, F., Radies, D., Matter, A., 2002. A 160,000 year record of dune development and atmospheric circulation in Southern Arabia. Science, vol. 296, pp. 2018-2020.

Preusser, F., Radies, D., Driehorst, F., Matter, A., 2005. Late Quaternary history of the coastal Wahiba Sands, Sultanate of Oman.

Prescott, JR., Hutton, JT., 1994. Cosmic ray contribution to dose rates for luminescence and ESR dating: large depths and long-term time variations. Radiation Measurements 23: 497-500.

Pugh J. 1997. The Quaternary desert sediments of the Al Liwa area, Abu Dhabi. PhD thesis, University of Aberdeen, UK.

Rodnight, H., Duller, G. A. T., Wintle, A. G., Tooth, S., 2006. Assessing the reproducibility and accuracy of optical dating of fluvial deposits. Quaternary Geochronology, vol. 1, pp. 109-120.

Rollin, E., Milton, E., 2003. Estimating spectral irradiance from measurements in seven spectral bands. Southampton, United Kingdom.

Schulz, E., Whitney, J. W., 1986. Upper pleistocene and holocene lakes in the An Nafud Saudi Arabia. Hydrobiologia, vol. 143, pp. 175-190.

Schulz, E., Whitney, J. W., 1986. Vegetation in North-Central Saudi Arabia. Journal of arid environments pp. 10, 175–186.

Schwertmann, U., 1993. Relations between iron oxides, soil colour and soil formation. Soil science society of America. USA, vol 31, pp. 51-69.

Staubwasser M, Weiss H. 2006. Holocene climate and cultural evolution in late prehistoric–early historic West Asia. Quaternary Research 66: 372–387.

Stokes, S., Horrocks, J., 1998. A reconnaissance survey of the linear dunes and loess plains of North-Western Nigeria: Granulometry and geochronology. Geology of Quaternary desert margins, Balkema. Rotterdam, pp. 165-174.

Stokes, S., Bray, H., 2005. Late pleistocene aeolian history of the Liwa region, Arabian Peninsula Geological Society of America, vol 117, pp. 1466-1480.

Stokes, S., Maxwell, T., Haynes, C., Horrocks, J., 1998. Latest pleistocene and holocene sand-sheet construction in the Selima Sand Sea, Eastern Sahara. Geology of Quaternary desert margins, Balkema. Rotterdam, pp. 175-181.

Stokes, S., Thomas, D., Washington, R., 1997. Multiple episodes of aridity in Southern Africa since the last interglacial period. Nature Macmillan Publishers Ltd., vol 338, pp. 154-158.

Tamers, D., Hood, R., 2010. Report for radiocarbon dating results for study samples, prepared by Bata Analytic Inc Lab. Miami, Florida, USA.

Telfer, M.W. and Thomas, D.S.G. 2007: Late Quaternary linear dune development of the southwestern Kalahari: Implications for aeolian palaeoclimatic reconstructions. Quaternary Science Reviews, 26(19-21): 2617-2630.

Tierney, J., 2010. An organic geochemical perspective on tropical East African paleoclimate. A dissertation submitted in partial fulfilment of the requirements for the degree of Doctor of Philosophy in The Department of Geological Sciences at Brown University.

Thomas, D., Connor, P., Stokes, S., 1998. Late Quaternary aridity in the South-Western Kalahari Desert. New contribution from optically stimulated luminescence OSL dating of aeolian deposits, Northern Cape Province, South Africa. Geology of Quaternary desert margins, Balkema. Rotterdam, pp. 209-224.

Thomsen, K. J., Murray, A. S., Bøtter-Jensen, L., Kinahan, J., 2007. Determination of burial dose in incompletely bleached fluvial samples using single grains of quartz. Radiation Measurements 42, pp. 370–379.

Torrent, J., Schwertmann, U., Schulze, G., 1980. Iron oxide mineralogy of some soils of two river terrace sequences in Spain. Geoderma, 23: 191-208

Tuenter, E., Weber, S., Hilgen., F., Loirens, L., 2003. The response of the African summer monsoon to remote and local forcing due to precession and obliquity. Global and Planetary Change, vol 36, pp. 219–235.

Viles, H. A., Pentecost, A., 2007. Tufa and Travertine. Chapter six in Geochemical sediments and landscapes. Edited by Nash, J., McLaren, S. Blackwell Publishing, Australia

Waldmann, N., Torfstein, A., Stein, M., 2010. Northward intrusions of low and mid latitude storms across the Saharo Arabian belt during past interglacials. Geological Society of America, vol 6, pp. 567-570.

Warne, A., Stanley, D., 1993. Late Quaternary evolution of the Northwest Nile Delta and adjacent coast in the Alexandria region, Egypt. Journal of coastal research, vol. 9, no. 1 (Abstract).

Whalen, N., Killick, A., James, N., Morsi, G., Kamal, M. 1980. Saudi Arabian archaeological reconnaissance. (Report on the western Province survey, Atlal, 5 43-58.

White, K., Goudie, A., Parker, A., Al Farraj, A., 2001. Mapping the geochemistry of the Northern Rub al Khali using multispectral remote sensing techniques. Earth surface and landforms, vol. 26, pp. 735-748.

Whitney, J., 1982. Overview of the geomorphology of Western Saudi Arabia. United States Geological Survey, Report USGSOF 02-6.

Whitney, J., Faulkender, D., Rubin, M. 1983. The environmental history and present condition of northern sand sea of Saudi Arabia. United States Geological Survey, Report USGSOF 03-95.

Willoughby, P.R., 2007. The evolution of modern humans in Africa a comprehensive guide. AltaMira Press, a division of Rowman and Littlefield publishers, United States of America.

Appendix

Appendix 1

Table 1.1 Main statistical parameters of the particle size composition of different facies of the QA.08.02 section. Letters in the table indicate the sand size and sorting (VC= Very Coarse, VF= Very Fine, M= Medium, F= fine, sd= Sand and M-S= Moderately sorted).

Sample Number	Mean (phi)		Median (phi)		Dispersion (phi)	
QA.08.02.01	0.22	C-sd	0.14	C-sd	0.81	M-S
QA.08.02.02	0.73	C-sd	0.68	C-sd	1.0	M-S
QA.08.02.03	0.53	VC-sd	0.66	VC-sd	1.0	M-S
QA.08.02.04	0.94	VC-sd	0.95	C-sd	0.79	M-S
QA.08.02.05	0.76	VC-sd	0.82	C-sd	0.72	M-S
QA.08.02.06	1.07	M-sd	0.95	C-sd	0.95	M-S
QA.08.02.07	0.56	C-sd	0.55	C-sd	0.90	M-S
QA.08.02.08	0.94	C-sd	0.95	C-sd	0.83	M-S
QA.08.02.09	0.94	C-sd	0.68	C-sd	1.0	M-S
QA.08.02.10	2.16	F-sd	2.16	F-sd	1.0	M-S

Table 1.2: Main statistical parameters of the particle size composition of different facies of the QA.08.17 section. Letters in the table indicate the sand size and sorting (VC= Very Coarse, VF= Very Fine, M= Medium, F= fine, sd= Sand, VP-S= Very Poorly sorted and P-S= Poorly sorted .

Sample Number	Mean (phi)		Median (phi)		Dispersion (phi)	
QA.08.17.01	4.08	C-Sl	3.37	F-sd	2.83	VP-S
QA.08.17.02	4.27	C-Sl	3.64	F-sd	2.09	VP-S
QA.08.17.03	4.90	C-Sl	4.99	C-Sl	2.23	VP-S
QA.08.17.04	3.22	F-sd	2.70	F-sd	2.10	VP-S
QA.08.17.05	2.42	F-sd	1.76	M-sd	2.22	VP-S
QA.08.17.06	3.61	F-sd	2.97	F-sd	2.18	VP-S
QA.08.17.07	2.42	F-sd	1.89	M-sd	1.96	P-S
QA.08.17.08	3.22	F-sd	2.84	F-sd	2.22	VP-S
QA.08.17.10	3.82	F-sd	2.43	F-sd	1.43	P-S

Table 1.3: Main statistical parameters of the particle size composition of different facies of the QA.08.21 section. Letters in the table indicate the sand size and sorting (VC= Very Coarse, VF= Very Fine, M= Medium, F= fine, sd= Sand, VP-S= Very Poorly sorted, P-S= Poorly sorted and M-S= Moderately sorted).

Sample Number	Mean (phi)		Median (phi)		Dipersion (phi)	
QA.08.21.01	7.44	F-Sl	7.41	F-Sl	1.06	P-S
QA.08.21.02	5.02	C-Sl	4.99	VC-Sl	2.43	VP-S
QA.08.21.03	7.35	F-Sl	7.28	F-Sl	1.14	P-S
QA.08.21.04	7.26	F-Sl	7.14	F-Sl	1.10	P-S
QA.08.21.05	5.84	C-Sl	5.66	C-Sl	1.79	P-S
QA.08.21.06	7.69	F-Sl	7.68	F-Sl	1.01	M-S
QA.08.21.07	7.81	F-Sl	7.81	F-Sl	1.52	P-S
QA.08.21.08	5.62	M-Sl	5.39	M-Sl	1.93	P-S
QA.08.21.09	7.69	F-Sl	7.68	F-Sl	1.10	P-S
QA.08.21.10	7.92	F-Sl	7.95	F-Sl	0.97	M-S
QA.08.21.11	6.89	M-Sl	7.14	F-Sl	1.69	P-S
QA.08.21.12	6.54	M-Sl	6.74	M-Sl	1.83	P-S
QA.08.21.13	6.05	M-Sl	6.20	M-Sl	2.18	VP-S
QA.08.21.14	6.96	M-Sl	7.41	F-Sl	2.31	VP-S
QA.08.21.15	6.68	M-Sl	7.01	F-Sl	2.13	VP-S
QA.08.21.16	4.39	VC-Sl	4.05	VC-Sl	2.16	VP-S
QA.08.21.17	4.58	VC-Sl	4.32	VC-Sl	2.48	VP-S
QA.08.21.18	6.41	M-Sl	6.87	M-Sl	2.37	VP-S
QA.08.21.19	4.27	VC-Sl	3.64	VF-sd	2.30	VP-S
QA.08.21.20	7.25	F-Sl	7.68	F-Sl	2.47	VP-S
QA.08.21.21	6.77	M-Sl	7.01	F-Sl	1.94	P-S
QA.08.21.22	4.06	VC-Sl	3.51	VF-sd	2.04	VP-S
QA.08.21.23	7.26	F-Sl	7.28	F-Sl	1.25	P-S

Table 1.4: Main statistical parameters of the particle size composition of different facies of the QA.08.14 section. Letters in the table indicate the sand size and sorting (VC= Very Coarse, VF= Very Fine, M= Medium, F= fine, sd= Sand, VP-S= Very Poorly sorted, P-S= Poorly sorted and M-S= Moderately sorted).

Sample Number	Mean (phi)		Median (phi)		Dispersion (phi)	
QA.08.14.01	9.22	Clay	9.29	Clay	3.11	VP-S
QA.08.14.02	1.17	M-sd	0.55	C-sd	2.00	P-S
QA.08.14.03	6.72	F-Sl	6.87	F-Sl	1.90	P-S
QA.08.14.04	1.40	M-sd	1.36	M-sd	0.78	M-S

Table 1.5 Main statistical parameters of the particle size composition of different facies of the QA.08.10 section. Letters in the table indicate the sand size and sorting (VC= Very Coarse, VF= Very Fine, M= Medium, F= fine, sd= Sand, P-S= Poorly sorted and M-S= Moderately sorted).

Sample Number	Mean (phi)		Median (phi)		Dispersion (phi)	
QA.08.10.01	1.48	M-sd	1.58	M-sd	1	M-S
QA.08.10.02	4.45	VF- sd	4.67	VF- sd	1	M-S
QA.08.10.03	1.75	M-sd	2.07	M-sd	1	M-S
QA.08.10.04	3.51	F-sd	2.97	M-sd	2.0	P-S

Table 1.6 Main statistical parameters of the particle size composition of different facies of the QA.08.15, QA.08.16 and QA.08.05 sections. Letters in the table indicate the sand size and sorting (VC= Very Coarse, VF= Very Fine, M= Medium, F= fine, sd= Sand and M-S= Moderately sorted).

Sample Number	Mean (phi)		Median (phi)		Dispersion (phi)	
QA.08.15.01	2.70	F-sd	3.09	F-sd	1.0	M-S
QA.08.15.02	2.57	F-sd	2.58	F-sd	0.95	M-S
QA.08.16.01	2.07	F-sd	2.16	F-sd	1.0	M-S
QA.08.16.02	1.3	M-sd	1.0	M-sd	1.0	M-S
QA.0.2.05.01A	3.25	VF-sd	3.10	VF-sd	1.0	M-S
QA.0.2.05.01B	2.94	F-sd	2.84	F-sd	1.0	M-S
QA.08.05.02A	1.29	M-sd	1.09	M-sd	1.0	M-S
QA.08.05.02B	1.40	M-sd	1.22	M-sd	0.93	M-S
QA.08.05.02C	2.01	M-sd	2.16	M-sd	0.81	M-S

Table 1.7 Main statistical parameters of the particle size composition of different facies of the QA.08.07 and QA.08.08 sections. Letters in the table indicate the sand size and sorting (VC= Very Coarse, VF= Very Fine, M= Medium, F= fine, sd= Sand, and M-S= Moderately sorted).

Sample Number	Mean (phi)		Median (phi)		Dispersion (phi)	
QA.08.07.01	1.76	M-sd	1.76	M-sd	0.72	M-S
QA.08.07.02	1.59	M-sd	1.49	M-sd	1.0	M-S
QA.08.08.01	1.68	M-sd	1.62	M-sd	1.0	M-S
QA.08.08.02	1.74	M-sd	1.76	M-sd	0.70	M-S
QA.08.08.03	1.80	M-sd	1.76	M-sd	0.69	M-S
QA.08.08.04	2.31	F-sd	2.16	F-sd	1.0	M-S
QA.08.08.05	1.67	M-sd	1.49	M-sd	0.98	M-S

Table 1.8 Main statistical parameters of the particle size composition of different facies of the QA.08.06 section. Letters in the table indicate the sand size and sorting (M= Medium, F= fine, sd= Sand, P-S= Poorly sorted and M-S= Moderately sorted).

Sample Number	Mean (phi)		Median (phi)		Dispersion (phi)	
QA.08.06.01	2.57	F-sd	1.89	F-sd	2.0	P-S
QA.08.06.02	2.10	F-sd	1.89	F-sd	1.0	M-S
QA.08.06.03	2.31	F-sd	2.03	F-sd	1.0	M-S
QA.08.06.04	1.46	M-sd	1.36	M-sd	0.82	M-S
QA.08.06.05	0.77	C-sd	0.82	C-sd	0.72	M-S

Table 1.9: Main statistical parameters of the particle size composition of different facies of the QA.08.18 and 19 and 20 sections. Letters in the table indicate the sand size and sorting (VC= Very Coarse, VF= Very Fine, M= Medium, F= fine, sd= Sand, VP-S= Very Poorly sorted and M-S= Moderately sorted).

Sample Number	Mean (phi)		Median (phi)		Dispersion (phi)	
QA.08.18.01	2.36	F-sd	2.30	F-sd	0.97	M-S
QA.08.18.02	3.60	F-sd	2.97	F-sd	2.13	VP-S
QA.08.18.03	4.03	F-sd	3.64	F-sd	2.27	VP-S
QA.08.19.01	4.58	VC-Sl	5.26	VC-Sl	2.35	VP-S
QA.08.19.02	3.61	VF-sd	3.37	F-sd	2.26	VP-S
QA.08.19.03	5.33	C-Sl	5.66	C-Sl	2.09	VP-S
QA.08.19.04	2.49	F-sd	1.89	M-sd	2.08	VP-S
QA.08.20.01	2.42	F-sd	2.16	F-sd	1.0	M-S
QA.08.20.02	1.79	M-sd	1.76	M-sd	0.87	M-S

Table 1.10: Main statistical parameters of the particle size composition of different facies of the QA.08.01, QA.08. 25, QA.08 26 and QA.08.28 sections. letters in the table indicate the sand size and sorting (VC= Very Coarse, VF= Very Fine, M= Medium, F= fine, sd= Sand and M-S= Moderately sorted).

Sample Number	Mean (phi)		Median (phi)		Dispersion (phi)	
QA.08.01W	1.71	M-sd	1.76	M-sd	1.0	M-S
QA.08.01E	1.22	M-sd	1.09	M-sd	1.0	M-S
QA.08.26W	1.55	M-sd	1.36	M-sd	1.0	M-S
QA.08.26E	1.83	M-sd	1.76	M-sd	0.61	M-S
QA.08.25W	2.04	F-sd	2.03	F-sd	0.55	M-S
QA.08.25E	2.13	F-sd	2.16	F-sd	0.41	M-S
QA.08.27W	1.85	M-sd	1.89	M-sd	0.91	M-S
QA.08.27E	0.74	C-sd	0.68	C-sd	1.0	M-S
QA.08.28W	1.04	M-sd	0.68	C-sd	0.97	M-S
QA.08.28E	1.21	M-sd	0.68	C-sd	1.0	M-S

Table 1.11: Main statistical parameters of the particle size composition of different facies of the sections QA.08.03and QA.08.04. VP-S= Very Poorly sorted, P-S= Poorly sorted and M-S= Moderately sorted).

Sample Number	Mean (phi)		Median (phi)		Dispersion (phi)	
QA.08.03.01	3.55	VF-sd	3.24	VF-sd	1.81	P-S
QA.08.03.02	3.13	VF-sd	2.84	F-sd	1.60	P-S
QA.08.03.03	3.07	VF-sd	2.84	F-sd	1.62	P-S
QA.08.03.04	2.09	VF-sd	1.89	M-sd	1.12	P-S
QA.08.03.05	1.94	VF-sd	1.76	M-sd	1.16	P-S
QA.08.03.06	3.72	VF-sd	3.51	VF-sd	1.73	P-S
QA.08.03.07	2.84	F-sd	2.57	F-sd	1.51	P-S
QA.08.03.08	2.85	F-sd	2.70	F-sd	1.35	P-S
QA.08.03.09	2.60	F-sd	2.43	F-sd	1.31	P-S
QA.08.03.10	2.60	F-sd	2.43	F-sd	1.33	P-S
QA.08.03.11	2.61	F-sd	2.43	F-sd	1.40	P-S
QA.08.03.12	2.12	F-sd	2.03	F-sd	0.91	M-S
QA.08.03.13	2.39	F-sd	2.30	F-sd	1.15	P-S
QA.08.03.14	2.36	F-sd	2.30	F-sd	1.14	P-S
QA.08.03.15	2.43	F-sd	2.30	F-sd	1.26	P-S
QA.08.03.16	3.43	VF-sd	3.24	VF-sd	1.37	P-S
QA.08. 04-00A	2.93	F-sd	2.70	F-sd	1.90	P-S
QA.08.04-00B	4.79	VC-Sl	4.99	VC-Sl	2.24	VP-S
QA.08.04-01	2.37	F-sd	2.43	F-sd	0.83	M-S
QA.08. 04-02	1.88	M-sd	1.62	M-sd	1.74	P-S
QA.08.04-03	3.51	VF-sd	3.24	VF-sd	1.79	P-S
QA.08. 04-04	3.72	VF-sd	3.51	VF-sd	1.66	P-S
QA.08.04-05A	3.82	VF-sd	3.51	VF-sd	2.15	VP-S
QA.08.04-05B	3.19	VF-sd	2.84	F-sd	1.91	P-S
QA.08.04-06A	3.13	VF-sd	2.84	F-sd	1.75	P-S
QA.08.04-06B	3.60	VF-sd	3.37	VF-sd	1.79	P-S
QA.08. 04-06C	3.42	VF-sd	3.24	VF-sd	1.62	P-S
QA.08. 04-06D	3.42	VF-sd	3.24	VF-sd	1.60	P-S
QA.08. 04-07	2.75	F-sd	2.70	F-sd	1.10	P-S

Appendix 2

Table2.1: Directions of the dunes axis in the study area*

Nafud	Interval	Angle (A)	Frequency (F)	A×F	Average (Degree)	Average %	10/%
Nafud Al Mazhur	0-180	110	1	110	132°	100	10
		115	3	345			
		120	10	1200			
		140	10	1400			
		145	10	1450			
Nafud Burydah (W)	0-180	170	10	1700	175°	66	6.6
		180	10	1800			
	181-360	210	10	2100	210°	33	3.3
Nafud Al Tarafiyah	0-180	170	10	1700	175°	66	6.6
		180	10	1800			
	181-360	220	10	2200	220	30	3
Nafud Uyun Al Jiw	0-180	110	2	220	147	78	7.8
		120	2	240			
		125	4	500			
		170	10	1700			
	181-360	210	5	1050	210	27	2.7
Nafud Al Qwarh	0-180	130	20	2600	130°	66	6.6
	181-360	190	10	1900	190°	33	3.3

***The dune axis measured by a random selection of Nafud direction along extended in different parts in the study area used GPS, and then computed the average of direction each Nafudsas well as the percent of each direction. This methods of data represented in adopted from Mohamed, 2002 and Al dughairi, 2003.**

Appendix 3

Table 3.1: Summary of quantitative XRD analyses have been completed on British Geological survey during 2009.

sample Number	Quartz (%)	Albite (%)	K-Feldspr (%)	Amphibole (%)	Calcite (%)	Aragonite (%)	Dolomite (%)	Gypsum (%)	Celestine (%)	Halite (%)	Hematite (%)	Palygorskite (%)	Chlorite (%)	Kaolinite (%)	Mica (%)
QA-08-02-08	66.5	14.5	18.3												0.7
QA-08-02-09	60.6	13.1	16.5		0.7			8.4							0.7
QA-08-02-10	83.6	4.9	7.4		1.7		<0.5				<0.5	0.6			1.3
QA-08-03-01	32.2	5.0	9.4				1.1		4.0			1.8	39.2	1.9	5.4
QA-08-03-08	37.1	4.3	8.7		39.6					0.5	<0.5	3.4		1.6	4.7
QA-08-03-14	4.7				5.6	88.8									0.9
QA-08-03-16	62.5	9.2	13.9	<0.5	5.1					<0.5	<0.5	1.9	2.1	1.1	3.8
QA-08-04-04	38.4	4.5	8.5		40.0		0.9					3.3		1.2	3.2
QA-08-04-05A	19.6	2.1	5.8		69.1		0.7					0.5		1.1	1.1
QA-08-04-07	11.3	1.3	3.5		83.5							<0.5			
QA-08-06-02	68.7	3.5	3.7		20.9		0.5					1.3			1.4
QA-08-07-01	91.4	3.9	4.3		<0.5						<0.5				
QA-08-07-03	86.7	5.3	6.1		<0.5						<0.5			<0.5	1.1
QA-08-08-01	90.7	3.2	4.2		0.8						<0.5				1.0
QA-08-08-03	87.8	4.2	4.7		1.9						<0.5				1.2
QA-08-08-05	83.9	3.2	4.4		7.0						<0.5	1.0		<0.5	
QA-08-10-01	86.0	4.9	4.6		1.9						<0.5	0.7		0.5	1.2
QA-08-10-02	71.8	5.9	6.6		7.0		<0.5				<0.5	2.2	1.7	1.0	3.3
QA-08-10-04	79.2	6.3	6.2		2.9		0.5					1.7		0.7	2.5
QA-08-11-02	1.1				10.8			84.4	3.7						
QA-08-12-03	7.6	0.8			80.4			6.1		1.8		1.0		0.6	1.8
QA-08-12-05	5.9				93.4							0.7			
QA-08-14-01	85.8	3.7	3.4		1.0						<0.5	2.5		0.7	2.8
QA-08-14-03	56.0	5.1	6.8		7.2						<0.5	6.2	5.0	3.4	10.2
QA-08-17-06	66.1	2.5	8.6		13.3						<0.5	4.5		1.6	3.3
QA-08-17-10	77.9	3.3	4.3		11.0						<0.5	1.8		0.7	0.9
QA-08-19-01	63.4	0.9	2.0		11.9		14.2	5.2				2.5			

sample Number	Quartz (%)	Albite (%)	K-Feldspr (%)	Amphibole (%)	Calcite (%)	Dlomite (%)	Gypsum (%)	Halite (%)	Hematite (%)	Palygorskite (%)	Smectie (%)	Chlorite (%)	Kaolinite (%)	Mica (%)
QA-08-19-02	51.5	1.0	1.2		14.2	12.3	18.2			1.7				
QA-08-19-03	59.0	1.5	2.6		23.3	2.0	4.9			6.7				
QA-08-19-04	41.2	<0.5	0.8		9.5	18.2	28.8			1.6				
QA-08-21-06	9.9	2.3	1.7		31.0		1.3	0.9	<0.5	14.8		6.1	2.9	29.0
QA-08-21-09	8.6	1.4	4.9		27.8	<0.5		1.9	<0.5	14.1		7.6	3.1	30.0
QA-08-21-13	15.5	1.9	5.0		12.1		12.0	1.6	<0.5	10.8		8.9	4.4	27.8
QA-08-21-15	7.1	1.7	3.2	<0.5	20.8		28.4	1.2		8.4		5.5	2.5	21.2
QA-08-21-20	9.0	2.0	3.7		21.4		3.9		0.5	14.1		8.4	4.2	32.9
QA-08-04-00B	41.1	3.0	6.3		39.1		4.7			4.9	<0.5	<0.5	<0.5	0.9
QA-08-11-01	7.0	2.2	6.2	<0.5			43.1			14.7	2.6	4.2	2.0	18.0
QA-08-12-00	20.9	1.0	2.9		63.1			0.6		3.7	1.1	2.2	1.0	3.5
QA-08-12-01	75.6	1.9	3.0		8.1			0.6	<0.5	4.9	0.8	0.8	0.6	3.6
QA-08-17-01	67.9	4.3	10.0		5.8				<0.5	5.5	3.0	1.3	2.0	
QA-08-17-02	65.4	2.8	9.7		5.6					7.6	3.8	2.1	3.0	
QA-08-18-01	80.1	0.7	1.6		10.8	3.5				2.7		0.6		
QA-08-18-02	47.1	1.4	4.2		20.9	2.1	17.4			4.2		1.0	0.5	1.2
QA-08-18-03	55.3	2.9	4.1		27.2					6.2		1.5	1.0	1.8
QA-08-20-01	76.1	1.5	3.5		4.3	13.1				1.0	<0.5	<0.5	<0.5	
QA-08-20-02	55.4	1.6	3.1		7.1	32.4				<0.5	<0.5			
QA-08-21-01	9.9	3.1	3.0		25.6		22.8			9.5	3.4	4.8	2.9	15.0
QA-08-21-02	8.3	2.2	1.7	<0.5	13.1		50.7			4.4	3.2	3.5	2.1	10.7
QA-08-21-03	11.0	3.7	2.9		24.6		20.5			9.0	3.7	5.1	3.2	16.3
QA-08-21-05	14.8	3.8	3.1	<0.5	17.5		22.6			7.0	4.7	5.7	3.8	16.9
QA-08-21-19	12.4	4.7	3.5		13.6		16.3		<0.5	9.1	5.7	8.0	4.6	22.0
QA-08-21-21	9.9	4.0	3.3		16.6		28.5			6.8	4.7	6.0	3.5	16.8
QA-08-21-23	11.8	4.0	4.0		16.6		16.1			9.2	5.9	7.0	5.3	20.0

KEY: 'mica' - undifferentiated mica species including muscovite, biotite, illite and illite/smectite etc; 'kaolin' - one of the kaolin group minerals including halloysite, kaolinite etc.; red figures represent Mg-calcite

Table 3.2: Summary of the clay minerals analyses have been completed on British Geological survey during 2009

Sample number	Smectite (%)	Illite (%)	Kaolinite(%)	Chlorite (%)	Palygorskite	Non-clay minerals
QA-08-04-00B	39	19	12	30	minor	calcite, quartz, K-feldspar, albite
QA-08-11-01	42	32	11	15	major	-
QA-08-12-00	39	29	12	20	minor	calcite, quartz
QA-08-12-01	20	37	19	24	major	calcite, quartz
QA-08-17-01	86	0	4	11	minor	calcite, quartz
QA-08-17-02	87	0	3	11	minor	calcite, quartz
QA-08-18-01	not detected	61	39	0	dominant	calcite, dolomite
QA-08-18-02	not detected	46	28	25	dominant	calcite, dolomite
QA-08-18-03	not detected	35	28	37	major	calcite, quartz
QA-08-20-01	13	41	18	28	dominant	calcite, dolomite
QA-08-20-02	100	not detected	not detected	not detected	dominant	dolomite, quartz, calcite
QA-08-21-01	16	36	22	25	minor	calcite, quartz
QA-08-21-02	12	41	23	24	minor	calcite, quartz, K-feldspar, albite
QA-08-21-03	21	34	21	25	minor	calcite, quartz, K-feldspar, albite
QA-08-21-05	9	41	24	27	minor	calcite, quartz, K-feldspar, albite
QA-08-21-19	9	41	25	26	minor	calcite, quartz, K-feldspar, albite
QA-08-21-21	13	43	21	23	minor	calcite, quartz, K-feldspar, albite
QA-08-21-23	12	36	25	27	minor	calcite, quartz, K-feldspar, albite

Appendix 4

CALIBRATION OF RADIOCARBON AGE TO CALENDAR YEARS

(Variables: C13/C12=-22.5:lab. mult=1)

Laboratory number: **Beta-279238**

Conventional radiocarbon age: **10310±60 BP**

2 Sigma calibrated results: **Cal BC 10430 to 10020 (Cal BP 12380 to 11970) and**
(95% probability) **Cal BC 9920 to 9890 (Cal BP 11870 to 11840)**

Intercept data

Intercept of radiocarbon age with calibration curve: Cal BC 10130 (Cal BP 12080)

1 Sigma calibrated results: Cal BC 10270 to 10270 (Cal BP 12220 to 12220) and
(68% probability) Cal BC 10210 to 10080 (Cal BP 12160 to 12040)

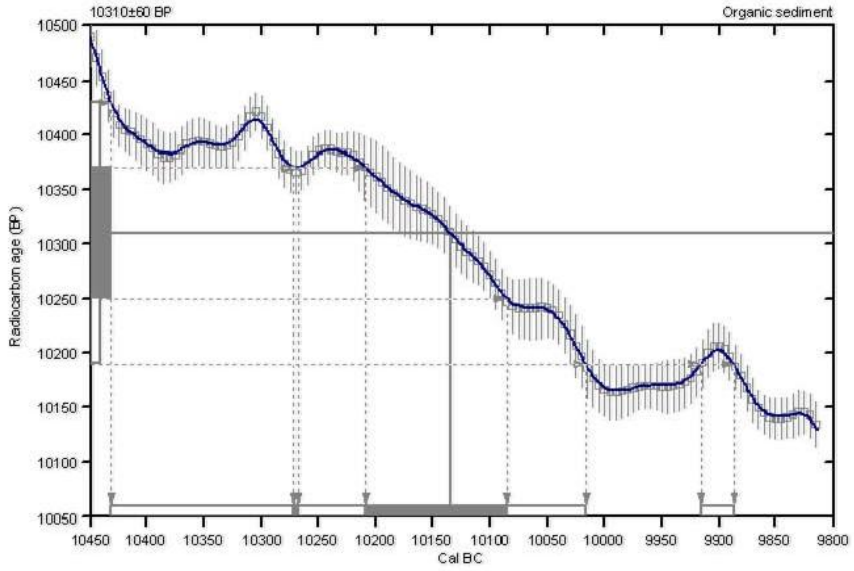

References:

Database used
INTCAL04
Calibration Database
INTCAL04 Radiocarbon Age Calibration
IntCal04: Calibration Issue of Radiocarbon (Volume 46, nr 3, 2004).
Mathematics
A Simplified Approach to Calibrating C14 Dates
Talma, A. S., Vogel, J. C., 1993, Radiocarbon 35(2), p317-322

Beta Analytic Radiocarbon Dating Laboratory

4985 S.W. 74th Court, Miami, Florida 33155 • Tel: (305)667-5167 • Fax: (305)663-0964 • E-Mail: beta@radiocarbon.com

Figure 4.1: Presents the results of calibration curve for sample QA.08.21.06 of Wadi Al Rimah deposit within Nafud Burydah

CALIBRATION OF RADIOCARBON AGE TO CALENDAR YEARS

(Variables: C13/C12=-28.6:lab. mult=1)

Laboratory number: **Beta-279237**

Conventional radiocarbon age: **11030±60 BP**

2 Sigma calibrated result: (95% probability) **Cal BC 11120 to 10920 (Cal BP 13080 to 12870)**

Intercept data

Intercept of radiocarbon age with calibration curve: Cal BC 10980 (Cal BP 12930)

1 Sigma calibrated result: (68% probability) Cal BC 11030 to 10950 (Cal BP 12980 to 12900)

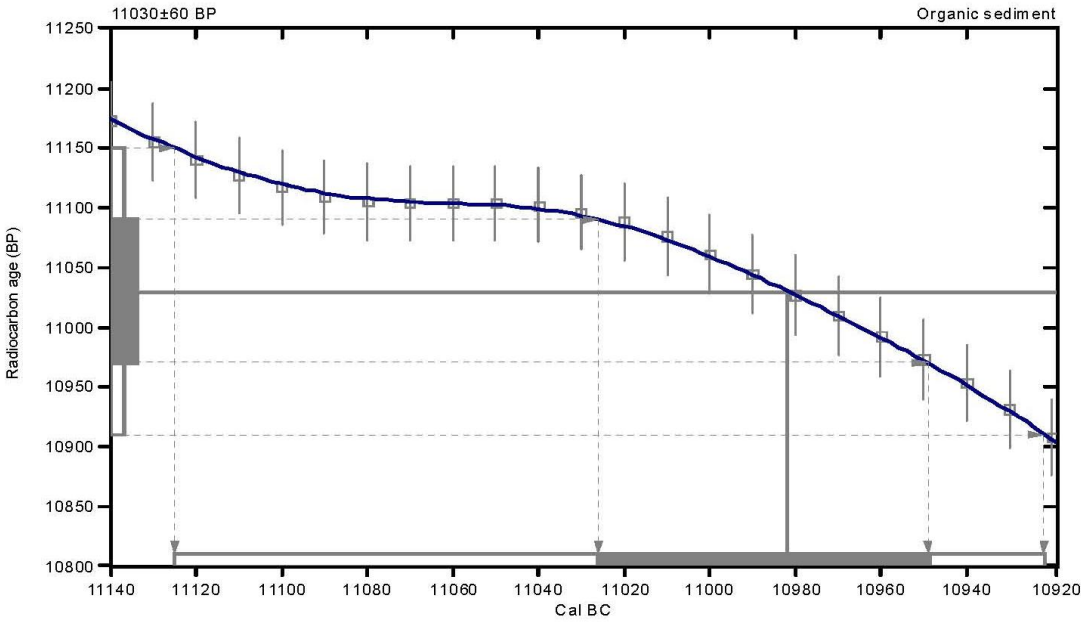

References:

Database used

INTCAL04

Calibration Database

INTCAL04 Radiocarbon Age Calibration

IntCal04: Calibration Issue of Radiocarbon (Volume 46, nr 3, 2004).

Mathematics

A Simplified Approach to Calibrating C14 Dates

Talma, A. S., Vogel, J. C., 1993, Radiocarbon 35(2), p317-322

Beta Analytic Radiocarbon Dating Laboratory

4985 S.W. 74th Court, Miami, Florida 33155 • Tel: (305)667-5167 • Fax: (305)663-0964 • E-Mail: beta@radiocarbon.com

.

Figure 4.2: Presents the results of calibration curve for sample QA.08.21.04 of Wadi Al Rimah deposit within Nafud Burydah

CALIBRATION OF RADIOCARBON AGE TO CALENDAR YEARS

(Variables: C13/C12=-1.6:lab. mult=1)

Laboratory number:	**Beta-279229**
Conventional radiocarbon age:	**9790±70 BP**
2 Sigma calibrated result: (95% probability)	**Cal BC 9350 to 9170 (Cal BP 11300 to 11120)**

Intercept data

Intercept of radiocarbon age with calibration curve:	Cal BC 9260 (Cal BP 11220)
1 Sigma calibrated result: (68% probability)	Cal BC 9300 to 9230 (Cal BP 11240 to 11180)

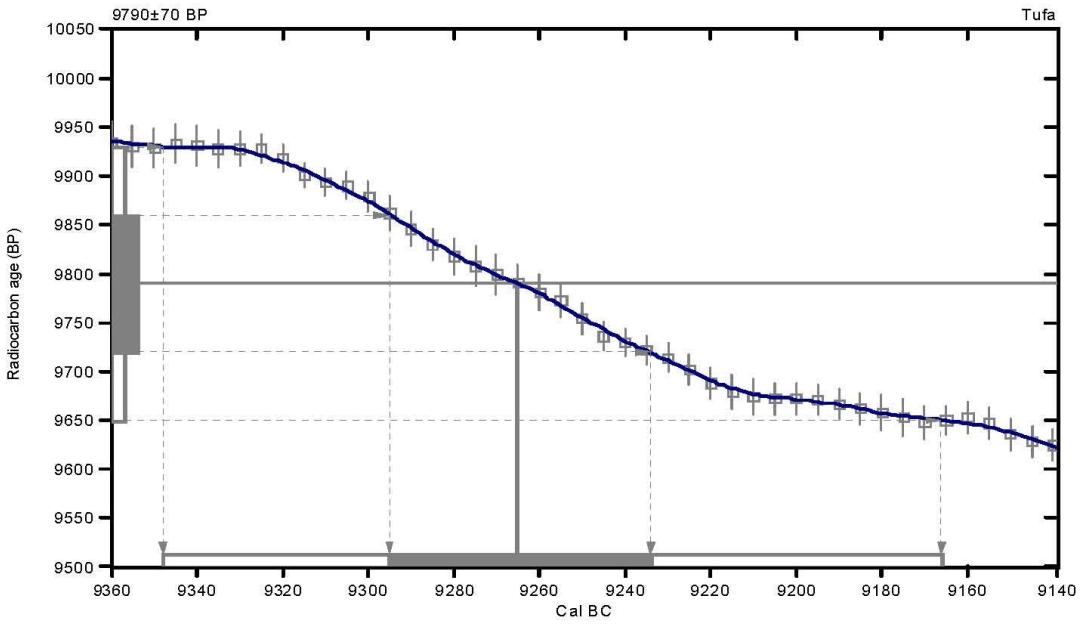

References:

Database used

INTCAL04

Calibration Database

INTCAL04 Radiocarbon Age Calibration

IntCal04: Calibration Issue of Radiocarbon (Volume 46, nr 3, 2004).

Mathematics

A Simplified Approach to Calibrating C14 Dates

Talma, A. S., Vogel, J. C., 1993, Radiocarbon 35(2), p317-322

Beta Analytic Radiocarbon Dating Laboratory

4985 S.W. 74th Court, Miami, Florida 33155 • Tel: (305)667-5167 • Fax: (305)663-0964 • E-Mail: beta@radiocarbon.com

Figure 4.3: Presents the results of calibration curve for sample QA.08.03.02of tufa deposit within Nafud Burydah

CALIBRATION OF RADIOCARBON AGE TO CALENDAR YEARS

(Variables: C13/C12=-2.7:lab. mult=1)

Laboratory number:	**Beta-282891**
Conventional radiocarbon age:	**9940±50 BP**
2 Sigma calibrated results: (95% probability)	**Cal BC 9660 to 9570 (Cal BP 11610 to 11520) and Cal BC 9550 to 9290 (Cal BP 11500 to 11240)**

Intercept data

Intercept of radiocarbon age with calibration curve:	Cal BC 9360 (Cal BP 11320)
1 Sigma calibrated result: (68% probability)	Cal BC 9450 to 9310 (Cal BP 11400 to 11260)

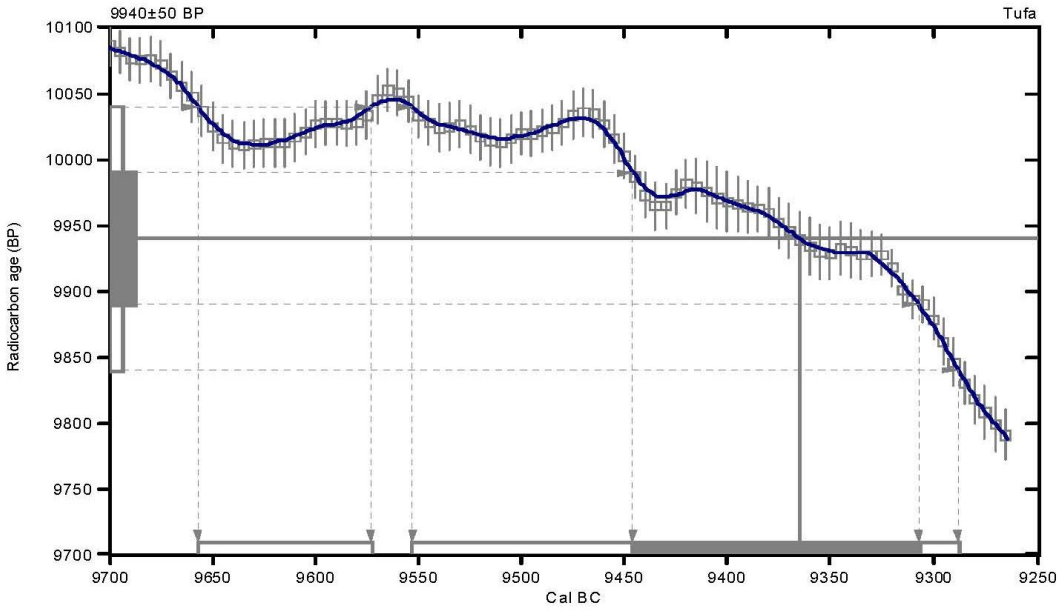

References:

Database used

INTCAL04

Calibration Database

INTCAL04 Radiocarbon Age Calibration

IntCal04: Calibration Issue of Radiocarbon (Volume 46, nr 3, 2004).

Mathematics

A Simplified Approach to Calibrating C14 Dates

Talma, A. S., Vogel, J. C., 1993, Radiocarbon 35(2), p317-322

Beta Analytic Radiocarbon Dating Laboratory

4985 S.W. 74th Court, Miami, Florida 33155 • Tel: (305)667-5167 • Fax: (305)663-0964 • E-Mail: beta@radiocarbon.com

Figure 4.4: Presents the results of calibration curve for sample QA.08.03.04 of tufa deposit within Nafud Burydah

CALIBRATION OF RADIOCARBON AGE TO CALENDAR YEARS

(Variables: C13/C12=-4.9:lab. mult=1)

Laboratory number:	**Beta-282892**
Conventional radiocarbon age:	**8280±50 BP**
2 Sigma calibrated result: (95% probability)	**Cal BC 7480 to 7170 (Cal BP 9440 to 9120)**

Intercept data

Intercept of radiocarbon age with calibration curve:	Cal BC 7340 (Cal BP 9290)
1 Sigma calibrated results: (68% probability)	Cal BC 7450 to 7400 (Cal BP 9400 to 9350) and Cal BC 7370 to 7300 (Cal BP 9320 to 9250) and Cal BC 7220 to 7190 (Cal BP 9170 to 9140)

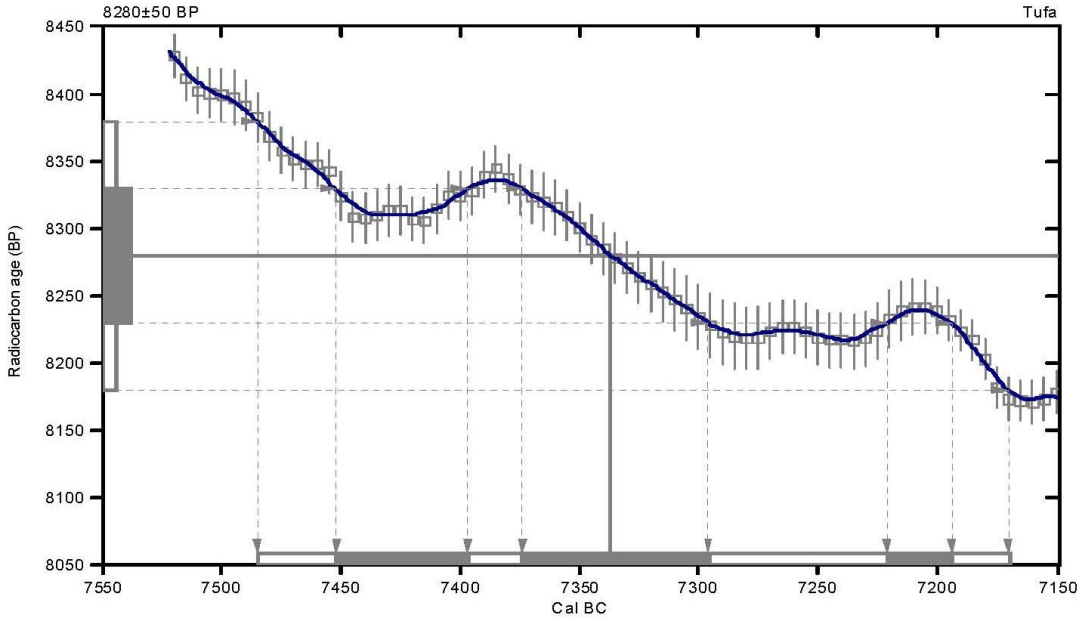

References:

Database used

INTCAL04

Calibration Database

INTCAL04 Radiocarbon Age Calibration

IntCal04: Calibration Issue of Radiocarbon (Volume 46, nr 3, 2004).

Mathematics

A Simplified Approach to Calibrating C14 Dates

Talma, A. S., Vogel, J. C., 1993, Radiocarbon 35(2), p317-322

Beta Analytic Radiocarbon Dating Laboratory

4985 S.W. 74th Court, Miami, Florida 33155 • Tel: (305)667-5167 • Fax: (305)663-0964 • E-Mail: beta@radiocarbon.com

Figure 4.5: Presents the results of calibration curve for sample QA.08.03.06A of tufa deposit within Nafud Burydah

CALIBRATION OF RADIOCARBON AGE TO CALENDAR YEARS

(Variables: C13/C12=-5.9:lab. mult=1)

Laboratory number:	**Beta-279230**
Conventional radiocarbon age:	**7430±60 BP**
2 Sigma calibrated result: (95% probability)	**Cal BC 6430 to 6210 (Cal BP 8380 to 8160)**

Intercept data

Intercepts of radiocarbon age with calibration curve:	Cal BC 6340 (Cal BP 8290) and Cal BC 6310 (Cal BP 8260) and Cal BC 6260 (Cal BP 8210)
1 Sigma calibrated result: (68% probability)	Cal BC 6390 to 6230 (Cal BP 8340 to 8180)

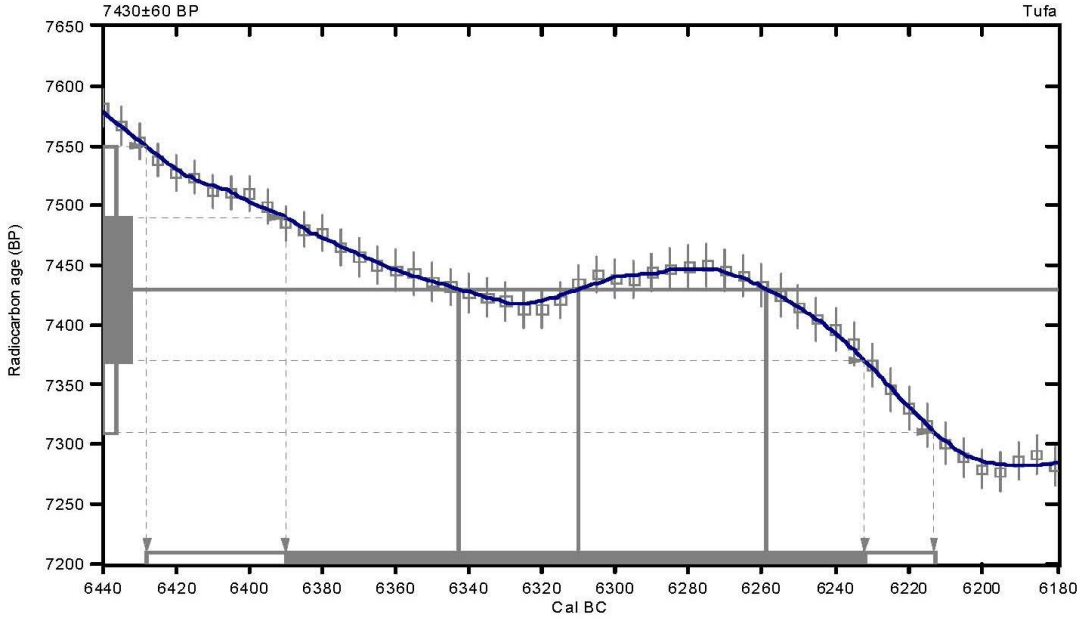

References:

Database used

INTCAL04

Calibration Database

INTCAL04 Radiocarbon Age Calibration

IntCal04: Calibration Issue of Radiocarbon (Volume 46, nr 3, 2004).

Mathematics

A Simplified Approach to Calibrating C14 Dates

Talma, A. S., Vogel, J. C., 1993, Radiocarbon 35(2), p317-322

Beta Analytic Radiocarbon Dating Laboratory

4985 S.W. 74th Court, Miami, Florida 33155 • Tel: (305)667-5167 • Fax: (305)663-0964 • E-Mail: beta@radiocarbon.com

Figure 4.6: Presents the results of calibration curve for sample QA.08.03.08 of tufa deposit within Nafud Burydah

CALIBRATION OF RADIOCARBON AGE TO CALENDAR YEARS

(Variables: C13/C12=-6:lab. mult=1)

Laboratory number: **Beta-282893**

Conventional radiocarbon age: **6980±40 BP**

2 Sigma calibrated results: **Cal BC 5980 to 5940 (Cal BP 7930 to 7890) and**
(95% probability) **Cal BC 5930 to 5750 (Cal BP 7880 to 7700)**

Intercept data

Intercept of radiocarbon age with calibration curve: Cal BC 5880 (Cal BP 7830)

1 Sigma calibrated result: (68% probability) Cal BC 5900 to 5830 (Cal BP 7850 to 7780)

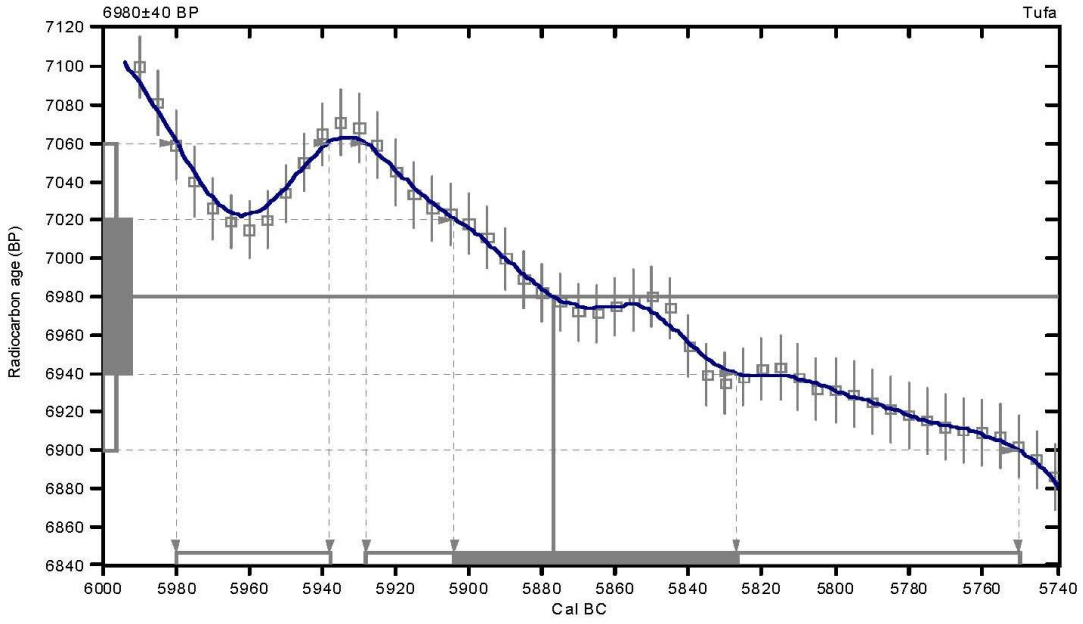

References:

Database used

INTCAL04

Calibration Database

INTCAL04 Radiocarbon Age Calibration

IntCal04: Calibration Issue of Radiocarbon (Volume 46, nr 3, 2004).

Mathematics

A Simplified Approach to Calibrating C14 Dates

Talma, A. S., Vogel, J. C., 1993, Radiocarbon 35(2), p317-322

Beta Analytic Radiocarbon Dating Laboratory

4985 S.W. 74th Court, Miami, Florida 33155 • Tel: (305)667-5167 • Fax: (305)663-0964 • E-Mail: beta@radiocarbon.com

Figure 4.7: Presents the results of calibration curve for sample QA.08.03.10 of tufa deposit within Nafud Burydah

CALIBRATION OF RADIOCARBON AGE TO CALENDAR YEARS

(Variables: C13/C12=-3.9:lab. mult=1)

Laboratory number: **Beta-282894**

Conventional radiocarbon age: **6800±40 BP**

2 Sigma calibrated result: (95% probability) **Cal BC 5740 to 5630 (Cal BP 7690 to 7580)**

Intercept data

Intercept of radiocarbon age with calibration curve: Cal BC 5710 (Cal BP 7660)

1 Sigma calibrated result: (68% probability) Cal BC 5720 to 5650 (Cal BP 7670 to 7600)

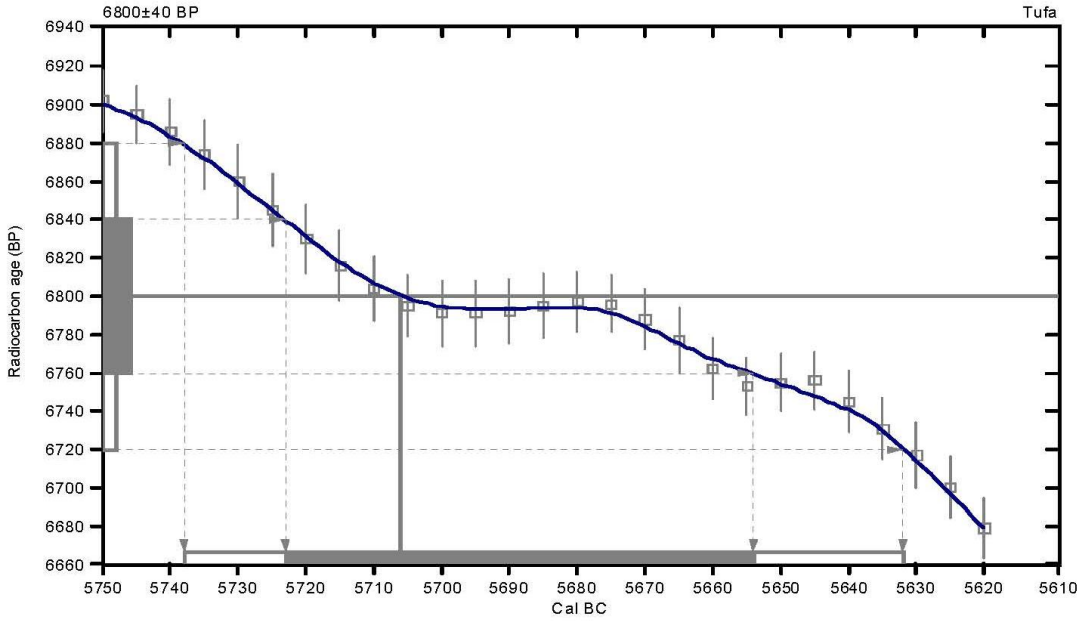

References:

Database used

INTCAL04

Calibration Database

INTCAL04 Radiocarbon Age Calibration

IntCal04: Calibration Issue of Radiocarbon (Volume 46, nr 3, 2004).

Mathematics

A Simplified Approach to Calibrating C14 Dates

Talma, A. S., Vogel, J. C., 1993, Radiocarbon 35(2), p317-322

Beta Analytic Radiocarbon Dating Laboratory

4985 S.W. 74th Court, Miami, Florida 33155 • Tel: (305)667-5167 • Fax: (305)663-0964 • E-Mail: beta@radiocarbon.com

Figure 4.8: Presents the results of calibration curve for sample QA.08.03.12 of tufa deposit within Nafud Burydah

CALIBRATION OF RADIOCARBON AGE TO CALENDAR YEARS

(Variables: C13/C12=-3:lab. mult=1)

Laboratory number: **Beta-279231**

Conventional radiocarbon age: **6800±50 BP**

2 Sigma calibrated result: (95% probability) **Cal BC 5750 to 5630 (Cal BP 7700 to 7580)**

Intercept data

Intercept of radiocarbon age with calibration curve: Cal BC 5710 (Cal BP 7660)

1 Sigma calibrated result: (68% probability) Cal BC 5730 to 5650 (Cal BP 7680 to 7600)

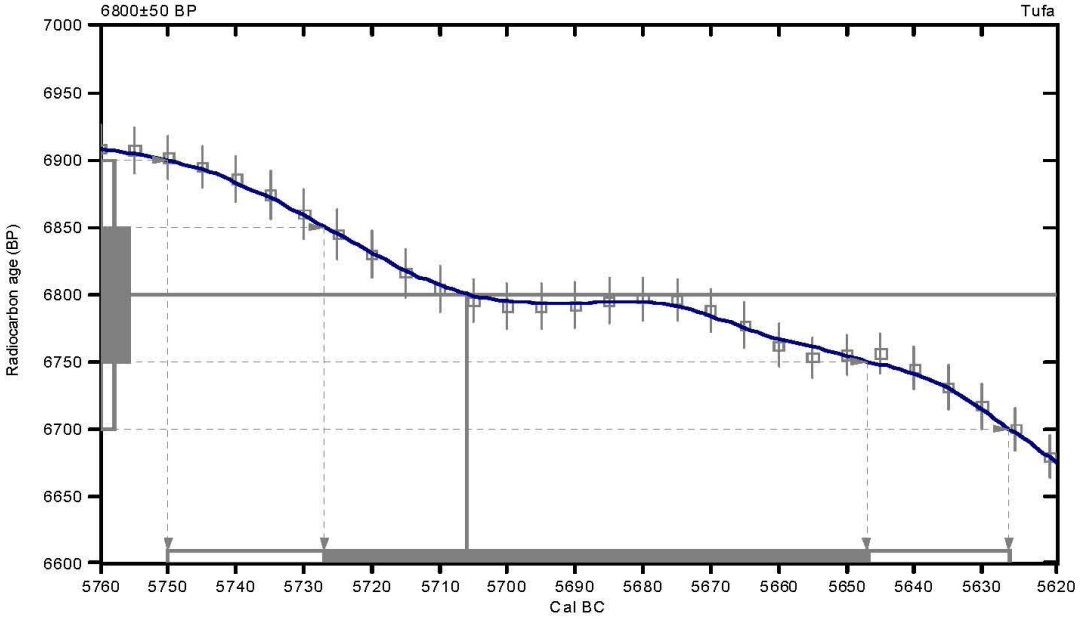

References:

Database used

INTCAL04

Calibration Database

INTCAL04 Radiocarbon Age Calibration

IntCal04: Calibration Issue of Radiocarbon (Volume 46, nr 3, 2004).

Mathematics

A Simplified Approach to Calibrating C14 Dates

Talma, A. S., Vogel, J. C., 1993, Radiocarbon 35(2), p317-322

Beta Analytic Radiocarbon Dating Laboratory

4985 S.W. 74th Court, Miami, Florida 33155 • Tel: (305)667-5167 • Fax: (305)663-0964 • E-Mail: beta@radiocarbon.com

Figure 4.9: Presents the results of calibration curve for sample QA.08.03.14 of tufa deposit within Nafud Burydah

CALIBRATION OF RADIOCARBON AGE TO CALENDAR YEARS

(Variables: C13/C12=-6.6:lab. mult=1)

Laboratory number: **Beta-279232**

Conventional radiocarbon age: **8950±60 BP**

2 Sigma calibrated result: (95% probability) **Cal BC 8280 to 7950 (Cal BP 10230 to 9900)**

Intercept data

Intercept of radiocarbon age with calibration curve: Cal BC 8220 (Cal BP 10180)

1 Sigma calibrated results: (68% probability) Cal BC 8250 to 8180 (Cal BP 10200 to 10130) and
Cal BC 8110 to 8090 (Cal BP 10060 to 10040) and
Cal BC 8070 to 8060 (Cal BP 10020 to 10010) and
Cal BC 8040 to 7990 (Cal BP 9990 to 9940)

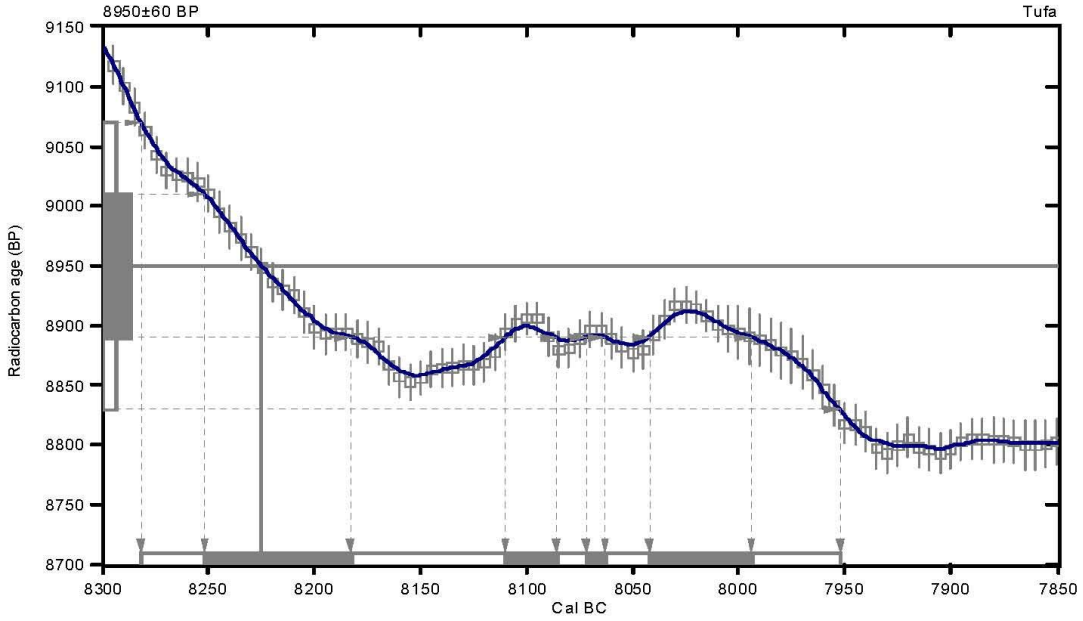

References:

Database used

INTCAL04

Calibration Database

INTCAL04 Radiocarbon Age Calibration

IntCal04: Calibration Issue of Radiocarbon (Volume 46, nr 3, 2004).

Mathematics

A Simplified Approach to Calibrating C14 Dates

Talma, A. S., Vogel, J. C., 1993, Radiocarbon 35(2), p317-322

Beta Analytic Radiocarbon Dating Laboratory

4985 S.W. 74th Court, Miami, Florida 33155 • Tel: (305)667-5167 • Fax: (305)663-0964 • E-Mail: beta@radiocarbon.com

Figure 4.10: Presents the results of calibration curve for sample QA.08.04.00 of tufa deposit within Nafud Burydah

CALIBRATION OF RADIOCARBON AGE TO CALENDAR YEARS

(Variables: C13/C12=-6.3:lab. mult=1)

Laboratory number: **Beta-282895**

Conventional radiocarbon age: **10580±60 BP**

2 Sigma calibrated result: (95% probability) **Cal BC 10840 to 10440 (Cal BP 12790 to 12390)**

Intercept data

Intercept of radiocarbon age with calibration curve: Cal BC 10720 (Cal BP 12670)

1 Sigma calibrated results: (68% probability) Cal BC 10790 to 10660 (Cal BP 12740 to 12610) and Cal BC 10500 to 10460 (Cal BP 12450 to 12410)

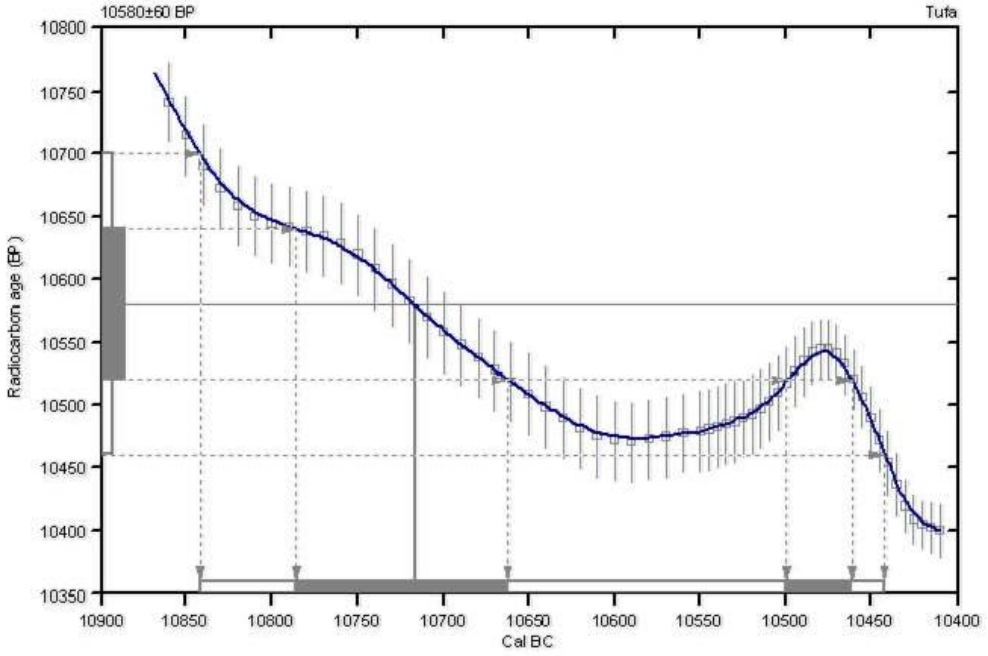

References:

Database used
INTCAL04
Calibration Database
INTCAL04 Radiocarbon Age Calibration
IntCal04: Calibration Issue of Radiocarbon (Volume 46, nr 3, 2004).
Mathematics
A Simplified Approach to Calibrating C14 Dates
Talma, A. S., Vogel, J. C., 1993, Radiocarbon 35(2), p317-322

Beta Analytic Radiocarbon Dating Laboratory

4985 S.W. 74th Court, Miami, Florida 33155 • Tel: (305)667-5167 • Fax: (305)663-0964 • E-Mail: beta@radiocarbon.com

Figure 4.11: Presents the results of calibration curve for sample QA.08.04.05A of tufa deposit within Nafud Burydah

CALIBRATION OF RADIOCARBON AGE TO CALENDAR YEARS

(Variables: C13/C12=-4.5:lab. mult=1)

Laboratory number: **Beta-279233**

Conventional radiocarbon age: **10910±60 BP**

2 Sigma calibrated result: (95% probability) **Cal BC 10980 to 10880 (Cal BP 12930 to 12830)**

Intercept data

Intercept of radiocarbon age with calibration curve: Cal BC 10920 (Cal BP 12870)

1 Sigma calibrated result: (68% probability) Cal BC 10950 to 10900 (Cal BP 12900 to 12850)

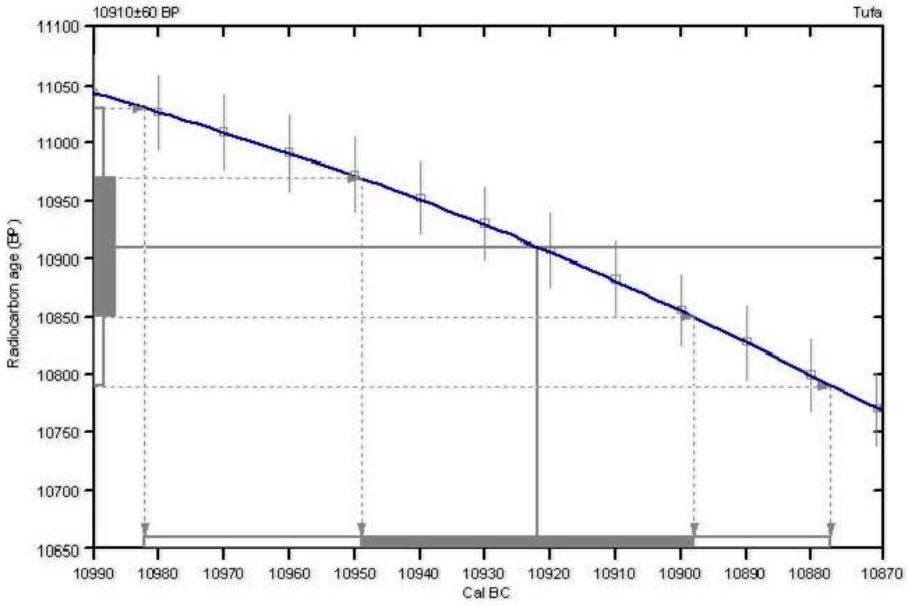

References:

Database used
INTCAL04
Calibration Database
INTCAL04 Radiocarbon Age Calibration
IntCal04: Calibration Issue of Radiocarbon (Volume 46, nr 3, 2004).
Mathematics
A Simplified Approach to Calibrating C14 Dates
Talma, A. S., Vogel, J. C., 1993, Radiocarbon 35(2), p317-322

Beta Analytic Radiocarbon Dating Laboratory

4985 S.W. 74th Court, Miami, Florida 33155 • Tel: (305)667-5167 • Fax: (305)663-0964 • E-Mail: beta@radiocarbon.com

Figure 4.12: Presents the results of calibration curve for sample QA.08.04.06Aof tufa deposit within Nafud Burydah

CALIBRATION OF RADIOCARBON AGE TO CALENDAR YEARS

(Variables: C13/C12=-5.4:lab. mult=1)

Laboratory number: **Beta-282896**

Conventional radiocarbon age: **10300±70 BP**

2 Sigma calibrated result: (95% probability) **Cal BC 10440 to 9870 (Cal BP 12390 to 11820)**

Intercept data

Intercept of radiocarbon age with calibration curve: Cal BC 10130 (Cal BP 12080)

1 Sigma calibrated results: (68% probability) Cal BC 10270 to 10270 (Cal BP 12220 to 12220) and Cal BC 10210 to 10040 (Cal BP 12160 to 11990)

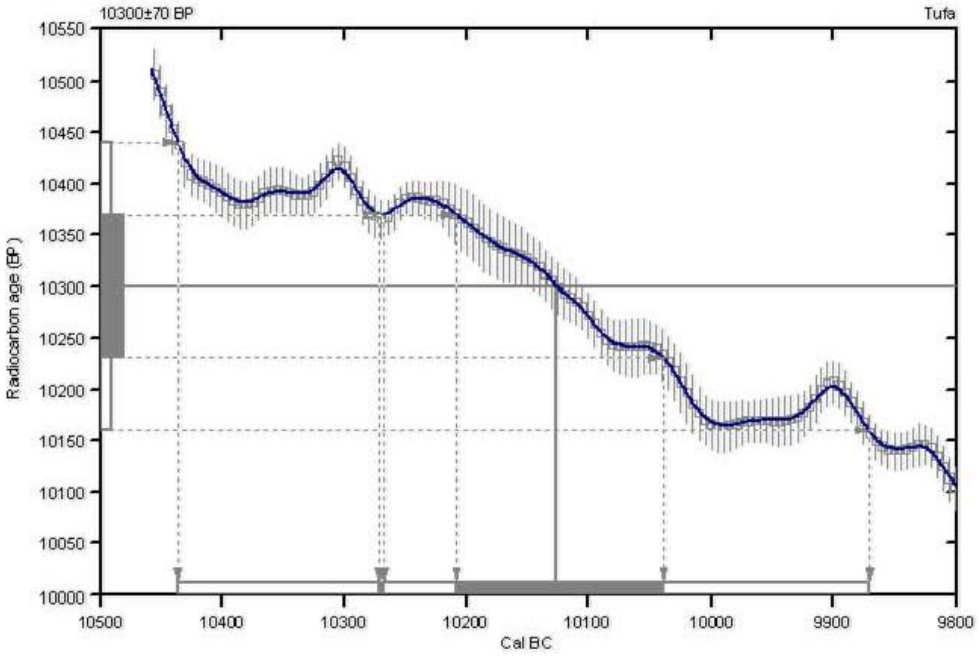

References:

Database used
INTCAL04
Calibration Database
INTCAL04 Radiocarbon Age Calibration
IntCal04: Calibration Issue of Radiocarbon (Volume 46, nr 3, 2004).
Mathematics
A Simplified Approach to Calibrating C14 Dates
Talma, A. S., Vogel, J. C., 1993, Radiocarbon 35(2), p317-322

Beta Analytic Radiocarbon Dating Laboratory

4985 S.W. 74th Court, Miami, Florida 33155 • Tel: (305)667-5167 • Fax: (305)663-0964 • E-Mail: beta@radiocarbon.com

Figure 4.13: Presents the results of calibration curve for sample QA.08.04.06Bof tufa deposit within Nafud Burydah

CALIBRATION OF RADIOCARBON AGE TO CALENDAR YEARS

(Variables: C13/C12=-4.6:lab. mult=1)

Laboratory number:	**Beta-279234**
Conventional radiocarbon age:	**9680±60 BP**
2 Sigma calibrated results: (95% probability)	**Cal BC 9270 to 9110 (Cal BP 11220 to 11060) and Cal BC 9080 to 9050 (Cal BP 11030 to 11000) and Cal BC 9020 to 8840 (Cal BP 10970 to 10790)**

Intercept data

Intercept of radiocarbon age with calibration curve:	Cal BC 9210 (Cal BP 11160)
1 Sigma calibrated results: (68% probability)	Cal BC 9240 to 9140 (Cal BP 11190 to 11090) and Cal BC 8970 to 8940 (Cal BP 10920 to 10890)

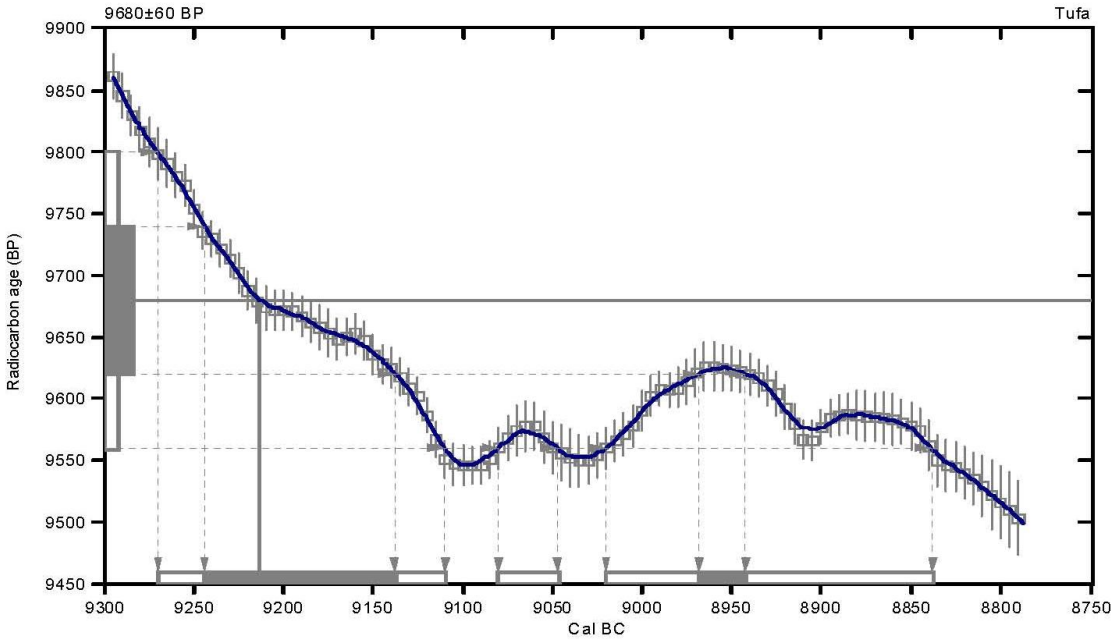

References:

Database used

INTCAL04

Calibration Database

INTCAL04 Radiocarbon Age Calibration

IntCal04: Calibration Issue of Radiocarbon (Volume 46, nr 3, 2004).

Mathematics

A Simplified Approach to Calibrating C14 Dates

Talma, A. S., Vogel, J. C., 1993, Radiocarbon 35(2), p317-322

Beta Analytic Radiocarbon Dating Laboratory

4985 S.W. 74th Court, Miami, Florida 33155 • Tel: (305)667-5167 • Fax: (305)663-0964 • E-Mail: beta@radiocarbon.com

Figure 4.14: Presents the results of calibration curve for sample QA.08.04.06D of tufa deposit within Nafud Burydah

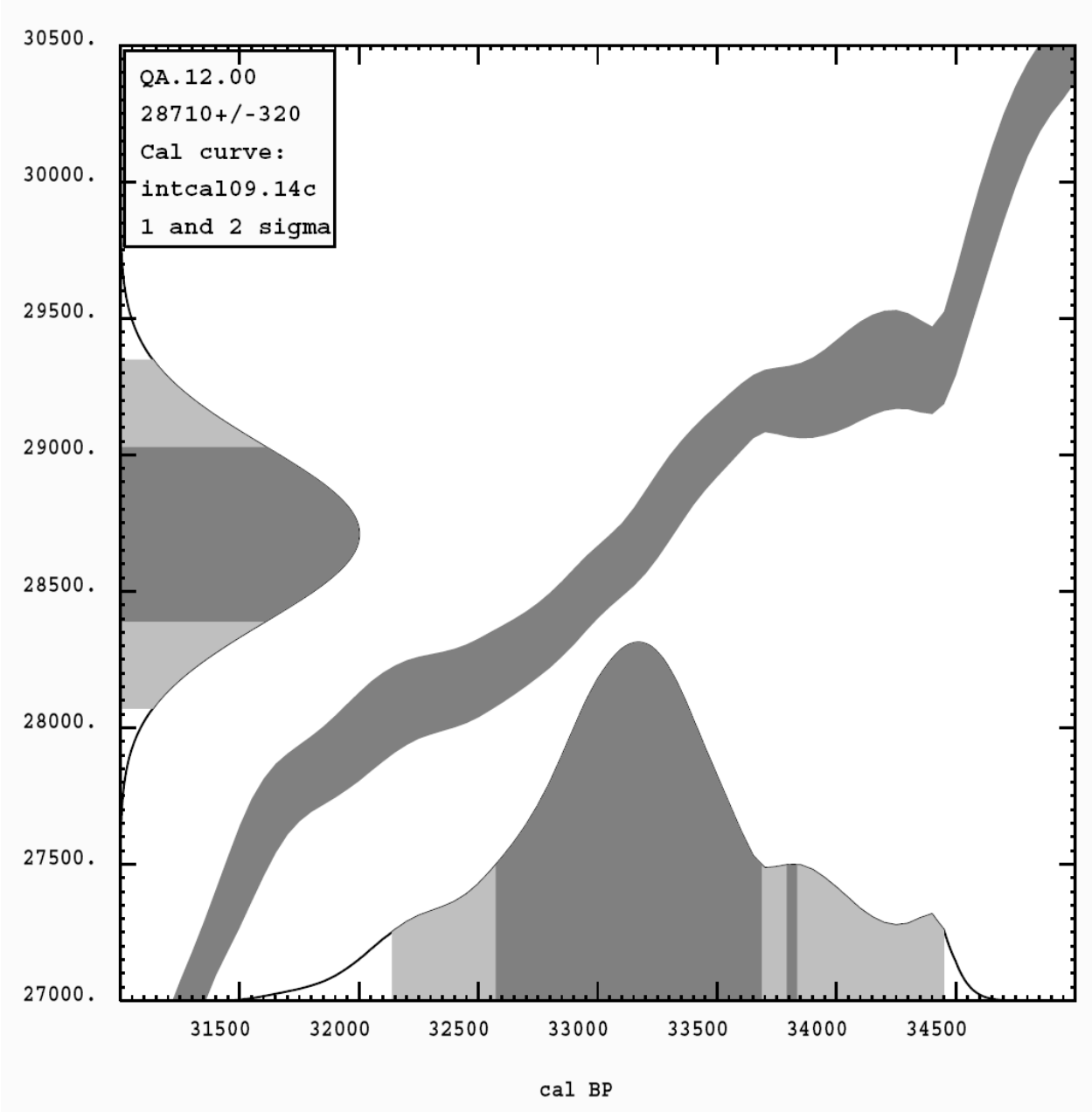

Figure 4.15: Presents the results of calibration curve for sample QA.08.12.00 of Lake deposits within Nafud Al Mazhur

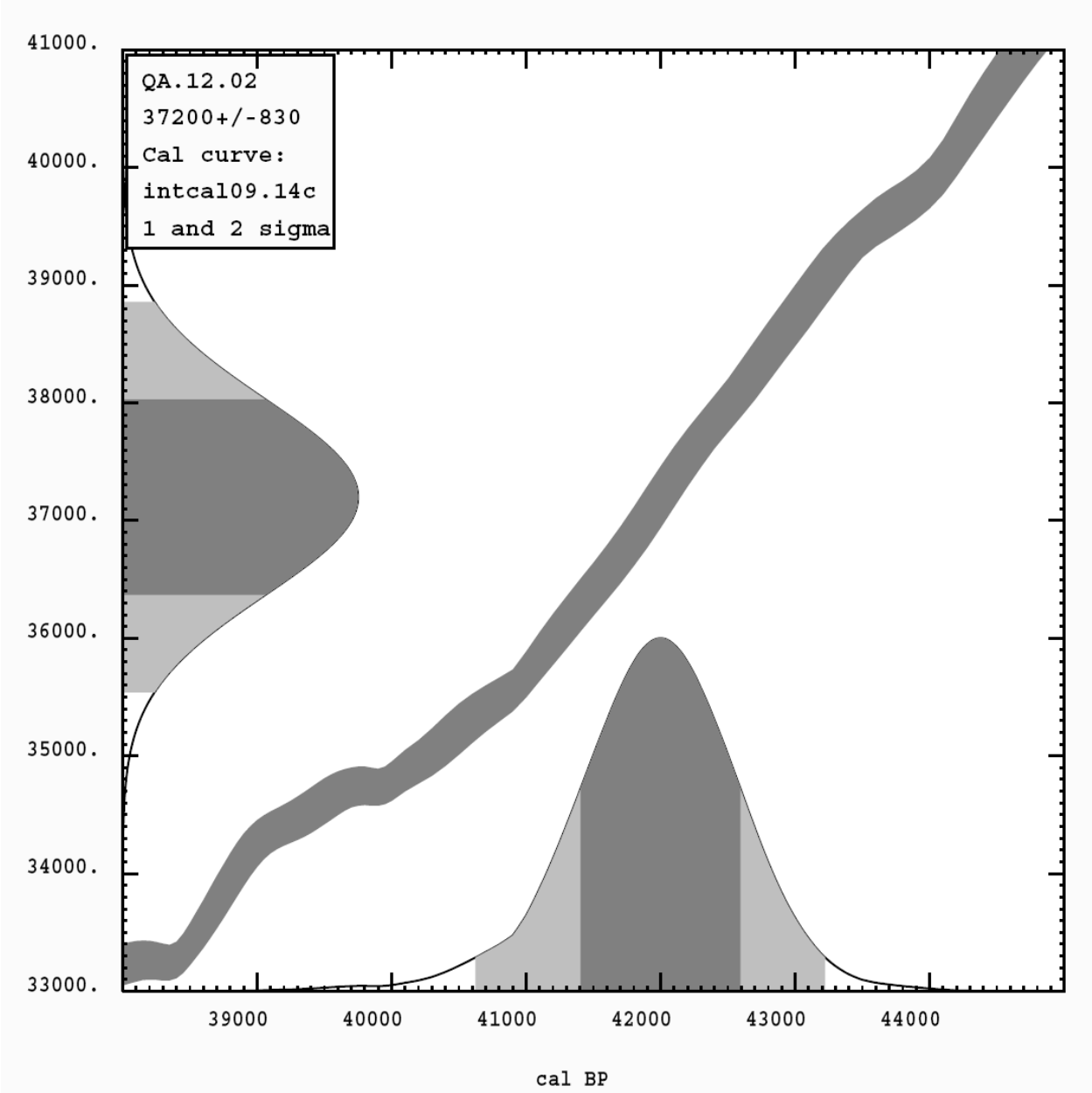

Figure 4.16: Presents the results of calibration curve for sample QA.08.12.02 of Lake deposits within Nafud Al Mazhur

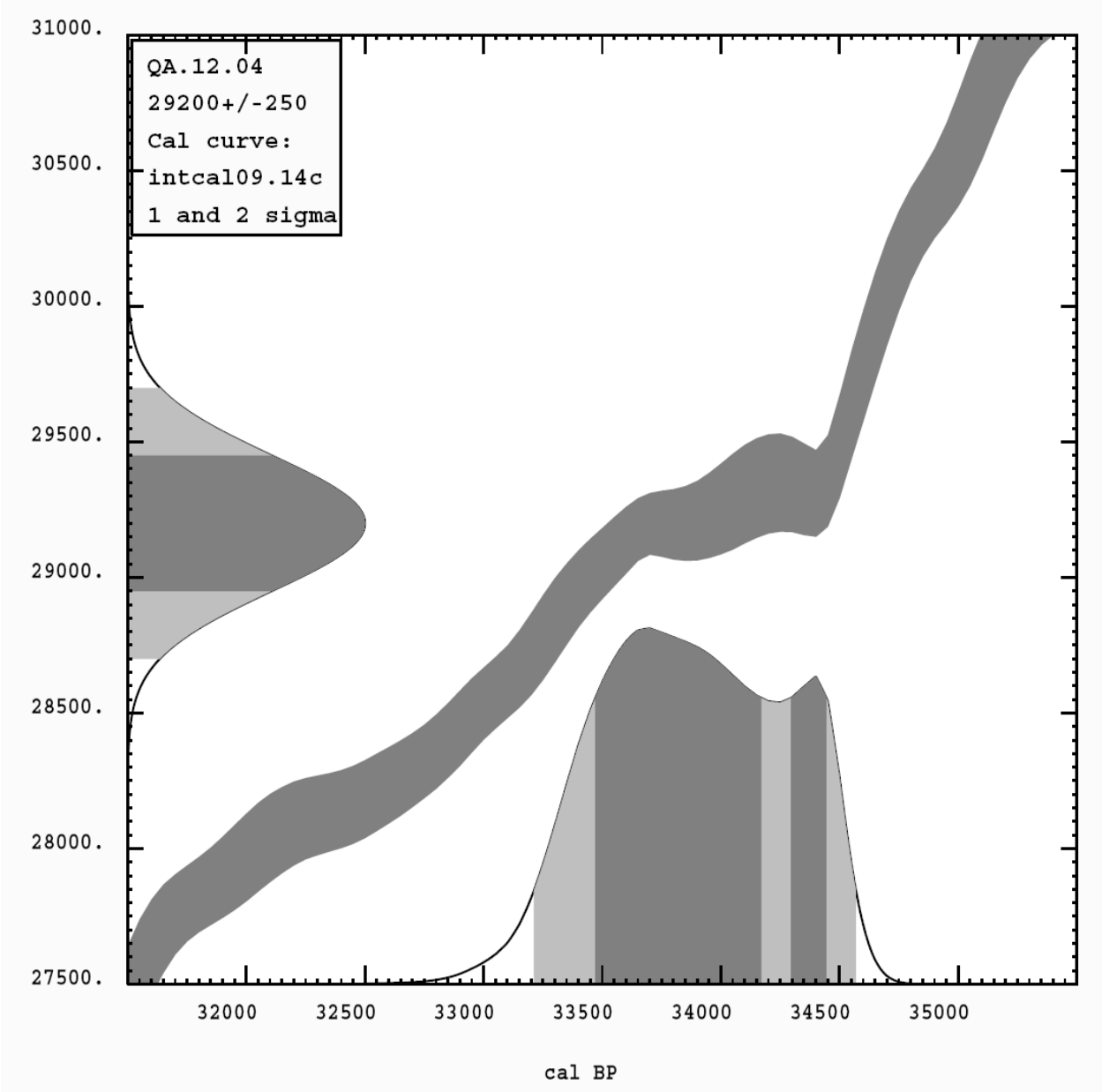

Figure 4.17: Presents the results of calibration curve for sample QA.08.12.04 of Lake deposit within Nafud Al Mazhur

Appendix 5

Lab Cod	Field Code	Range Finder (°C)	R1 (°C)	R2 (°C)	R3 (°C)	R4 (°C)	R5 (°C)
Shfd09 123	05-02A	197-156	100	200	300	25	100
Shfd09 133	05-02B	235-233	100	200	300	25	100
Shfd09 134	05-02C	263-172	100	200	300	25	100
Shfd09 135	02.-01	1300-1300	200	2000	3000	4000	200
Shfd09 136	02.-09	1600-1300	200	2000	3000	4000	200
Shfd09 137	10.-01	330-320	200	350	500	0	200
Shfd09 138	10.03	330-263	200	300	400	0	200
Shfd09 139	14.-01	1400-1800	200	1600	2200	3000	200
Shfd09 140	16.-01	128-155	100	150	250	0	100
Shfd09 141	16.-02	92-104	50	100	150	0	50
Shfd09 142	17.02	978-224	100	250	350	0	100
Shfd09 143	21.08	269-256	100	250	350	0	100

Table 5.1 Summary of 12 samples shows the range of regeneration values were prepared for OSL dating

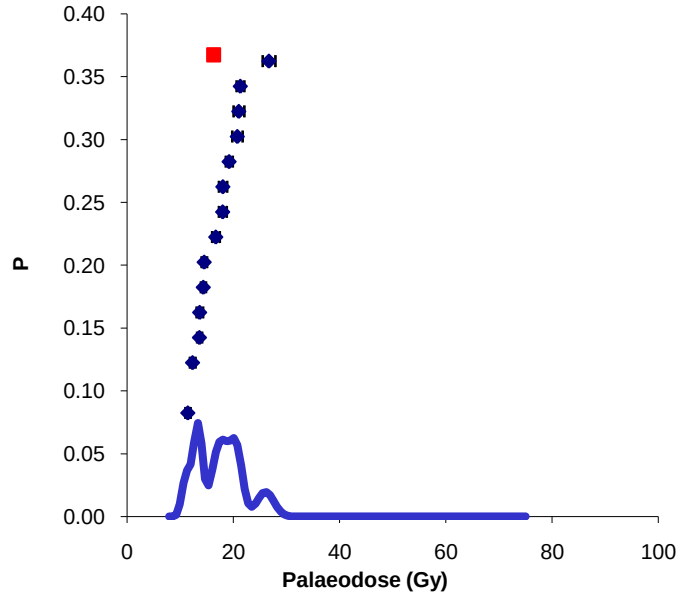

(A)

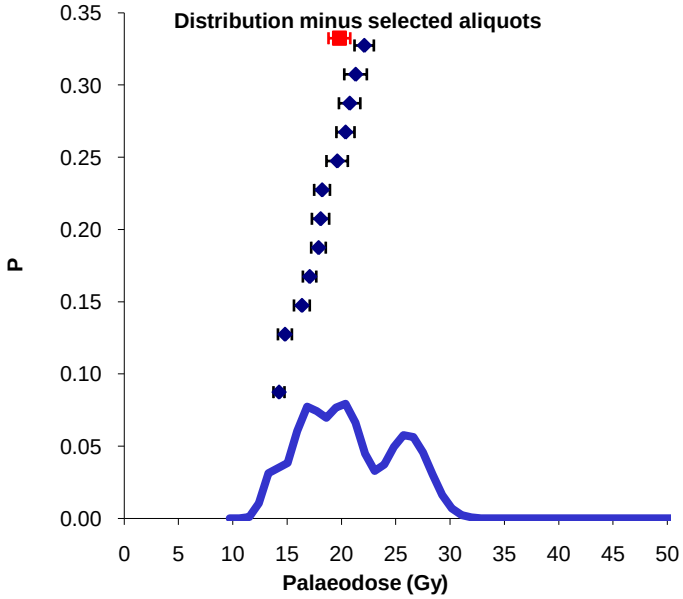

(B)

Figure 5.2 Example for De distribution Fluvial sands (A) Shfd135 and (B) Shfd137

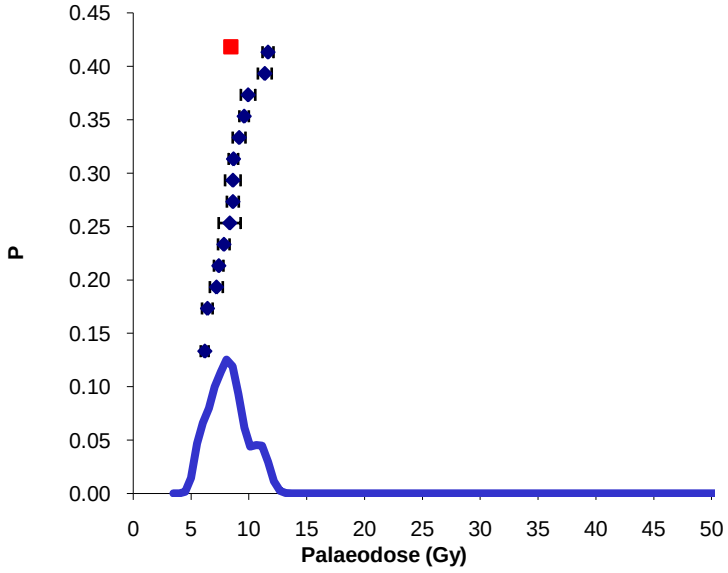

A

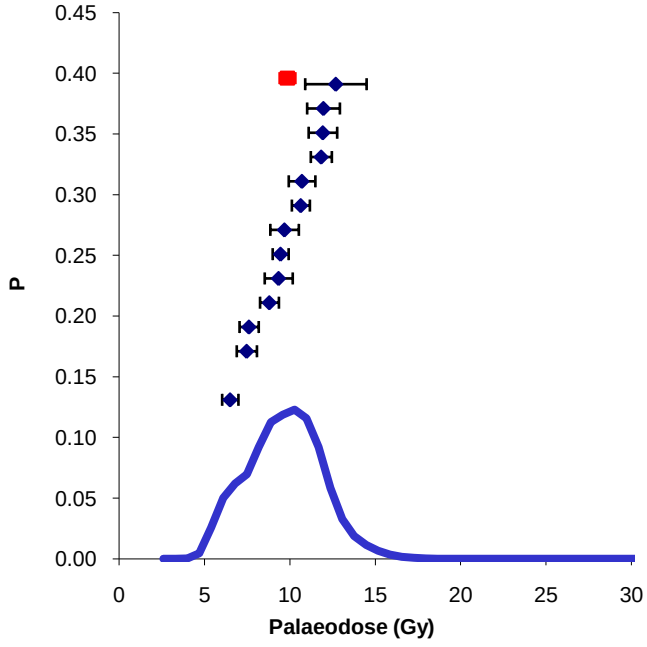

B

Figure 5.3 Example for De distribution from linear dunes of Nafud Uyun Al Jiwa (A) Shfd140 and (B) Shfd141

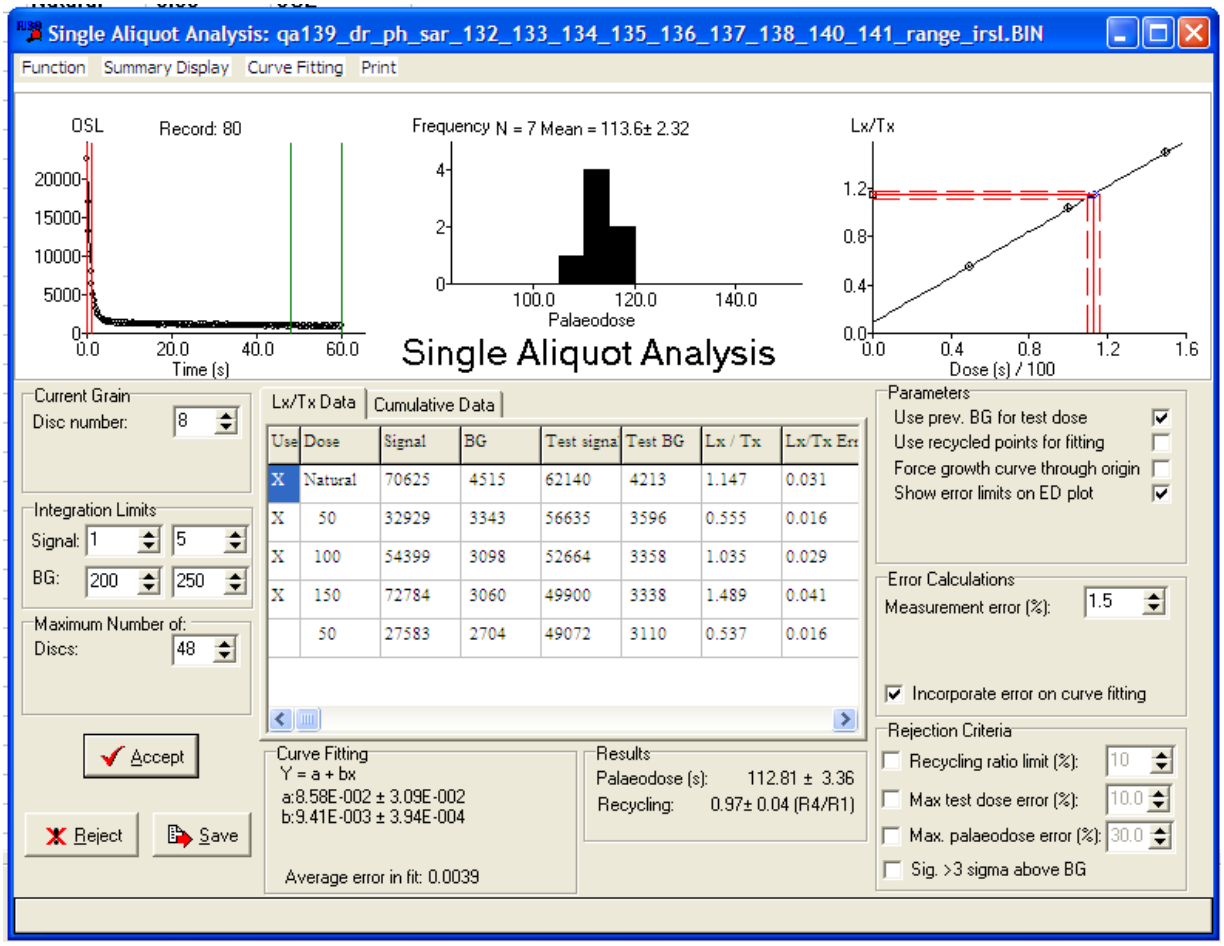

Figure 5.4. Results of a SAR test of the sample QA 08 14 01, showing the sample decay curve (top left) and growth curve (top right), the values recycling rate (bottom right,) and the histogram resulting from accepting aliquots (top centre).

Appendix 6

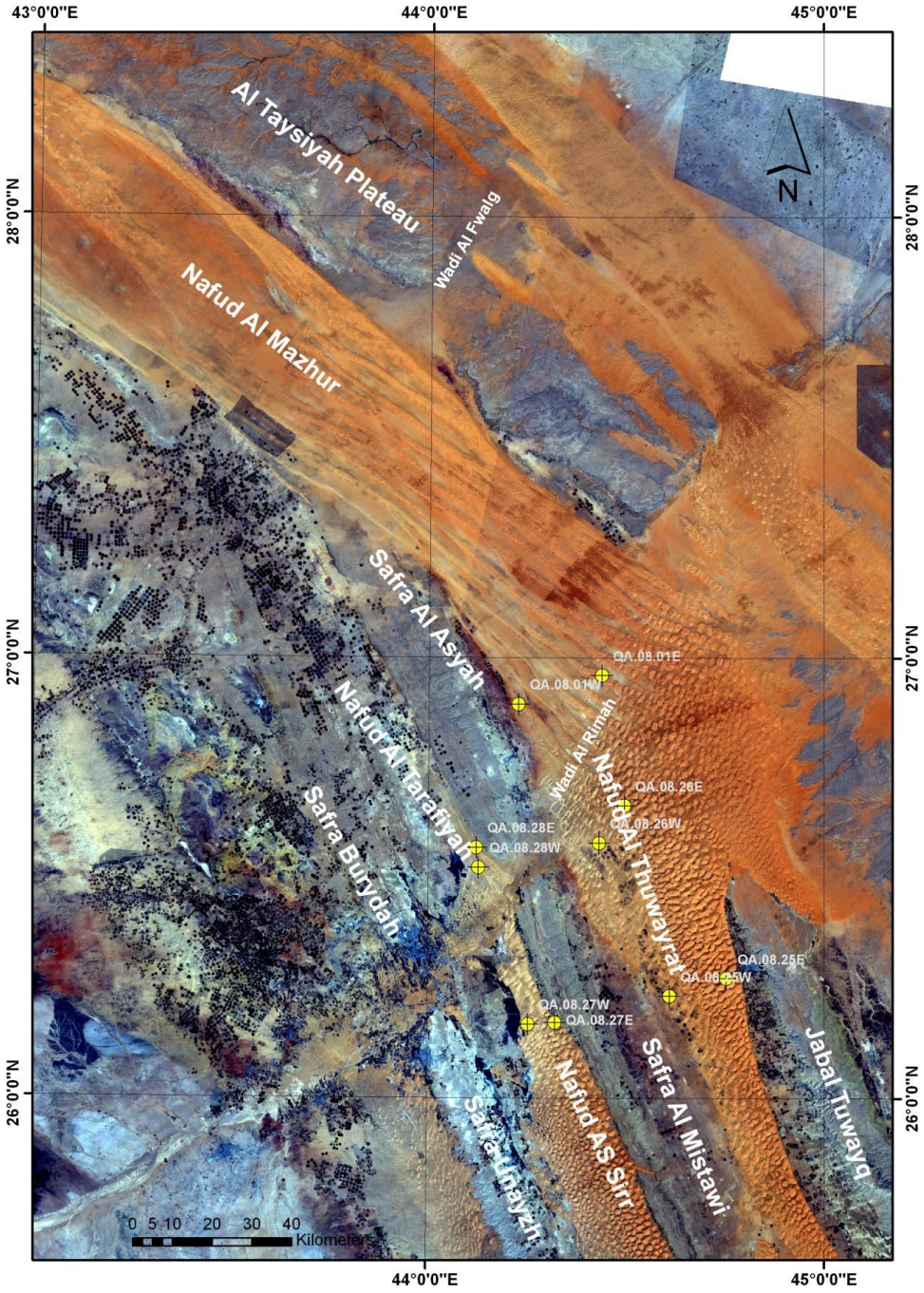

Figure 6.1: The ETM Image (bands 1.2.3) shows the sand dunes distributions in the study area, Linear dunes of Nafud Al Tarafiyah (middle), Nafud As Sirr (middle lower) and Nafud Al Thuwayrat are seen on the right and Nafud Al Mazhur in the upper image.

BAND	LMAX	LMIN
1	293.700	-6.200
2	300.900	-6.400
3	234.400	-5.000
4	*241.100*	*-5.100*
5	*47.570*	*-1.000*
7	16.540	-0.350
METADATA ETM7 SUN ASIMUTH 62.652596 SUN DISTANCE 1.00573		

Figure 7: the Metadata used to generated the COST method by Erdas